U.S. Department of Transportation

Federal Railroad Administration

Alternative Occupied Volume Integrity (OVI) Tests and Analyses

Office of Research
and Development
Washington, DC 20590

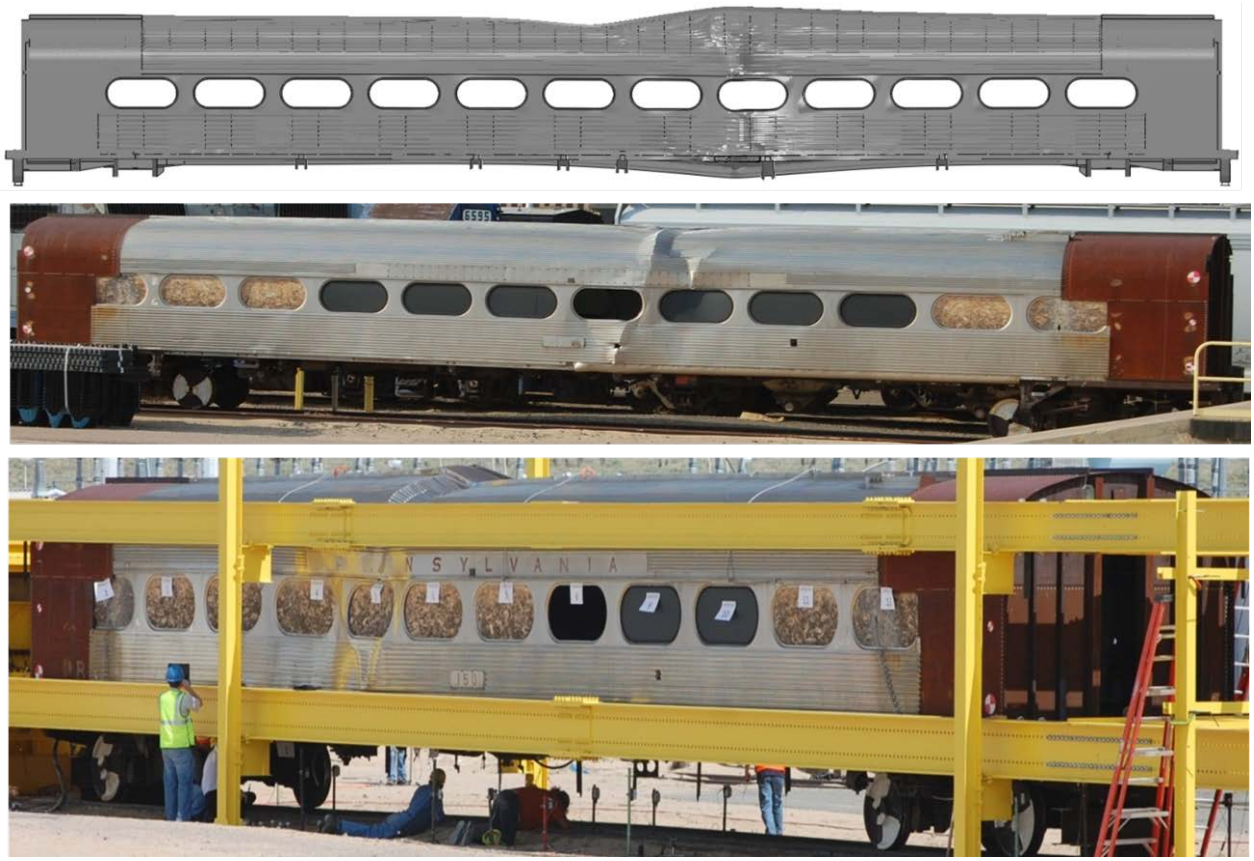

DOT/FRA/ORD-13/46

Final Report
October 2013

NOTICE

This document is disseminated under the sponsorship of the Department of Transportation in the interest of information exchange. The United States Government assumes no liability for its contents or use thereof. Any opinions, findings and conclusions, or recommendations expressed in this material do not necessarily reflect the views or policies of the United States Government, nor does mention of trade names, commercial products, or organizations imply endorsement by the United States Government. The United States Government assumes no liability for the content or use of the material contained in this document.

NOTICE

The United States Government does not endorse products or manufacturers. Trade or manufacturers' names appear herein solely because they are considered essential to the objective of this report.

REPORT DOCUMENTATION PAGE

Form Approved
OMB No. 0704-0188

1. AGENCY USE ONLY (Leave blank)	2. REPORT DATE	3. REPORT TYPE AND DATES COVERED
	October 2013	

4. TITLE AND SUBTITLE
Alternative Occupied Volume Integrity (OVI) Testing and Analyses

5. FUNDING NUMBERS
RR28A1/JG343
RR28A2/JL649
RR28A2/KL649

6. AUTHOR(S) and FRA COTR
Authors: Michael Carolan, Benjamin Perlman, David Tyrell

COTR: Melissa Shurland, Jeff Gordon

7. PERFORMING ORGANIZATION NAME(S) AND ADDRESS(ES)
John A. Volpe National Transportation Systems Center
55 Broadway
Cambridge, MA 02142

8. PERFORMING ORGANIZATION REPORT NUMBER

9. SPONSORING/MONITORING AGENCY NAME(S) AND ADDRESS(ES)
U.S. Department of Transportation
Federal Railroad Administration
Office of Research and Development
1200 New Jersey Avenue, SE
Washington, DC 20590

10. SPONSORING/MONITORING AGENCY REPORT NUMBER
DOT/FRA/ORD – 13/46

11. SUPPLEMENTARY NOTES

12a. DISTRIBUTION/AVAILABILITY STATEMENT
This document is available to the public through the FRA Web site at http://www.fra.dot.gov/eLib/Find, or by calling (202) 493-1300.

12b. DISTRIBUTION CODE

13. ABSTRACT (Maximum 200 words)

FRA, supported by the Volpe Center, conducted research on alternative methods of evaluating occupied volume integrity (OVI) in passenger railcars. Guided by this research, an alternative methodology for evaluating OVI that ensures an equivalent or greater level of safety than that provided by the current Federal regulations was developed. The alternative methodology moves the evaluation loads to the collision load path and includes three sets of load magnitudes and pass-fail criteria. This methodology also permits a combination of elastic testing and finite element (FE) analysis to be used. This research program applied the alternative methodology to a passenger railcar. Three tests were performed in concert with FE analyses. The first test was a conventional 800,000-pound buff strength test. The results of this test were used to validate an FE model of the car. The FE model was used to estimate the ultimate, or crippling, load of the car. Two destructive crippling tests were then performed. The crippling FE analysis results were compared with the crippling test results and found to describe the general behavior of the tested cars. The FE analysis estimated a crippling load of 1.19 million pounds, and the two test cars had crippling loads of 1.15 and 1.19 million pounds. The results of this program provide a technical basis for the alternative OVI methodology. The load magnitudes in the new methodology have been shown to be reasonable descriptions of the OVI capacity of conventionally designed passenger railcars.

14. SUBJECT TERMS
Occupant volume integrity, testing, finite element analysis, passenger equipment, crashworthiness

15. NUMBER OF PAGES
143

16. PRICE CODE

17. SECURITY CLASSIFICATION OF REPORT	18. SECURITY CLASSIFICATION OF THIS PAGE	19. SECURITY CLASSIFICATION OF ABSTRACT	20. LIMITATION OF ABSTRACT
Unclassified	Unclassified	Unclassified	

NSN 7540-01-280-5500

Standard Form 298 (Rev. 2-89)
Prescribed by ANSI Std. 239-18
298-102

METRIC/ENGLISH CONVERSION FACTORS

ENGLISH TO METRIC	METRIC TO ENGLISH
LENGTH (APPROXIMATE)	**LENGTH (APPROXIMATE)**
1 inch (in) = 2.5 centimeters (cm)	1 millimeter (mm) = 0.04 inch (in)
1 foot (ft) = 30 centimeters (cm)	1 centimeter (cm) = 0.4 inch (in)
1 yard (yd) = 0.9 meter (m)	1 meter (m) = 3.3 feet (ft)
1 mile (mi) = 1.6 kilometers (km)	1 meter (m) = 1.1 yards (yd)
	1 kilometer (km) = 0.6 mile (mi)
AREA (APPROXIMATE)	**AREA (APPROXIMATE)**
1 square inch (sq in, in^2) = 6.5 square centimeters (cm^2)	1 square centimeter (cm^2) = 0.16 square inch (sq in, in^2)
1 square foot (sq ft, ft^2) = 0.09 square meter (m^2)	1 square meter (m^2) = 1.2 square yards (sq yd, yd^2)
1 square yard (sq yd, yd^2) = 0.8 square meter (m^2)	1 square kilometer (km^2) = 0.4 square mile (sq mi, mi^2)
1 square mile (sq mi, mi^2) = 2.6 square kilometers (km^2)	10,000 square meters (m^2) = 1 hectare (ha) = 2.5 acres
1 acre = 0.4 hectare (he) = 4,000 square meters (m^2)	
MASS - WEIGHT (APPROXIMATE)	**MASS - WEIGHT (APPROXIMATE)**
1 ounce (oz) = 28 grams (gm)	1 gram (gm) = 0.036 ounce (oz)
1 pound (lb) = 0.45 kilogram (kg)	1 kilogram (kg) = 2.2 pounds (lb)
1 short ton = 2,000 pounds (lb) = 0.9 tonne (t)	1 tonne (t) = 1,000 kilograms (kg)
	= 1.1 short tons
VOLUME (APPROXIMATE)	**VOLUME (APPROXIMATE)**
1 teaspoon (tsp) = 5 milliliters (ml)	1 milliliter (ml) = 0.03 fluid ounce (fl oz)
1 tablespoon (tbsp) = 15 milliliters (ml)	1 liter (l) = 2.1 pints (pt)
1 fluid ounce (fl oz) = 30 milliliters (ml)	1 liter (l) = 1.06 quarts (qt)
1 cup (c) = 0.24 liter (l)	1 liter (l) = 0.26 gallon (gal)
1 pint (pt) = 0.47 liter (l)	
1 quart (qt) = 0.96 liter (l)	
1 gallon (gal) = 3.8 liters (l)	
1 cubic foot (cu ft, ft^3) = 0.03 cubic meter (m^3)	1 cubic meter (m^3) = 36 cubic feet (cu ft, ft^3)
1 cubic yard (cu yd, yd^3) = 0.76 cubic meter (m^3)	1 cubic meter (m^3) = 1.3 cubic yards (cu yd, yd^3)
TEMPERATURE (EXACT)	**TEMPERATURE (EXACT)**
[(x-32)(5/9)] °F = y °C	[(9/5) y + 32] °C = x °F

QUICK INCH - CENTIMETER LENGTH CONVERSION

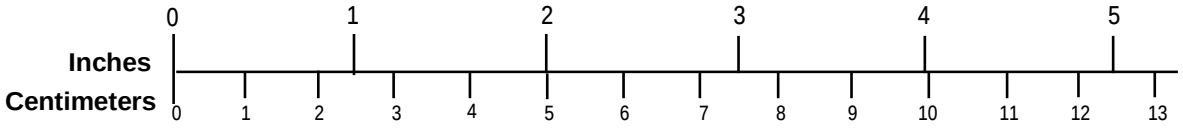

QUICK FAHRENHEIT - CELSIUS TEMPERATURE CONVERSIO

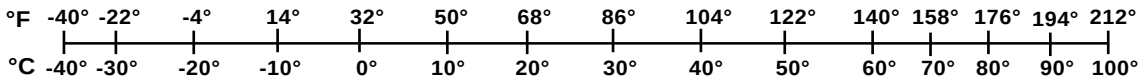

For more exact and or other conversion factors, see NIST Miscellaneous Publication 286, Units of Weights and Measures. Price $2.50
SD Catalog No. C13 10286

Updated 6/17/98

Contents

Illustrations

Tables

Executive Summary

The Federal Railroad Administration (FRA), with the assistance of the John A. Volpe National Transportation Systems Center (Volpe Center), has been conducting research on alternative methods of evaluating occupied volume integrity (OVI) in passenger rail equipment. As a result of this research, an alternative methodology for evaluating OVI has been developed that ensures an equivalent or greater level of safety than that provided by the current Federal regulations. The alternative methodology moves the applied load away from the line of draft to the collision load path, more closely representing the type of loading the occupant volume would experience during a collision. This methodology permits application of one of three sets of evaluation load magnitudes and corresponding pass-fail criteria. Additionally, this methodology permits a combination of elastic testing and finite element (FE) analysis to be used in the evaluation of a car design, whereas the conventional methodology only permits the use of testing. The new methodology requires that an elastic test be used to validate an FE model of the car undergoing evaluation. Once validated with elastic test data, the model can be used to demonstrate that the car's OVI satisfies one of the three pass-fail criteria.

This research program sought to establish confidence in the alternative methodology as a means of evaluating OVI. The research methodology was applied to a Budd Pioneer passenger railcar. A pair of destructive crippling tests was performed to confirm that analysis performed according to the new methodology could reliably estimate the crippling behavior of a passenger railcar. The testing program applied the new methodology by first performing a conventional 800,000-pound line of draft buff strength test. The results of this test were used to validate an FE model of the car to which the test loading conditions were applied. The now-validated FE model was then used to estimate the ultimate, or crippling, load for this type of car.

The second test performed as part of this research program was a limited-instrumentation "shakedown" test that loaded a Pioneer car to its crippling load along its collision load path. The third test performed was a fully instrumented crippling test of a second Pioneer car along its collision load path.

Data collected during the tests include the incremental load versus displacement behavior of each car, the longitudinal strains in major structural members, and the vertical, lateral, and longitudinal displacements of the underframe. The elastic FE analysis results were compared with the results of the elastic test and found to be in reasonable agreement. The crippling FE analysis results were compared with the crippling test results and were found to describe the general load versus displacement behavior of the two tested cars. The crippling FE analysis estimated a crippling load of 1.19 million pounds. The first tested car crippled after reaching a load of 1.15 million pounds, and the second car slightly exceeded 1.19 million pounds before it crippled.

The results of this testing and analysis program have provided a technical basis for the alternative OVI evaluation methodology. The load magnitudes adopted as a part of the new methodology have been shown to be reasonable descriptions of the capacity of the OVI of conventionally designed passenger railcars.

1. Introduction

1.1 Background

The FRA Office of Research and Development supports the safety rulemaking and enforcement programs of the FRA Office of Railroad Safety. The Volpe Center provides engineering support to the Office of R&D.

Presently, FRA's *Passenger Equipment Safety Standards* are located within the Code of Federal Regulations at 49 CFR 238. These standards provide design and performance requirements for ensuring an appropriate level of safety for various locations and components of passenger railcars. The purpose of these standards is described in 49 CFR 238.1(a) as follows:

> *The purpose of this part is to prevent collisions, derailments, and other occurrences involving railroad passenger equipment that cause injury or death to railroad employees, railroad passengers, or the general public; and to mitigate the consequences of such occurrences to the extent they cannot be prevented.*

One of the techniques employed in mitigating the consequences of accidents is the use of structural standards to establish a baseline level of performance for various structures that make up the car body. Among the structural requirements given in 49 CFR 238 are the compressive strength of the car body (§238.203), the collision posts (§238.211), the corner posts (§238.213), the rollover strength (§238.215), and the side structure (§238.217). These structures are intended to prevent loss of occupied volume in the event of an accident that is not prevented through other measures.

The *Passenger Equipment Safety Standards* are applied to all passenger equipment that operates over the general railroad system of the United States. Because different structural standards are applied to railroad vehicles built for service in other parts of the world, FRA has received several requests for waivers of the domestic structural requirements [1, 2, 3, 4]. These waiver requests seek to permit rail vehicles built to different structural standards to operate on the general railroad system of the United States. The entity seeking the waiver must generally demonstrate that the subject vehicle provides an equivalent level of safety as a vehicle that complies with the requirements of the CFR.

To help facilitate the waiver application process, in 2009 FRA's Railroad Safety Advisory Committee (RSAC) established its Engineering Task Force (ETF). The ETF was responsible for generating a set of technical criteria and procedures to demonstrate that trainsets developed to meet alternative standards provide a level of safety equal to the domestic standard. Compliance with the criteria and procedures may be demonstrated when a waiver is sought to permit an alternatively designed trainset to operate in the United States [5]. ETF members included rail vehicle manufacturers, railroad operators, industry consultants, and FRA and Volpe Center staff. The recommendations proposed by the ETF were published as a report, "Technical Criteria and Procedures for Evaluating the Crashworthiness and Occupant Protection Performance of Alternatively Designed Passenger Rail Equipment for Use in Tier I Service" [6]. The final version of this report was posted on FRA's Web site in October 2011.

One of the structural requirements addressed in the ETF's report is used to demonstrate that an equivalent level of safety for the occupant volume integrity (OVI) exists between the vehicle in question and a conventional vehicle meeting the requirements of the CFR. The existing CFR requirement places an 800,000-pound compressive load along the line of draft of the car, and the car is required to experience no permanent deformation under this load. The ETF alternative offers the choice of one of three optional load magnitudes, applied along the collision load path of the car, each with a corresponding pass-fail criterion. The existing OVI requirement and the proposed ETF methodology for ensuring OVI are discussed in this section.

1.1.1 Existing OVI Requirement

The current OVI requirement for all passenger equipment traveling on the general railroad system is contained in the CFR at 49 CFR 238.203 and reads, in part, as follows:

> *(a)(1) Except as further specified in this paragraph or in paragraph (d), on or after November 8, 1999 all passenger equipment shall resist a minimum static end load of 800,000 pounds applied on the line of draft without permanent deformation of the body structure.*
>
> *(2) For a passenger car or a locomotive, the static end strength of unoccupied volumes may be less than 800,000 pounds if:*
> *(i) Energy absorbing structures are used as part of a crash energy management design of the passenger car or locomotive, and*
> *(ii) The passenger car or locomotive resists a minimum static end load of 800,000 pounds applied on the line of draft at the ends of its occupied volume without permanent deformation of the body structure.*

The line of draft is an imaginary line that runs from the structure of the car just inboard of the coupler at one end to just inboard of the coupler at the opposite end. This line represents the line-of-action of the tensile (draft) and compressive (buff) forces introduced into a railcar through its couplers by the adjacent cars. Based on the specific design of a passenger car, an actual structure may or may not exist along the line of draft. The line of draft is illustrated schematically in Figure 1 for a generic, conventionally designed passenger railcar.

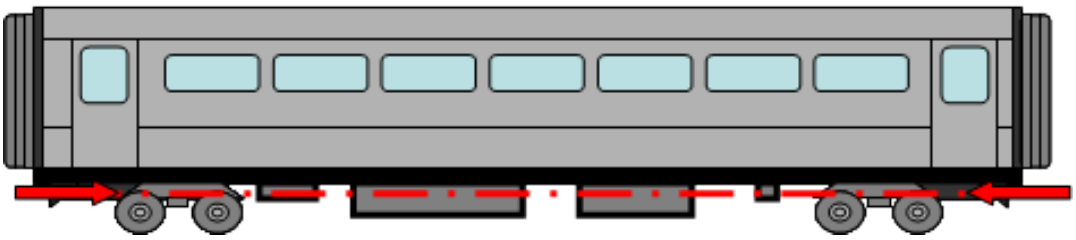

Figure 1. Line of Draft Illustrated on Generic Conventional Passenger Railcar

A large compressive load applied to the line of draft of a passenger railcar has been in place as a standard or recommended practice since the first half of the twentieth century [7], and was codified in 1999 as a Federal regulation applicable to all passenger equipment on the general railroad system [8]. Historically, this loading requirement was used to ensure a baseline resistance to loss of occupant volume through longitudinal crush.

The 800,000-pound requirement has several positive attributes that have contributed to its continued use. Because the OVI requirement has traditionally been evaluated through the use of

a quasi-static test, verification of a railcar's success in meeting the requirement is straightforward. The criterion for "no permanent deformation" may be verified through visual inspection of the car, as well as through the use of strain gages installed on the structural members of the car. For a car that has been designed and constructed to meet the 800,000-pound requirement, a successful test is nondestructive. If a car structure succeeds in resisting 800,000 pounds without permanent deformation, that structure may then have its assembly completed and be delivered to the customer as a functional rail vehicle. This ability to utilize a structure as both test article and deliverable product gives this test an economic advantage over destructive testing.

However, there are several disadvantages associated with the existing OVI requirement. The regulation places the full 800,000-pound load along the line of draft for all vehicles, regardless of the design of the body structure. While a conventionally designed railcar may have the ability to support that load at the line of draft, vehicles with a partial low-floor section, an articulation at one or both ends, an alternative load path, or an otherwise nonconventional design may not.

A modern development in railcar crashworthiness design is the use of sacrificial unoccupied areas designed to permanently deform and absorb collision energy in a controlled manner. This approach to design, known as crash energy management (CEM), is more frequently being included in the design of passenger railcars as a means to increase safety in the event of a collision. In order to function as intended in a collision, the CEM system must crush at a lower force than it takes to crush the occupant volume. The car's OVI must be sufficient to prevent crush of the occupied areas before the CEM system has fully exhausted.

The current CFR requirement makes allowance for CEM designs, permitting the evaluation load to be applied to the car inboard of the designated energy absorbing structures. However, the 800,000-pound load must still be applied along the line of draft. In a CEM-equipped railcar, the normal service loads may still be transmitted along the line of draft. Nevertheless, in a collision with sufficient severity to activate the CEM system, the load path into the occupant volume will be altered. During crush of the CEM components, the collision forces will travel through the energy absorbing elements and into the occupant volume where these elements are attached to it. Because these elements may not be attached to the car along its line of draft, the collision load path for a CEM car may differ significantly from its normal service load path. Therefore, although applying 800,000 pounds along the line of draft determines some level of resistance to loss of occupant volume, it does not evaluate the car in the manner in which it was designed to be loaded in a collision.

1.1.2 Previous FRA Research on OVI

For several years, FRA, in support of the advancement of improved safety standards for passenger rail vehicles, has sponsored work at the Volpe Center investigating alternative ways of evaluating OVI. This research was intended to identify an alternative manner of evaluating the OVI that would ensure a level of safety equivalent to that provided by the conventional requirement. Such an alternative would permit nonconventional passenger car designs to be introduced into service in the United States.

This research first set out to investigate the behavior of a conventionally designed passenger railcar when subject to the conventional 800,000-pound (800 kip) line of draft load [9]. Using a simplified FE model, the 800-kip load was applied to a generic representation of a conventional

passenger car. The effect of this loading was to impart to the railcar a large bending moment as well as a significant compressive load.

The next step in this research program was to determine whether a conventionally designed passenger railcar could be loaded in an alternative manner and develop a similar state of stress as a conventionally loaded railcar subjected to the 800-kip compressive line of draft load. Again using a simplified FE model, alternative loading schemes were evaluated on a generic single-level passenger railcar of conventional construction. Because the line of draft may be difficult to define for some rail cars, or may be easily defined but not descriptive of the path traveled by collision loads through the structure, alternative loading locations that were easily definable and descriptive of the collision load path were examined. The alternate loading scheme examined a 1 million-pound load applied across the floor of the endframe of the car in concert with a 200,000-pound load applied across the roof of the endframe of the car. The combined 1.2 million-pound load, distributed across the floor and roof of the endframe, resulted in a state of stress in the car's structural members that was more severe than the stress state developed by the conventional 800,000-pound load along the line of draft.

By moving the load away from the line of draft and onto the end structure of the car, the previous research program sought to make the compressive strength requirement applicable to a wider range of passenger car designs than could readily be evaluated with the conventional test. The suggested approach to alternative loading also sought to provide an equivalent level of occupant protection as the existing 800,000-pound requirement by selecting loads that placed an equal or greater demand on the car's structure. These preliminary results indicated that a conventional car's structure was capable of supporting compression loads above the conventional 800,000-pound load, if the loads were introduced into the structure at a location other than the line of draft.

A general strategy for evaluating passenger cars of an alternative design was developed; it employed a combination of elastic analysis, elastic testing, and plastic analysis. Because placing large compressive loads in several locations on a car may be difficult to accomplish during a test, FE analysis was considered a possible method of evaluating an occupant volume's response to loads at several locations. Any FE model will have certain assumptions, simplifications, and approximations built in; therefore, it is essential that a model be validated by comparing a modeled load case with the results of a test under the same conditions. If the model is capable of closely estimating the results of an elastic load test, there is greater confidence in the model's results for a load case that is not also tested. If simulating the response of the carbody to loads that induce plastic behavior, the FE model may be validated with test data obtained for loads producing elastic behavior. The plastic response for greater load magnitudes may then be extrapolated using the model alone. With this methodology, the test article is not subjected to loads that would cause plastic deformation.

A 2009 technical paper outlined the general strategy of using a combination of elastic analysis, elastic testing, and plastic analysis to estimate the crippling behavior of a passenger car loaded in an alternative manner [10]. Following the development of this alternative approach to loading the passenger car structure, the next objective of the research program was to apply these alternative loads to an exemplar railcar in a quasi-static test. A preliminary testing strategy was developed that placed alternative loads along the collision load path of a passenger railcar equipped with CEM.

1.1.3 Adopted ETF OVI Methodology

In 2009, the ETF was tasked with developing a set of technical criteria and procedures that would help determine whether an alternatively designed rail vehicle would perform as well as a vehicle designed to meet the *Passenger Equipment Safety Standards*. The ETF examined current requirements for OVI as detailed by 49 CFR 238.203. FRA and the Volpe Center were active participants in the ETF and presented information on the ongoing OVI research program as well as future testing plans. Additionally, railcar manufacturers provided technical information on OVI requirements in other parts of the world as well as test and simulation results for alternatively designed passenger railcars. The ETF adopted a set of technical criteria and procedures for evaluating the OVI of alternatively designed passenger equipment, in lieu of applying the requirements of 49 CFR 238.203 [6].

In the ETF's report, the criteria are defined as the loading conditions to be applied and the acceptable behavior of the vehicle under those conditions. The procedures are the required tests and/or analyses that are employed to demonstrate compliance with the criteria. The ETF's criteria and procedures are intended to allow for flexibility with respect to car design methodology and evaluation procedure while maintaining an equivalent level of safety as equipment designed to meet and be evaluated against the existing 800,000-pound buff strength requirement.

In developing alternative criteria and procedures for evaluating OVI, the ETF examined some of the reasons waivers are sought for alternatively designed equipment. In recognition of a variety of passenger car designs that could be the subject of potential waiver applications, the ETF adopted three loading options consisting of pairs of load magnitudes and corresponding pass-fail criteria. To meet the alternative OVI requirement, a passenger railcar design must satisfy one of the three options. The three options for demonstrating a vehicle's OVI are provided in Table 1.

Table 1. ETF OVI Criteria

ETF Option	Criteria for Each Option
Option A	Passenger equipment shall resist a minimum quasi-static end load of 800,000 pounds applied on the collision load path without permanent deformation of the occupied volume.
Option B	Passenger equipment shall resist a minimum quasi-static end load of 1 million pounds applied on the collision load path with limited permanent deformation of the occupied volume. Limited permanent deformation means that local plastic strains must be less than 5 percent and vehicle shortening must not exceed 1 percent over any 15 feet of occupied volume.
Option C	Passenger equipment shall resist a minimum quasi-static end load of 1.2 million pounds applied on the collision load path without crippling the body structure.

The ETF adopted a two-stage procedure as the general approach to demonstrating OVI. The first stage consists of simulating an elastic compression test with an FE model. An elastic test is then performed and the data collected during the test is used to validate the FE model. In the second stage, the now-validated FE model is used to demonstrate that the modeled car satisfies one of the three options. The ETF's report discusses the procedures that may be used to evaluate any of the three options, as well as particular procedures unique to each option. The ETF's general approach to ensuring OVI is the same as that employed for conventional cars, that is, a large compressive load is applied to the occupant volume. However, the ETF's procedures include two major changes from the current OVI evaluation methodology.

The first major difference is the placement of the load. The CFR requires the load to be placed along the line of draft for all equipment under evaluation. Recognizing that collision loads pose a greater threat to the integrity of the occupant volume than service loads and that a vehicle may be designed to transmit collision loads at a location other than the line of draft, the applied evaluation load was moved to the ends of the collision load path.

Placing the load along the collision load path offers a better approximation of the type of loading the car will actually experience during a collision. This change also permits CEM-equipped cars to be evaluated in the manner in which they were designed to be loaded during a collision. By removing the specific language of "line of draft" and allowing loads to be applied along the collision load path specific to the vehicle undergoing evaluation, the ETF's procedures represent a design-neutral approach to evaluating OVI.

The second major change to procedures adopted by the ETF involves allowing a combination of testing and analysis to be used to demonstrate a vehicle's OVI. The 800,000-pound buff strength requirement has been demonstrated using a quasi-static test. Although analysis may be used during the development of a design, testing has traditionally been used to demonstrate the ability of the vehicle to support the 800,000-pound load without permanent deformation. Because two of the ETF's options permit some permanent deformation to occur in a successful demonstration of OVI, the use of analysis is necessary to avoid performing a destructive test. Although the

ETF's procedures do not prevent a destructive test from being used to demonstrate compliance, it was envisioned that a combination of nondestructive (elastic) testing and analysis would more typically be applied.

Permitting the combined use of nondestructive (elastic) testing and analysis (as a surrogate for potentially destructive testing) is a significant step away from the conventional approach of permitting only testing to be used to demonstrate compliance. Because of the uncertainties introduced in an analysis, it is important to verify that the model being analyzed is capable of producing reasonably accurate results. The ETF procedures do not permit a total abandonment of testing, but contain a methodology where testing and analysis are both utilized to increase the confidence in the analytical results.

Under the ETF procedures, model results may be used to demonstrate that a vehicle complies with Option A, Option B, or Option C only if the model has been previously validated with elastic test data. Specifically, the vehicle being evaluated must be tested under a longitudinal load that meets a recognized national or international testing standard. The applied load must be no less than 337,000 pounds, regardless of the standard being applied. A model should be used to analyze the behavior of the car in this test. If the strain and displacement results from the model and the data from the test are within the tolerances adopted by the ETF, the model is considered validated and may be used to demonstrate compliance with any of the three OVI options. A flowchart of the ETF's procedures is shown in Figure 2.

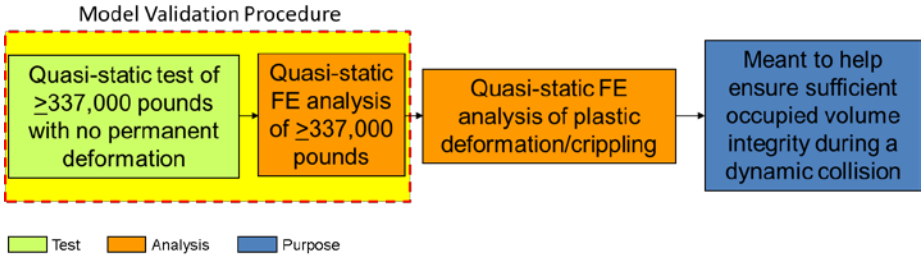

Figure 2. Summary of ETF OVI Procedures

1.2 Objectives

The ETF criteria and procedures represent a departure from the existing 800,000-pound buff strength requirement. This alternative methodology for demonstrating OVI permits a wider variety of equipment designs to be evaluated through a waiver process using criteria that place loads on the equipment in the manner in which it was designed to support load. This alternative methodology permits the use of modern engineering analysis techniques to demonstrate a rail vehicle's OVI. However, as this procedure is relatively new, additional progress needs to be made in applying the methodology to evaluate the OVI of a passenger railcar. FRA, with the support of the Volpe Center, has conducted a series of full-scale, quasi-static compression tests of passenger rail equipment in concert with FEA of each test. The goal of this testing program was to develop confidence in using the elastic test and crippling analysis methodology adopted by the ETF to estimate the crippling behavior of passenger rail equipment. The results of the research program could verify the load magnitudes adopted by the ETF as representative of the performance of conventionally designed equipment. Application of the research findings would also provide confidence that the methodology of elastic analysis, elastic testing, and plastic

extrapolation analysis is capable of describing the behavior of a passenger railcar when loaded up to its crippling load.

The series of tests undertaken in this research program consisted of a conventional 800-kip line of draft elastic test and two collision load path crippling tests. Two Budd Pioneer cars were used in this program. The three tests are summarized in Table 2. An FE model was used to simulate the elastic line of draft test, and a second model was used to simulate the crippling test. The results of the testing and analyses were compared using the ETF's criteria to evaluate whether the modeling provided a reasonable estimate of the behaviors of the cars under the given test conditions.

Table 2. Descriptions of Tests in FRA Research Program

Test	Test Date	Test Article	Description
800,000-pound line of draft	January 2011	Pioneer 244	Elastic test used to verify structural integrity of Car 244 and provide data for FE validation.
"Shakedown" crippling test	May 2011	Pioneer 248	Verify performance of newly constructed test frame and newly installed hydraulic control system.
Fully instrumented crippling test	May 2011	Pioneer 244	Establish whether the loading options considered in the ETF's methodology reasonably reflect the OVI of a conventionally designed passenger railcar.

1.3 Organization of the report

The body of this report contains five sections that are as follows.

This section, section one, includes the introduction, background information on OVI, and a description of the objectives of this research program.

Section two discusses the first test, the 800-kip elastic verification test, which was conducted in this series. The general test setup and the instrumentation used to collect data are presented. A detailed description of the test article, Pioneer 244, used in the elastic test and one crippling test is also provided in this section of the report. In addition, section two presents the FE model that was used to simulate the 800-kip elastic test. Discussion of the FE model includes the history of the model's development, the boundary conditions placed on the model, and the loading mechanism used to simulate the elastic test. Validation of the FE model using strain and displacement data from the 800-kip elastic test is discussed in this section of the report.

Section three examines the crippling tests that were performed in this research program. Both the limited-instrumentation crippling test of Car 248 and the fully instrumented crippling test of Car 244 are considered. This section also provides a discussion of the test setup, a description of the physical condition of the two test cars, and a listing of the instrumentation that was installed on both cars during their crippling tests. The FE model that was used to simulate the crippling tests is presented. The discussion in this section touches on the modifications made to the elastic model to create the crippling model, the boundary conditions placed on the model, and the loading mechanism used in the crippling simulation.

In section four, the results of the two crippling tests are compared with one another, as well as with the results obtained from the FE model. This section includes a detailed discussion of the damage observed in each test. For both tests, the load-versus-displacement measurements are compared with the load-versus-displacement calculations made by the FE model. For the fully instrumented crippling test, the vertical mode of deformation and the strain results on key longitudinal members of the body structure are also discussed. These results are compared with the results calculated by the FE model.

Section five contains concluding remarks. The major results of the research program are summarized. This section also touches on the relevance of the results to the criteria and procedures that were adopted by the ETF.

2. 800-kip Validation Test and Analysis

The first test performed in this research program was a conventional 800,000-pound line of draft loading. This test was performed to verify the structural integrity of Budd Pioneer Car 244 and to validate the FE model of the car. The car was instrumented during this test to measure the applied load, strains in the major longitudinal members, and displacements of the underframe along its length.

2.1 Description of Test Article

The test article selected for this program was the Budd Pioneer car. Two Pioneer cars were used: Car 244 and Car 248. These two cars were used in commuter rail service for approximately 30 years before being retired. The cars were donated to FRA by the Southeastern Pennsylvania Transportation Authority (SEPTA). The Pioneer was originally designed to comply with the 800-kip line of draft load requirement. Cars of this design utilized a conventional draft sill and underframe arrangement featuring a center sill and two side sills capable of meeting the 800-kip requirement. The Pioneer design made extensive use of high-strength stainless steels for the structural members as a means of ensuring a lightweight vehicle. Budd Pioneer Car 244 is shown in Figure 3 in its original condition.

Figure 3. Car 244 in Original Condition

Prior to their use in the OVI testing program, both cars were used in a previous FRA research program. This previous program used the cars in a series of dynamic impact tests [11]. Following the collision tests, each car was repaired and retrofitted with a CEM system designed to dissipate collision energy through controlled permanent deformation. The CEM system featured energy absorbing elements at both the floor level and roof level of the car. The CEM-equipped cars were then subjected to a second series of impact tests designed to evaluate the

performance of the CEM systems. Pioneer 248 is shown in Figure 32 with its CEM system highlighted.

Figure 4. Car 248 with CEM System

The design of this particular CEM system provides two paths for longitudinal loads through the occupant volume. During normal operations, the service loads are transmitted on the conventional load path along the line of draft. In the event of a collision, trigger elements are activated and the energy absorbing components begin to crush. Once the energy absorbing elements begin crushing, the collision loads are transmitted through these elements and into the occupant volume at the energy absorber support structures. Figure 5 shows Car 248 with its CEM components removed. The energy absorber supports at one end of the occupant volume are indicated in this figure.

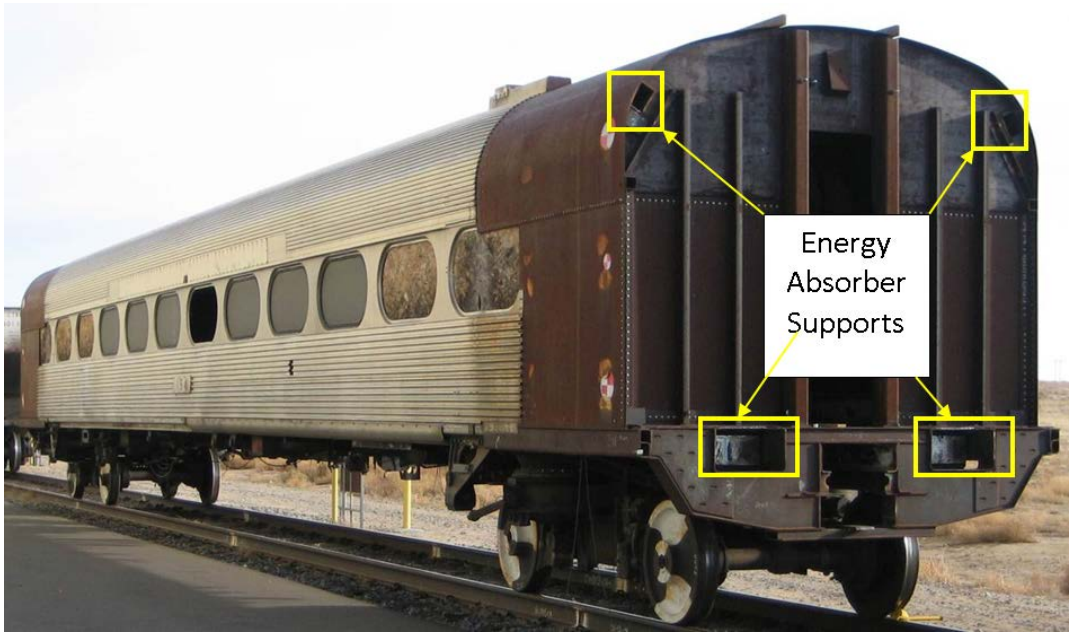

Figure 5. Car 248 Energy Absorber Support Locations

2.2 Elastic Test Setup

Because Car 244 had previously been involved in a series of high-energy dynamic impacts [11], a test was needed to ensure the structural integrity of the car and verify its suitability for further OVI testing. Additionally, the ETF procedures require that an elastic test be used to validate the FE model used to simulate the crippling behavior of the car. The 800-kip line of draft test was chosen to accomplish both of these tasks. Because the Pioneer Cars were originally designed to meet the 800-kip line of draft load requirement, their ability to support this load would verify their structural integrity. The 800-kip magnitude of load applied also exceeds the minimum load of 337,000 pounds required by the ETF procedures for an elastic validation test. Therefore, the results of this test can also be used to validate the FE model of the car. The validated model would then be modified slightly to simulate loading up to crippling.

The 800-kip elastic verification test was performed on January 19, 2011, at Transportation Technology Center (TTC) in Pueblo, CO. A previous 800-kip elastic verification test had been performed on this car on January 10, 2010 [11]; however, during review of the test results, several anomalies were discovered. These anomalies included indication of a lateral shift of the test frame that was not captured by any instrumentation. This behavior caused difficulty in comparing the test results and the results of the corresponding FE analysis. Additionally, post-test examination of the car revealed several small cracks in one side sill. The decision was made to perform a second buff test on the car. A doubler plate was installed over the side sill cracks, with a second patch placed on the other side sill to maintain symmetry. Figure 6 shows a photograph of one of the crack patches that was added to the side sill of Car 244. Following the addition, the test frame was better restrained against unintended lateral motion. Finally, additional string potentiometers were installed on the underframe of the car so that motion in the vertical, lateral, and longitudinal directions could be resolved into its components.

Figure 6. Patch Installed on Car 244 Side Sill

During the test, Car 244 remained on its trucks. Because the line of draft represents the service load path taken by normal operational loads, the CEM endframes of the car were left intact for this test. Load was applied to the A-end buff stops through a hydraulic actuator with a capacity of 1 million pounds. The car was restrained at the B-end buff stops by the test frame's cross member. The test frame itself was composed of two longitudinal beams running the length of the car connected by two large lateral cross members. These longitudinal beams are themselves supported by a series of sawhorses, preventing the beams from moving downward but offering no resistance to uplift. The lateral cross member is attached to the ground at the live end but is free to move longitudinally at the restraint end. Figure 7 shows Car 244 in the test frame during the January 2011 test. The CEM endframes are indicated in this figure at both ends of the car.

Figure 7. Car 244 in Test Frame, 800-kip Verification Test

2.3 Instrumentation

In the 800-kip verification test, Car 244 was instrumented with uniaxial strain gages installed on the longitudinal members and string potentiometers (string pots) having vertical, lateral, and longitudinal orientations. A single load cell with a capacity of 1,000 kips was installed in-line with the hydraulic actuator at the live end of the car. A summary of the instrumentation used in this test is provided in Table 3.

Table 3. Instrumentation Summary for 800-kip Verification Test

Type of Instrumentation	Number of Channels
Uniaxial Strain Gages	64
String Potentiometer	27
1,000 kip Load Cell	1
Total	**92**

2.3.1 Load Cell

A single load cell with a 1,000-kip capacity was used in the 800-kip elastic verification test. The load cell was installed in series between the hydraulic actuator and a column used to transmit load to the buff stops within the draft sill of the car. The single load cell used in this test is shown in Figure 8.

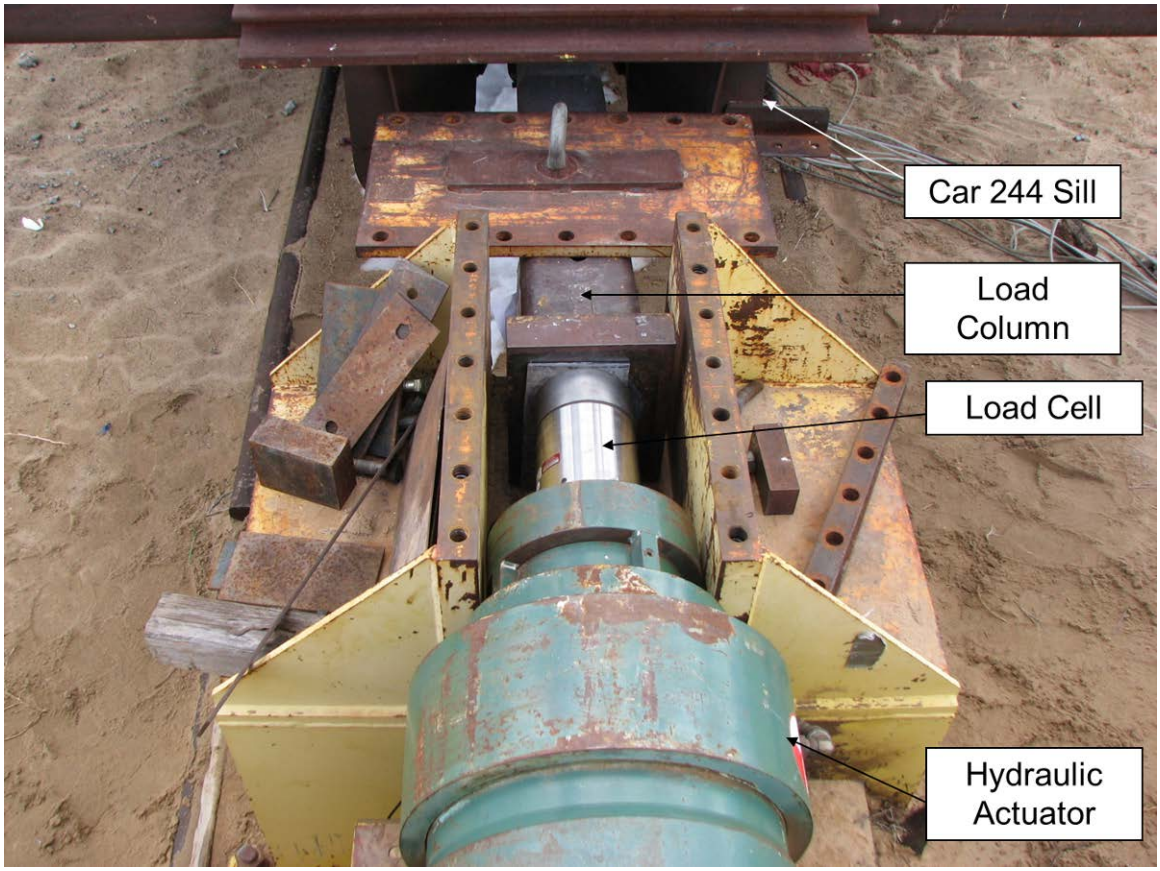

Figure 8. Load Cell in 800-kip Verification Test

2.3.2 String Potentiometers

Each string pot reports the change in string length between its grounded end and its attachment point on the car. Because the point on the car can experience simultaneous motion in all three directions, the change in length reported by any one string could include components in all directions. Vertical, lateral, and longitudinal (VLL) arrays of string pots were installed at each instrumented point on the underframe of the car in the 800-kip test. By attaching three string pots to a single point on the car, the reported change in length of each string can be used to resolve the VLL motion of the point on the car. The procedures for resolving the motion of a single point into its components are discussed in Appendix D. An exemplar VLL array is shown in Figure 9.

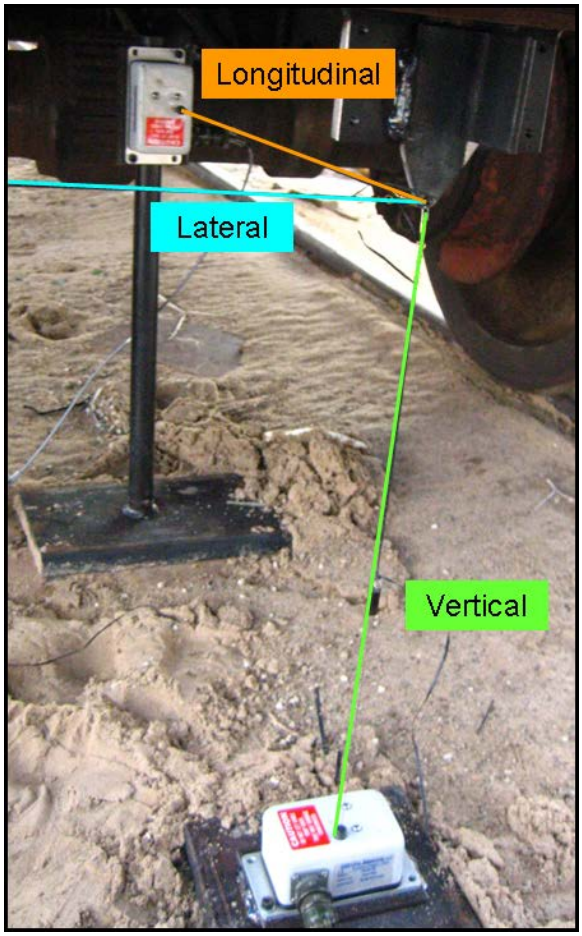

Figure 9. VLL Array of String Pots

In the elastic verification test of Car 244, a total of nine VLL arrays were installed on the underframe of the car. At both ends of the car, arrays were placed on the side sills and the lateral member at the end of the occupant volume. Between the two body bolsters, VLL arrays were attached to the center sill of the car. Figure 10 shows the nine locations and the names of the VLL arrays used in the elastic verification test of Car 244. This image shows an inverted view of the car, taken from the FE model.

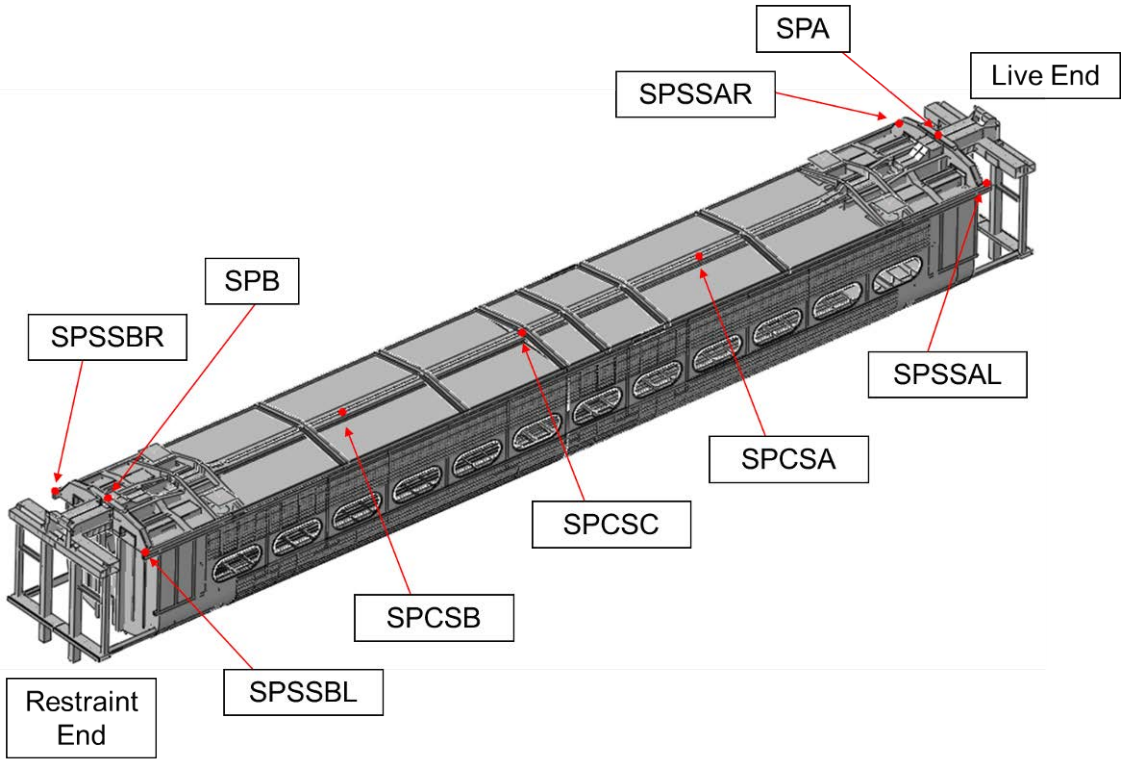

Figure 10. String Pot Arrays in 800-kip Verification Test (Underside View)

2.3.3 Strain Gages

Uniaxial strain gages were installed on Car 244 at six cross-sections, as shown in Figure 11 below. This figure also indicates the locations on Car 244's underframe where string pot arrays were installed during the elastic verification test.

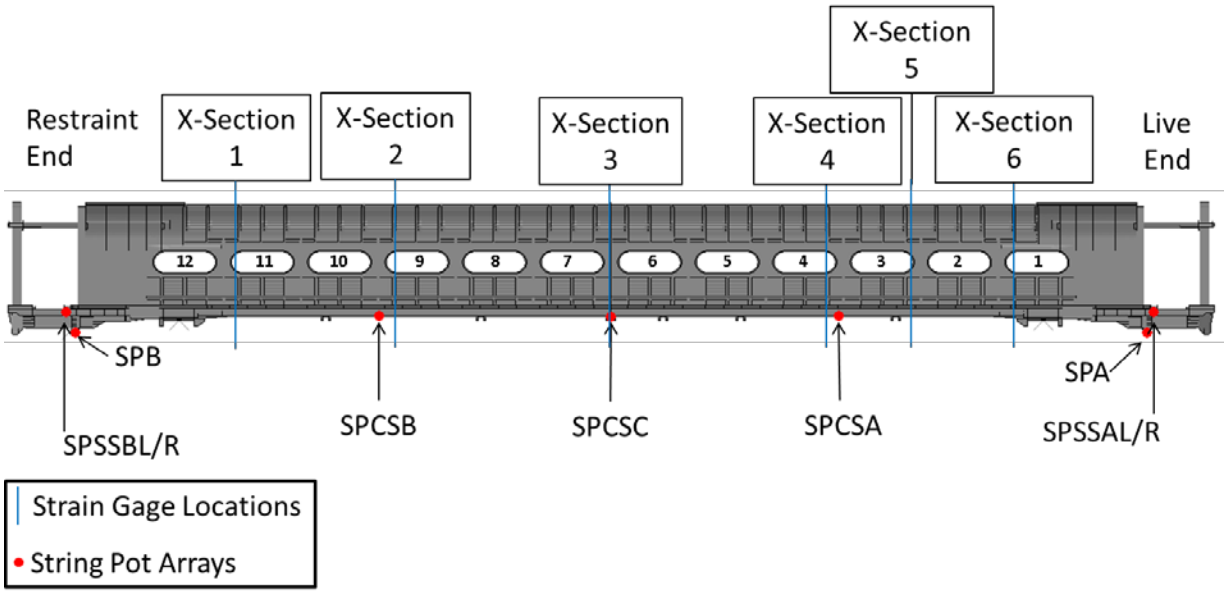

Figure 11. Strain Gage and String Pot Locations in 800-kip Verification Test

At cross-sections 1–5, strain gages were installed on the center sill, side sills, belt rails, roof rails, and purlins on both the left and right sides of the car. At cross-section 6, strain gages were installed on the side sills and belt rails. Figure 12 shows the locations on each longitudinal member where the strain gages were placed.

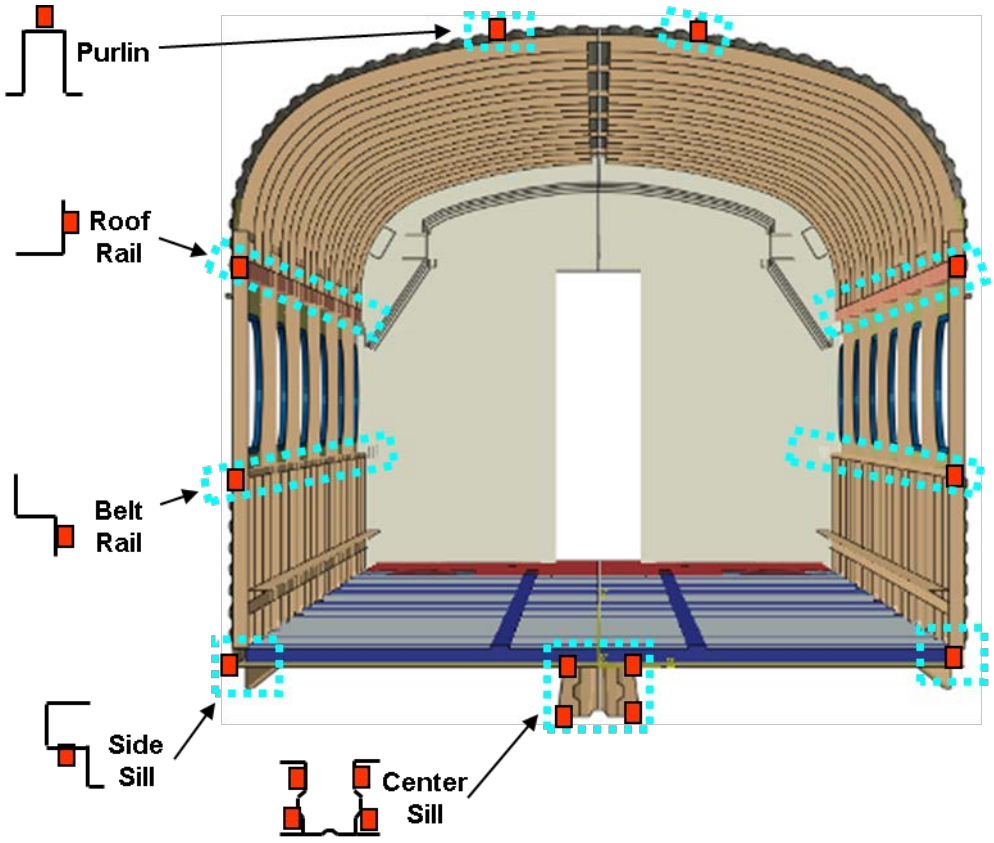

Figure 12. Strain Gage Placement on Cross-Section of Car

2.4 FE Modeling of 800-kip Verification Test

In the ETF's procedures, analysis used to demonstrate the OVI of a passenger car must first be validated with elastic test data. Accordingly, FE analysis was used to simulate the 800-kip elastic verification test. The ETF's report provides guidelines for acceptable tolerances between test measurements and analysis results for successful validation of the model.

The ETF's guidance procedures were followed in this research program. Because the 800-kip test being performed to verify the structural integrity of Car 244 met the ETF requirement of an elastic test with a load greater than 337 kips, this test was also used to validate an FE model. The FE model used in this research program was derived from models used in several previous tests. This FE model was first constructed to simulate the impact tests of unmodified Pioneer cars [12]. The FE model was then modified to include CEM components when the Pioneer cars themselves had CEM components installed [13]. Finally, the model was modified in this OVI research program to accommodate the quasi-static loading that would take place during the elastic test. The model used to simulate the CEM system only featured the occupied volume directly behind one CEM end of the car. The full-length of the car was modeled for the 800-kip test load case. The doublers that were installed on the side sills of Car 244 were also included in the model. Finally, the energy absorbing components that were removed from the test cars following the dynamic impact testing program were removed from the model used to simulate the 800-kip test.

The FE model represented the full-length of the car and half of its width. A symmetry boundary condition was applied along the vertical-longitudinal midplane of the car to account for the half-width condition. The model featured a total of 223,888 elements and 220,986 nodes. The model had a characteristic element length of 1.37 inches. The car structure was modeled almost entirely with shell elements. A small number of solid (brick) elements were used around the window frames and in the endframes to represent geometry too thick to be effectively modeled using shell elements. Other element types used in the model included rigid elements to represent the ground and spring elements to represent the suspension. Figure 13 shows the FE model as it existed during simulation of the buff strength test.

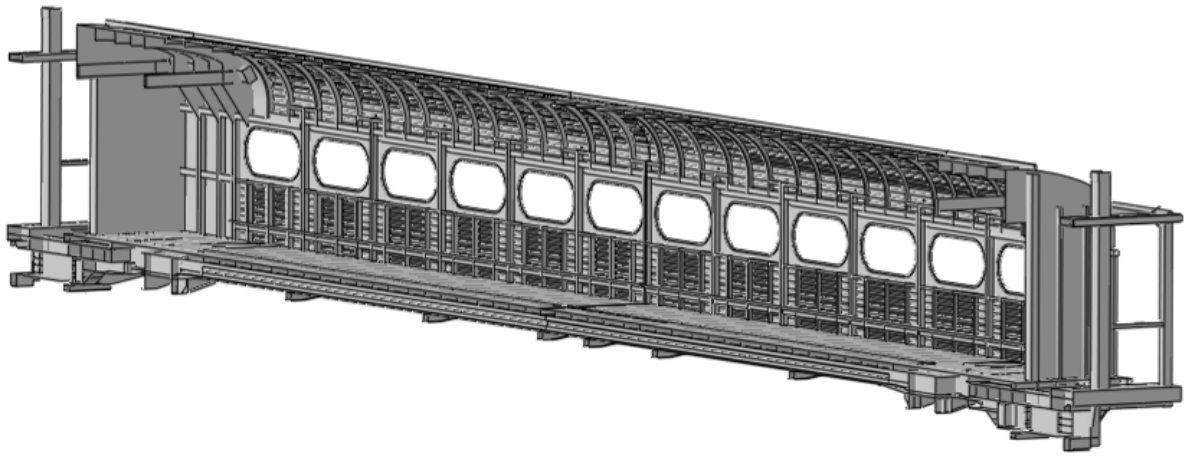

Figure 13. Half-Symmetric FE Model used for Buff Strength Analysis

Because the 800-kip test and the corresponding FE analysis were performed with the goal of validating the FE model to be used to simulate crippling, certain aspects of the buff strength

analysis were performed with this objective in mind. Although the 800-kip test is intended to be a nondestructive elastic test, the materials that were used in the model included elastic and plastic stress-strain behavior. The plastic behavior was included so that the same material models could be used for the buff strength simulation and the crippling simulation.

Because the 800-kip model was derived from models previously used to simulate dynamic impacts, elastic-plastic material models were already defined for the materials in the car [12, 13]. These existing material properties were defined in the models used to simulate the 800-kip test and the subsequent crippling test. The majority of the structural members of the car were made of steel. Steel material properties featuring different yield and ultimate strengths were included in this model. The simplest representation of elastic-plastic material properties was a bilinear characteristic. The first part of this characteristic represents the stress-strain behavior in the elastic range with a line of one slope. The second part of this characteristic represents the plastic behavior from the yield strength up to the ultimate strength of the material. The model did not employ any damage initiation, damage progression, or element removal techniques. A simple bilinear stress-strain characteristic is shown in Figure 14.

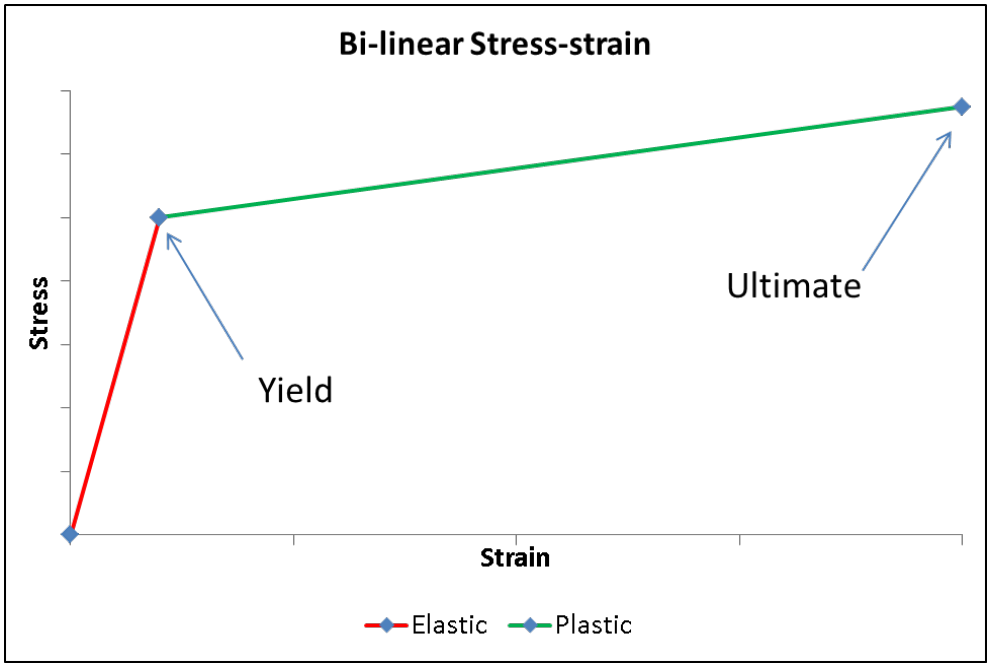

Figure 14. Example Bilinear Stress-Strain Behavior

Although the buff strength test was initially to be performed quasi-statically, an explicit FE solver (Abaqus/Explicit) [14] was used in anticipation of the follow-on crippling simulation. An explicit solver was intended to simulate the crippling behavior of the car due to the expectation of nonlinear geometric and material behaviors. Because one goal of the elastic test was validation of the FE model that would be used to estimate crippling, it was important to ensure that the elastic model used was substantially representative of the crippling model. An explicit solver was expected to simulate the crippling test to capture the plastic and crippling behaviors of the car; therefore, this solver was also chosen to execute the buff strength model.

2.4.1 Boundary Conditions

Boundary conditions were applied to the FE model of Car 244 to simulate the support conditions of the test car within its frame. A lateral symmetry condition was applied along the longitudinal-vertical midplane of the model. This boundary condition prevented any lateral motion of nodes along this plane. Because the boundary condition extends along the length of the car, it also serves to prevent gross lateral motion of the entire car.

Vertical support to the model was provided by nonlinear springs at the body bolsters where the secondary suspension attaches to the carbody. The nonlinear spring characteristic used in the model has a stiffness of $1x10^6$ pounds/inch in compression and 1/1000 pounds/inch in tension. This prevents the car from moving downward, but offers only a small resistance to upward motion. In the physical car, the body is resting on the trucks. Thus, contact of the car body and the truck prevents downward motion of the car body, but the truck does not impede upward motion of the body. The car's own weight serves to impede vertical uplift.

The spring at each body bolster is attached to the ground. The ground is represented by a rigid plate beneath each body bolster. This plate is free to move in the longitudinal direction, simulating the truck's ability to roll down the track in response to the applied buff load. The ground is prevented from moving in either the lateral or vertical direction. An inverted view of the car, the suspension spring, and the ground plate at one body bolster location is shown in Figure 15.

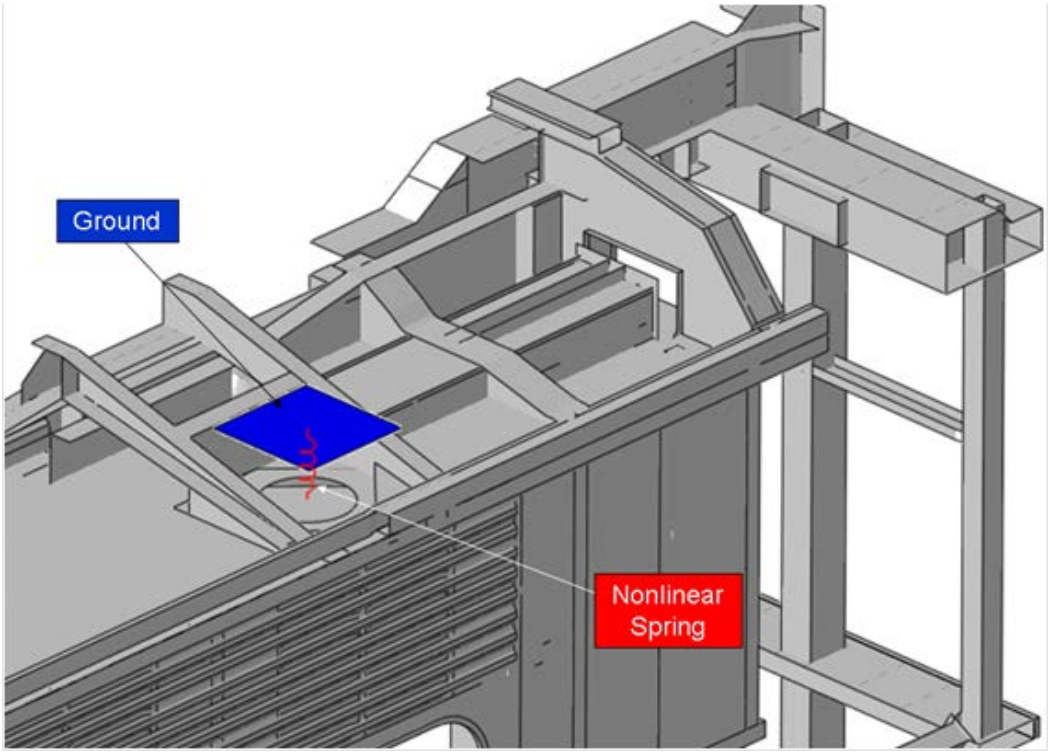

Figure 15. Vertical Spring Assembly, 800-kip FE Model

Additional vertical constraint was provided at the back end buff lugs. Upon review of the test data it was apparent that the rear end of the car was limited in its ability to move downward but free to lift upward. As an approximation of this limitation, a vertical nonlinear spring was

attached to the buff stop at the rear end of the car; this attachment offered a high resistance to downward motion of the buff stop but a very small resistance to upward motion. No such spring was used on the live end of the model.

In both the model and the test, longitudinal restraint was accomplished through the buff stops on the reaction end of the car. In the model, a zero-displacement boundary condition was applied to nodes on the rear buff stop to prevent longitudinal motion. Because the buff stops were not prevented from pivoting during the test, the nodes used in the boundary condition were permitted to rotate in response to the applied load. The FE solver calculated the restraint force necessary to maintain zero longitudinal displacement at each of the nodes in this boundary condition.

On the live end of the car, a corresponding set of nodes on the buff stop was used to apply the load to the car. The nodes were given a prescribed displacement-time behavior. The FE solver calculated the longitudinal force needed to achieve the prescribed displacement. The analysis was run until the applied load reached 800 kips. The displacement boundary condition was only applied to the longitudinal degree-of-freedom on these nodes. The nodes were free to pivot as the structure responded to the applied load. The loading location on the live end buff stop of the FE model is shown in Figure 16.

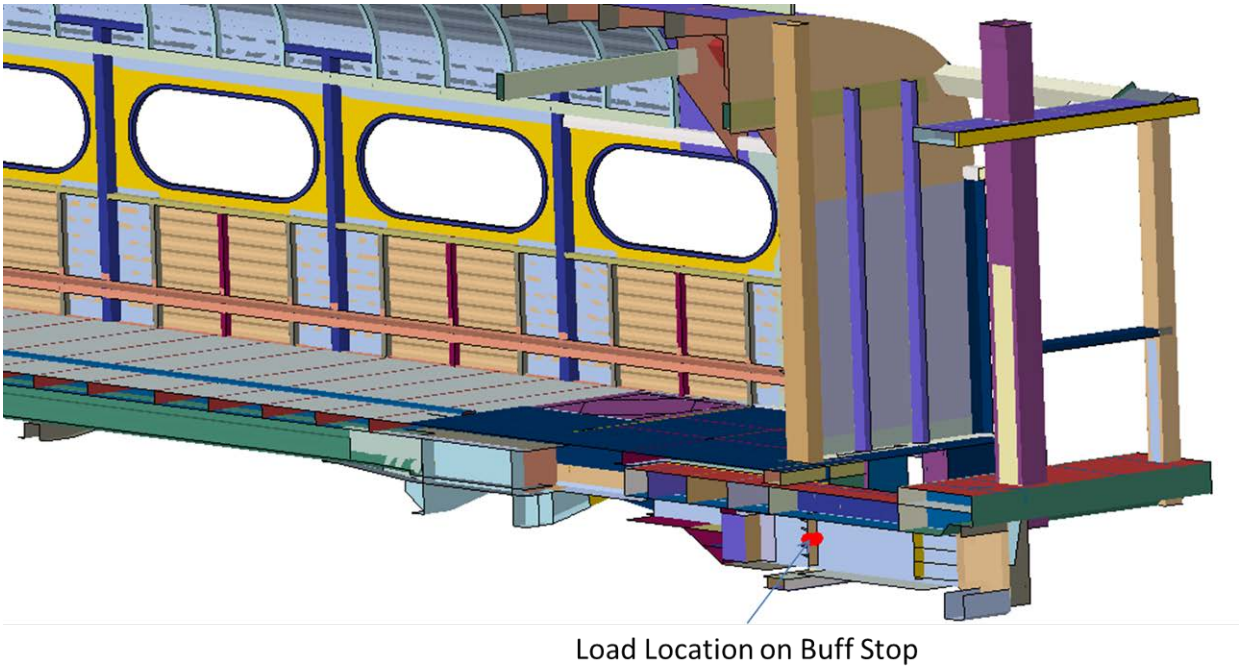

Figure 16. Loading Location on Live End Buff Stop, 800-kip FE Model

2.5 Elastic Test Results and FE Model Validation

The elastic verification test of Car 244 was used both to verify the car's structural integrity and to validate the FE model that would be used to estimate the crippling behavior of the car. The ETF procedures report provides target tolerances for validating a model with test data; those tolerances were used in comparing the results of the test with the results of the FE model.

The key results that were compared between the test and the FE model are the longitudinal load versus displacement behavior, the vertical deformation shape, and the strains in key longitudinal members. There is very good agreement between the measured and modeled longitudinal load versus displacement behavior. The model results also indicate good agreement with the vertical mode of deformation of the tested car. The strain results for the center sill, side sills, and purlins have good agreement between test and analysis. The strain results from the roof rail and belt rail do not agree with the model as well as the results in the other longitudinal members. These two members are fairly lightly loaded members with thin cross-sections. In general, the FE results effectively captured the behavior of the tested car. The model has been determined to be suitable for use in simulating the crippling tests.

2.5.1 Verification of Quasi-Static Behavior in FEA

Because the line-of-draft testing and modeling effort was meant to validate the FE model that would be used to simulate crippling, the same explicit solver was used to execute both models. It was important to verify that the line-of-draft model was sufficiently free of dynamic effects to be considered quasi-static before comparing test results with analysis calculations. The ETF report provides two procedures for determining if a model may be considered quasi-static. Although only one method needs to be used as a part of the ETF's procedures, both methods were used in this research program. The following two conditions are taken directly from the ETF's report:

ETF Condition One

> For a given simulated load rate, the load at the live end of the model should be the same as the load at the fixed end. Load at the reaction end may vary by up to +/-5 percent of the load at the live end of the model for the analysis to be considered quasi-static.

ETF Condition Two

> The ratio of kinetic energy-to-strain energy within the structure should be small (< 5 percent). The ratio of kinetic energy-to-strain energy may exceed 5 percent during the first 10 percent of the total simulation time without invalidating the analysis as quasi-static.

Evaluation of Condition One

Loading in the 800-kip model was accomplished by applying a prescribed displacement-time boundary condition to a row of nodes on the live end buff stops. The FE solver calculated the force that was applied to each node to achieve the desired displacement. Similarly to the loading on the live end, a row of nodes on the rear end buff stops was prevented from moving longitudinally. The solver calculated the force that was applied to each node to prevent it from

moving. The total live end load and total restraint load are plotted alongside a +/-5 percent envelope in Figure 17.

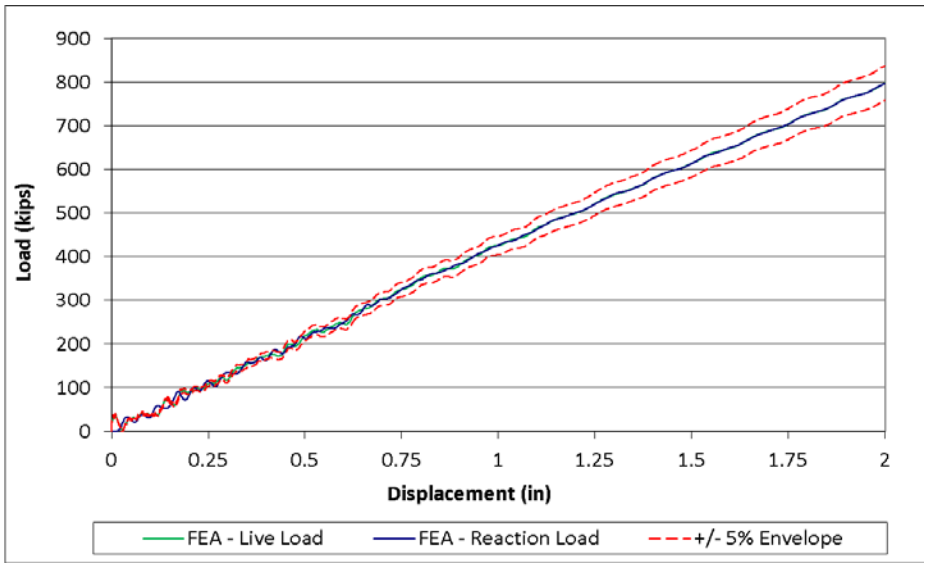

Figure 17. Live Load and Reaction Load with +/-5 % Envelope, 800-kip Elastic FEA

This figure shows that at loads above approximately 200 kips the live load and reaction load are very close and well within the 5 percent envelope on the live end force. Because the envelope gets larger as the applied load is increased, at low loads the reaction end load may be outside the envelope. Both the live and reaction end loads are noisier at the beginning of the analysis but stabilize as the load magnitude increases. One possible alternative to applying a 5 percent envelope to the live load that varies in magnitude over the course of the simulation is to apply a constant-width envelope of 5 percent of the target load. In the case of the 800,000-pound load, this means a constant width envelope of +/-40 kips. The live and reaction loads are plotted against this envelope in Figure 18. The simulation is deemed to be quasi-static using ETF Condition One.

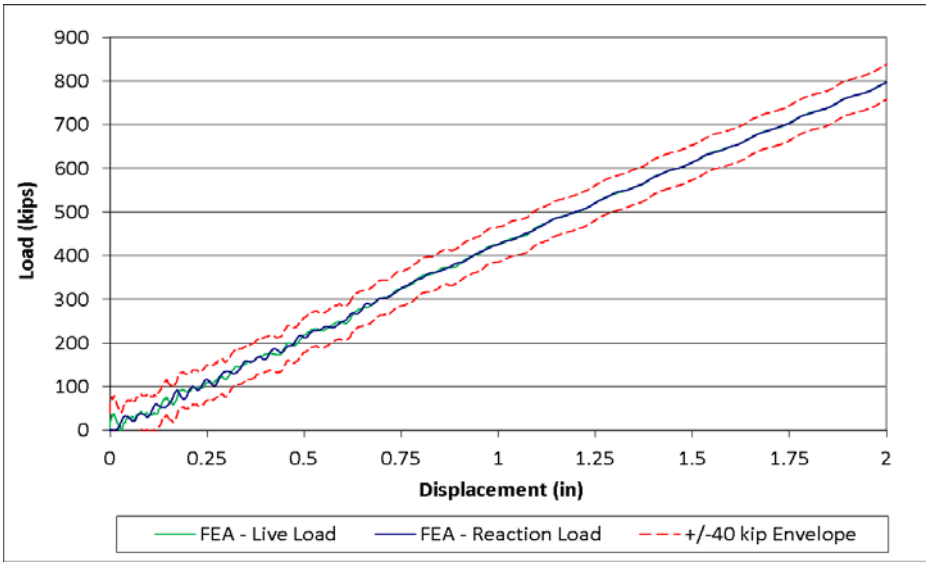

Figure 18. Live Load and Reaction Load with +/-40 kip Envelope, 800-kip Elastic FEA

Evaluation of Condition Two

Because the load applied to the car was dynamic, the FE solver calculated the total kinetic energy in the model. The solver also calculated the total internal energy, which is the total strain energy in the model. The ratio of kinetic energy to internal energy in the model of the 800-kip buff simulation is plotted in Figure 19 against the normalized time of the analysis. The energy is plotted on a logarithmic scale because it decreases by multiple orders of magnitude as loading progresses.

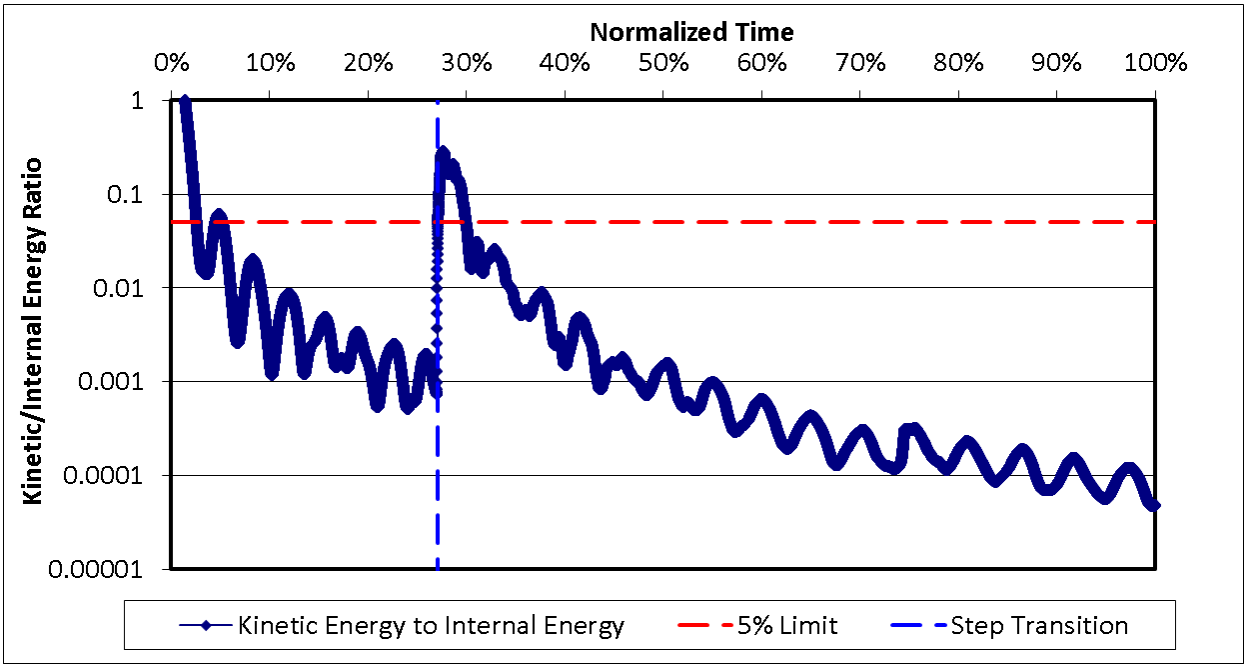

Figure 19. Ratio of Kinetic to Internal Energies, 800-kip Elastic Model

The car was loaded in two steps. In the first step, gravity was applied and the car responded by settling. In the second step, the longitudinal load was applied. In both steps, the energy ratio quickly drops below the 5 percent limit. This behavior indicates that the model quickly stabilizes and the dynamic effects are minimal, especially at the critical load of 800 kips. The simulation is deemed to be quasi-static using ETF Condition Two.

2.5.2 Load-Displacement Results

The applied load is plotted against the change in the car's length in Figure 20 for both the 800-kip test and the corresponding FE analysis. A +/-10 percent envelope on the test load magnitude is also plotted in this figure. This figure shows good agreement between the overall longitudinal load-displacement behavior measured during the test and calculated during the analysis.

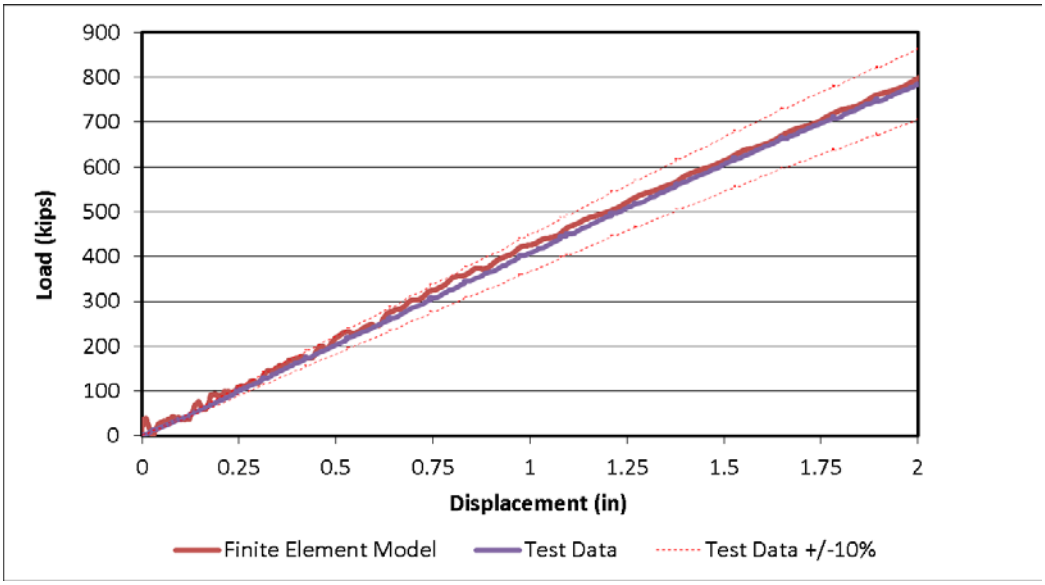

Figure 20. Load-Displacement Data for 800-kip Test and FE Analysis, Car 244

2.5.3 Vertical Displacement Results

Vertical displacement of the underframe of the car was measured during the test by a series of string pots. The locations and channel names of the string potentiometers used in this test are shown in Figure 10. The vertical displacement along the length of the car is plotted in Figure 21 at a series of load increments. In these two plots, the horizontal axis has its datum at the end of the side sill at the live end of the car. The distance between each instrumented location and the live end datum is given as the initial distance between these points and is not updated to reflect any longitudinal travel by the instrumented point of the car. The data points correspond to the instrumented locations, and the lines have been interpolated between adjacent locations. The left side plot shows the data measured during the 800-kip test, and the right side plot shows the calculated vertical displacement at the corresponding locations in the FE model. Each plot marks the location of the live and restraint end body bolsters where the car is supported in both the test and the model.

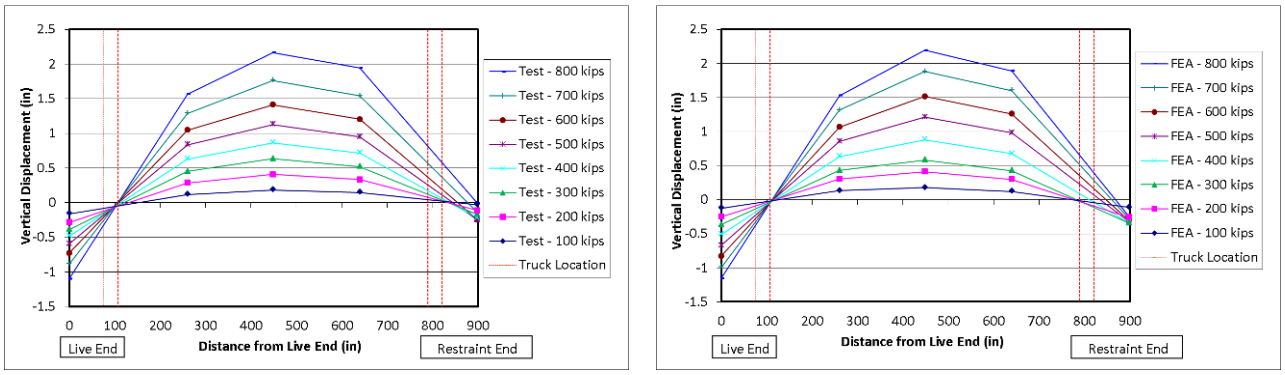

Figure 21. Vertical Displacements along Length of Car, 800-kip Test (L) and FEA (R)

Figure 21 indicates a strong similarity between the global vertical behaviors of the car in both the test and the analysis at a given load. At the live end, the car moves downward in both test and analysis. At the live end truck, the displacement crosses from downward to upward in both sets of results. This indicates the live end truck is acting like a pivot for the car body. At the rear end, the truck does not act as a pivot. Figure 21 demonstrates that the FE model is capturing the global bending behavior of the car under line-of-draft loading conditions.

The vertical displacement measurement from each string pot in the 800-kip test was compared with the calculated vertical deflection at the corresponding location in the FE analysis and, for most locations, good agreement was observed between the two results. The full set of comparison plots is provided in Appendix D. The vertical displacement measurements at the three locations on the center sill between the trucks of the car are plotted against the FE results in Figure 22, Figure 23, and Figure 24. At all three locations, the FE results are within +/-10 percent of the test data when the load is greater than approximately 200 kips. Similar to the +/-10 percent envelope applied to the longitudinal force-displacement results, the envelope applied to the vertical displacement data increases in width as the displacement value increases. The FE results are outside the +/-10 percent envelope at low loads because of the small displacement magnitude measured and the correspondingly small envelope.

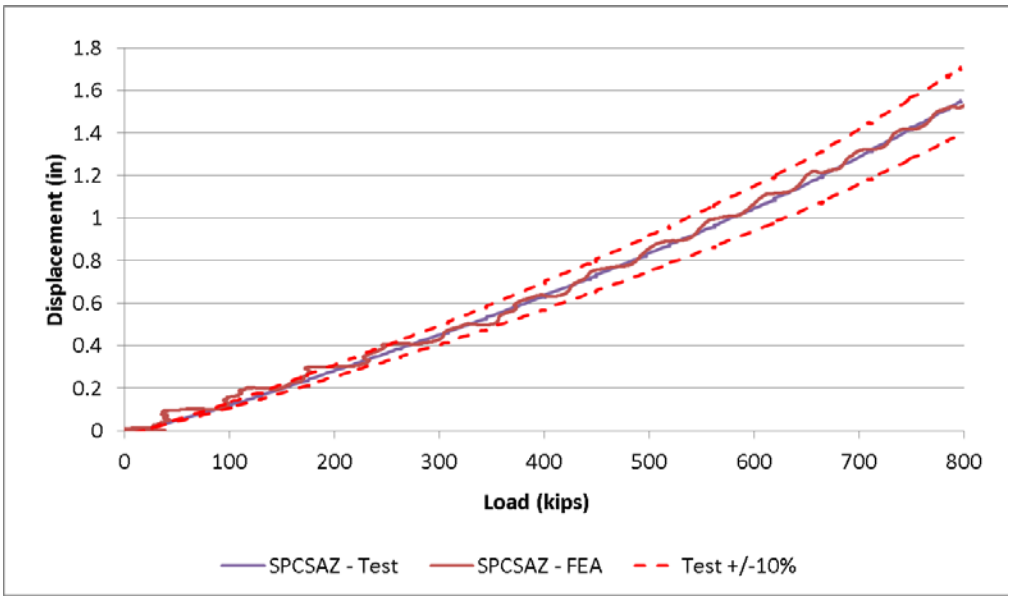

Figure 22. Vertical Deflection of Center Sill at A-end of Car, 800-kip Test

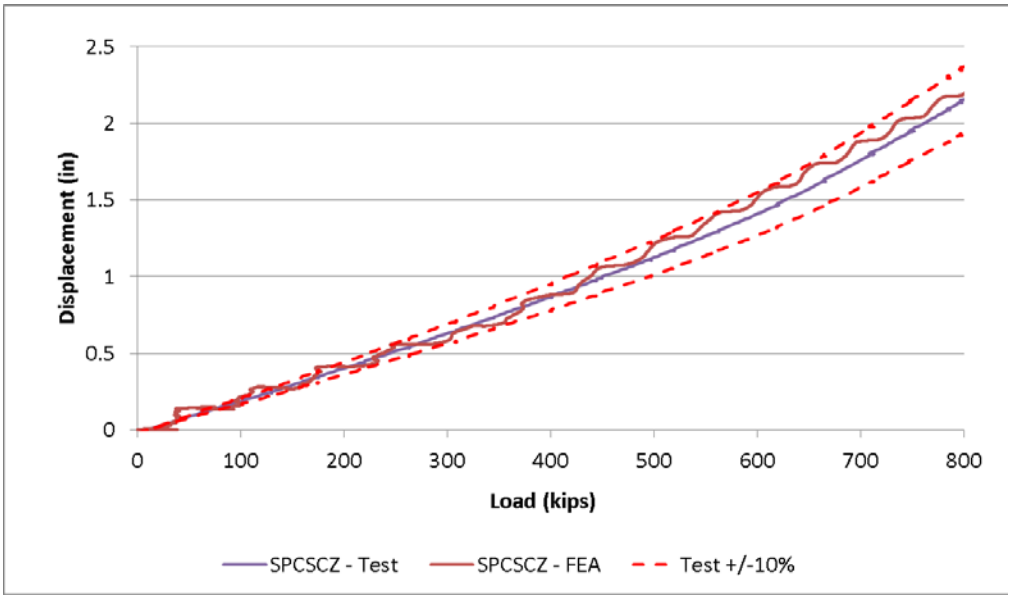

Figure 23. Vertical Deflection of Center Sill at Center of Car, 800-kip Test

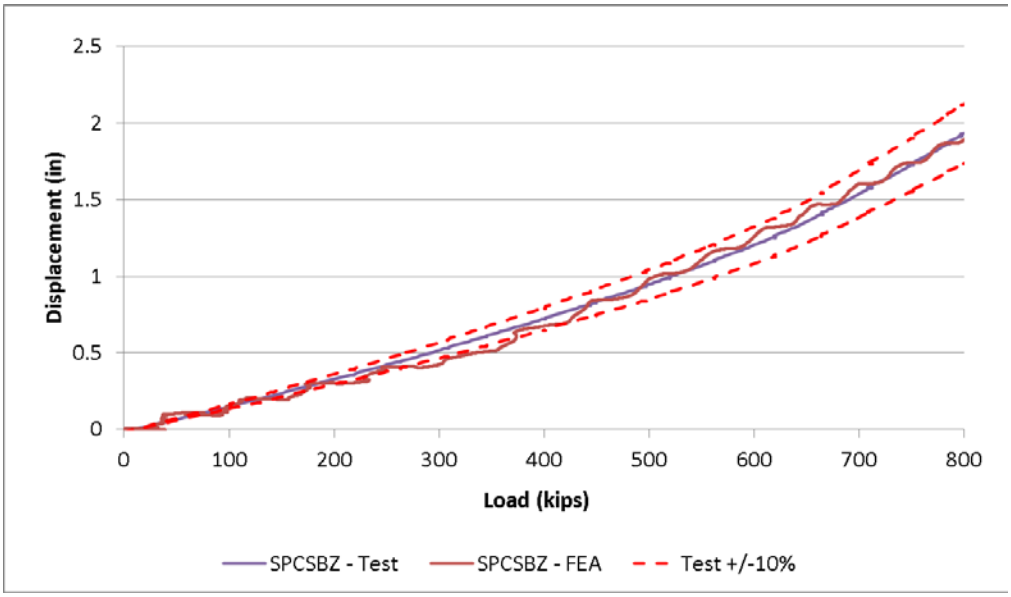

Figure 24. Vertical Deflection of Center Sill at B-end of Car, 800-kip Test

2.5.4 Longitudinal Strain Results

A total of 64 longitudinal strain gages were installed on Car 244 for the 800-kip test. These gages were installed on nine longitudinal members (Figure 12) at six cross-sections along the length of the car (Figure 11). The complete set of strain gage results is provided in Appendix C. The ETF report provides a target tolerance of +/-20 percent for validating an FE model using strain data. That value is used for comparing the strain data with the calculated strains in the FE model.

The strain results discussed in this section are organized by structural member. For each member, the strain measurement at each location on that member is plotted against the longitudinal location of the corresponding strain gage. For strain data, the longitudinal datum in the elastic test of Car 244 is the center of the restraint end body bolster. Because of the orientation of the car within the test frame, the following strain-versus-distance graphs have the restraint end of the car at the left (i.e., small distances) and the live end of the car at the right (i.e., at the large distances). The strain measurements plotted in this section have all been recorded at an applied load of 800 kips. In each plot, the longitudinal strain along the length of a given member has also been calculated in the FE model and plotted alongside the measured data. The test data appear as a series of discrete points and the FE model data as a continuous line.

Figure 25 is a plot of the longitudinal strain in the center sill under a load of 800 kips. At each cross-section, the center sill was instrumented with 4 strain gages: top left, top right, bottom left, and bottom right. Each plot in the figure contains three data series: test data from the left side of the member, test data from the right side, and the calculated strain along the length of the member in the FE analysis. The error bars plotted for each point of test data represent the ETF's adopted tolerance of +/-20 percent.

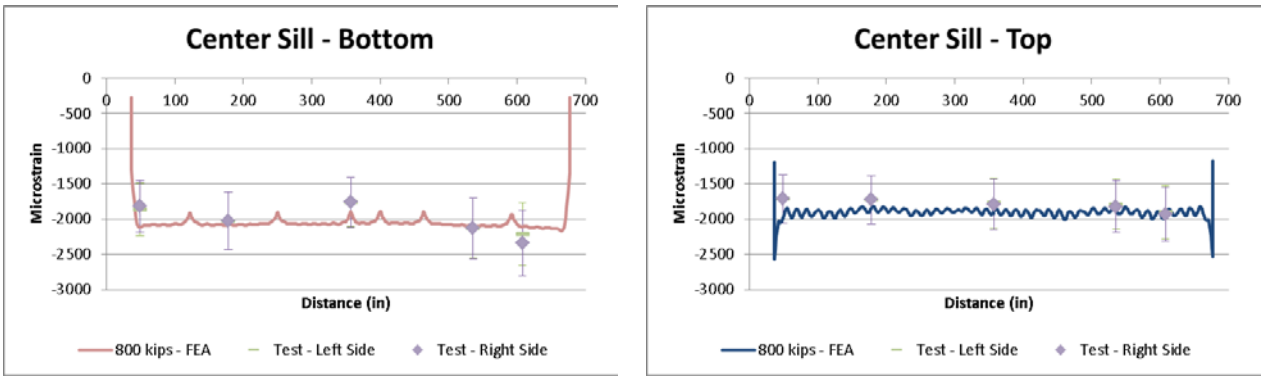

Figure 25. Strain in Bottom (Left) and Top (Right) of Center Sill at 800 kips, 800-kip Test and FEA

The longitudinal strains obtained from the FE analysis agree well with the strains measured in the test. At all locations on the center sill, the FE results are within the 20 percent envelope on the test data. Additionally, both the test measurements and the FEA results indicate a fairly stable state of strain in the center sill under a load of 800 kips. The FE results indicate a steep strain gradient at the ends of the center sill. The center sill ends at the body bolster at each end of the car. Although the strain results are within the tolerance at these locations, the presence of such a steep gradient underscores the need for careful strain gage placement in a test article. In

areas of high gradient, moving the strain gage by only a few inches could result in a large difference in measured value.

Figure 26 is a plot of the longitudinal strain in the side sills under a load of 800 kips. The solid line represents the FE results along the length of the side sill, and the points represent the measurements recorded at the strain gages at each location during the test. Although the FE result exhibits more peaks and valleys than the calculation for the center sill, the strain level is roughly constant in the side sill under a load of 800 kips. This "noise" is likely seen in the model due to the presence of many vertical wall supports and floor members that are attached to the side sill. The test data indicate good agreement with the model predictions. As was observed in the center sill strain results, the side sill test data show similar levels of strain in the left and right sides of the car, indicating that both side sills are carrying roughly equal loads. The decrease in strain that occurs at distances between 400 and 450 inches, as seen in the model results, corresponds to the location where a doubler plate had been added to the side sill to act as a patch over two small cracks that were discovered during inspection of the car prior to the test.

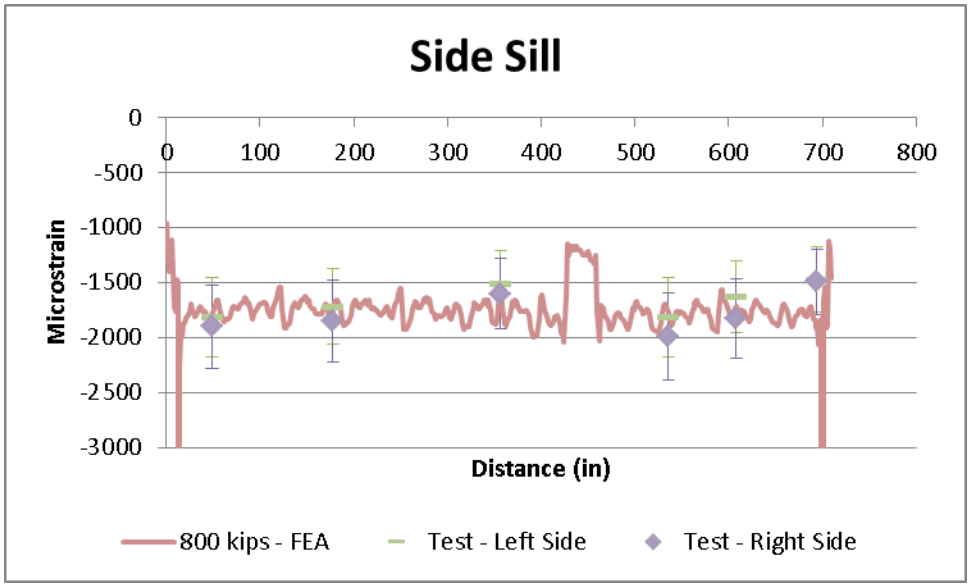

Figure 26. Strain in Side Sills at 800 kips, 800-kip Test and FEA

Figure 27 is a plot of the longitudinal strain in the purlin under a load of 800 kips. The FEA and test both exhibit the same arched shape. Because the 800-kip compressive load is applied along the line of draft, the car experiences both compression and bending. The underframe of the car is placed in compression, while the bending stresses that develop in the roof result in tensile stresses. However, the FEA results indicate a higher tensile strain than the strains measured in the test, which suggests that the tested car develops lower bending stresses in the roof than were developed in the model. Overall, however, the model is capturing the behavior of the tested car. The test results show very good agreement between the measurements on the left purlin and the right purlin of the car, indicating that the load is being shared equally between the left and right sides of the car. The left and right side measurements are nearly the same at each location, leading the two data points to overlay one another.

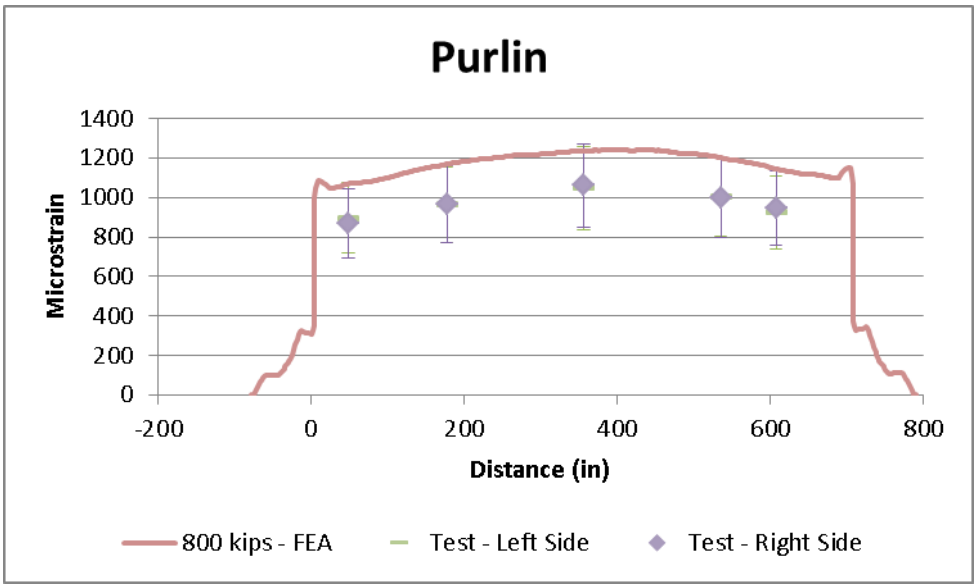

Figure 27. Strain in Purlin at 800 kips, 800-kip Test and FEA

Figure 28 is a plot of the longitudinal strain in the belt rail under a load of 800 kips. In this particular car, the belt rail is a relatively thin z-shaped member located just below the window line (see Figure 12). The belt rail carries relatively little load compared to the members making up the underframe. The FE results indicate a relatively constant level of strain along the length of the member, with intermittent peaks corresponding to locations where wall supports are attached to the belt rail. The test results indicate more variation in the strains measured in the belt rails than the model. The test results also indicate differing levels of strain in the test car's left and right side belt rails.

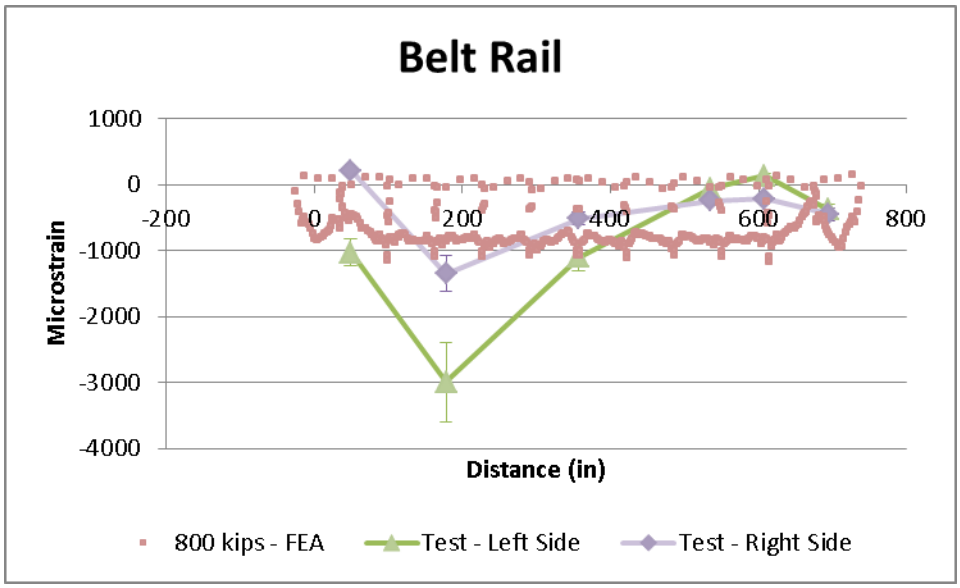

Figure 28. Strain Results in Belt Rail at 800 kips, 800-kip Test and FEA

Figure 29 is a plot of the strains along the length of the roof rail from the test and from the analysis under a longitudinal load of 800 kips. The roof rail is a fairly thin L-shaped member

located above the window line in this car's design (see Figure 12). In both the test and the analysis, the roof rail indicates a low state of stress (for steel, +/-100 microstrain is approximately equal to +/-3 ksi). In the FE model, the roof rail is under a fairly constant low level of tensile strain. The intermittent peaks correspond to the locations of roof stiffeners. In the test data, the strain state ranges from slightly compressive to slightly tensile. The left and right sides of the test car exhibit slight differences in strain level at each location.

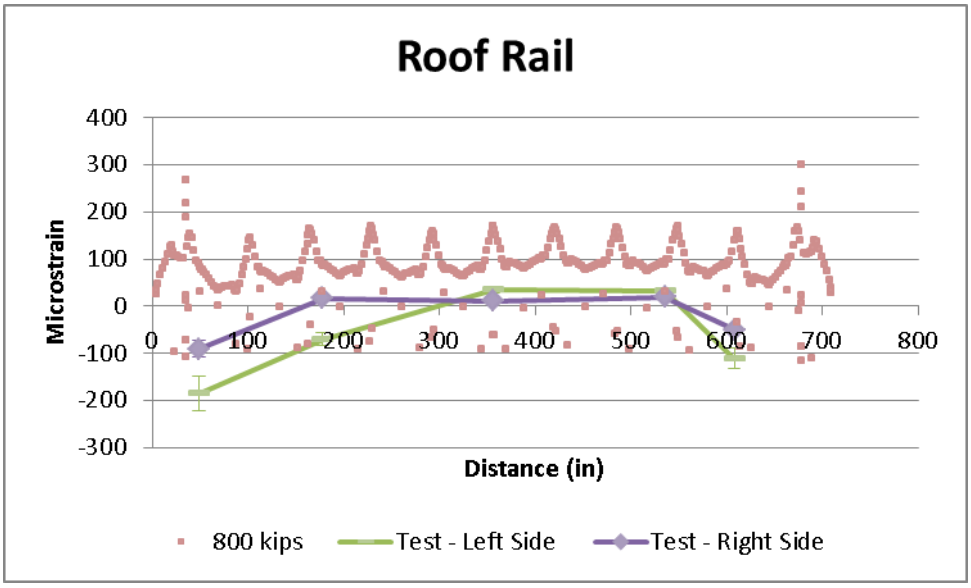

Figure 29. Strain Results in Roof Rail at 800 kips, 800-kip test and FEA

A total of 64 longitudinal strain gages were installed on the major structural members of Car 244 during the 800-kip buff strength test. Of these, eight strain gages reported strains that corresponded to stresses less than 2200 psi. This measurement is less than 4 percent of the yield strength for the materials to which they are attached. These eight gages were all located on the belt or roof rails. Because of the low stress reported by these gages, they are omitted from the statistical assessment performed in this section.

For the remaining 56 strain gages used in the test, the stress measured in the test was compared with the stress at the corresponding location in the FE model. The difference between the two values was normalized by the measured stress. The resulting percentage differences between the test data and the FE results for the strain data are plotted in Figure 30.

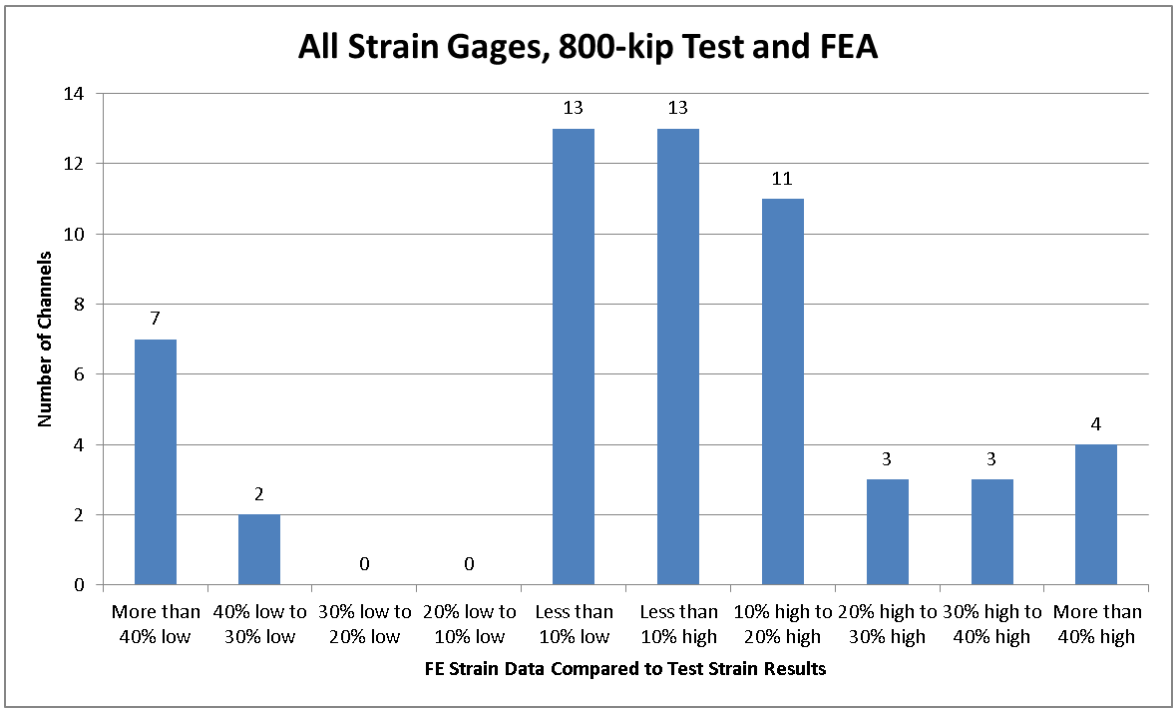

Figure 30. FE Strain Data Compared with Test Strain Results, All Gages in 800-kip Test

The ETF has established a threshold of +/-20 percent for comparing strain gage data with strain results in an FE model. As seen in the figure above, 37 out of 56 gages fall within the threshold. The majority of the gages that fall outside of this range were installed on the roof rail and the belt rail, which indicated poor agreement with the FE model in this test and low stress/strain.

If the strain gages considered in the comparison between test and model are limited to the longitudinal members with the largest load-carrying capacity (i.e., the center sill, side sills, and purlin), a total of 42 gaged locations remain. The histogram in Figure 31 shows the distribution of strain levels at these 42 locations in the test and in the analysis. The same 37 gages included in the previous figure fall within the +/-20 percent threshold. Only five gages fall outside the +/-20 percent threshold when the comparison is limited to the center sill, side sills, and purlins.

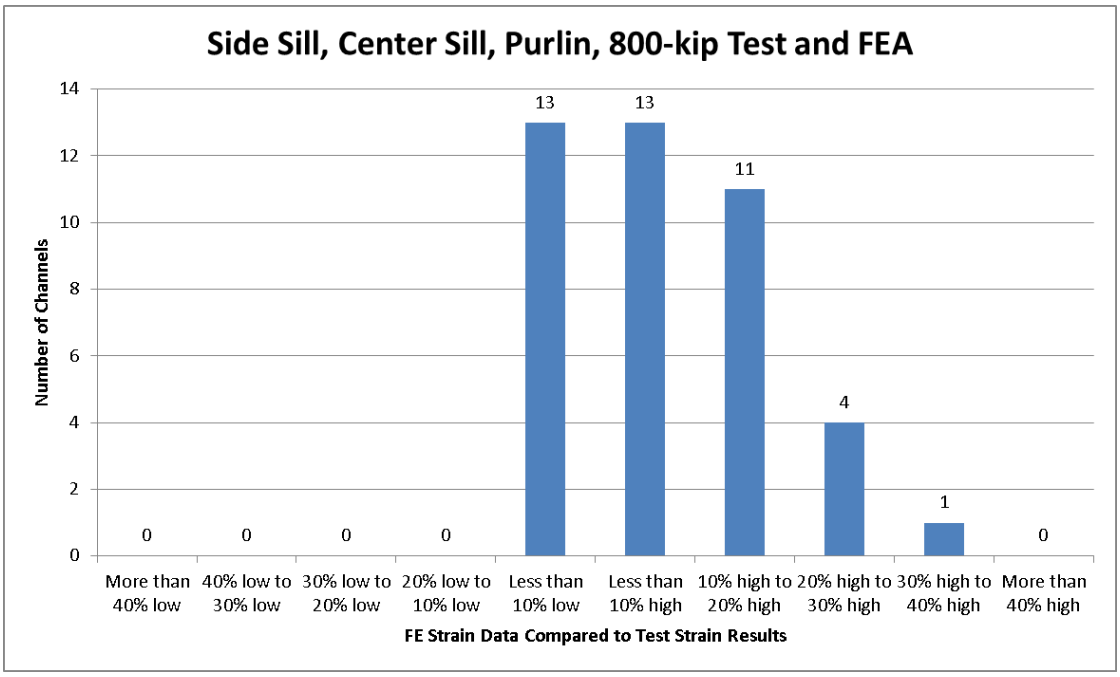

Figure 31. FE Strain Data Compared with Test Strain Results, Limited Gages in 800-kip Test

Details on the five gages that are outside the +/-20 percent range are shown below, in Table 4. Three of the five gages that are outside the +/-20 percent range reported strains that are less than 22 percent different from the model's estimates at the corresponding locations. Although the differences are outside the +/-20 percent envelope, the exceedance is very small. These values may be within the uncertainty introduced into the measurement either through the precision of the instrumentation or the precision of the model. The remaining two gages provided measurements that are different from the model's calculations by 30 percent or more. These gages are located on the left and right side sills at cross-section 6, the cross-section nearest to the live end of the car. These data points can be seen at the far right of Figure 26. As shown in this figure, the model reports a very high strain gradient in this region, owing to a change in cross-section of the side sill.

Table 4. Strain Gages Outside of +/-20 % Threshold, 800-kip Test

Channel Name	Location	Delta Strain (FEA-Test)/(Test)	Comments
S1PR	Cross-Section 1, Right Purlin	20.1 %	Slightly outside +/-20 %
S2PL	Cross-Section 2, Left Purlin	20.2 %	Slightly outside +/-20 %
S5PL	Cross-Section 5, Left Purlin	21.7 %	Slightly outside +/-20 %
S6SSL	Cross-Section 6, Left Side Sill	31.5 %	High strain gradient area (see Figure 26)
S6SSR	Cross-Section 6, Right Side Sill	30.0 %	High strain gradient area (see Figure 26)

The stress/strain measurements made during the 800-kip test were compared with the stress/strain calculations made during the simulation of the 800-kip test. With the exception of the roof rail and belt rail, which experienced fairly low levels of stress in the test, the remaining locations on the center sill, side sills, and purlins exhibited good agreement between test and analysis. The FE model appears capable of capturing both the global deformation behaviors of the tested car and the stress states of the major longitudinal load-carrying members.

3. Crippling Test Setup

Two crippling tests were performed in this research program. A limited-instrumentation "shakedown" test of Pioneer 248 was conducted at TTC on June 15, 2011. The purpose of this test was to evaluate the operation of a newly installed hydraulic loading system, determine that the test frame was capable of loading and restraining a car simultaneously at the floor and roof levels, assess the procedures that had been developed for performing a crippling test, and examine the response of a passenger car under crippling conditions. Because Car 248 had structural damage likely caused by a previous dynamic testing program, this car was chosen for the limited-instrumentation test. The test frame was instrumented to measure the applied load and the stroke length of the hydraulic actuators introducing that load.

A fully instrumented crippling test was conducted on June 21, 2011, at TTC. This second test used Pioneer 244 as the test article. This car was fully instrumented with string potentiometers and strain gages, and the test frame was instrumented with load cells and displacement transducers.

3.1 Crippling Test Description

In both crippling tests, the desired load scheme was to introduce compression loads into the car at the ends of the collision load path. Because each Pioneer car was equipped with a CEM system, the points where the CEM elements attached to the occupied volume were chosen as the load and restraint locations. For this particular CEM system design, these elements included two floor-level energy absorbers and two roof-level energy absorbers at each end of the car. Pioneer 248, with its CEM system indicated, is shown in Figure 4.

Each car was installed into a test frame and remained on its trucks during the test. The test frame was designed to enable simultaneous loading of a structure at two different heights. In the case of the Pioneer cars, these heights correspond to the roof and floor of the car. Car 248 is shown within the test frame in Figure 32.

Figure 32. Car 248 in Test Frame, Crippling Test

The energy absorbing components and endframes at each end of each car were removed to allow for loads to be applied directly to the energy absorber support structures at the ends of the occupied volume. The support structures are the locations where collision loads would be introduced into the occupied volume and are therefore the end points along the collision load path. The roof and floor loading locations are shown on one end of the car in Figure 5.

In both crippling tests, the car was loaded simultaneously at the floor energy absorber supports and the roof energy absorber supports. Four independent hydraulic actuators were used to apply load at the four locations. A displacement control scheme was used so that the four hydraulic actuators maintained equal displacements during the loading of the car. The amount of force exerted by each actuator was dependent on the stiffness of the car's structure and was allowed to vary from actuator to actuator.

Because of the need to simultaneously load the car at the floor and roof levels, the load frame used in the crippling tests is significantly different from the load frame used in the 800-kip buff strength test. The crippling load frame consisted of four longitudinal beams, two at the floor-level and two at the roof-level of the car, as seen in Figure 32. At the floor-level and the roof-level, a lateral restraint block was installed between the two longitudinal beams. This lateral block provided a support for the hydraulic actuators on the live end of the car and a bearing surface for the load cells at the restraint end of the car. The roof-level arrangement at the restraint end of the car is shown in Figure 33. A similar setup is used at the floor level of the restraint end, with 1,000 kip capacity load cells used in place of the 500 kip capacity load cells used at the roof.

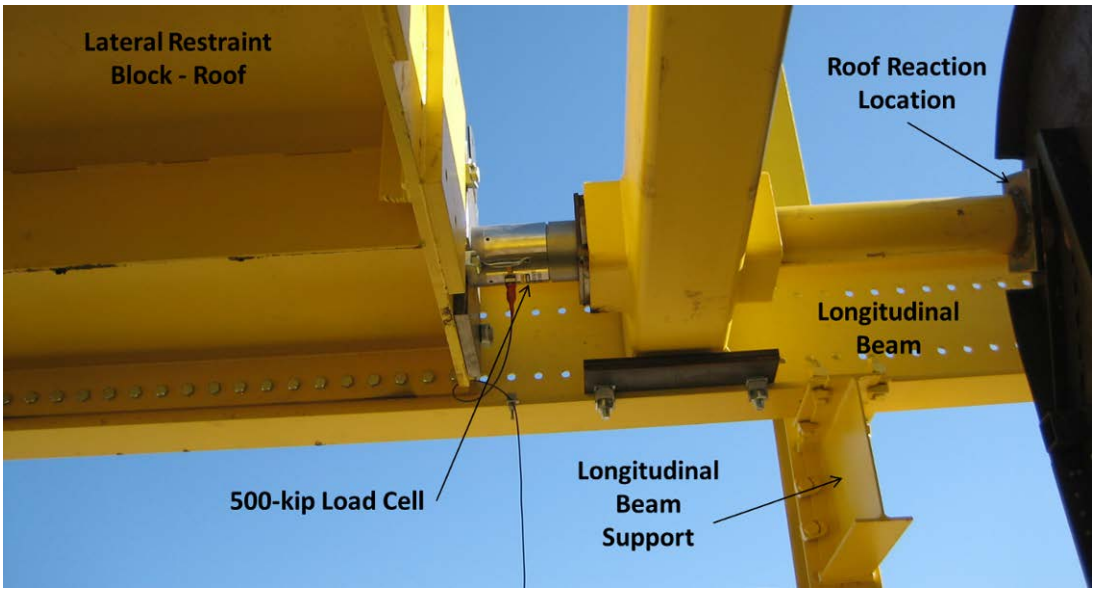

Figure 33. Restraint End Roof Setup in Crippling Tests

3.2 Description of Test Articles

3.2.1 Pioneer Car 248

Pioneer Car 248 has a testing history similar to that of Car 244. Car 248 was previously used in a series of impact tests, was retrofitted with a CEM system, and was then used in a second series of impact tests. However, Car 248 experienced more structural damage to its occupant volume during this series of impact tests than Car 244 did. Because of its existing damage, Car 248 was considered structurally compromised for use in a fully instrumented crippling test, as the damaged area could affect the crippling behavior of the car. However, Car 248 was used in the "shakedown" test to verify the performance of testing frame and hydraulic control system.

Both Car 244 and Car 248 were inspected prior to the beginning of this test program. Damage was found in several longitudinal members in Car 248. Damage to the two floor longerons was readily apparent during a walkthrough of the car and is noted on the left side of Figure 34. These two channels run the length of the occupant volume and both have an observable dent caused by high longitudinal loading in the previous impact tests. The floor damage is located in the vicinity of the sixth window from the live end of Car 248.

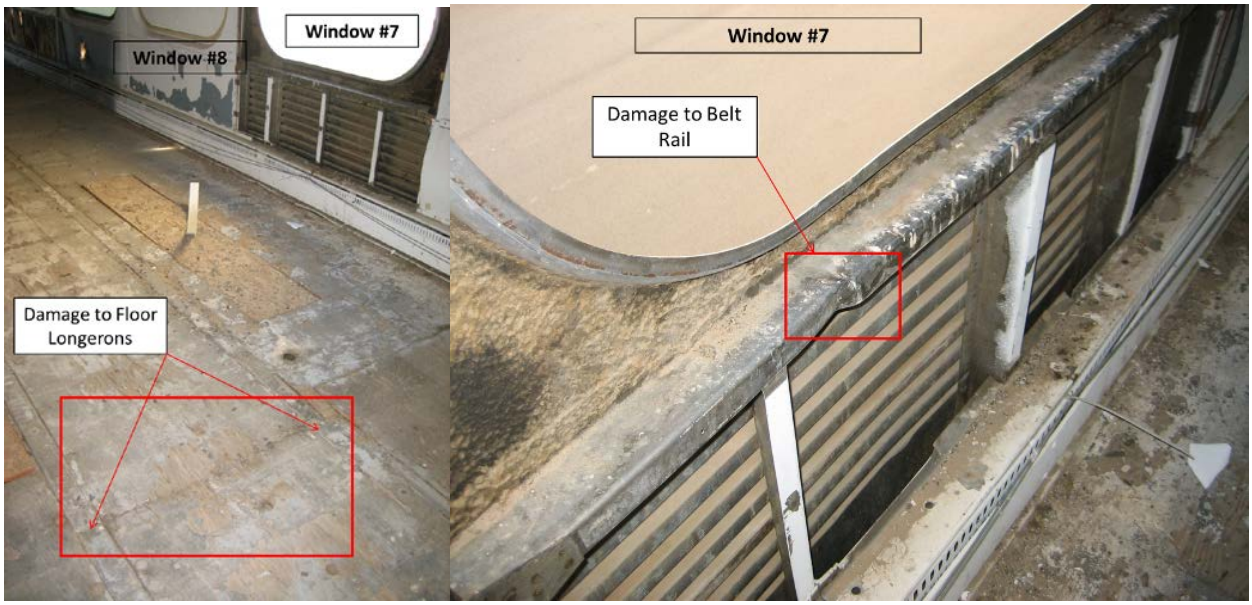

Figure 34. Pretest Damage to Occupied Volume in Car 248

In the same area as the deformed longerons, the belt rail on the left side of the car had an observable wrinkle in it adjacent to the seventh window from the live end of the car. This damage was also likely caused by high longitudinal loading during the previous impact testing program. This damage is shown on the right side of Figure 34.

Because the testing methodology called for applying loads directly to the energy absorber support locations on the ends of the occupant volume, some of the CEM components of the car needed to be removed to provide access to these locations. At each end of the car, the endframe components were removed from the car. The primary energy absorbers were removed from the floor level of each end of the car, and the energy absorber supports had any remaining weld material ground down to provide a flat bearing surface for the load to be introduced into the car.

Figure 4 shows the car with its energy absorbers and endframes intact, and Figure 5 shows Car 248 in its crippling test configuration.

3.2.2 Pioneer Car 244

Following the successful 800-kip elastic verification test of Car 244, the car was deemed structurally sufficient for use in the crippling test. The endframes of the car and the primary energy absorbing components were removed from the ends of the car to provide access to the loading locations at the ends of the occupant volume. A more detailed discussion of Pioneer Car 244's history is provided in Section 2.1.

3.3 Instrumentation

The shakedown test of Car 248 was intended to verify the capabilities of the newly installed load frame and hydraulic control system in supporting the car. It was also performed to verify the ability of the testing setup to successfully load a car to crippling and assess the test procedures to be followed. Because this was a preliminary test, only a limited number of instrumentation channels were used. The primary data recorded in this test were the applied load and stroke length of each live end hydraulic actuator and the restraint load at each restraint location. Laterally mounted string potentiometers were installed to monitor any lateral shift that may have occurred in the carbody during the test. The instrumentation used in this test is summarized in Table 5.

Table 5. Instrumentation Summary for Shakedown Test of Car 248

Type of Instrumentation	Number of Channels
500 kip Load Cell	4
1000 kip Load Cell	4
Displacement Transducer (within hydraulic actuator)	4
Pressure Transducer (within hydraulic actuator)	4
Lateral String Potentiometers	2
Total	**18**

In the crippling test of Car 244, instrumentation was used to measure the load-displacement behavior of the live end of the car, strains in key longitudinal structural members, and the vertical, lateral, and longitudinal displacements of several points on the underframe of the car. String potentiometers were installed at the rear end of the car to measure the stretching of the frame in response to the applied loads. A summary of the instrumentation used in the crippling test of Car 244 is provided in Table 6.

Table 6. Instrumentation Summary for Fully Instrumented Crippling Test of Car 244

Type of Instrumentation	Number of Channels
500 kip Load Cell	4
1000 kip Load Cell	4
Displacement Transducers (within hydraulic actuators)	4
Pressure Transducer (within hydraulic actuators)	4
String Potentiometers	41
Uniaxial Strain Gages	76
Temperature Sensor	1
Total	**134**

A total of eight load cells were used in each crippling test. One load cell was placed in-line with each load application or restraint location so that the total load on both ends of the occupied volume could be measured. The names and locations for the eight load cells are listed in Table 7.

Table 7. Load Cell Names and Locations, Crippling Tests

Channel Name	Capacity	Car End	Side	Height
Load Cell 1	1000 kips	Live	Left	Floor
Load Cell 2	1000 kips	Live	Right	Floor
Load Cell 3	500 kips	Live	Left	Roof
Load Cell 4	500 kips	Live	Right	Roof
Load Cell 5	1000 kips	Restraint	Left	Floor
Load Cell 6	1000 kips	Restraint	Right	Floor
Load Cell 7	500 kips	Restraint	Left	Roof
Load Cell 8	500 kips	Restraint	Right	Roof

The live end floor loading setup used in both crippling tests is shown in Figure 35. There are two hydraulic actuators installed at the floor-level with a load cell installed between each actuator and the energy absorber support on the car. A similar arrangement of hydraulic actuators and load cells is installed at the roof-level of the car. At the restraint end of the car, load cells are installed between the roof and floor reaction points and the load frame. This arrangement allows the load through each load or reaction point to be measured independently. This load measurement arrangement was designed to help measure the load path traveled through the structure, as well as to ensure that the load introduced at the live end was only exiting the car structure through the designated reaction locations on the back end.

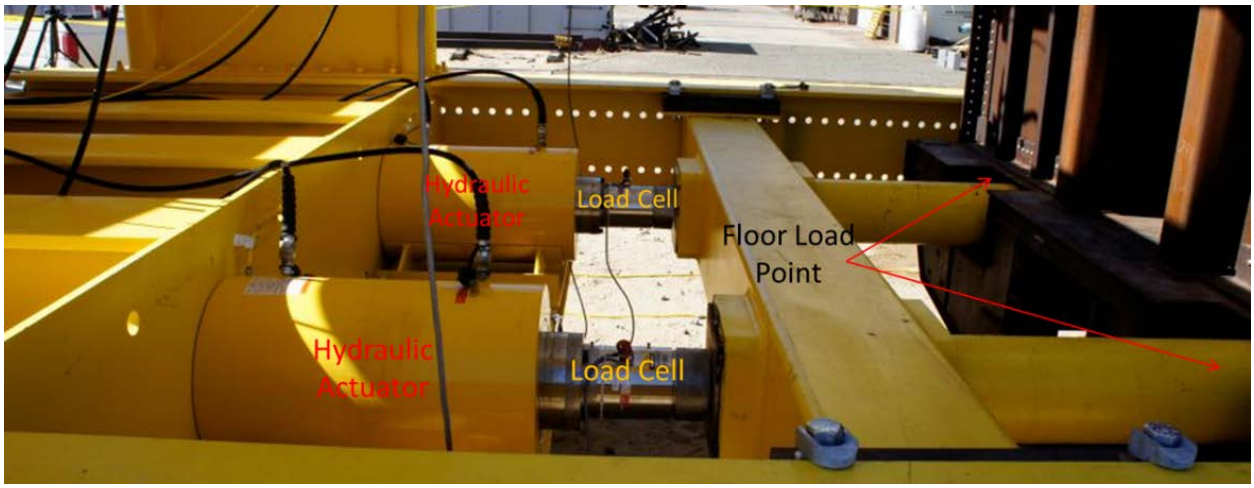

Figure 35. Live End Floor Load Setup

3.3.1 String Potentiometers in Car 244 Crippling Test

String potentiometers were used to measure the displacements of various points on Car 244. Two arrangements of string pots were used in this test. A single, longitudinally oriented string pot was installed between each loading or reaction point on the car and a ground point. These

string pots were used to measure the longitudinal displacement of each load and reaction location. Exemplar longitudinal string pots are shown in Figure 36.

Figure 36. Typical Longitudinal String Potentiometer Setup, Car 244

The second string pot arrangement used in this test was a VLL array of string pots attached to a single point on the underframe of the car. In the crippling test of Car 244, a total of 11 VLL arrays were installed on the underframe of the car. At both ends of the car, arrays were placed on the side sills and the lateral member at the end of the car. Between the two body bolsters, VLL arrays were attached to the center sill of the car. Figure 37 shows the 11 locations instrumented with VLL arrays, as well as the names of the arrays in the crippling test of Car 244. This image shows an inverted view of the car taken from the FE model.

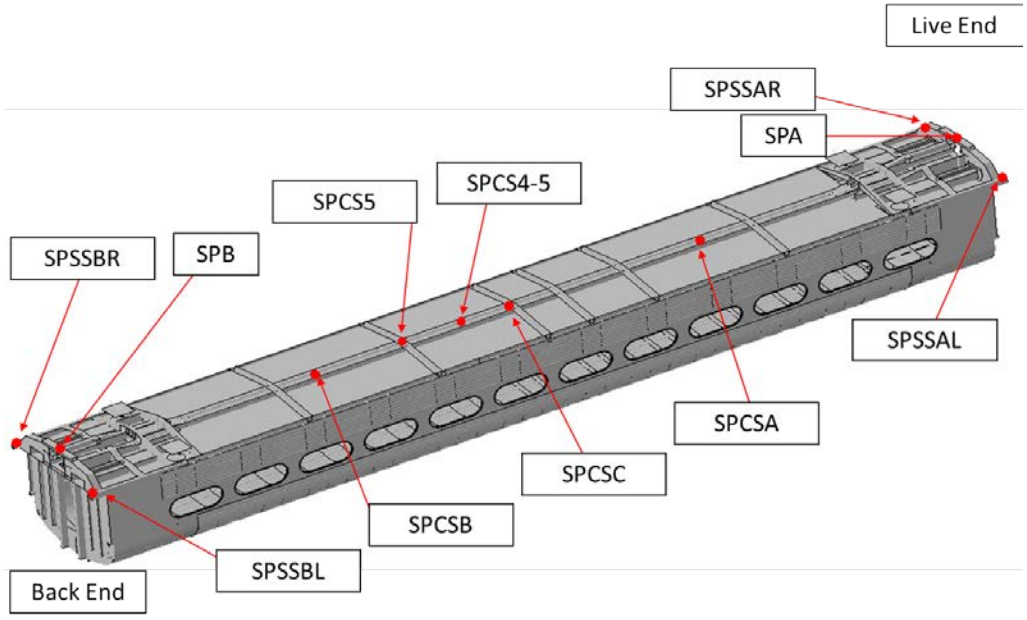

Figure 37. String Pot VLL Arrays on Car 244 (Underside View)

3.3.2 Strain Gages in Car 244 Crippling Test

Uniaxial strain gages were installed on Car 244 prior to the 800-kip elastic test. These gages were placed on the major longitudinal structural members of the car at six cross-sections. The six cross-sections are shown in Figure 11, and the instrumented members at each cross-section are shown in Figure 12. These same locations were instrumented during the crippling test of Car 244. In addition to these locations, gages were added in the vicinity of the floor and roof energy absorber supports at the live and restraint ends of the car. These gages were added to measure the local strains at the ends of the collision load path, where load is introduced or reacted through the occupant volume.

At the floor-level, two strain gages were added to each of the four energy absorber supports, for a total of eight floor-level strain gages. The first location instrumented at each support is on the longitudinal channel supporting the lateral face where the load was applied. The second location instrumented with a strain gage at each floor-level support was on the longitudinal channel inboard of the first lateral member of the car. The strain gages at a floor-level energy absorber support are shown in Figure 38.

Outboard Floor EA Strain Gage

Inboard Floor EA Strain Gage

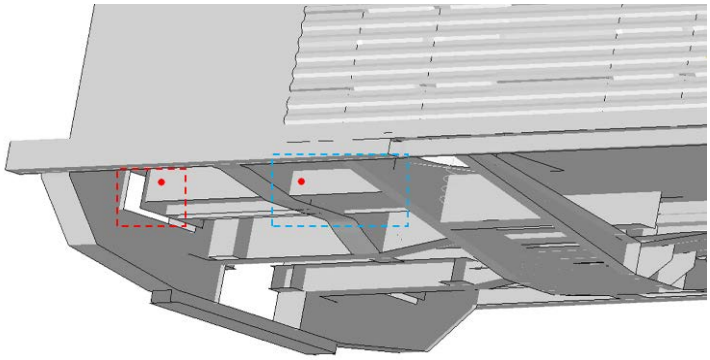

Figure 38. Strain Gages at Floor-Level Energy Absorber Support

Strain gages were also placed at the roof energy absorber support location. The roof support consists of a longitudinal tube that passes through the bulkhead of the car and is attached to the roof structure within the occupant volume of the car. One additional strain gage was placed on the interior of the car's roof just inboard of the bulkhead at each roof loading or restraint location. A typical location is shown in Figure 39.

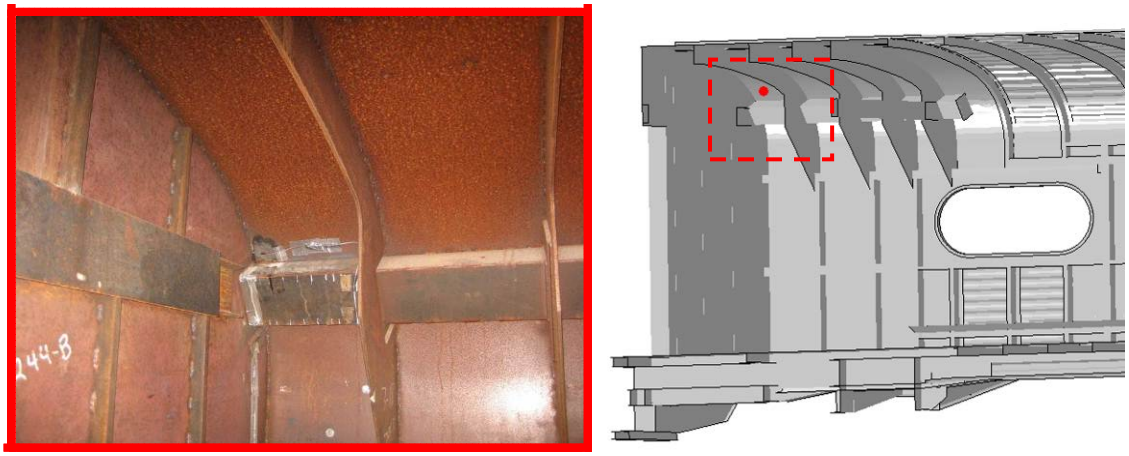

Figure 39. Strain Gage at Roof-Level Energy Absorber Support

3.4 FE Modeling of Crippling Tests

FE modeling of the crippling tests was performed as a part of this research program. One goal of this research program was to demonstrate the efficacy of the proposed ETF methodology of validating an FE model with elastic test data, then using the FE model to simulate loading conditions that include plastic deformation and crippling of the structure. The FE model was executed prior to conducting the crippling tests and was used to help design the tests.

The FE model for the 800-kip buff strength test was used as a starting point for the crippling model. Because the endframes and CEM components were removed from the Pioneer cars prior to the crippling tests, these structures were removed from the FE model as well. The section thickness and plastic stress-strain behavior assigned to the center sill and the plastic stress-strain behavior assigned to the side sills were adjusted to reflect the properties used in the original Pioneer car FE model. Additionally, because the lateral-vertical symmetry used in the 800-kip model could suppress a potential lateral buckling mode in the crippling model, the existing structure was mirrored to create a full-car model. The full-car model contained a total of 381,700 elements. This model is shown in Figure 40.

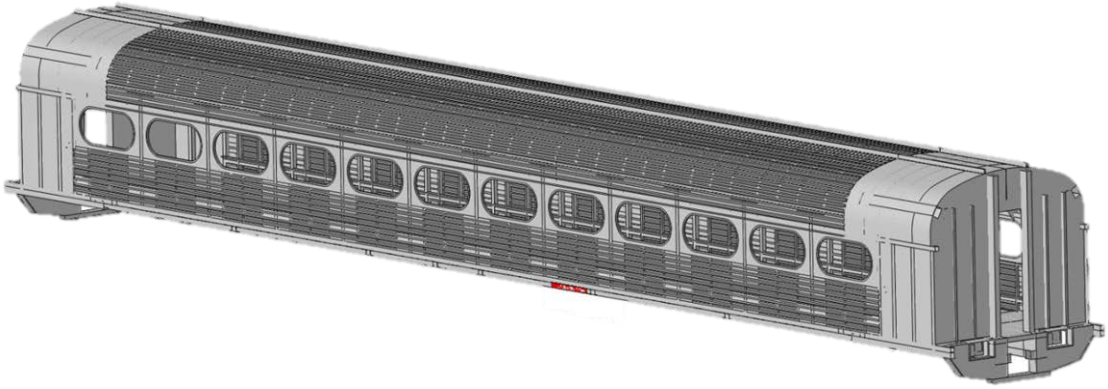

Figure 40. FE Model Used in Crippling Analysis

The crippling analysis was executed using the commercial FE software Abaqus/Explicit. An explicit finite-element solver was chosen for the analysis because of the expectation of large deflections and of plastic deformation. The load was slowly applied dynamically as an approximation of the quasi-static test condition.

3.4.1 Boundary Conditions

Suspension springs were placed at each of the four body bolster locations where the trucks would interface with the physical car body to support the car vertically. The springs had the same nonlinear characteristics and ground attachment as were used in the 800-kip FE analysis. The car-spring-ground attachment is shown in Figure 15.

Four locations on the live end of the car were used as loading locations. The corresponding locations on the back end of the car were used to restrain the car. The car was loaded at the floor-level energy absorber supports and at the inboard end of the roof energy absorber tubes. At each of the four load locations, a single row of nodes was selected and given a prescribed 2 inch/second longitudinal velocity. Because only the longitudinal motion was controlled and only

a single row of nodes at each load area was selected, each load application or restraint location was free to rotate as a result of this boundary condition. At the rear end of the car, corresponding rows of nodes were selected at each restraint location and were restricted from longitudinal motion. The nodes to which the boundary condition was applied are shown in Figure 41 for one end of the FE model.

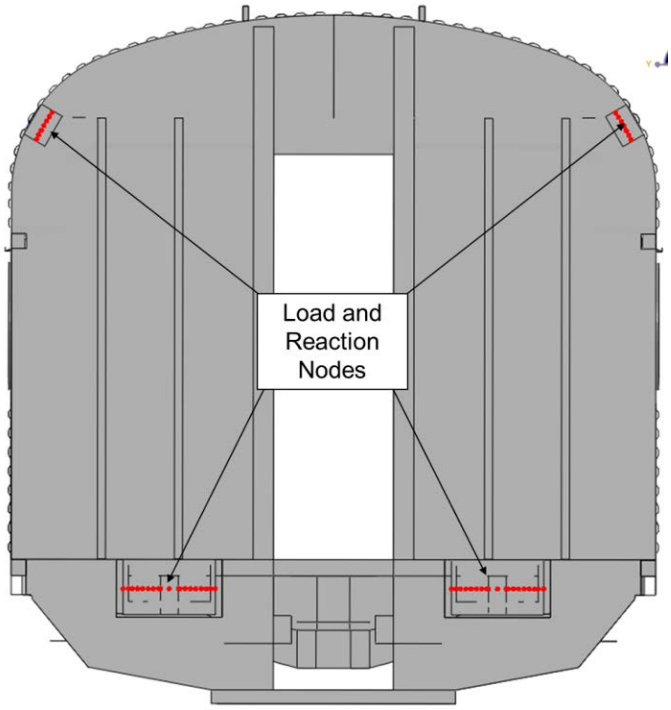

Figure 41. Load and Reaction Nodes, Crippling test FE Model

Using this loading technique, the FE solver calculated the force necessary to maintain the prescribed displacement at each node on the live end. In this way, the applied (live) load is calculated independently for each load application location, thus replicating the test condition. Similarly, the software calculated the force necessary to maintain zero longitudinal displacement at the back end of the car for the reaction locations. Because only a single row of nodes was subject to the longitudinal boundary condition at each location, each load or restraint location was able to move laterally, vertically, and rotate in response to the loads that developed.

Because the loading technique used in the FE model does not allow the rear end of the car to displace in the longitudinal direction, the displacement measurements on the front end will be equal to the overall shortening of the car. Because the test frame in the physical test stretches in response to the loads applied to the car, the rear end of the test car has a nonzero longitudinal displacement. The FE results for load-displacement obtained using this approach can be directly compared with the test data only if longitudinal displacement data is collected at the rear of the car. Because longitudinal displacement was only measured at the live end of the car during the shakedown test of Car 248, the displacements measured in this test include the change in length of both the car and the test frame that was restraining it. To compare the load-displacement results from the FE model with the test data, the stretching of the frame must be incorporated

into the model results. The longitudinal stiffness of each frame beam is estimated in Appendix B of this report.

4. Crippling Test and Analysis Results

Results are presented in this section for the crippling tests of Cars 248 and 244 as well as the FE analysis of the crippling load cases. These results include the load versus displacement behavior and discussion of the observed damage to both tested cars. Additional results from the test of Car 244 include strain measurements and displacements of the underframe. Results are compared, as necessary, between the two tested cars and the FE calculations.

4.1 Car 248 Shakedown Crippling Test Results

The limited-instrumentation shakedown test of car 248 was performed at TTC on June 15, 2011. An initial longitudinal load was used to settle the car within the test frame. The car was then loaded in 200-kip increments, with a return to a nominal load of approximately 20 kips between increments. Once a load of 800 kips was reached, the load was not actively removed between loading increments. The load was paused at 800 kips to permit the data recorded up to that point to be reviewed. Loading increased beyond 800 kips until the roof buckled, at which point the test was paused to permit inspection of the data collected and photographs of the car to be taken. Loading then resumed until crippling was reached. The load versus time data from the four live end load cells are plotted in Figure 42 for the final load increment, from the nominal load to 800 kips, and then up to crippling. This figure also includes the sum of the four load cell measurements plotted against time.

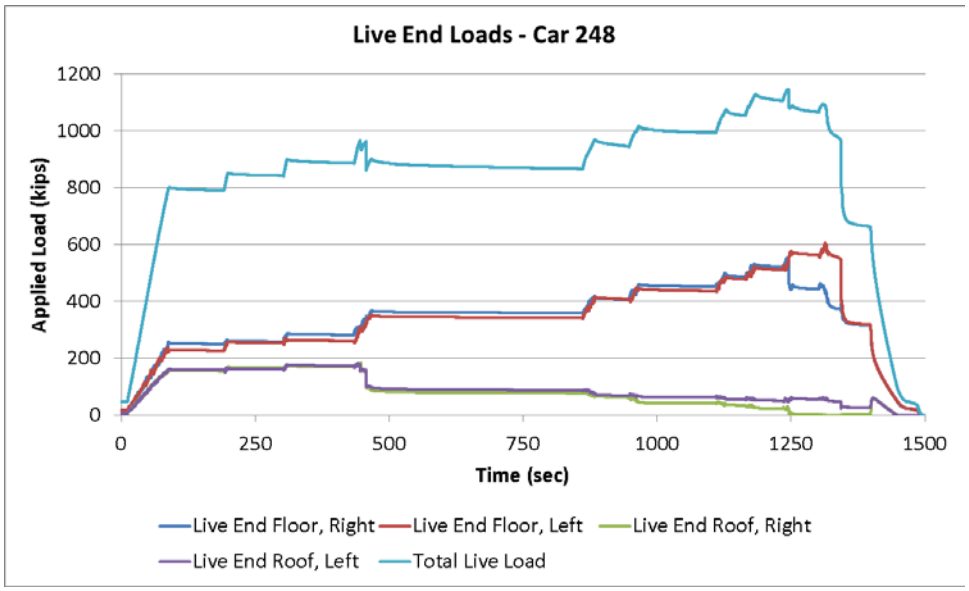

Figure 42. Live End Loads versus Time, Car 248 Crippling Test

The load from each individual load cell is plotted against the corresponding actuator displacement in Figure 43 for the load cells at the live end of the car. As seen in this figure, the two load cells at the roof recorded very similar load-displacement characteristics. The roof's stiffness was approximately the same for both the left and right sides, and both sides reached nearly identical peak loads. The right load cell recorded a peak load of 185 kips, and the left load cell recorded a peak load of 183 kips.

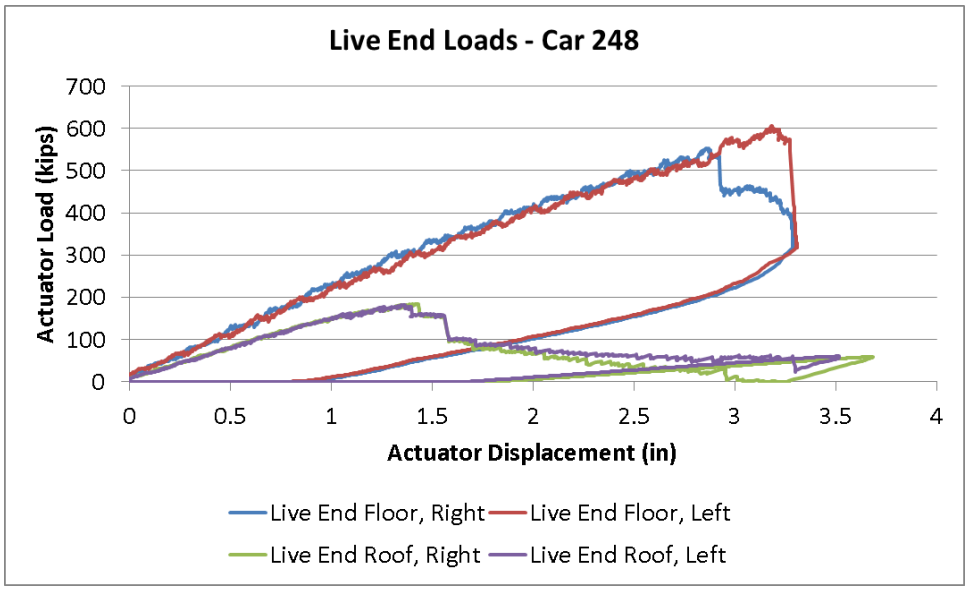

Figure 43. Live End Loads and Displacements, Car 248

At the floor-level, both load cells recorded similar load-displacement characteristics. There is a larger variance in peak load between the floor-level load cells than was seen at the roof-level. The right load cell recorded a peak load of 554 kips, and the left recorded a peak load of 607 kips. The left side load begins to decrease at a smaller displacement than the load on the right side. This behavior may be an indication of the left side sill crippling before the right side sill. Because of the limited instrumentation employed in the test of Car 248, additional information on the progression of damage to the carbody is not available.

The loads in the individual load cells at the restraint end of the car are plotted in Figure 44 against the displacement of the corresponding actuator on the live end. The roof-level data are nearly identical for the left- and right-side load cells, as it was at the front end of the car. At the floor-level, the left and right side data have more variance than at the front end. The left-side load cell records a higher load at zero displacement than the load cell at the right. However, even with this offset taken into account, the right side load does not reach the same level as the left side load at the floor.

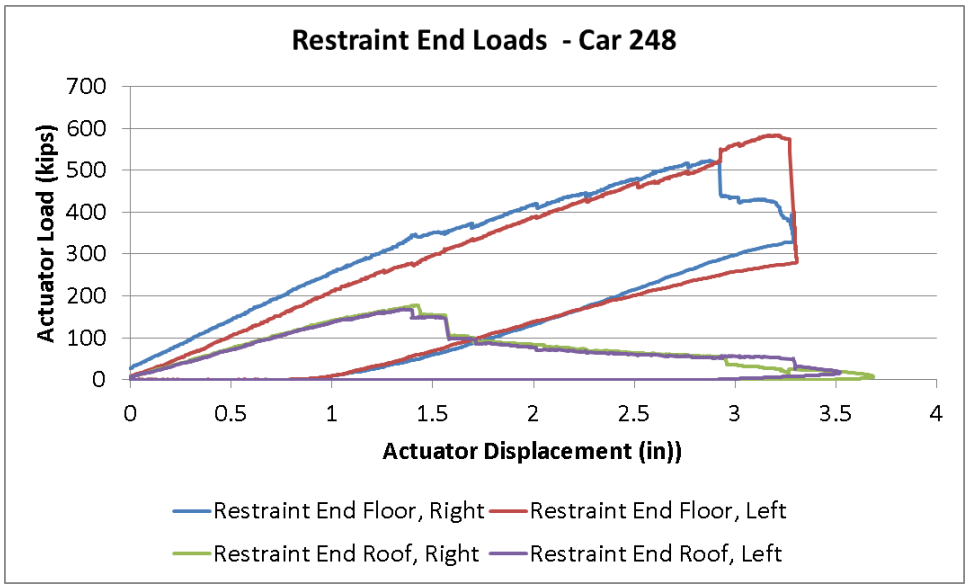

Figure 44. Restraint End Loads and Displacements, Car 248

The total applied load and total restraining load are obtained by summing the four load cell measurements at each respective end of the car. The total applied load and total restraint load are plotted against the average live end actuator displacement in Figure 45. These two values are in excellent agreement with each other. This indicates that the test is being conducted in a quasi-static manner, free from dynamic effects, and that the full load applied to the front end of the car is exiting the structure through the rear restraints. The load does not appear to be exiting the car through any uninstrumented locations or "short-circuits" in the load path.

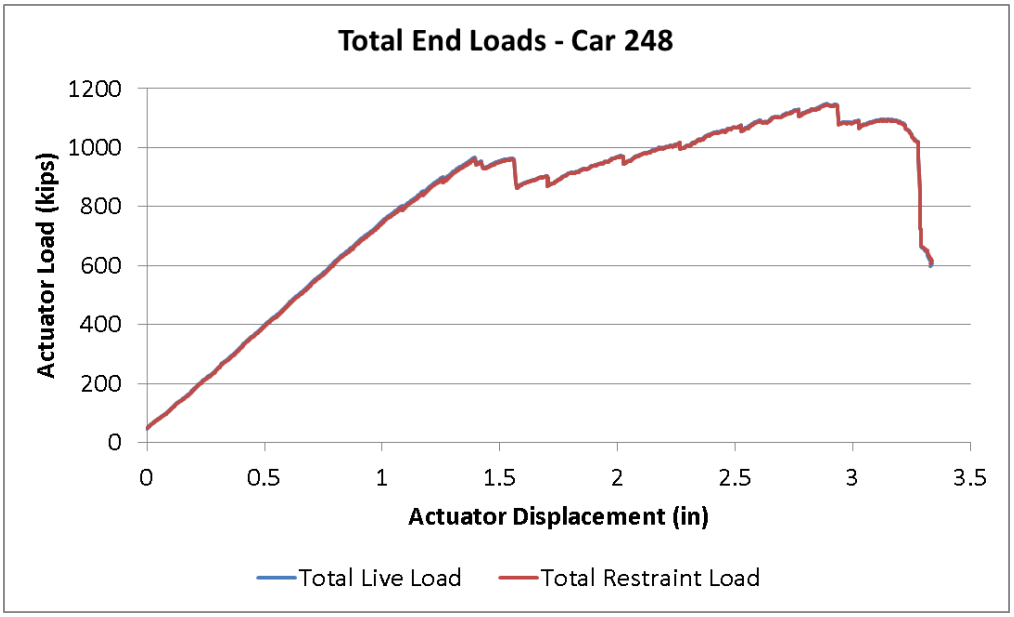

Figure 45. Total End Loads for Car 248 Shakedown Test

The load-displacement response is approximately linear to above 800 kips. At a total load of approximately 950 kips, the roof structure begins to buckle and the total load decreases. Because

the underframe has not yet exhausted its load-carrying capacity, the total applied load begins to climb again. At a global maximum of 1150 kips, the underframe begins to buckle, and the car has reached its crippling load.

4.1.1 Post-test Examination of Car 248

The car's structure was examined following the test. The center sill, side sills, sidewalls, and roof structure had all experienced buckling in at least one location.

Underframe Damage

The underframe of the car consists of three major longitudinal structural members: the center sill and the left and right side sills. These three members are attached by two types of lateral members: the body bolsters and cross-bearers. The body bolsters are located at the ends of the occupied volume and attach the trucks to the car body. A total of six cross-bearers are located at irregular intervals between the two bolsters. An underframe view of Pioneer 248, taken from the FE model of the car, is shown in Figure 46 with these structural members indicated.

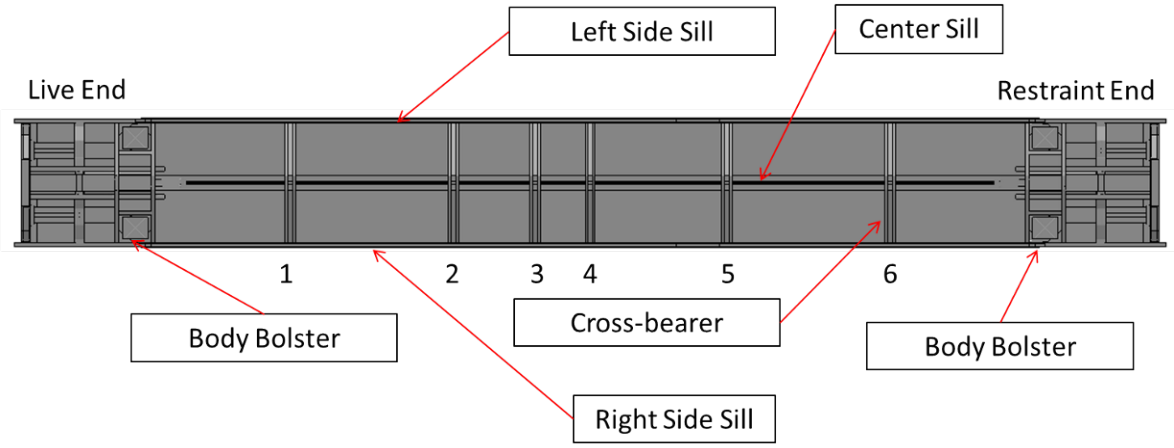

Figure 46. Annotated Underframe for Pioneer Cars

Damage occurred on the center sill and both side sills of Car 248. Because of the limited-instrumentation applied to this car during the shakedown test, it is unclear in what sequence the damage occurred. On the center sill, buckling was found to have occurred in two locations. The first location was approximately 44 inches toward the live end from the centerline of cross-bearer 5. This buckle occurred in the top half of the web of the center sill. A second buckle was found approximately 29 inches toward the restraint end, measured from the centerline of cross-bearer 5. This buckle was in the lower flange of the center sill. Both of these buckles are shown in Figure 47.

Figure 47. Damage to Underframe of Car 248

A third area of damage was observed on the center sill of car 248. A small buckle and failed welds were observed at the intersection of the center sill and cross-bearer 5. This area of damage is shown in Figure 48.

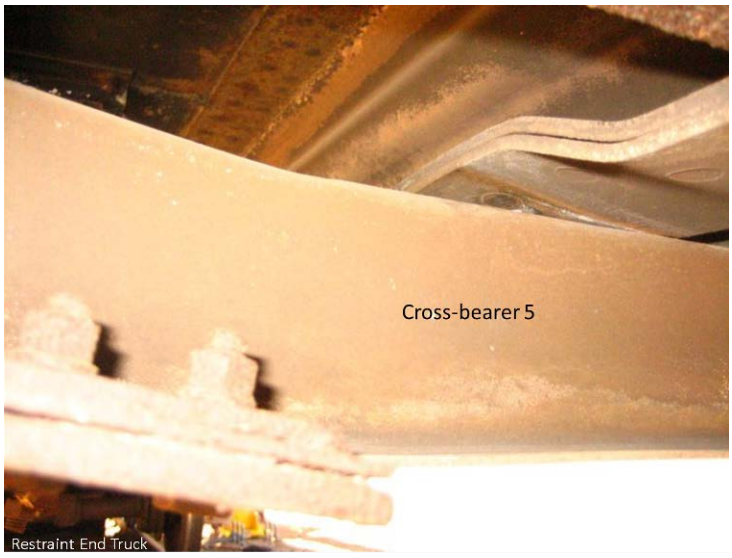

Figure 48. Buckle and Failed Welds in Center Sill at Cross-Bearer 5, Car 248

Damage was observed on both the left and right side sills of Car 248. On both side sills, the damage was located longitudinally between cross-bearers 4 and 5. On both sides, the damage

was in the form of a buckle to the lower portion of the side sill. Also, on both sides, the damage was proximate to observed damage in the sidewall structure of the car. The side sill damage is shown below in Figure 49.

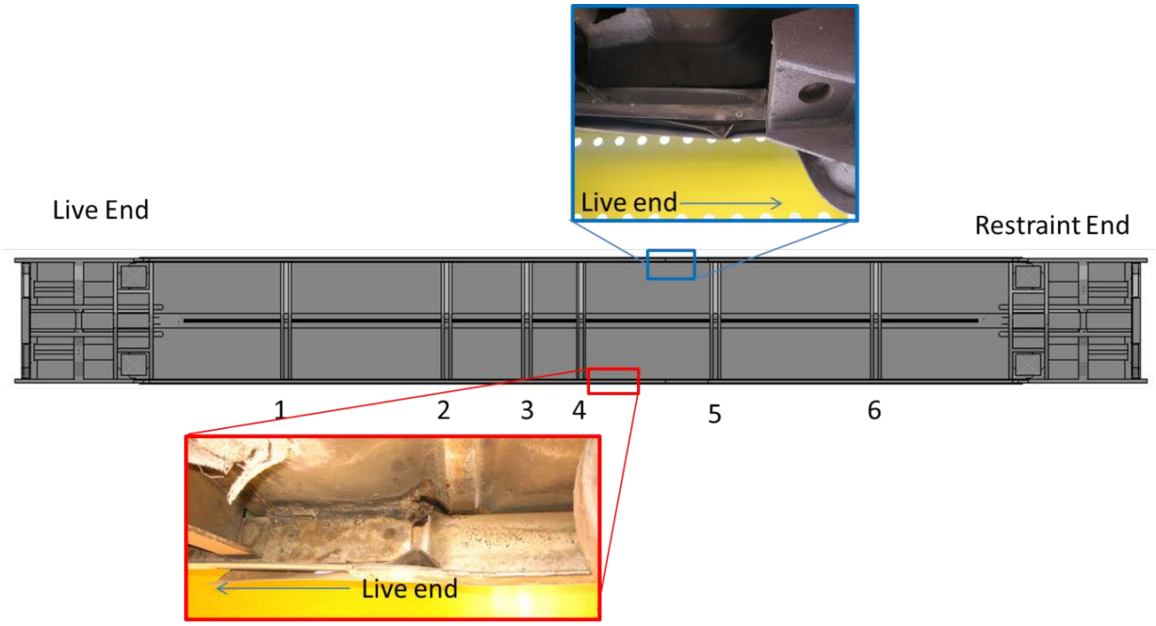

Figure 49. Damage to Sides Sills of Car 248

Right Side Damage

Structural damage was observed to the right sidewall of car 248 following the crippling test. On the exterior of the car, the sidewall of the car buckled inward at approximately the midpoint of the seventh window from the live end of the car. This location corresponds with the buckle observed on the right side sill. The buckled sidewall is shown in Figure 50.

Figure 50. Damage to Right Sidewall, Car 248

Left Side Damage

The left sidewall of Car 248 also had a visible buckle on the outside of the car. The sidewall buckled outward at the seventh window from the live end and buckled inward above the eighth window. The outward buckle of the sidewall is in approximately the same area as the buckle in the side sill on this side of car 248. The sidewall buckle is shown in Figure 51.

Figure 51. Damage to Left Sidewall, Car 248

The buckled area of the left sidewall was also examined from within the car. Because the interior finish and fittings had been removed, the structural members making up the skeleton of the superstructure were clearly visible in this area. On the left side of the car, the belt rail had fractured in two locations. The fractured belt rail is shown in Figure 52. These fractures occurred in an area of the car known to have had pre-existing damage. The pretest damage is shown in Figure 34.

Figure 52. Fractured Left Belt Rail, Car 248

Roof Damage

The roof and sidewalls of Car 248 buckled during the test at a total applied load of slightly less than 1 million pounds. The roof buckled outward on both the left and right sides of the car. The roof buckle does not extend laterally across the car in a straight line, but follows a zigzag pattern from left to right. The roof buckle on each side of the car connects with the sidewall buckle on each side. The roof buckle is shown from above in Figure 53.

Figure 53. Buckled Roof, Car 248

4.2 Car 244 Fully Instrumented Crippling Test Results

The fully instrumented crippling test of Car 244 was conducted at TTC on June 28, 2011. In addition to measuring the live and restraint end loads and live end displacements as was done in the test of Car 248, this test included strain gages along key structural members and arrays of string potentiometers designed to measure VLL deflections in the underframe of the car. Additional displacement transducers measured the longitudinal motion of the live and restraint ends of the car, permitting the overall change in car length to be calculated.

The loading procedures used in the test of Car 244 were similar to the procedures used on Car 248. In both tests, the car was secured within the frame by a small longitudinal load. The car was then loaded in 200-kip increments, with a return to a nominal load of approximately 20 kips between increments. Once a load of 800 kips was reached, the load was not actively reduced between increments. The actuators were pushed forward in 0.25-inch increments and then paused to allow the structure to settle. This approach was followed until crippling occurred. The individual live end loads and the total live end load are plotted against time in Figure 54 for the full sequence of loads.

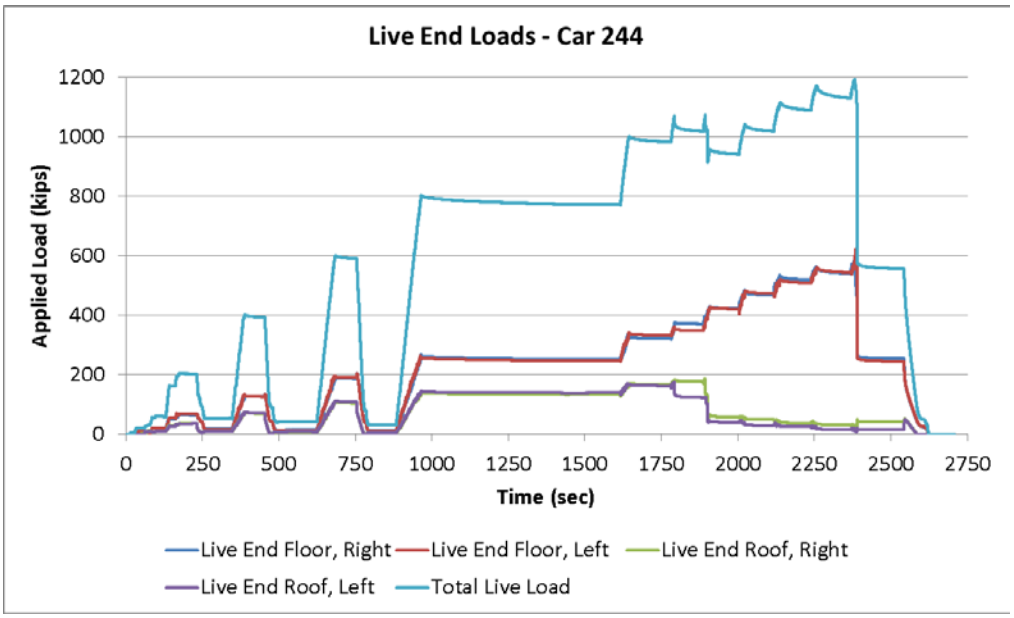

Figure 54. Live End Loads, Car 244 Crippling Test

The loads measured by each of the four live end load cells are plotted against the displacement of each hydraulic actuator in Figure 55. The load cell names and locations for the test of Car 244 are the same as were used for Car 248, as shown in Table 7. Both of the floor-level load cells recorded approximately the same load-displacement characteristic, with the left-side load cell measuring a slightly higher peak load than the right-side. The two roof load cells also recorded very similar load levels. The right load cell measured a slightly higher peak load than the left.

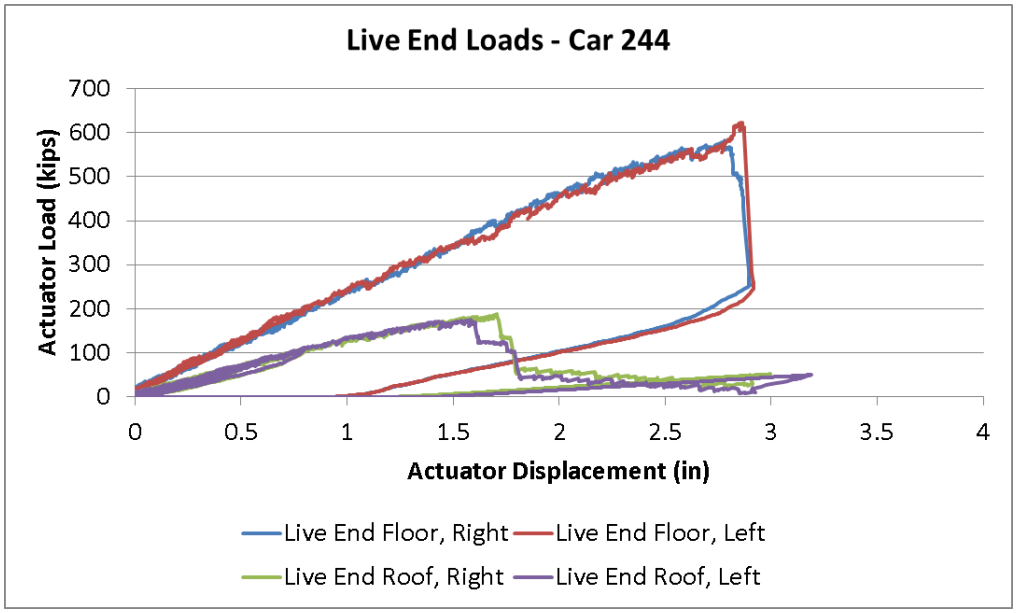

Figure 55. Live End Loads and Displacements (Car 244 Crippling Test)

The load at each restraint location is plotted against actuator displacement for the corresponding location on the live end for the four restraint end load cells in Figure 56. At both the floor and roof restraint locations, the left and right side loads are roughly equal. Comparing the loads at a

given displacement between the restraint end (Figure 56) and the live end (Figure 55), it is apparent that some portion of the load that is introduced to the car through the floor at the live end is being reacted through the roof at the restraint end of the car. The peak load in each floor location on the live end is approximately 600 kips, while the peak load in each floor location on the restraint end is slightly greater than 500 kips.

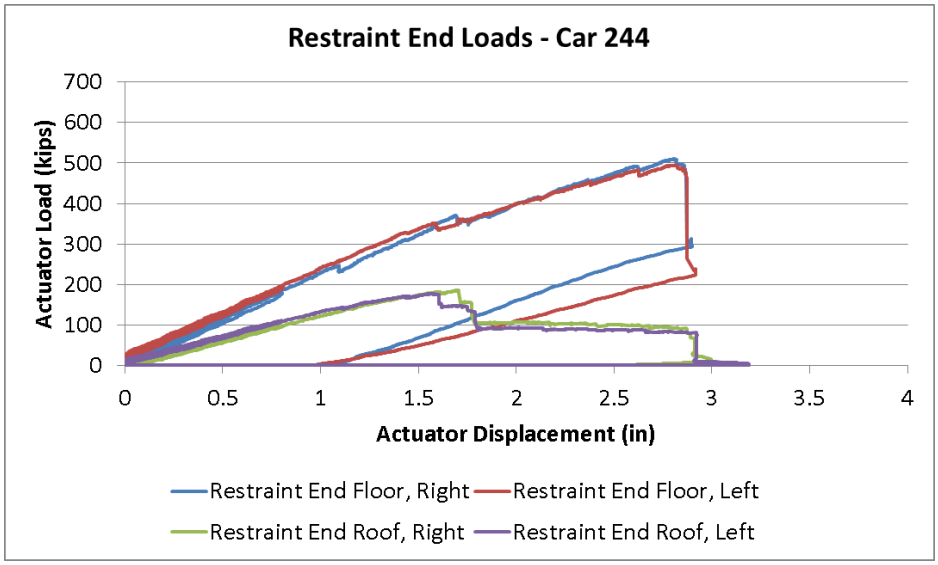

Figure 56. Restraint End Loads and Displacements (Car 244 Crippling Test)

In Figure 57, the total applied load on the live end of the car and the total reaction load from the restraint end of the car are plotted against the average displacement of the actuators on the live end. The live end and restraint end loads are approximately equal throughout the entire test. This verifies that the test is being run in a quasi-static manner, free from dynamic effects. Additionally, this result indicates that the longitudinal load is entering and exiting the car through the load cells without experiencing losses through any noninstrumented load paths.

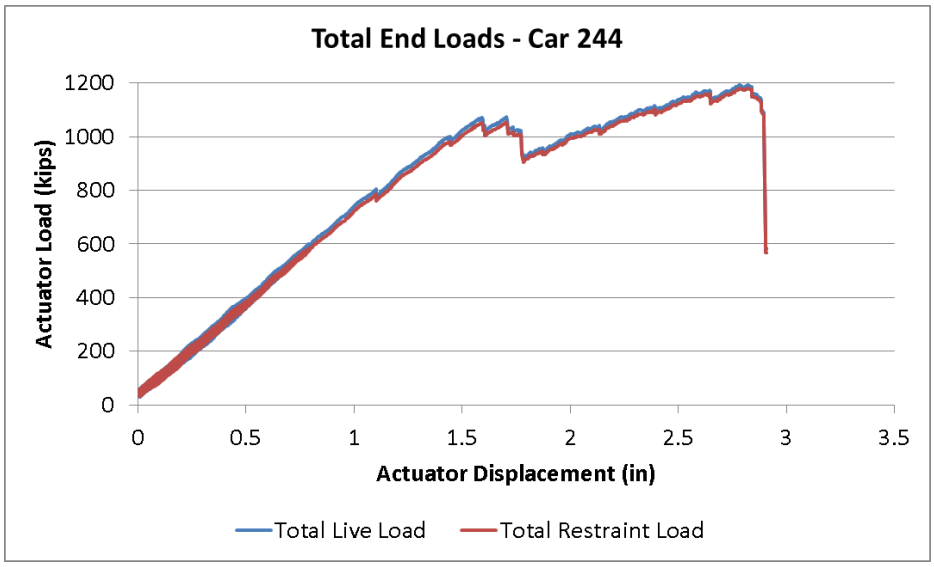

Figure 57. Total End Loads for Car 244 Crippling Test

The results from the crippling test of Car 244 are similar to the results from Car 248. The live end load versus actuator displacement from each car is plotted in Figure 58. In both cars, the roof structure buckles at a load of approximately 1 million pounds. In Car 248, the actual buckling load is slightly below 1 million pounds and in Car 244 this load is slightly above 1 million pounds. Because the underframe structure has not been compromised at the roof buckling load in either car, as the displacement continues to increase, the load is able to increase as well. Car 248 had a crippling load of 1.15 million pounds and Car 244 had a crippling load of more than 1.19 million pounds.

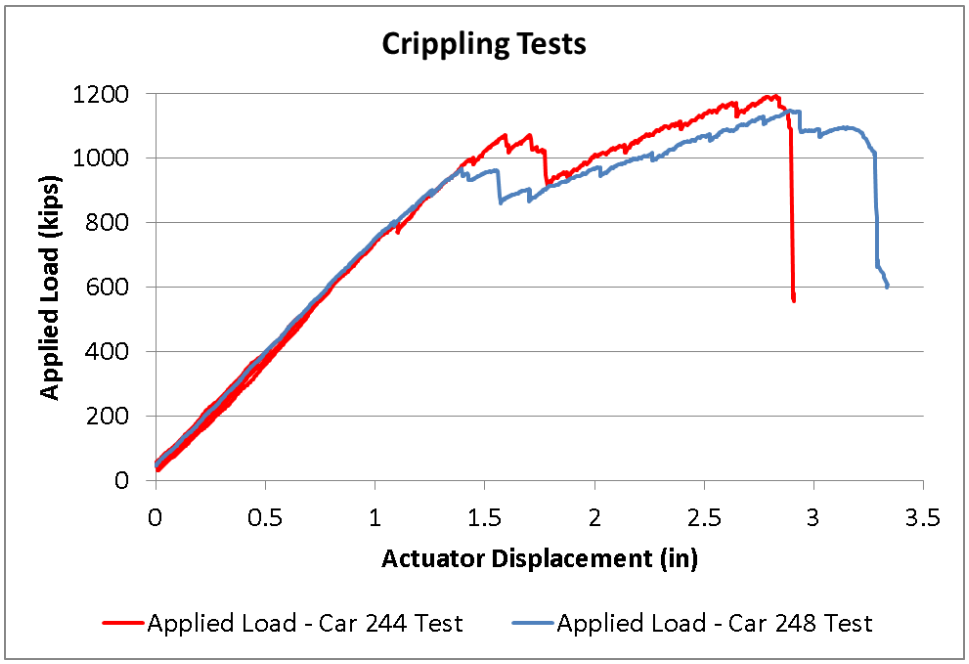

Figure 58. Load-Displacement Behavior for Car 248 and Car 244

4.2.1 Post-Test Examination of Car 244

Following the crippling test of Car 244, the structure of the car was inspected for damage. Damage was observed on the center sill, the side sills, and both sidewalls of the car. The damage to Car 244 occurred primarily between the live end of the car and the lateral-vertical midplane of the car. The conventions used in reference to "left" and "right" are the same as were used in the discussion of the damage to Car 248 and are shown in Figure 46.

Underframe Damage

The center sill buckled in multiple locations. One buckle occurred approximately 24 inches toward the live end from the first cross-member on the underframe. The bottom flange of the center sill folded into a "z" at this location. Figure 59 shows two photographs of the damaged center sill at this location, as well as the location on the underframe where the damage occurred. The figures also show the proximity of the cross-section 5 strain gages to the buckled flange.

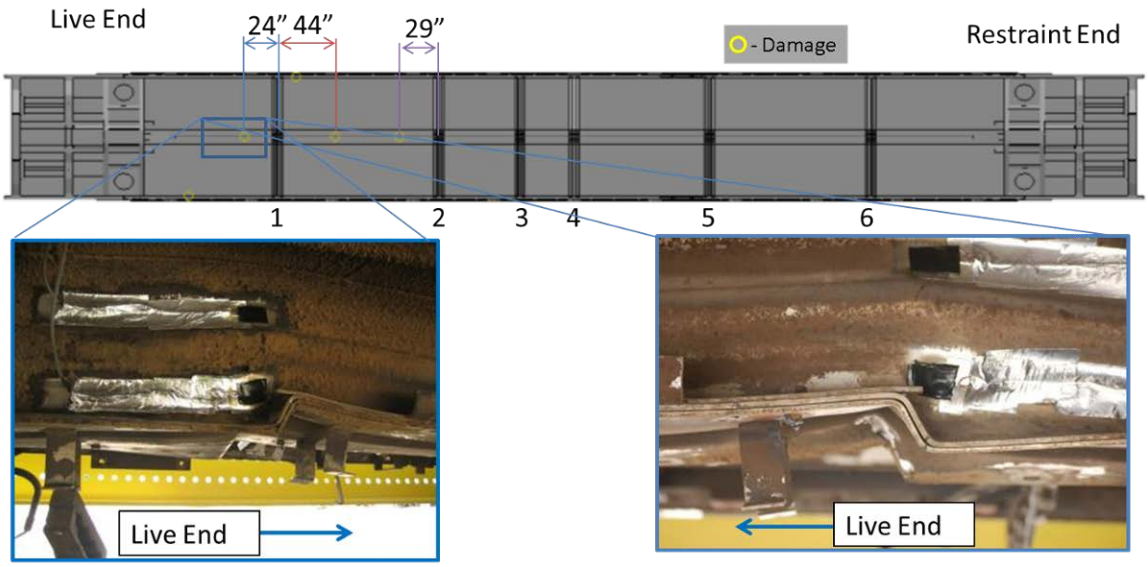

Figure 59. Damage to Car 244 Center Sill (1)

The bottom flange of the center sill experiences a change in geometry at this point, decreasing from three built-up sections to two. The three layers of the center sill flange can be seen in both photographs of Figure 59. The third layer of material is not connected to the other two by a continuous weld, but through a series of spot welds. This discontinuous connection allows two layers to fold and deform while the third layer remains straight.

A second buckle occurred on the center sill approximately 44 inches toward the restraint end from the first cross-bearer. This location experienced buckling primarily in the top flanges of the center sill. Two photographs of the damage, as well as the damaged location on the underframe of the car, are shown together in Figure 60. The photographs in this figure also show the proximity of the cross-section 4 strain gages to the damaged area of the center sill. A second, similar buckle in the top flange of the center sill was observed approximately 29 inches toward the A-end from the second cross-member.

Figure 60. Damage to Car 244 Center Sill (2)

Figure 61 shows the damage to the side sills of Car 244. On the left side, the side sill buckled at a point approximately 13 inches toward the restraint end from the first cross-bearer. On the right side, the side sill buckled at approximately 68 inches toward the live end from the first cross bearer. Both side sills buckled laterally.

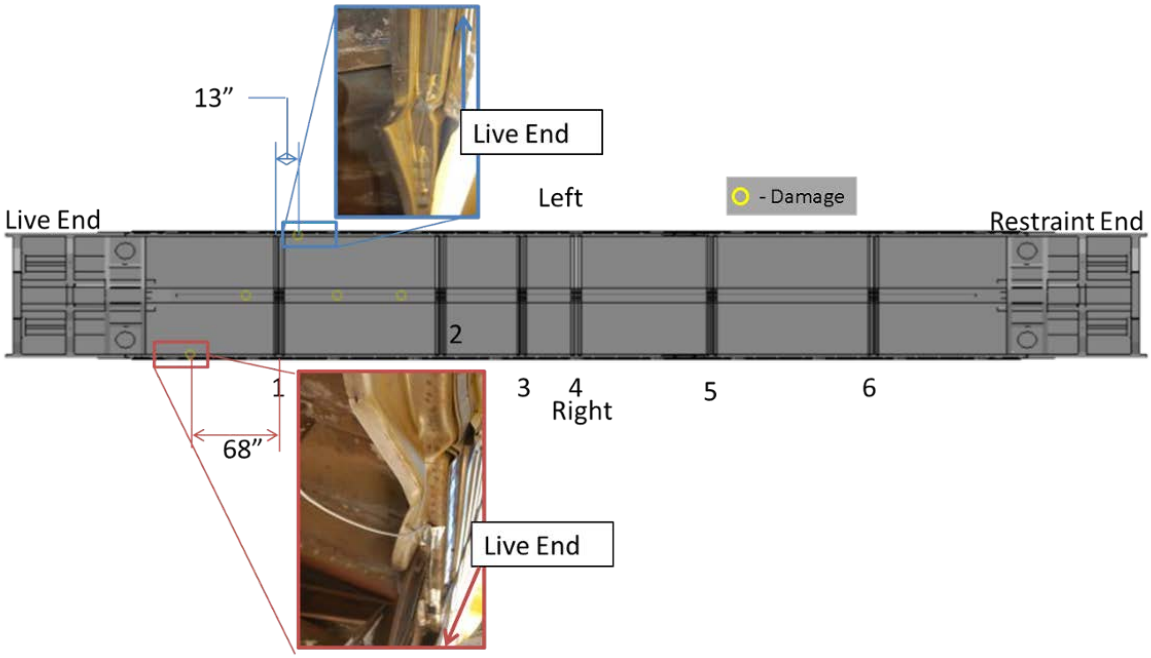

Figure 61. Damage to Car 244 Side Sills

Right Side Damage

Following the crippling test, large-scale buckles in the sidewall of Car 244 were visible on the right side. The main sidewall buckle occurred between window 4 and window 5 on this side. A second buckle was observed in the vicinity of window 2. In this area, a rectangular cutout in the outer skin of the car had been made to permit material testing during a previous testing program. The skin of the car buckled in the area around this cutout. The large buckle and this second buckle are both shown in Figure 62.

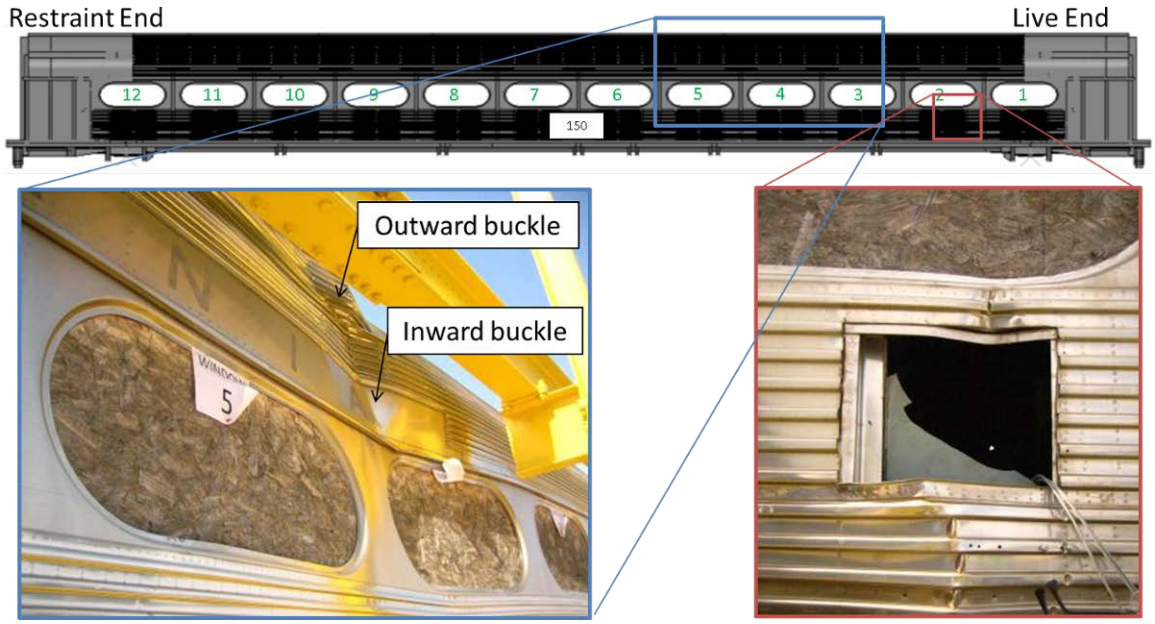

Figure 62. Damage to Right Side of Car 244

The damage to the right side of Car 244 was also inspected from the interior of the car. The sidewall between windows 4 and 5 protruded into the interior of the car by several inches. The belt rail in this region exhibited a gradual deformation without any sharp kinks or buckles. The right-side interior of the car is shown in Figure 63.

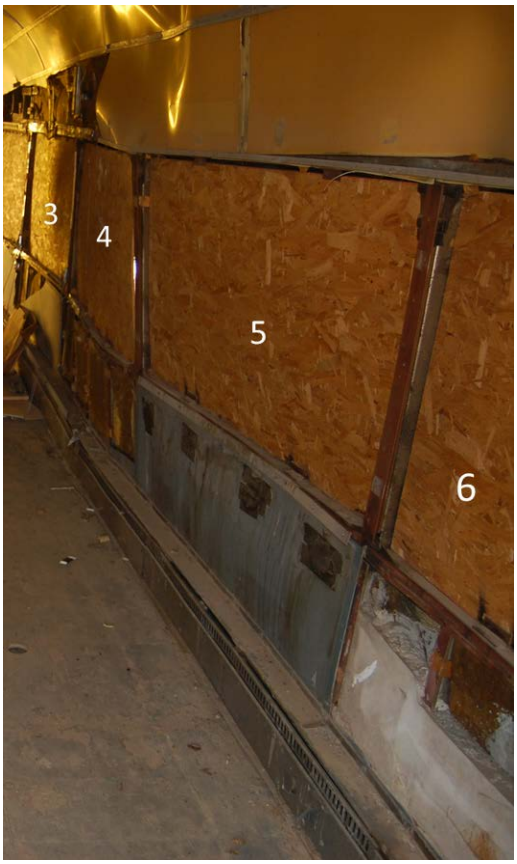

Figure 63. Damage to Right Side Interior of Car 244

Left Side Damage

The sidewall on the left side of Car 244 buckled over a large region of the car. At window 3, the sidewall buckle is outward and at window 5 the sidewall buckle is inward. The damage to the right side of the car was more localized than the damage to the left side of the car. The left side damage is shown in Figure 64.

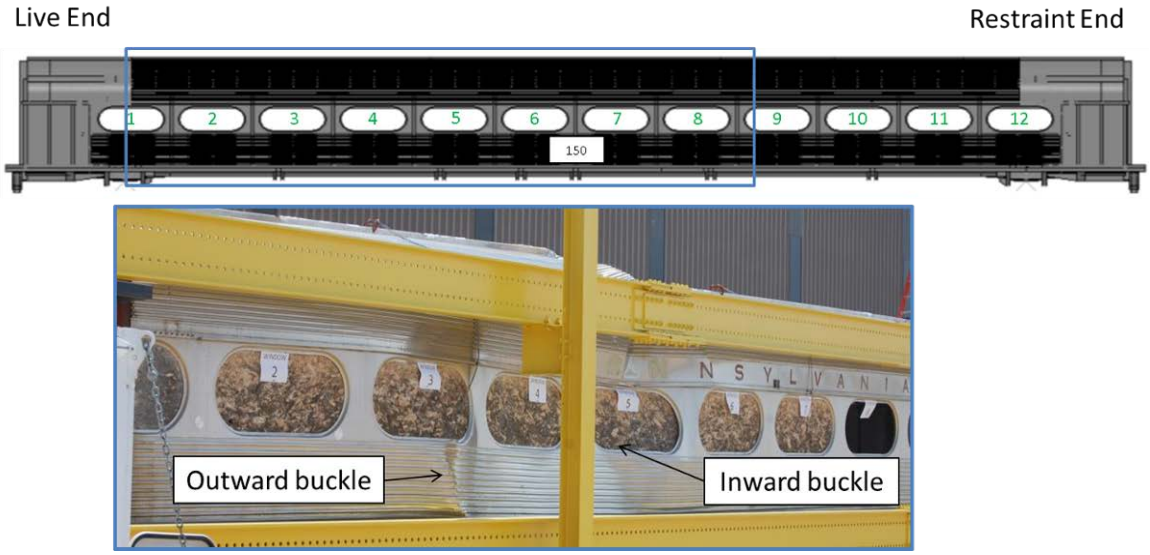

Figure 64. Damage to Left Side of Car 244

This damaged area was inspected from the interior of the car as well as the exterior. The belt rail on the left side of the car was buckled beneath window 3. The vertical supports below this window were also buckled. This damage can be seen in Figure 65.

Figure 65. Damage to Left Side Interior of Car 244

Roof Damage

The roof buckled during the test of Car 244 in a manner similar to the roof of Car 248's buckling. In both cars the roof buckled at a load of approximately 1 million pounds. As was the case with Car 248, the roof on Car 244 did not buckle laterally across the car, but buckled in a zigzag pattern across the width of the car. An overhead view of the roof buckle is shown in Figure 66.

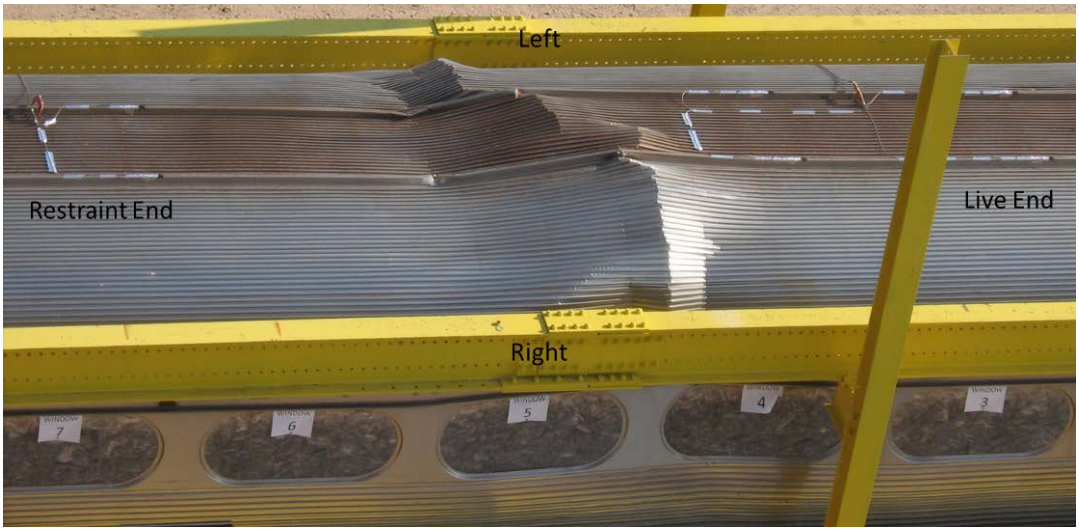

Figure 66. Roof Buckle in Car 244

4.3 FE Model Results

The FE model of the crippling test case was executed before the shakedown test of Car 248 and its results were used to prepare and execute both crippling tests. A single analysis was used to simulate both crippling tests. The model represented Car 244 and included the crack patches that had been installed prior to the elastic verification test. The results of this analysis are compared with the results from both the crippling test of Car 248 and the crippling test of Car 244.

4.3.1 Load-Displacement Results

Load versus displacement data were obtained independently for each loaded location on the live end of the car in the crippling analysis. Figure 67 shows the load-displacement behavior calculated by the FE analysis for each of the four live end load locations. In this figure, the horizontal axis represents the total shortening of the car.

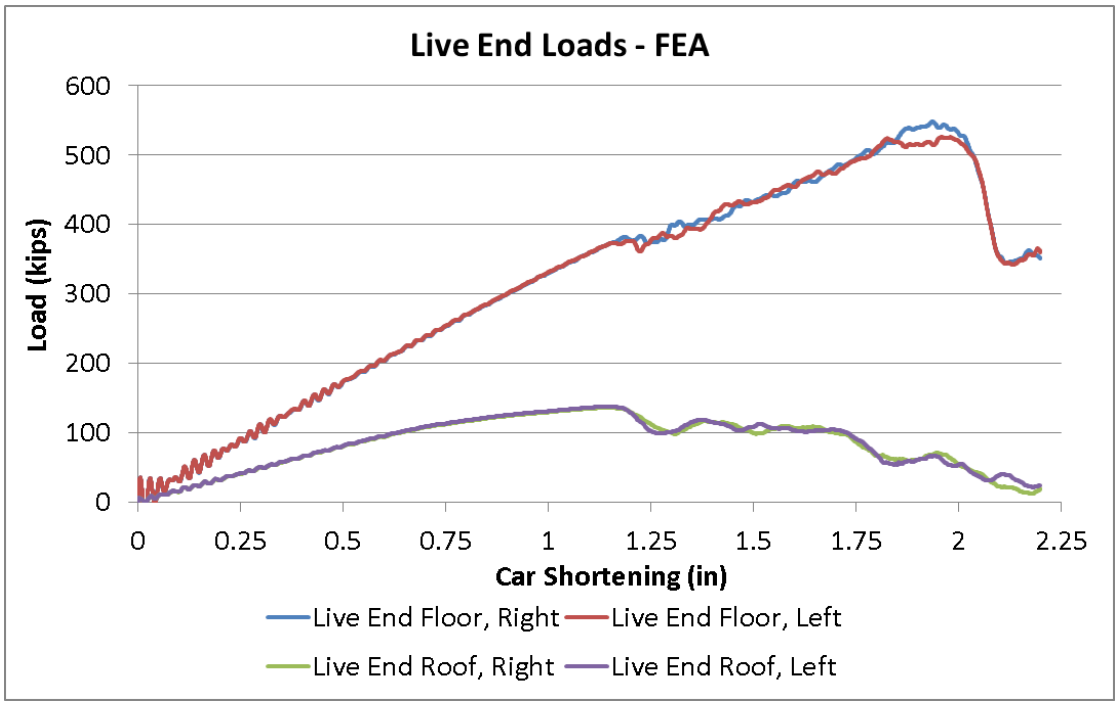

Figure 67. Live End Loads by Location (Crippling FEA)

A corresponding set of load versus displacement characteristics were generated for the restraint end of the car. These four characteristics are shown in Figure 68. Figure 67 and Figure 68 indicate that the load being reacted and the load being introduced into the car at the corresponding live end location are approximately the same. These results show the same qualitative behavior as was seen in the crippling tests of Cars 248 and 244.

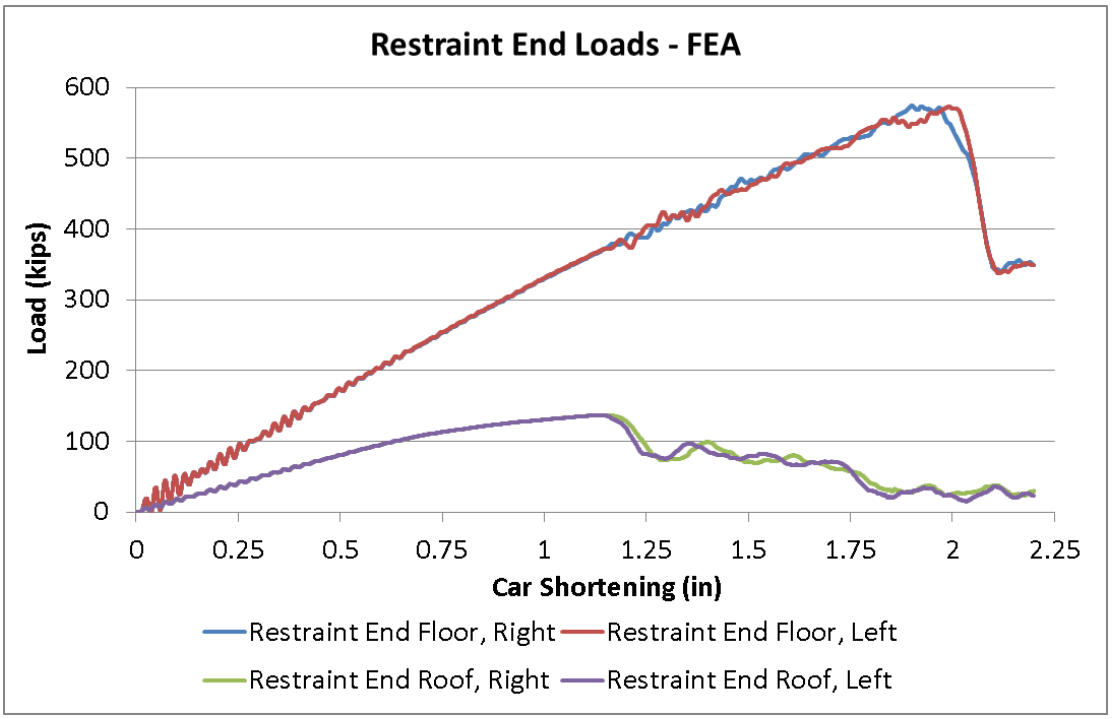

Figure 68. Restraint End Loads by Location (Crippling FEA)

4.3.2 Verification of Quasi-Static Behavior

In the ETF's report, two criteria are established for determining whether a slow, dynamic analysis is sufficiently free from dynamic effects to be considered quasi-static. While an analysis that meets only one of the two criteria qualifies as quasi-static, both methods of evaluation were used to examine the FE model in this study. The following two conditions are taken directly from the ETF's Report:

ETF Condition One

> For a given simulated load rate, the load at the live end of the model should be the same as the load at the fixed end. Load at the reaction end may vary by up to +/-5 percent of the load at the live end of the model for the analysis to be considered quasi-static.

Evaluation of Condition One

A displacement boundary condition was used to apply loads to the four live end locations in the FE model. The FE solver calculates the force that must be applied at each location to maintain the prescribed displacement. In this way, the load and displacement behavior at each live end location is calculated.

Similarly, at the back end of the car a zero-displacement boundary condition is enforced at each reaction location. The software calculates the force that must be applied to maintain zero displacement at the selected locations. The reaction load can then be determined for each of the restraint locations in the model.

For the purpose of applying the quasi-static condition, the four loads applied to the live end are added together and plotted versus the displacement of the live end. The four loads at the back end are also summed and plotted against the displacement of the live end. Because the restraint

end in the model cannot move, the live end displacement is the same measurement as the shortening of the car. A +/-5 percent envelope on the live end force is plotted alongside the two load-displacement characteristics in Figure 69.

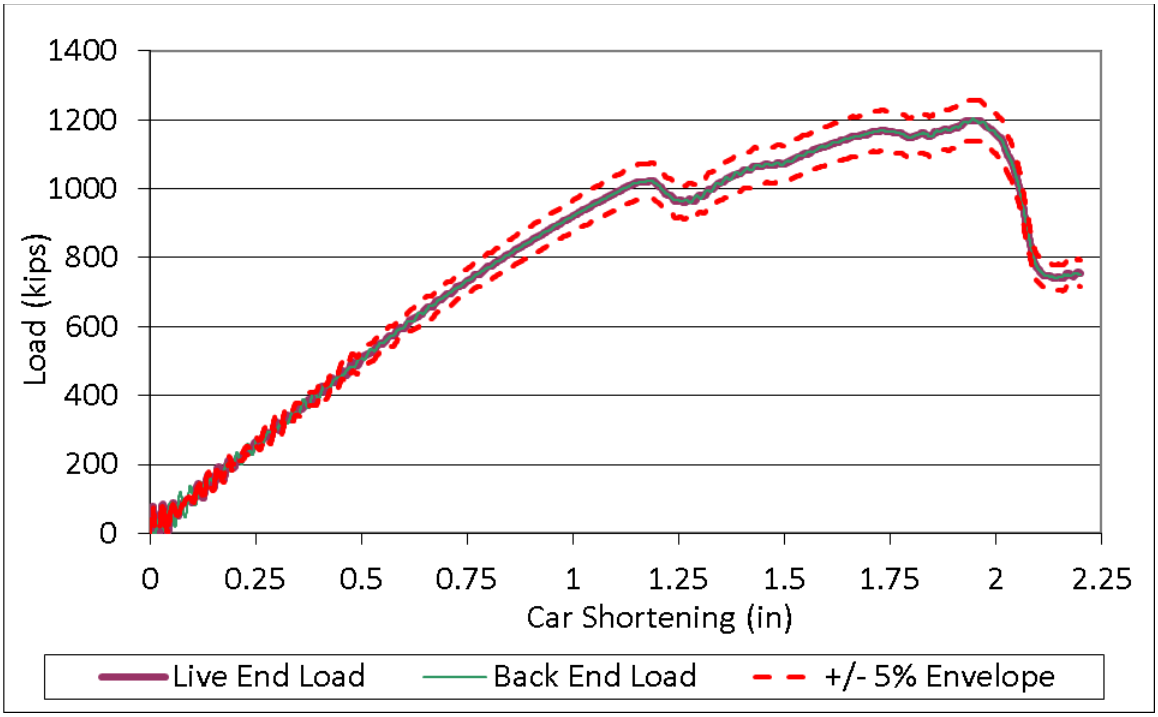

Figure 69. Live Load and Reaction Load for Crippling Analysis

ETF Condition Two

> The ratio of kinetic energy to strain energy within the structure should be small (< 5%). The ratio of kinetic energy-to-strain energy may exceed 5 percent during the first 10 percent of the total simulation time without invalidating the analysis as quasi-static.

Evaluation of Condition Two

Because an explicit FE solver was used to estimate the crippling load, the load that is applied is dynamic. The solver calculates the total amount of kinetic energy in the system, as well as the internal (strain) energy. Because the model initially experiences very little deformation, the ratio of kinetic energy to internal energy may exceed 5 percent for the first 10 percent of the simulation time.

The ratio of kinetic energy to internal energy for the crippling simulation is plotted in Figure 70. The simulation consisted of two steps: a gravity step and a compression load step. The transition between the two steps is indicated by a dashed vertical line in this figure. The energy ratio is plotted on a logarithmic scale because this quantity varies over several orders of magnitude during the course of the simulation.

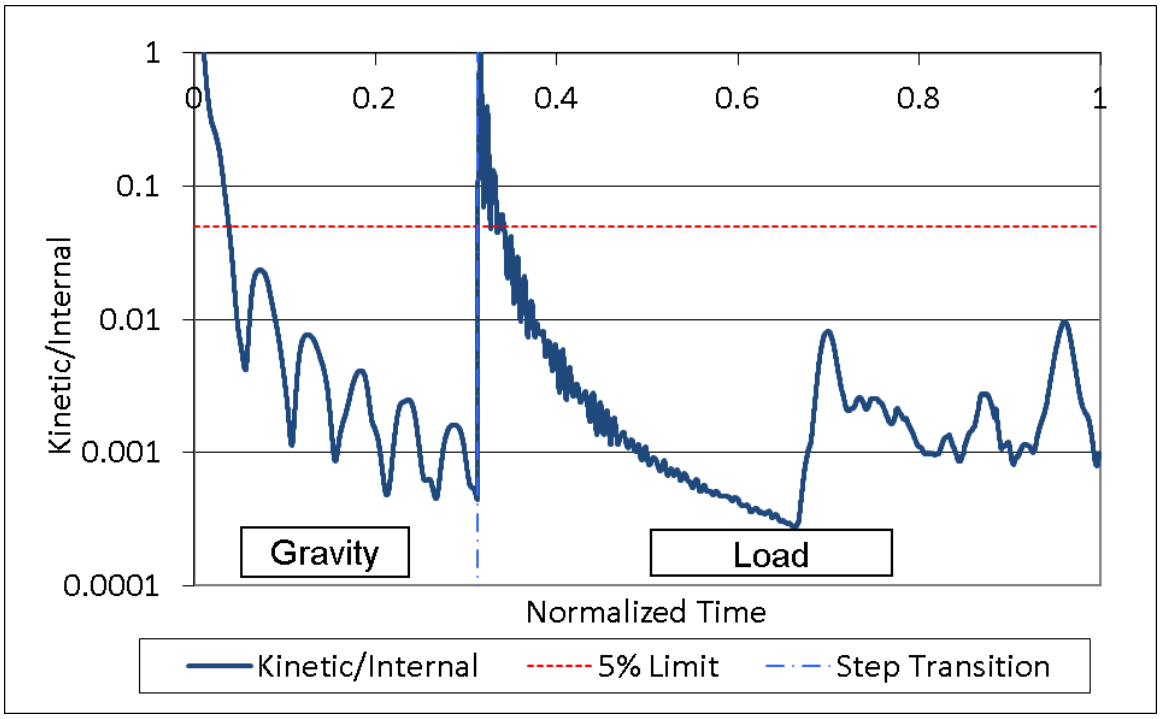

Figure 70. Ratio of Kinetic Energy to Internal Energy for Crippling Analysis

Figure 70 shows that the ratio of kinetic energy to internal energy is well below 5 percent for nearly the entire length of the simulation, except for the initial portion of each step. Based upon either of the ETF criteria, the crippling analysis can be considered quasi-static.

4.3.3 Comparison of Car 248 Test Results with FE Results

The longitudinal load-displacement behavior was the primary output data collected in the shakedown test of Car 248. This data is compared with the FE analysis results to determine if the FE model is providing a reasonable estimation of the car behavior as observed in the test. Because longitudinal displacement data were only measured on the live end actuators during the shakedown test, the behavior of the test frame must be incorporated into the FE results before the test and analysis results may be compared with one another. Each longitudinal frame beam is treated as an axially loaded member and its stiffness is calculated in Appendix B. For a given load magnitude, this stiffness is used to calculate the deflection of each frame member. The overall actuator displacement is the sum of the change in car length (directly calculated by the FE analysis) and the deflection of the test frame obtained through this approximation.

Figure 71 plots the load in the floor-level energy absorber supports in the test and the loads in the corresponding energy absorber supports in the FE model. There is generally good agreement between the floor-level load data from the test and the floor-level response of the FE model. The FE model is slightly stiffer than Car 248. The load through the left floor energy absorber support in the model reaches a maximum load of 525 kips, and the load on the right floor energy absorber reaches a maximum load of 550 kips.

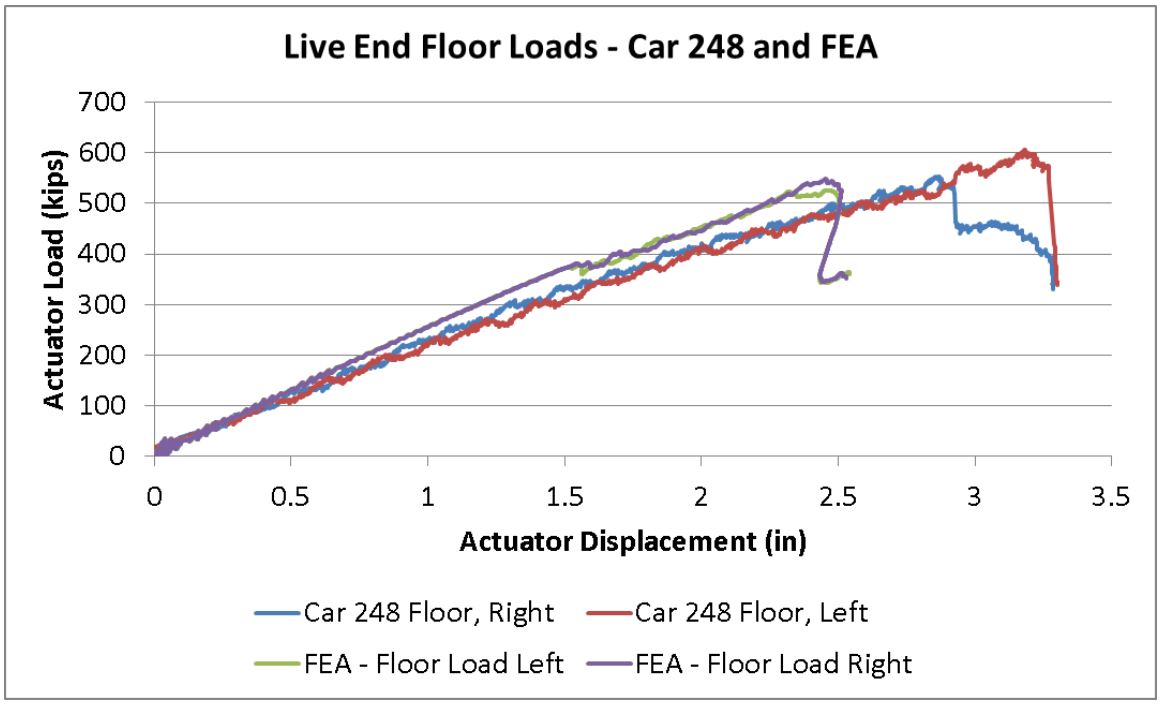

Figure 71. Live Load at Floor for Test of Car 248 and FE Model

The live end load-displacement responses of the roof-level energy absorber supports are plotted in Figure 72 for both the test of Car 248 and the analysis. In both the test and the analysis, the roof reaches its maximum load at an actuator displacement of approximately 1.5 inches. The roof in the model exhibits a softer response than the roof of the test car. Additionally, the model has a lower maximum load of approximately 135 kips at each roof load point, compared with approximately 180 kips at each roof load point in the test.

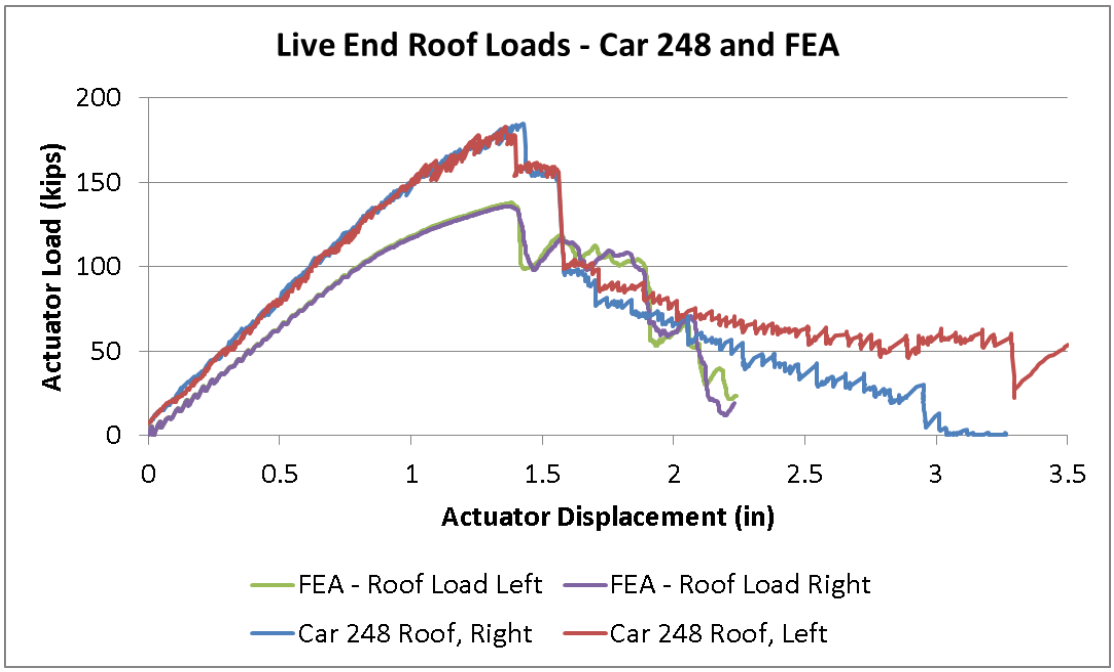

Figure 72. Live Load at Roof for Test of Car 248 and FE Model

The four live end load cell data channels are added together to obtain the total live end load for Car 248. Similarly, the four applied loads on the live end of the FE model are added together to obtain the total applied load. The total end load from the test of Car 248 and the FE model are plotted in Figure 73 against the actuator displacements.

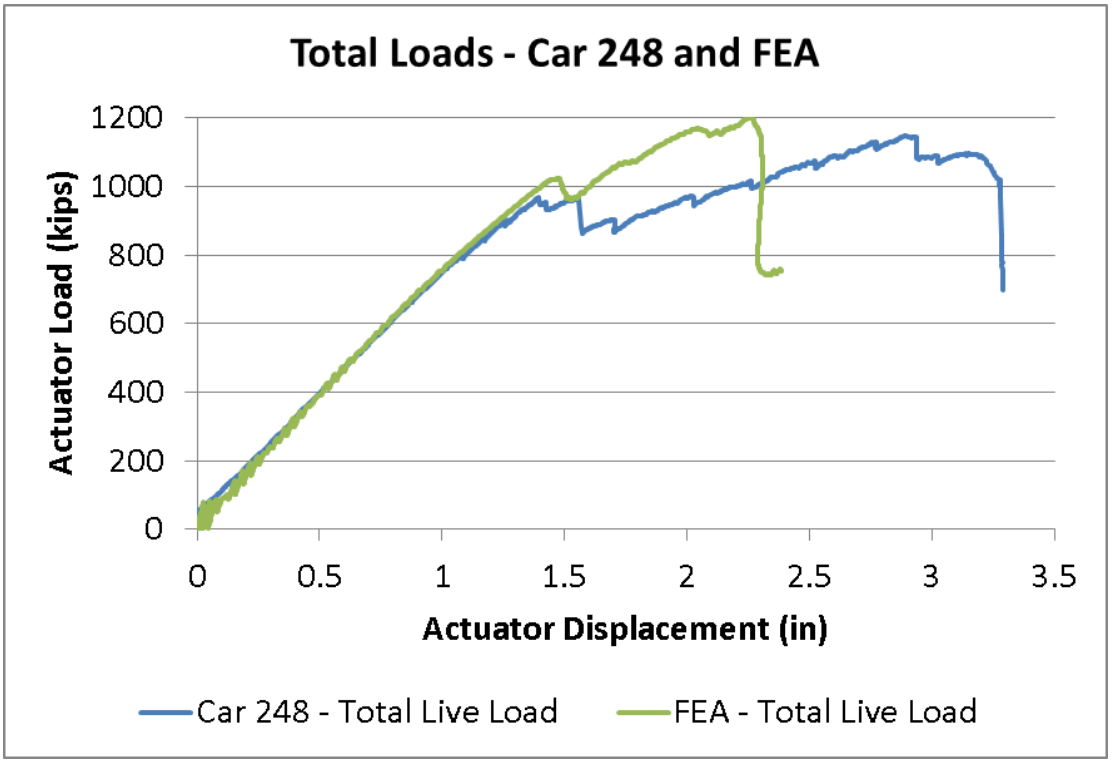

Figure 73. Total Live Loads for Test of Car 248 and FE Model

There is good agreement between the FE results and test data up to the point where the roof buckles at a total load of approximately 1 million pounds. At this point, the load reported in the test and calculated in the FE model both drop. Because the underframe structure has not yet crippled in either case, the total applied load begins to increase as the actuator displacement continues to increase. Following buckling of the roof structure, the FE results are greater than the test results. The FE results reach a global maximum load of approximately 1.2 million pounds and Car 248 reaches a global maximum load of approximately 1.15 million pounds. These maxima occur at different actuator displacements, owing to the model being stiffer than Car 248 actually was following buckling of the roof. Additionally, because the stiffness of the load frame was estimated and added to the displacement results for the FE model, the apparent difference in displacement at the time of crippling may be partially due to this approximation.

4.3.4 Comparison of Car 244 Test Results and FEA Results

Load, strain, and displacement data for Car 244 were collected during its crippling test. These results are compared with the results obtained by the FE analysis results to determine whether the FE analysis is producing a reasonable approximation of the test results.

Because displacement data were measured at both the live end and the restraint end of Car 244, the frame stiffness does not need to be accounted for in order to compare test results with the FE results. The reduction in the car's length was calculated by subtracting the displacement at the restraint end (owing to extension of the frame) from the actuator displacement at the live end of Car 244. Because the FE model was prevented from longitudinal movement at its restraint end, the displacements calculated at its live end are equal to the change in car length.

The floor-level loads from the test of Car 244 and the FE model are compared with one another in Figure 74. All four measurements follow approximately the same initial slope. At both the left and right FE locations the maximum sustained load is below the maximum load recorded during the test.

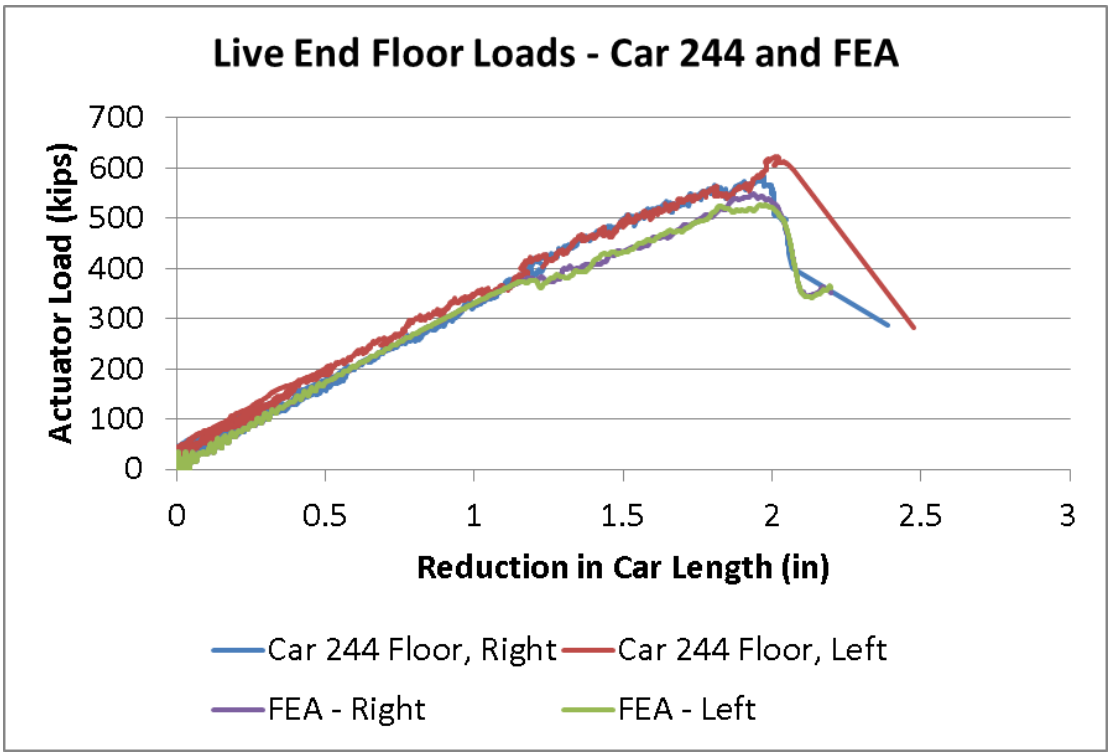

Figure 74. Live Load at Floor for Test of Car 244 and FEA

The live end load-displacement responses of the roof-level energy absorber supports are plotted in Figure 75 for both the test of car 244 and the FE analysis. Both the test results and the FE analysis results have the same shape. The model has an apparent lower stiffness in its roof than the test car did. The model reaches a lower peak load than the test on both the left and right sides. In both the test and the analysis, the roof reaches its peak load at approximately the same displacement.

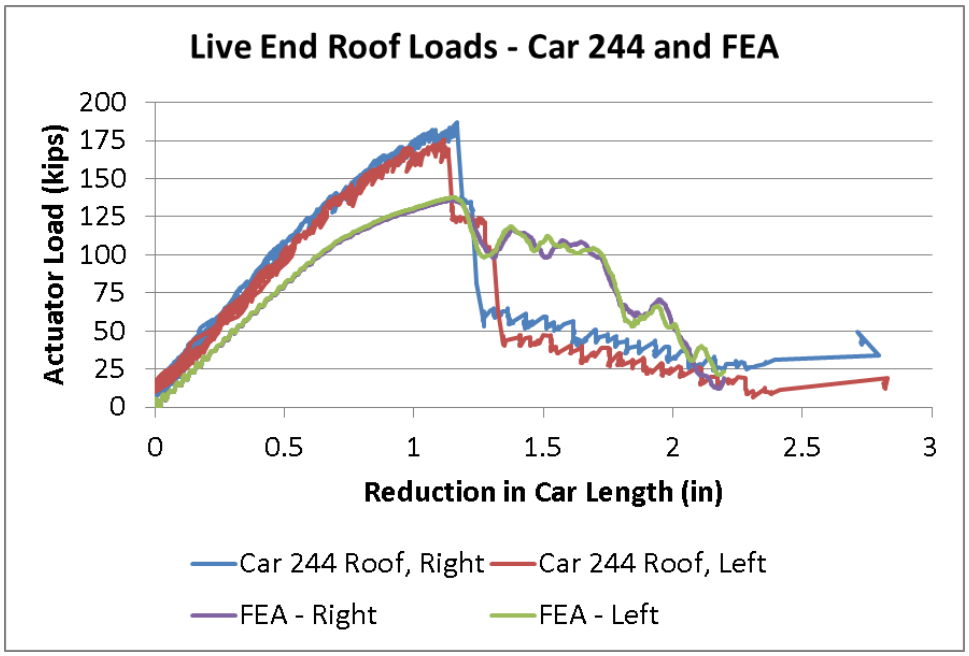

Figure 75. Live Load at Roof for Test of Car 244 and FEA

The post-crippling behavior of the roof is different between the test and analysis. In the test, both the left and right side channels record a sudden drop in load, followed by a more gradual decrease in load. In the FE analysis results, the peak is followed by a gradual drop in load.

The four live end load cell data channels are added together to obtain the total live end load placed on Car 244. Similarly, the four loads on the live end of the FE model are added together to obtain the total simulated applied load. The total end load from the test of Car 244 and the FE model are plotted against the reduction in car length in Figure 76.

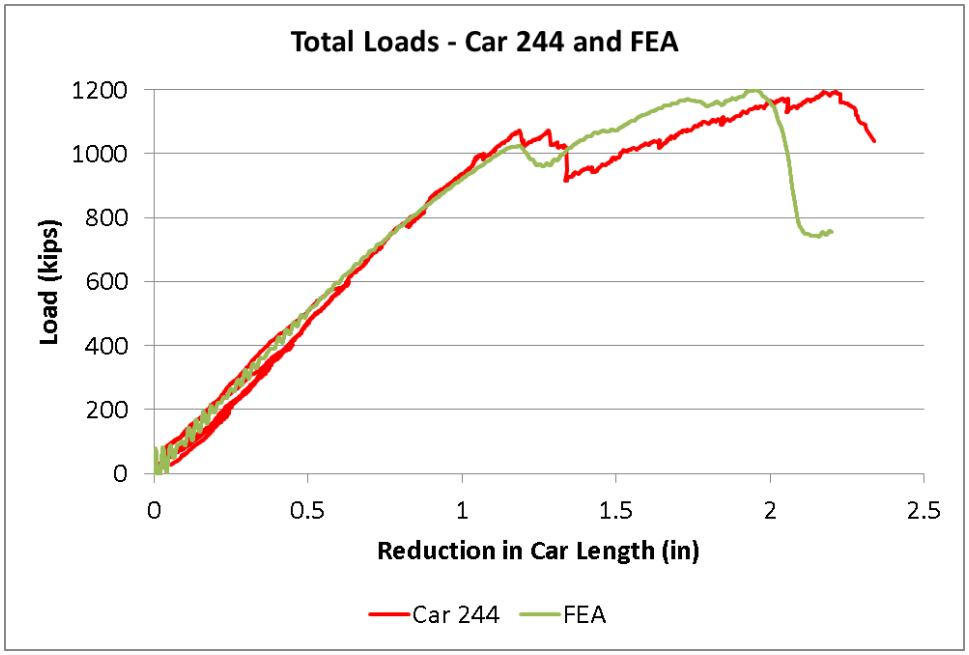

Figure 76. Total Live Loads for Test of Car 244 and FE Model

There is good agreement between the FE model and Car 244's test data prior to the point where the roof buckles. Both the test and the analysis experience a drop in load when the roof has begun to cripple at a load of approximately 1 million pounds. Since the floor structure has not yet crippled, the total load can begin to rise again. In both the test and the model, the second rise in load is along approximately the same slope. Both Car 244 and the model have a global crippling load of nearly 1.2 million pounds. The FE model reached its crippling load after a reduction in length of approximately 1.9 inches and Car 244 reached its crippling load after a reduction in length of approximately 2.2 inches.

The results of the crippling test of Car 244 and the FE analysis are both qualitatively and quantitatively similar to the results from the crippling test of Car 248. The three force-displacement results (two tests, one analysis) are plotted together in Figure 77. In this figure, the horizontal axis represents the live end (actuator) displacement for all three results. Because Car 244 and Car 248 were both tested within the same test frame, the actuator displacements may be directly compared. The FE results in this figure have been adjusted to include the estimated expansion of the test frame. The FE model reached its crippling load after an actuator displacement of approximately 2.2 inches. Car 244 reached its crippling load after an actuator displacement of approximately 2.8 inches, and Car 248 reached its crippling load after an actuator displacement of approximately 2.9 inches.

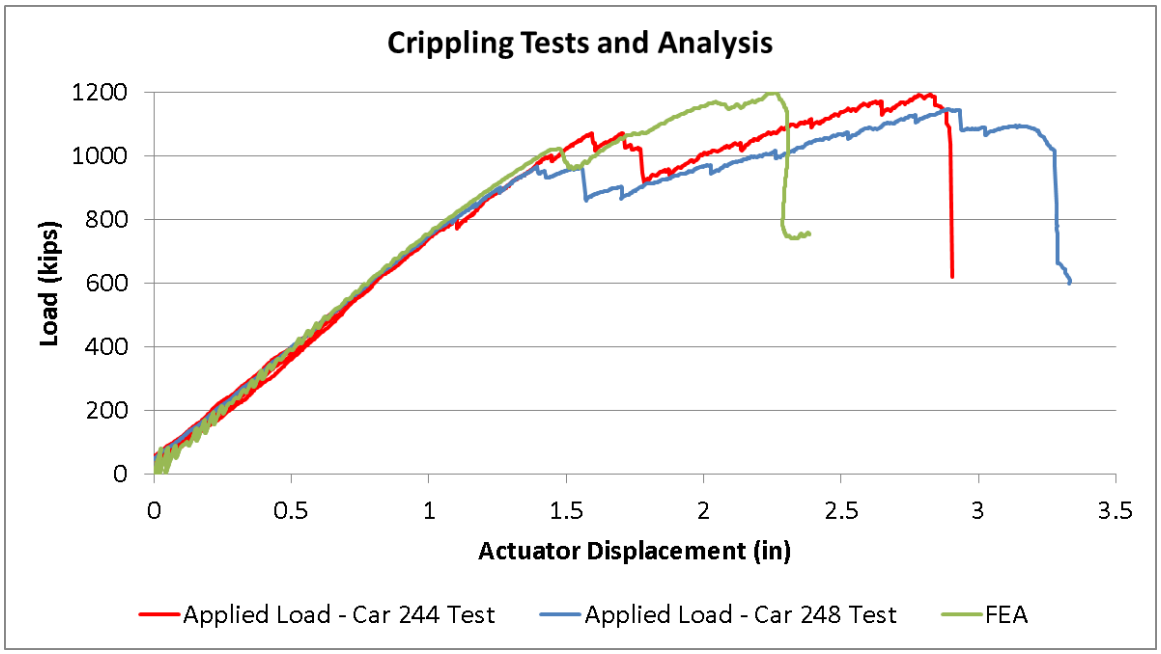

Figure 77. Load-Displacement Behavior for Both Tests and Analyses

There are slight variations in each of the results plotted in Figure 77. The analysis result exhibits slightly higher roof buckling and crippling loads than the test of Car 248, but a slightly lower roof buckling load than Car 244. Car 248's roof buckled at a load slightly below 1 million pounds, while Car 244's roof buckled at a load slightly above 1 million pounds. Car 244's crippling load of nearly 1.2 million pounds is slightly larger than the 1.15 million pound crippling load reached by Car 248. This is likely due to the damage known to preexist in Car 248. The two crippling load magnitudes measured in the tests vary by approximately 50 kips, which is approximately 4 percent of 1200 kips.

The FEA displacement results appear to correlate better in Figure 76 than in Figure 77. In Figure 76, the horizontal axis represents the reduction in car length. This quantity is derived entirely from the results of the FEA and from test data for Car 244. In Figure 77, the horizontal axis represents the displacement of the actuators at the live end of the test cars. The FE results in this figure must be adjusted to account for the stretching of the test frame. These two figures indicate that this approximation represents the behavior of the car well, up to the point of roof buckling. Beyond this point, the frame stiffness approximation results in an overestimate, resulting in an underestimation of the actuator displacement at a given amount of load.

4.3.5 Deformation Modes

In the FEA results the car first experiences buckling of the roof and sidewall structures. As seen in Figure 78, the roof buckle is a fairly long wavelength buckle, spanning from the sixth window to the eighth window. While buckling initiated at the roof and sidewalls, the underframe continued to carry load until the center sill reached its crippling load. In the FEA, the center sill buckled beneath the eighth window. The center sill also experienced a fairly gradual buckling, as can be seen in Figure 78.

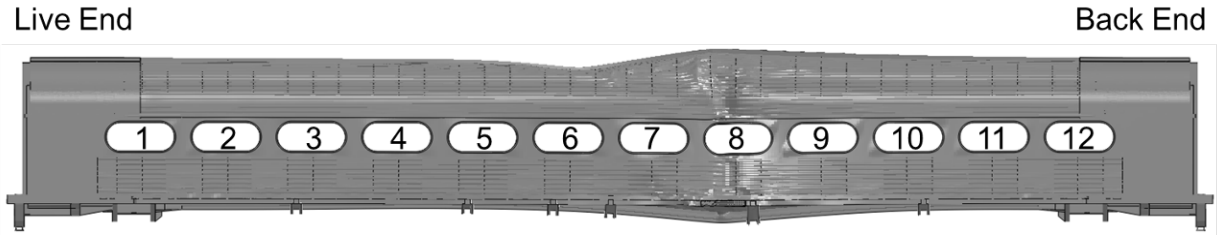

Figure 78. Deformed Shape of Crippled Car in FEA

In the FE model, buckling occurred at both side sills and on the center sill at approximately the same distance from the live end. In the model, each side sill experienced an inward buckling mode of its lower web and flange. The center sill buckled at its upper flange and web. The buckled center sill and one of the two buckled side sills are shown in Figure 79. The center sill has been given a different color from the other members to allow it to stand out in this figure.

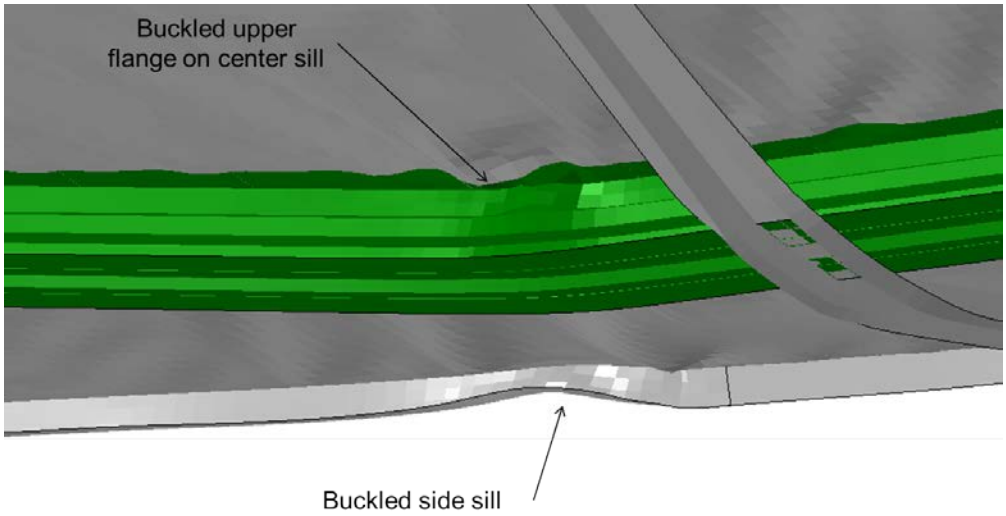

Figure 79. Detail Showing Buckled Center Sill and Side Sill in FEA

In both the test of Car 244 and the test of Car 248, the center sill experienced buckling at several locations along its length. The buckling mode that occurred in the FE model, where the top flange of the center sill buckled, was also observed in both tests. Figure 80 shows an image of the undamaged underframe (taken from the FE model) with photographs of damage from each of the three cases indicated. The approximate location of each upper flange buckle on the center sill is indicated on the underframe.

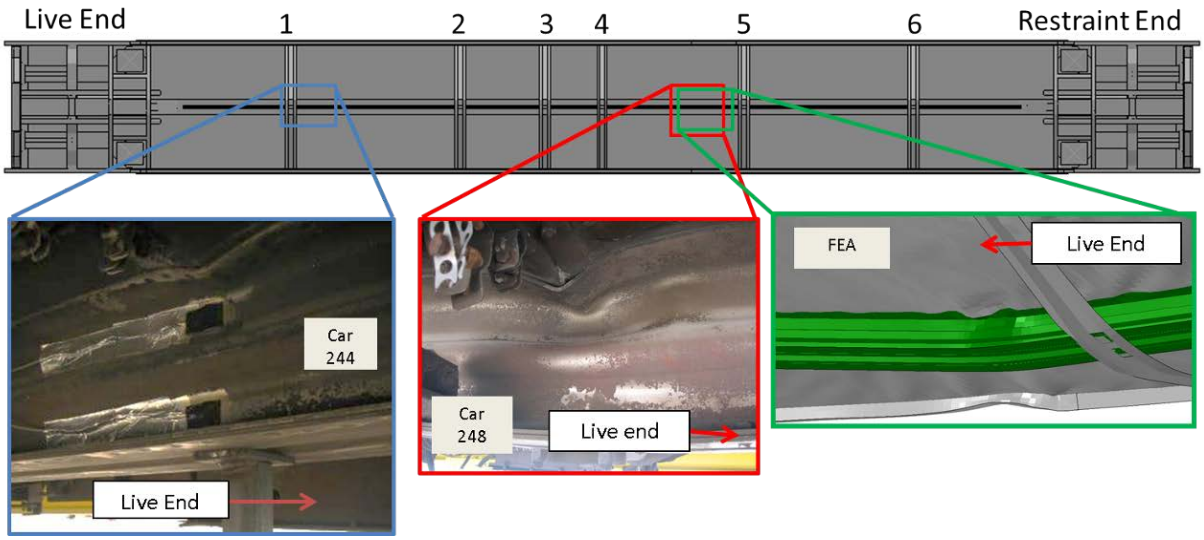

Figure 80. Center Sill Upper Flange Buckle in Car 244, Car 248, and FEA Result

4.3.6 Displacement Results

Displacement measurements were made between the underframe of Car 244 and the ground during its crippling test. At each instrumented location, a VLL array of string pots was used to capture motion in three directions. Displacement data were requested at the corresponding locations in the FE model. The string pot locations are indicated in Figure 37. The full set of string pot results from the crippling test of Car 244 is provided in Appendix D of this report.

The predominant deflections occurred parallel to the applied load, in the longitudinal direction. There is good agreement between the FE analysis and the test of car 244. An exemplar comparison between test and analysis is presented in Figure 81, which shows the longitudinal displacement measured at the center sill at the centerline of the car. The negative displacement indicates motion in the direction of the applied load in both the test and the model.

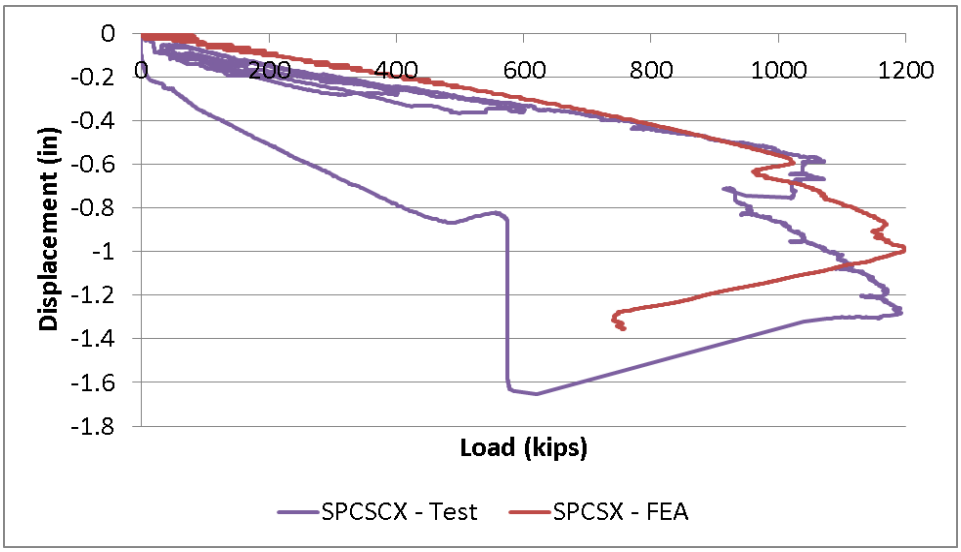

Figure 81. Longitudinal Displacement at Center Point of Car, Car 244 Test and FEA

Lateral displacement data were also collected during both the test and analysis. The lateral displacements were small compared to the longitudinal displacements for both the test of Car 244 and the analysis. The car exhibited very little lateral motion prior to the buckling of the roof. Lateral motion is observed from the onset of roof buckling through unloading of the car. The largest magnitude of lateral deflection in the test was measured at the center sill at the centerline of the car. This result is plotted in Figure 82 alongside the FE results for the same location. Although the FE model was not constrained against lateral motion, it does not exhibit very much lateral motion. A small amount of lateral motion occurs once buckling begins to occur, as was the case with the car in the test.

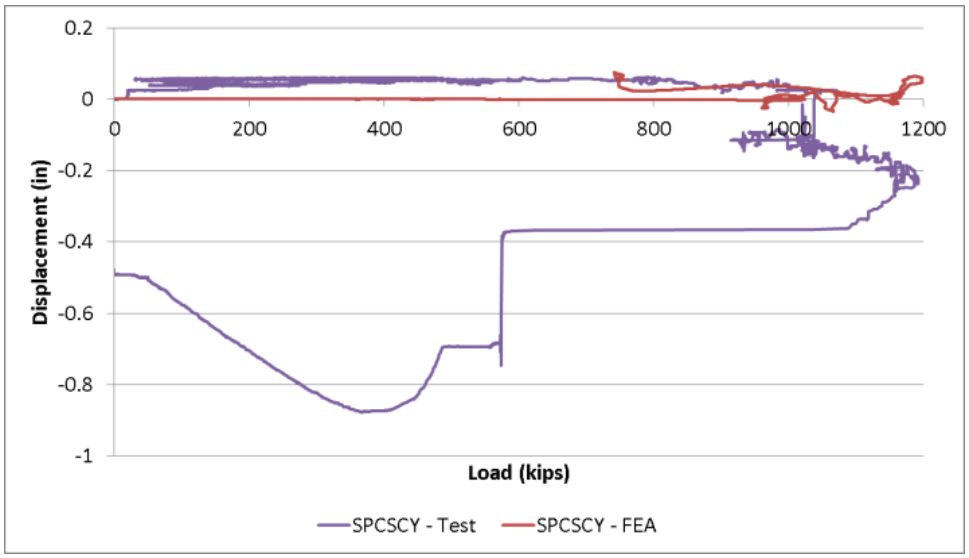

Figure 82. Lateral Displacement at Center Point of Car, Car 244 Test and FEA

Vertical displacement was measured at the same locations as longitudinal and lateral displacements in the test of Car 244. While Car 244 exhibited significant bending deflection during the conventional buff strength test (Figure 21), the car demonstrated a different behavior in the crippling test. In the 800-kip test, the load was applied and reacted at the buff stops,

within the draft sills. This single point load resulted in a significant bending moment developing in the car body. In the crippling test, load was applied to the energy absorber supports at the floor and roof levels. This loading scheme resulted in a smaller bending moment developing in the car, causing smaller vertical deflections to occur in the underframe.

The vertical displacement measured at each instrumented location on Car 244 is plotted against the distance of that instrumented location from the end of the side sill on the live end of the car in Figure 83. Each data series in this figure represents a "snapshot" of the mode of deformation at a particular load level. With a total applied load of 1 million pounds (1,000 kips) and less, the car experiences very little vertical deflection. Above 1 million pounds, buckling has started to occur within the body of the car. The largest deformations are measured near the live end of the car where the center sill crippled.

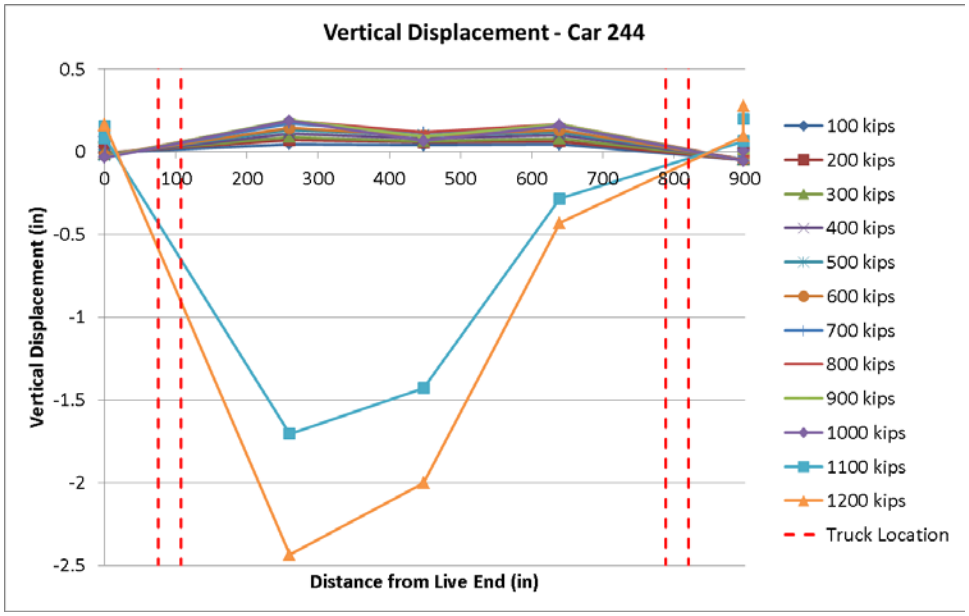

Figure 83. Vertical Displacement along Length of Car 244 in Crippling Test

An analogous plot was created for the FE results and is shown in Figure 84. As with the tested car, the FE model initially experiences very little vertical deflection. The test and the analysis both experienced different initial modes of deformation. Where Car 244 exhibited an "M" shaped bending mode with 2 inflection points, the FEA results indicate a shallow inverted "U" shaped mode. This may indicate that the FE model is underweight compared to Car 244, as the center of the model experiences greater vertical uplift under small bending moments.

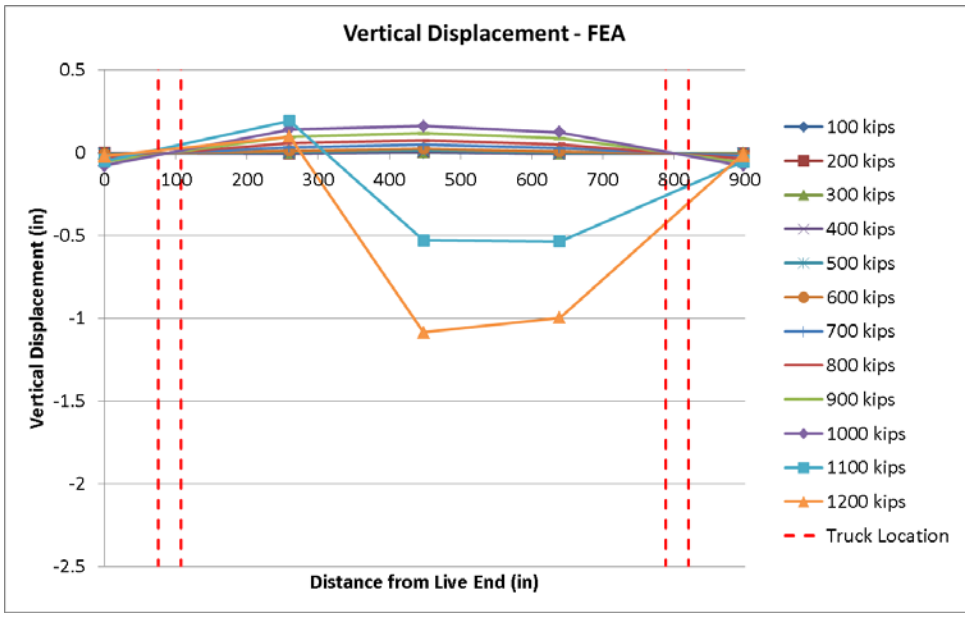

Figure 84. Vertical Displacement along Length of FE Model in Crippling Simulation

As the load increased beyond 1 million pounds, both the model and Car 244 began to exhibit fairly large vertical deflections. Because Car 244 and the FE model experienced center sill crippling at different locations along their lengths, the vertical bending modes are somewhat different as crippling occurs. Buckling occurs further away from the live end of the car in the model than was observed in the test. The model also indicates smaller downward deflections than were recorded during the test of Car 244.

4.3.7 Strain Results

Longitudinal strain measurements were made on the structural members shown in Figure 12. Selected strain results are discussed in this section of this report; the complete set of longitudinal strain data is provided in Appendix C.

Strain data were collected on the center sill at five cross-sections. At each cross-section one gage was placed on each quadrant of the center sill's webs (upper left, upper right, lower left, lower right). Figure 85 is a plot of the longitudinal strain in the center sill as measured in the gages on the bottom half of the member. The horizontal axis indicates the undeformed distance between the datum of the car (the center of the restraint end body bolster) and each strain gage. The strains in this figure are the result of an 830-kip total load applied to the car. The error bars on the test data indicate a +/-20 percent tolerance on the measured test data. The strains calculated along the length of the center sill in the FEA result are plotted as a continuous line in this figure.

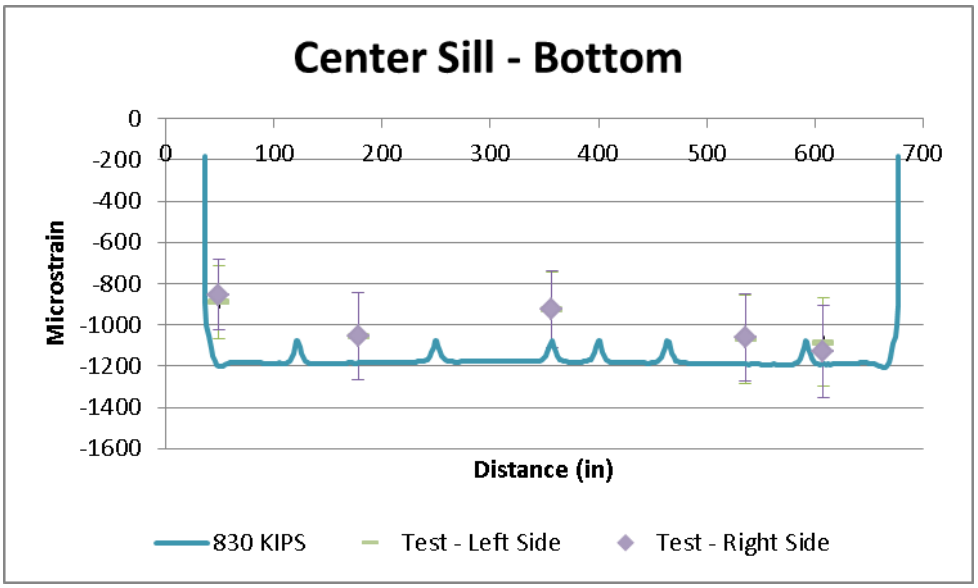

Figure 85. Longitudinal Strain in Center Sill at 830 kips, Crippling Test

The strain data measured in the test indicate a relatively constant level of strain in the center sill at this load. At each cross-section, the strain measured on the left and right sides of the center sill of the tested car are nearly equal. The FE results also indicate a constant level of strain along the length of the center sill. The peaks that occur along the plot of the FE result coincide with locations of the six cross members that connect the center sill with the side sills. At the ends of the center sill, the model indicates a steep strain gradient where the center sill ends at the body bolster. If this high gradient is present in the physical car as well as the model, it emphasizes the need to place strain gages with extreme care. A small difference in placement can result in a large difference in the strain measurement. Although the FE results are not within +/-20 percent of the FE results at the left-most cross-section in this figure, the test and analysis results would overlay one another if the strain gage were placed a few inches closer to the restraint end.

A second plot of longitudinal strain versus distance along the center sill for the strain measurements in the bottom half of the web is shown in Figure 85. In this figure the strain measurements are taken at a total applied load of approximately 1.18 million pounds. This load is just prior to crippling in both the test and the model. The test data at 1.18 million pounds are similar in appearance to the test data at a load of 830 kips (Figure 84) with the exception of the measurement location at approximately 600 inches. Because the datum point on this car is at the restraint end, this cross-section is the closest to the live end of the tested car. This set of center sill strain gages happened to be adjacent to an area of the center sill that buckled during the test (Figure 59).

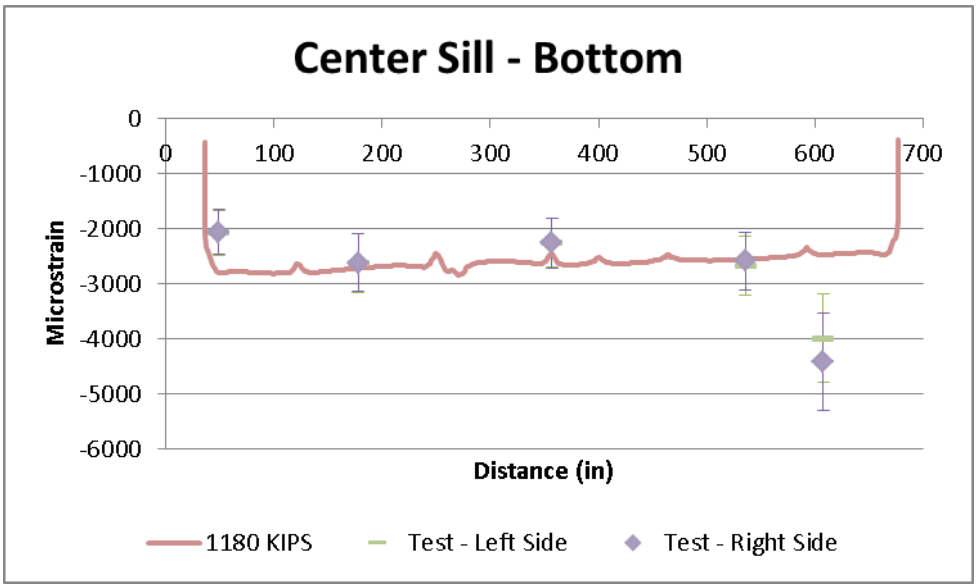

Figure 86. Longitudinal Strain in Center Sill at 1180 kips, Crippling Test

The strain gages adjacent to the buckle indicate a very high level of strain in the center sill at a load just prior to crippling. However, even though the crippling load is a global measurement for the entire car, the strain data in the previous figure indicate that the center sill's buckling is a localized behavior. The center sill remains elastic at the cross-section away from this local buckle even at a load just below the crippling load of 1.2 million pounds.

Figure 86 also contains the strain-distance results calculated from the FE model along the entire length of the center sill for elements in the lower half of the web. Except at the crippling cross-section, the FE results compare favorably with the test data. Because the FE model experienced crippling at a different location than Car 244, there is not a steep change in strain data at the same location as the test car. The FE model's center sill buckled at a location adjacent to a cross-bearer on the restraint end of the car (Figure 78). A small inflection between 200 and 300 inches can be observed in the FE results in Figure 86; this is the location where the incipient buckle will cripple the model.

While the FE model and the tested cars each experienced crippling at different locations, the overall crippling behaviors were very similar. Specifically, the global force-displacement characteristics and the sequences of structural failures were similar for all three results. In order to assess the strain behaviors of Car 244 and the FE model at the location where center sill buckling occurred, data from one location in the test but a different location in the model must be compared. Figure 87 shows an image of the crippled center sill from the FE model and a photograph of one buckled location on the center sill of Car 244. The approximate location of each of these areas of damage is indicated on a profile view of the undeformed car in this figure. Two elements are highlighted in the image of the center sill taken from the FE model, shown at the right in this figure. These two elements correspond to the approximate placement of strain gages on the web of the center sill of Car 244. Two such strain gages can be seen in the left hand side of this figure.

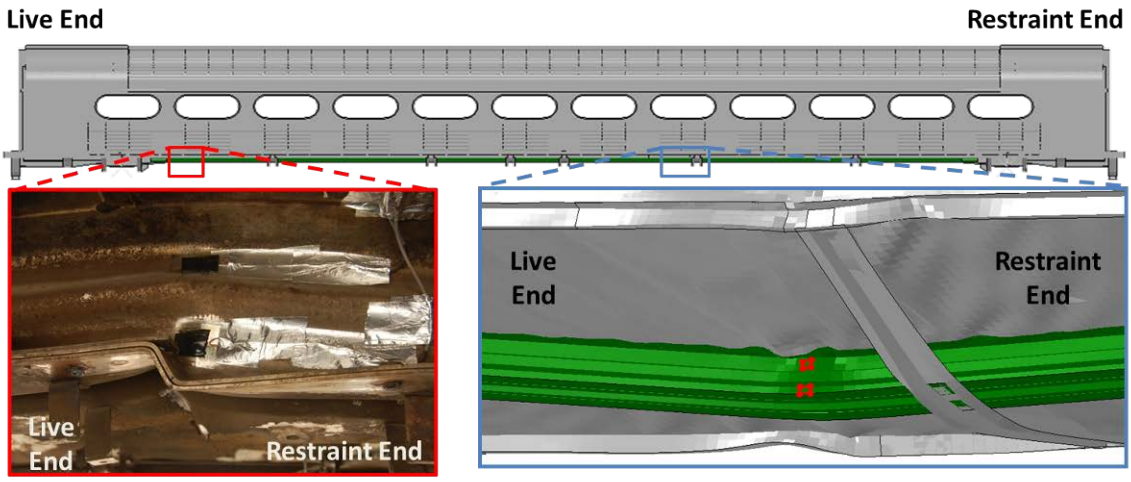

Figure 87. Crippling Locations for Strain Comparison, FEA (right) and Car 244 (left)

The strain versus applied load results from the crippled location on the center sill of Car 244 and the FEA result are plotted in Figure 88. This figure shows the measurements from the four test strain gages on the left; the right shows the calculated strains in the FEA from four elements at the corresponding locations on the center sill at the buckle.

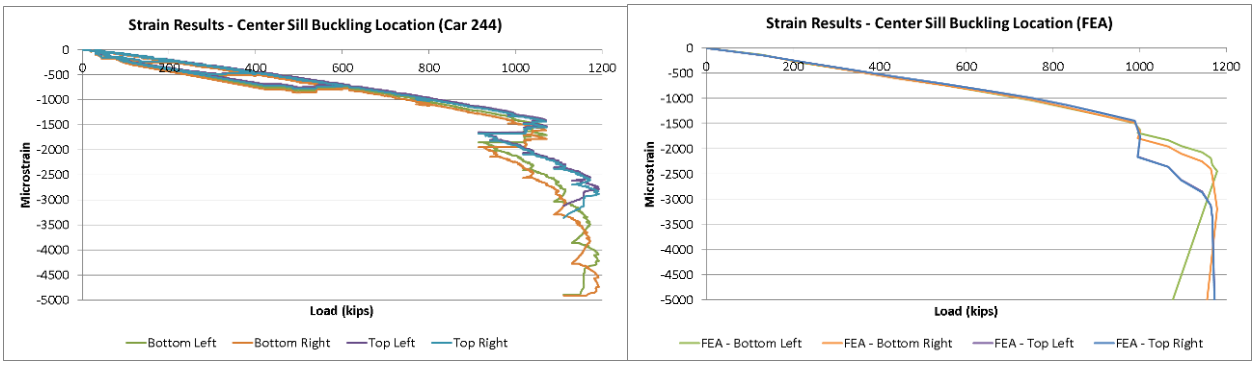

Figure 88. Strain vs. Load Behavior at Center Sill Buckling Locations, Test (left) and FEA (right)

In both the test and the analysis, the strain behaviors are very similar. In both cases, the four strain results overlay one another up to a load of approximately 1 million pounds. The inflection point at approximately 1 million pounds corresponds with buckling of the roof structure. Beyond this load the four strain results begin to diverge in both the test and the FEA. In the test, the two gages at the bottom of the center sill indicate a more rapid change in strain with additional load than do the two at the top. In the FE results, the two locations at the top of the center sill experience greater changes than the two locations at the bottom. Figure 87 shows that the FE results experienced a buckling in the top of the center sill while Car 244's center sill buckled at its bottom. The strain gauges installed on the car during this test had a maximum capacity of +/-3,000 microstrain. Although the gage reports values up to -5,000 microstrain, these results have greatly exceeded the intended range of the strain gage.

5. Conclusions

FRA has sponsored research at the Volpe Center examining the OVI of passenger cars since 2006. The ETF adopted criteria and procedures for evaluating OVI based, in part, on the results of this FRA research. In 2011, FRA performed a series of OVI tests as a means of evaluating the methodology developed by the ETF and developing confidence in the results obtained from applying the methodology. Two types of tests were performed in this series: a conventional 800,000-pound buff strength test and two destructive crippling tests. A corresponding FE analysis was performed for each type of test.

The test articles chosen for this program were two Budd Pioneer passenger cars that had been retrofitted with CEM systems during a previous FRA research program. These passenger cars were originally constructed to comply with the 800,000-pound line of draft load requirement. With the addition of the CEM components, these cars feature two different load paths for longitudinal loads: one load path for service loads and a different load path for collision loads. These cars represent an 800,000-pound compliant vehicle with a nonconventional collision load path. This particular design permitted the ETF's criteria and procedures for collision-path loading to be used to evaluate the load capabilities of a vehicle designed to the conventional elastic load requirement.

A conventional 800,000-pound buff strength test was used to demonstrate that a passenger car that had been involved in a series of crash tests was still structurally sound. This test was also used to provide data for validating an FE model of the passenger car. Car 244 received minor repairs prior to this test, including the placement of a patch on each side sill over an area with small cracks. The car successfully met the requirements of the test, and the results were in satisfactory agreement with the FE model. The key results that were compared between test and model were the longitudinal load-displacement behavior, the vertical deflection mode, and strains in key longitudinal members.

Following the successful validation of the FE model with the 800-kip test data, the model was modified to represent the condition of the test car in the crippling test. In order to permit loads to be applied along the collision load path, the endframes and energy absorbing components of the CEM system were removed. These components were also removed from the FE model. The model was used to simulate loading of the carbody up to its crippling load; it estimated a crippling load of approximately 1.19 million pounds.

A newly constructed loading frame and hydraulic control system at TTC were used to perform the crippling tests. A shakedown test was performed to ensure the proper operation of the new system before the crippling test of Car 244 was performed. The shakedown test featured limited instrumentation installed on a car of similar design, Pioneer Car 248. The car was loaded until crippling occurred at a load of 1.15 million pounds.

Following the successful shakedown test, the fully instrumented test of Car 244 was run. The instrumentation used in this test included displacement transducers on the underframe of the car, load cells at each loading and restraint location, and strain gages on key longitudinal members. Car 244 behaved similarly to Car 248 in reaching its crippling load. Both cars also experienced global behavior similar to the FE model, although there were differences in the locations where

buckling occurred in each case. Car 244 had a measured crippling load of nearly 1.2 million pounds.

This research program has demonstrated that a carefully executed program of elastic testing and model validation is capable of estimating the crippling behavior of a passenger railcar. This program has also confirmed the sound technical basis for the OVI criteria and procedures adopted by the ETF. The results of the tests and analyses performed in this program indicate that the alternative OVI methodology provides an effective means of evaluating the OVI of passenger rail equipment.

6. References

[1] Petition of Capital Metropolitan Transportation Authority for Shared Lease and Waiver of Federal Railroad Administration Regulations. Docket No. FRA-2006-25040.

[2] Petition of the Denton County Transportation Authority for Waiver Acceptance of non-Compliant Self-Propelled Rail Vehicles (Stadler GTW 2/6 Diesel Multiple Units). Docket No. FRA-2010-0180.

[3] Petition of Peninsula Corridor Joint Powers Board/Caltrain for Approval of Mixed Use and Waiver of Certain Federal Railroad Administration Regulations. Docket No.FRA-2009-0124.

[4] DesertXpress Enterprises, LLC's Petition for Waivers from Federal Railroad Administration Regulations. Docket No.FRA-2010-0098.

[5] Federal Register/Vol. 74, No. 156/ Friday, August 14, 2009/ Notices. Department of Transportation, Federal Railroad Administration [Docket No. FRA-2000-7257; Notice No. 56]. *Railroad Safety Advisory Committee (RSAC); Working Group Activity Update. Page 41181.*

[6] "Technical Criteria and Procedures for Evaluating the Crashworthiness and Occupant Protection Performance of Alternatively Designed Passenger Rail Equipment for Use in Tier I Service," U.S. Department of Transportation Report No. DOT-FRA-ORD-11/22. Washington, DC: Federal Railroad Administration, Office of Railroad Policy Research and Development, October 2011.

[7] White, J.H., "The American Passenger Railway Car," The John Hopkins University Press, 1978.

[8] U.S. Department of Transportation, Federal Railroad Administration, "49 CFR Part 216 et al., Passenger Equipment Safety Standards; Final Rule," Federal Register, May 12, 1999.

[9] Carolan, M., Perlman, B.A., Tyrell, D., "Evaluation of Occupant Volume Strength in Conventional Passenger Railroad Equipment," American Society of Mechanical Engineers, Paper No. RTDF2008-74026, September 2008.

[10] Carolan, M., Muhlanger, M., "Strategy for Alternative Occupant Volume Testing" American Society of Mechanical Engineers, Paper No. RTDF2009-18025, October 2009.

[11] Carolan, M., Muhlanger, M.P. "Update on Alternative Occupant Volume Testing." American Society of Mechanical Engineers, Paper No. JRC2010-36020., April 2010.

[12] Kirkpatrick, S., and MacNeil, R. “Development of a Computer Model for Prediction of Collision Response of a Railroad Passenger Car.” Proceedings of the 2002 IEEE/ASME Joint Railroad Conference, Institute of Electrical and Electronics Engineers, Catalog Number CH37356-TBR, 2002.

[13] Jacobsen, K., Tyrell, D., and Perlman, A.B. “Impact Test of a Crash-Energy Management Passenger Rail Car.” American Society of Mechanical Engineers, Paper No. RTD2004-66045, April 2004.

[14] Abaqus/Explicit Version 6.10. Dassault Systemes Simulia Corp., Providence, RI, USA. 2010.

[15] MathCAD 15. Parametric Technology Corporation, 2011.

Appendix A.
Estimated Car Stiffness

In the crippling tests of Pioneer 248 and 244, the displacement at each load point on the live end of the car was controlled so as to keep all four load points at the same displacement at any given point in time. Because the car was supported at the back end at the corresponding locations as on the front, the load was nearly entirely axial with little bending component. As a check on the FE results, the car was approximated as an axially loaded member and its stiffness was calculated.

For an axially loaded member:

$$\Delta = PL/AE \qquad \text{(Eq. 1)}$$

Where

Δ - change in axial length

P – applied load

L – member length

A – cross-sectional area

E – Young's modulus

$k = P/\Delta$

Through rearrangement and substitution,

$$k = EA/L \qquad \text{(Eq. 2)}$$

The Budd Company calculated the Pioneer car to have an effective cross-sectional area of 30.8 in^2. The length from the energy absorber supports on the live end to the energy absorber supports on the back end measures approximately 871.75 inches. The carbody is made of stainless steel, with a Young's modulus of 3×10^7 psi. Substituting these values in Equation 2 gives the estimated stiffness of the car as:

$$k_{car} = (3 \times 10^7)(30.8)/(871.75) = \underline{1{,}006 \text{ kips/inch}}$$

The estimated stiffness of the car is plotted against the applied load versus change-in-car-length data from Car 244 and the crippling FE analysis in Figure A 1.

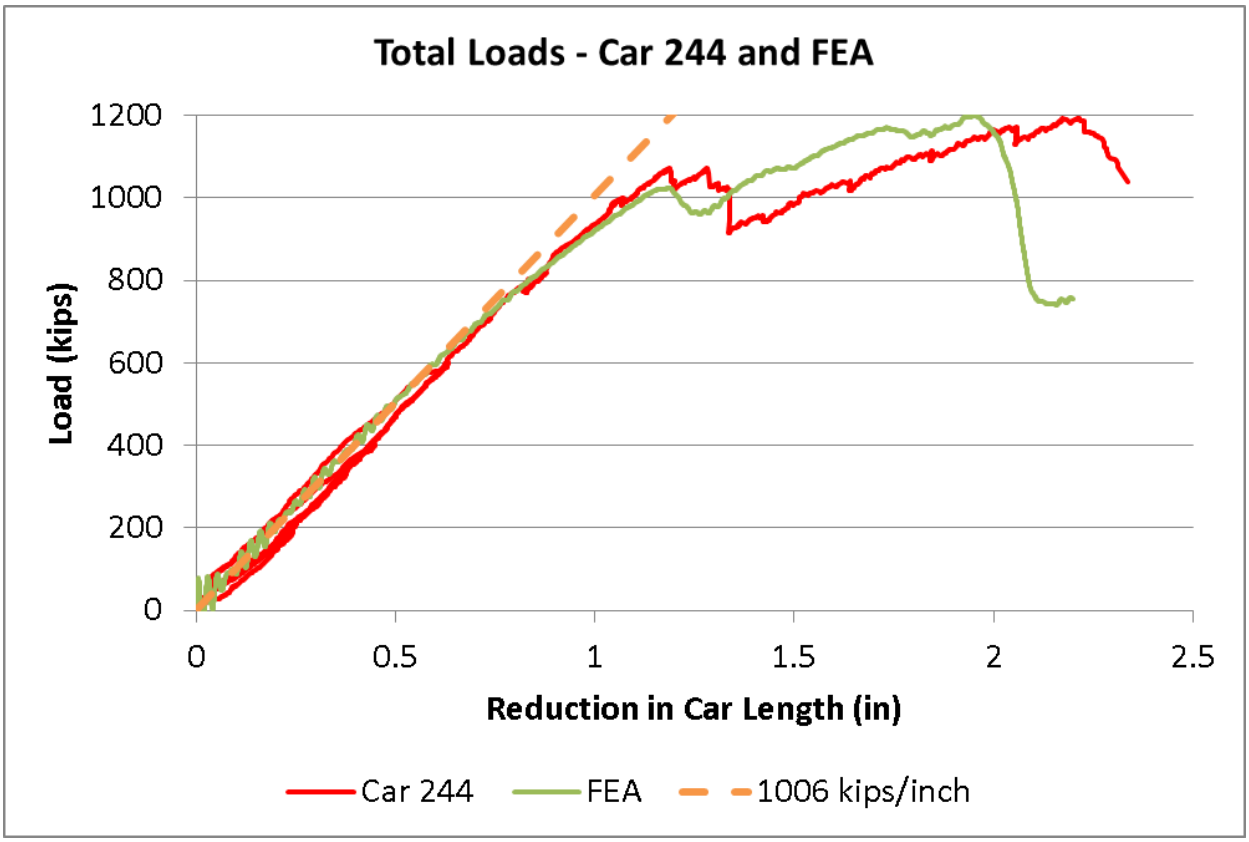

Figure A 1. Estimated Car Stiffness and Reduction in Car Length Results

Appendix B.
Estimated Frame Stiffness

During the shakedown test of Car 248, the only displacement measurements made were of the stroke length of each hydraulic actuator. Because the test frame expanded in response to the load transmitted through the car, the expansion of the frame must be taken into account when modeling the response of the system. The frame is made up of four longitudinal members: two upper beams and two lower beams. The stiffness of each type of member is calculated below.

Upper Member

Each beam is approximated as an axially loaded member. From Equation 2,

$$k=EA/L$$

For steel beams, Young's modulus is 3×10^7 psi. The measured length of the frame, from lateral end restraint at the live end to lateral end restraint at the restrained end, is 1017.5 inches. The upper members are beams having a cross-sectional area of 20.6 in^2. Substituting these values in Equation 2 gives the estimated upper member stiffness as

$$k_{upper} = (3x10^7)(20.6)/(1017.5) = 607 \text{ kips/inch}$$

Lower Member

Each beam is approximated as an axially loaded member. From Equation 2,

$$k=EA/L$$

For steel beams, Young's modulus is 3×10^7 psi. The measured length of the frame, from lateral end restraint at the live end to lateral end restraint at the restrained end, is 1017.5 inches. The lower members are beams having a cross-sectional area of 35.9 in^2. Substituting these values in Equation 2 gives the estimated upper member stiffness as

$$k_{lower} = (3x10^7)(35.9)/(1017.5) = 1{,}058 \text{ kips/inch}$$

System Stiffness

The four longitudinal beams making up the frame can be represented by a single spring of equivalent stiffness as follows:

$$k_{frame}=(2 \times k_{upper}) + (2 \times k_{lower}) = 3{,}330 \text{ kips/inch}$$

The combined stiffness of the car and frame is referred to as the system stiffness. Because the hydraulic actuators and the frame are grounded at the live end, the load-displacement outputs of these actuators describe the overall system behavior.

$$1/k_{sys} = 1/k_{car} + 1/k_{frame}$$

$$k_{sys} = \underline{773 \text{ kips/inch}}$$

The estimated system stiffness is plotted against the load-actuator displacement results from the two crippling tests and the crippling FEA in Figure A 2.

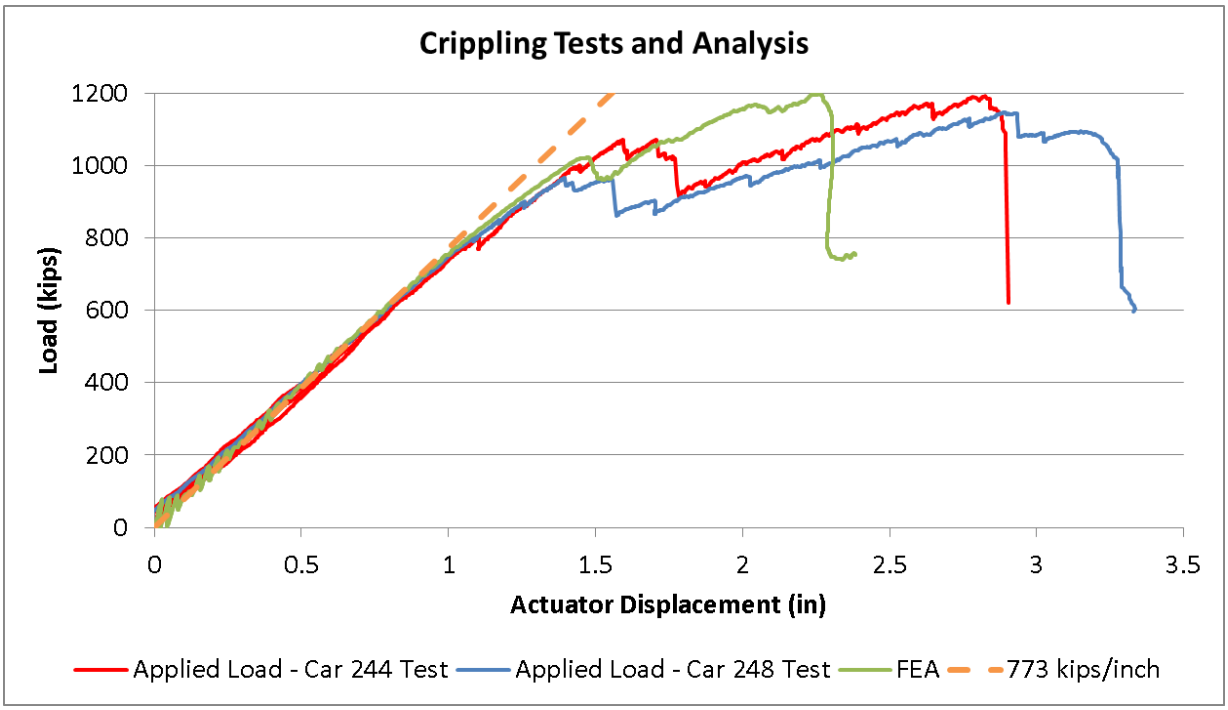

Figure A 2. Estimated System Stiffness and Load-Actuator Displacement Results

Appendix C.
Car 244 Strain Data and FE Results

A total of 64 single-axis strain gages were installed for both the 800-kip elastic test and the crippling test of car 244. In the crippling test, additional strain gages were placed at the roof and floor energy absorber supports where the load was applied and reacted. The strain gage channel names are provided in Table A 1.

Table A 1. Strain Gage Channel Names and Locations

Channel Name	Instrumented Member	Location
S1CSBL	Center Sill	Cross-Section 1, bottom left
S1CSTL	Center Sill	Cross-Section 1, top left
S1CSBR	Center Sill	Cross-Section 1, bottom right
S1CSTR	Center Sill	Cross-Section 1, top right
S1SSL	Side Sill	Cross-Section 1, left side
S1SSR	Side Sill	Cross-Section 1, right side
S1BRL	Belt Rail	Cross-Section 1, left side
S1BRR	Belt Rail	Cross-Section 1, right side
S1RRL	Roof Rail	Cross-Section 1, left side
S1RRR	Roof Rail	Cross-Section 1, right side
S1PL	Purlin	Cross-Section 1, left side
S1PR	Purlin	Cross-Section 1, right side
S2CSBL	Center Sill	Cross-Section 2, bottom left
S2CSTL	Center Sill	Cross-Section 2, top left
S2CSBR	Center Sill	Cross-Section 2, bottom right
S2CSTR	Center Sill	Cross-Section 2, top right
S2SSL	Side Sill	Cross-Section 2, left side
S2SSR	Side Sill	Cross-Section 2, right side
S2BRL	Belt Rail	Cross-Section 2, left side
S2BRR	Belt Rail	Cross-Section 2, right side
S2RRL	Roof Rail	Cross-Section 2, left side
S2RRR	Roof Rail	Cross-Section 2, right side
S2PL	Purlin	Cross-Section 2, left side
S2PR	Purlin	Cross-Section 2, right side
S3CSBL	Center Sill	Cross-Section 3, bottom left

Channel Name	Instrumented Member	Location
S3CSTL	Center Sill	Cross-Section 3, top left
S3CSBR	Center Sill	Cross-Section 3, bottom right
S3CSTR	Center Sill	Cross-Section 3, top right
S3SSL	Side Sill	Cross-Section 3, left side
S3SSR	Side Sill	Cross-Section 3, right side
S3BRL	Belt Rail	Cross-Section 3, left side
S3BRR	Belt Rail	Cross-Section 3, right side
S3RRL	Roof Rail	Cross-Section 3, left side
S3RRR	Roof Rail	Cross-Section 3, right side
S3PL	Purlin	Cross-Section 3, left side
S3PR	Purlin	Cross-Section 3, right side
S4CSBL	Center Sill	Cross-Section 4, bottom left
S4CSTL	Center Sill	Cross-Section 4, top left
S4CSBR	Center Sill	Cross-Section 4, bottom right
S4CSTR	Center Sill	Cross-Section 4, top right
S4SSL	Side Sill	Cross-Section 4, left side
S4SSR	Side Sill	Cross-Section 4, right side
S4BRL	Belt Rail	Cross-Section 4, left side
S4BRR	Belt Rail	Cross-Section 4, right side
S4RRL	Roof Rail	Cross-Section 4, left side
S4RRR	Roof Rail	Cross-Section 4, right side
S4PL	Purlin	Cross-Section 4, left side
S4PR	Purlin	Cross-Section 4, right side
S5CSBL	Center Sill	Cross-Section 5, bottom left
S5CSTL	Center Sill	Cross-Section 5, top left
S5CSBR	Center Sill	Cross-Section 5, bottom right
S5CSTR	Center Sill	Cross-Section 5, top right
S5SSL	Side Sill	Cross-Section 5, left side
S5SSR	Side Sill	Cross-Section 5, right side
S5BRL	Belt Rail	Cross-Section 5, left side
S5BRR	Belt Rail	Cross-Section 5, right side
S5RRL	Roof Rail	Cross-Section 5, left side

Channel Name	Instrumented Member	Location
S5RRR	Roof Rail	Cross-Section 5, right side
S5PL	Purlin	Cross-Section 5, left side
S5PR	Purlin	Cross-Section 5, right side
S6SSL	Side Sill	Cross-Section 6, left side
S6SSR	Side Sill	Cross-Section 6, right side
S6BRL	Belt Rail	Cross-Section 6, left side
S6BRR	Belt Rail	Cross-Section 6, right side
SRBL*	Roof EA Support	B-end, left side
SRBR*	Roof EA Support	B-end, right side
SBPEAM1L*	Primary EA Support	B-end, outboard, left side
SBPEAM2L*	Primary EA Support	B-end, inboard, left side
SBPEAM1R*	Primary EA Support	B-end, outboard, right side
SBPEAM2R*	Primary EA Support	B-end, inboard, right side
SRAL*	Roof EA Support	A-end, left side
SRAR*	Roof EA Support	A-end, right side
SAPEAM1L*	Primary EA Support	A-end, outboard, left side
SAPEAM2L*	Primary EA Support	A-end, inboard, left side
SAPEAM1R*	Primary EA Support	A-end, outboard, right side
SAPEAM2R*	Primary EA Support	A-end, inboard, right side

*Channel only used in crippling test

800-kip Buff Strength Test

Cross-Section 1

Purlins

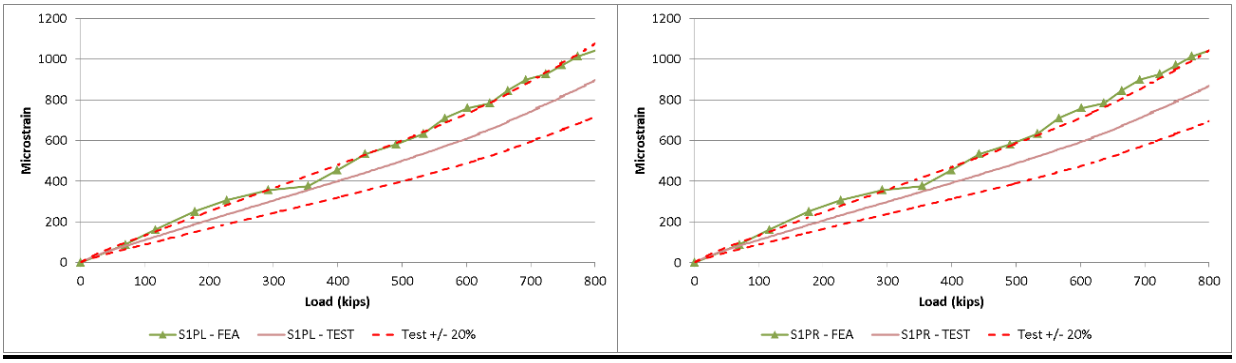

Roof Rails

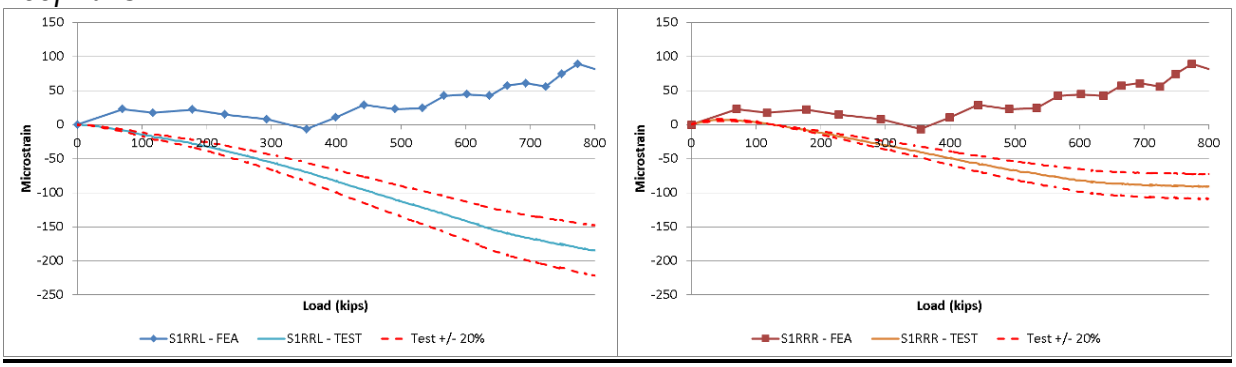

Belt Rails

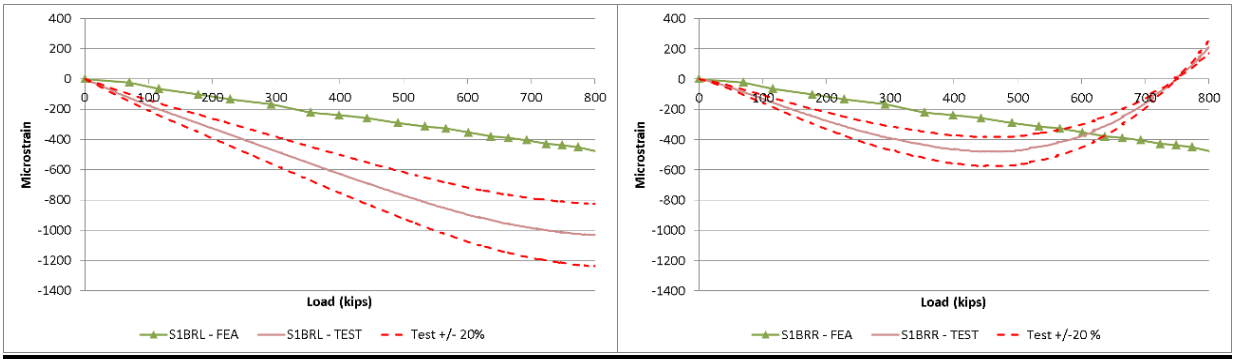

Side Sills

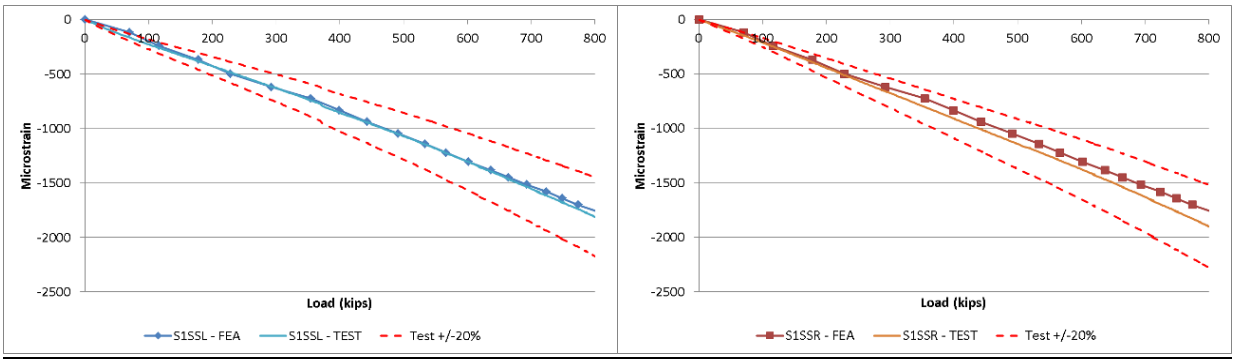

Center Sill, Top

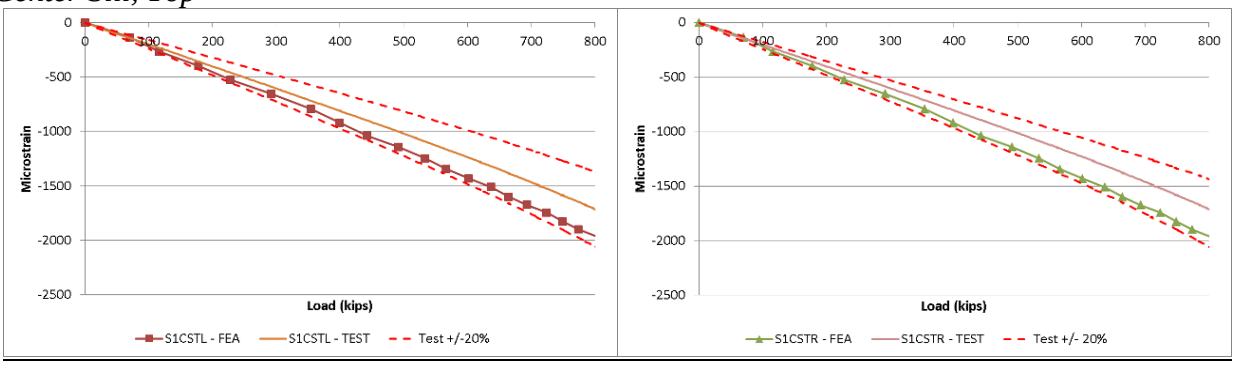

Center Sill, Bottom

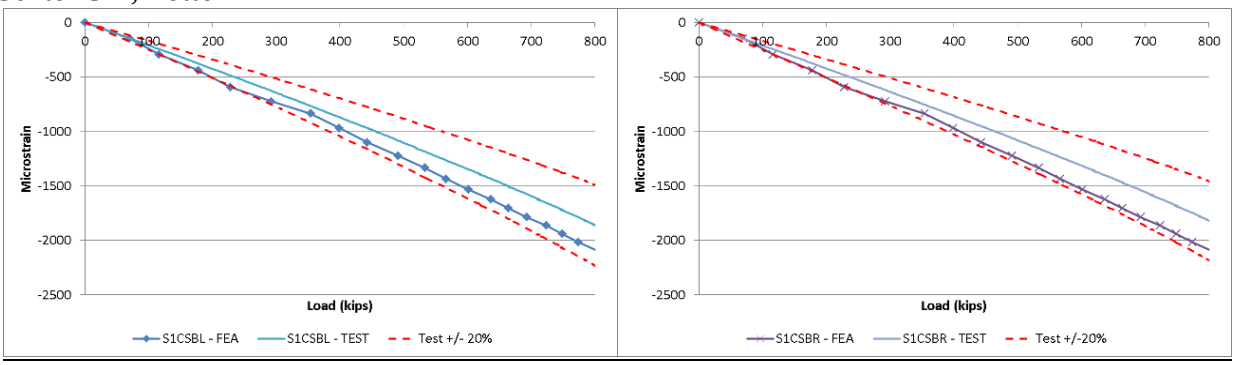

Cross-Section 2

Purlin

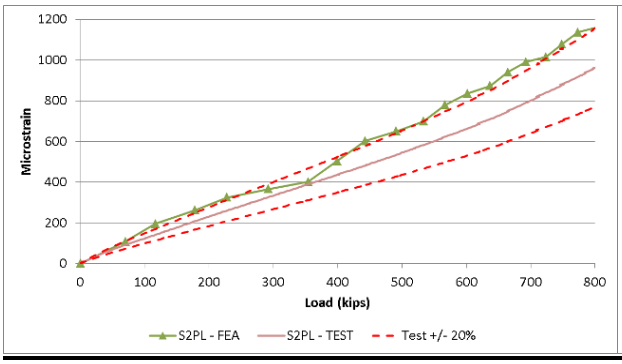

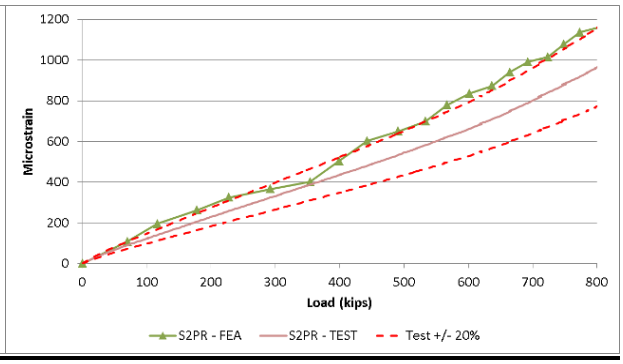

Roof Rail

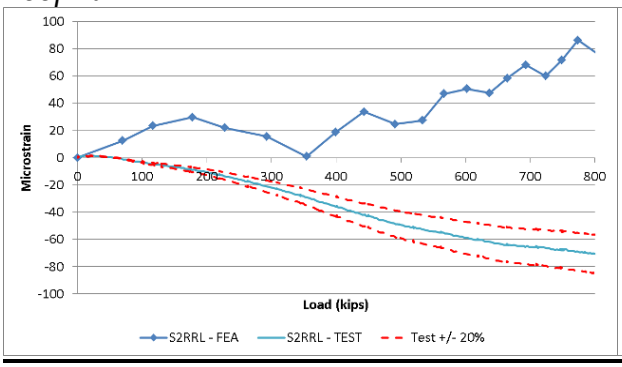

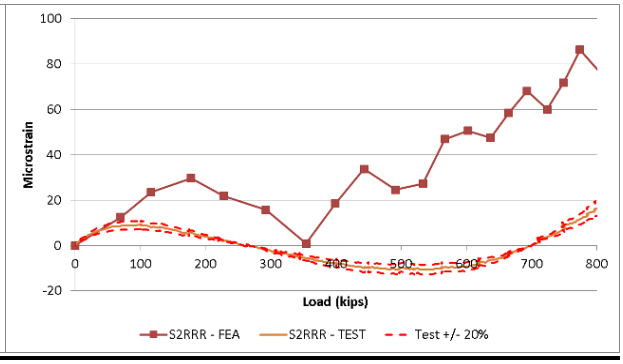

Belt Rail

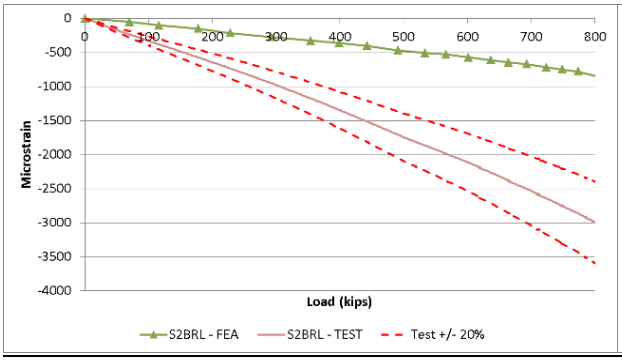

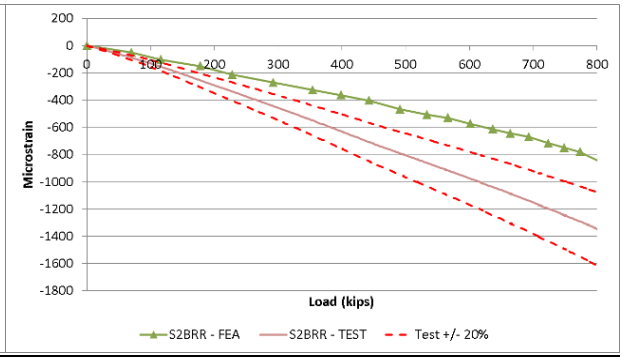

Side Sill

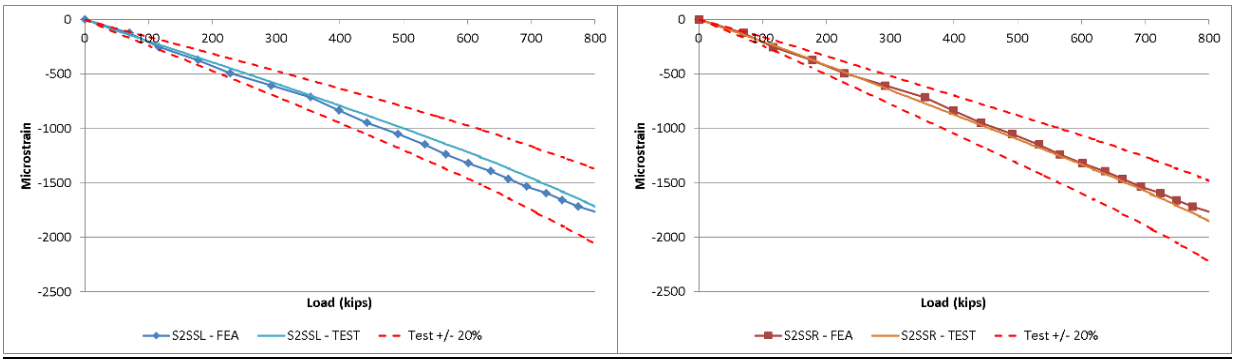

Center Sill, Top

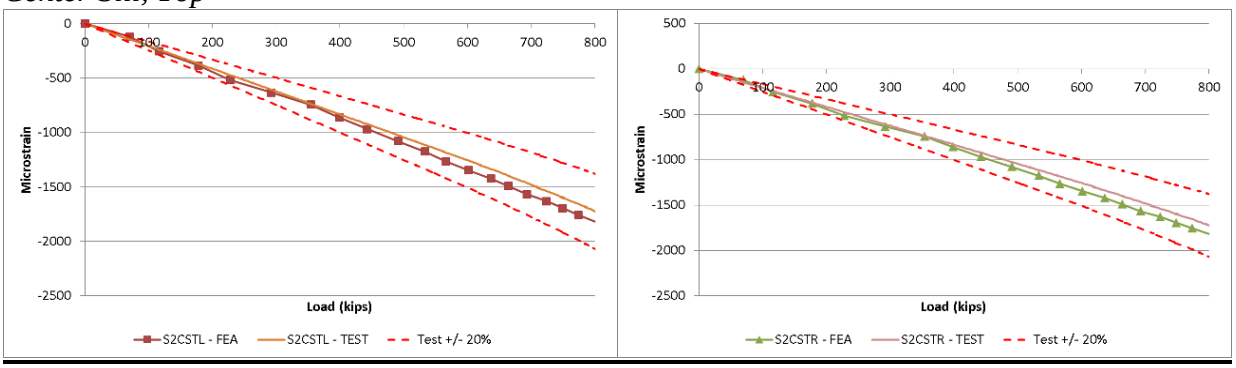

Center Sill, Bottom

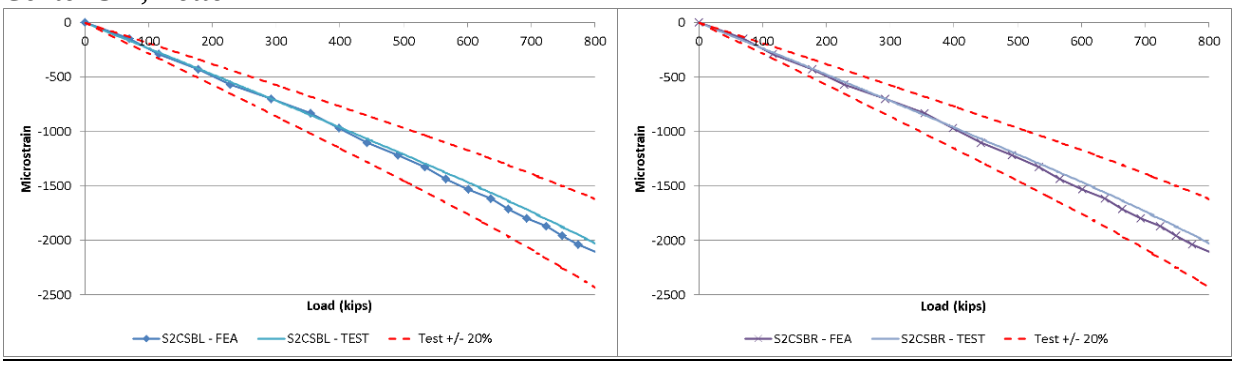

Cross-Section 3

Purlin

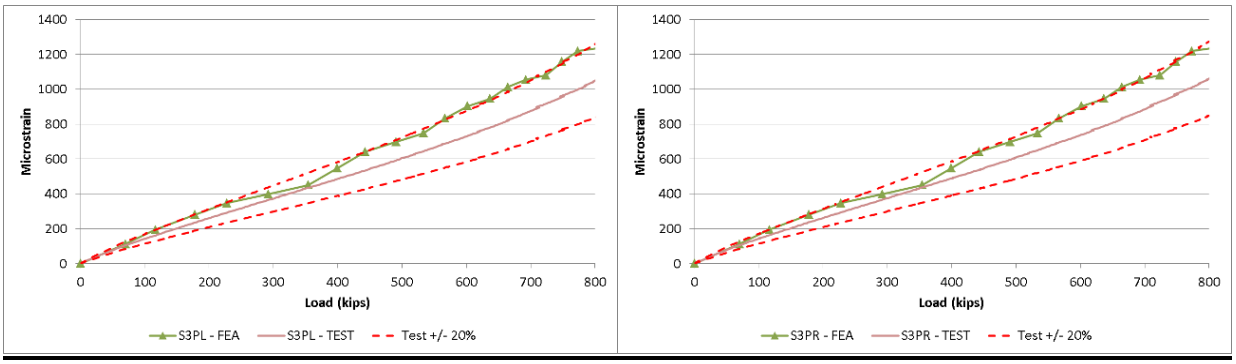

Roof Rail

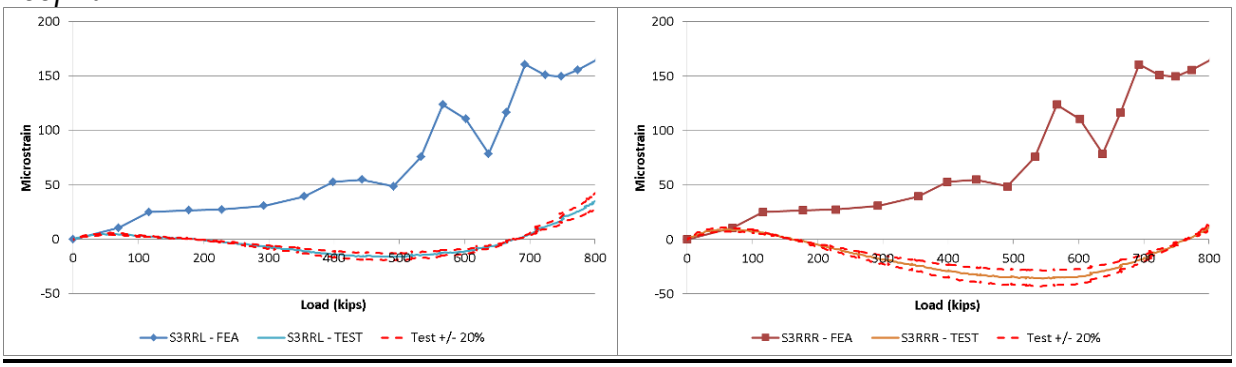

Belt Rail

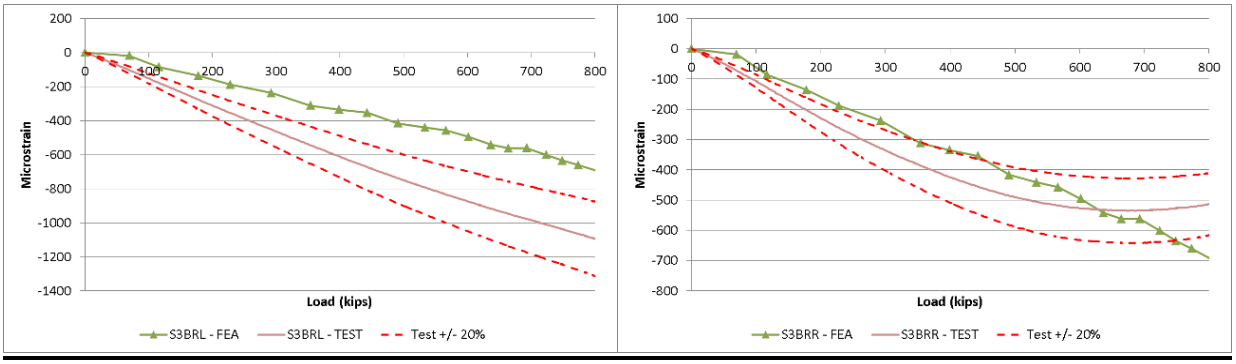

Side Sill

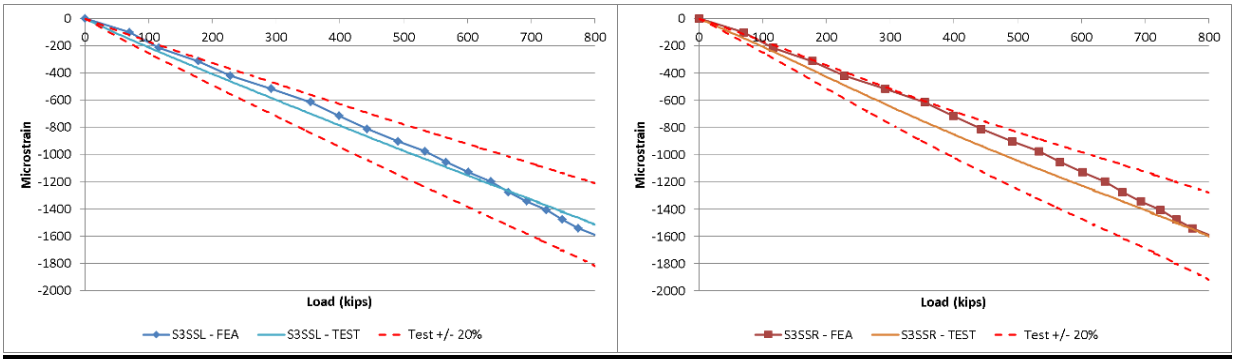

Center Sill, Top

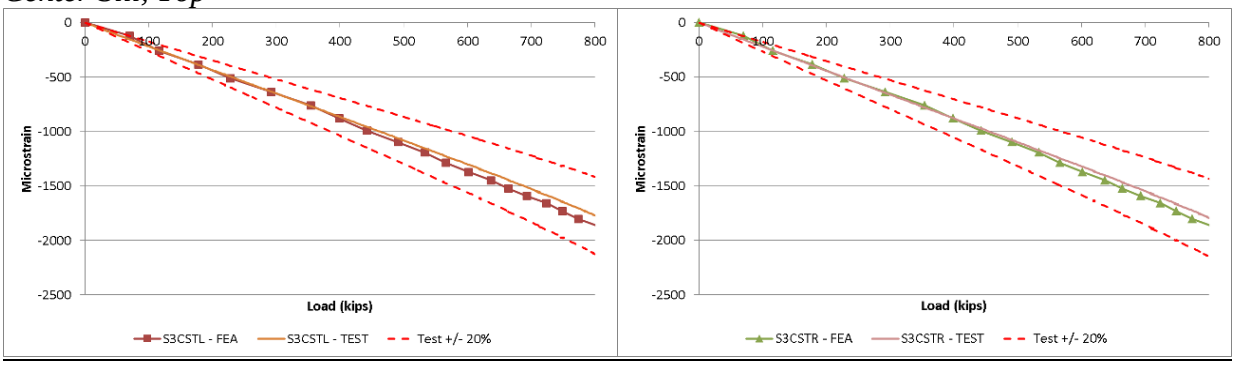

Center Sill, Bottom

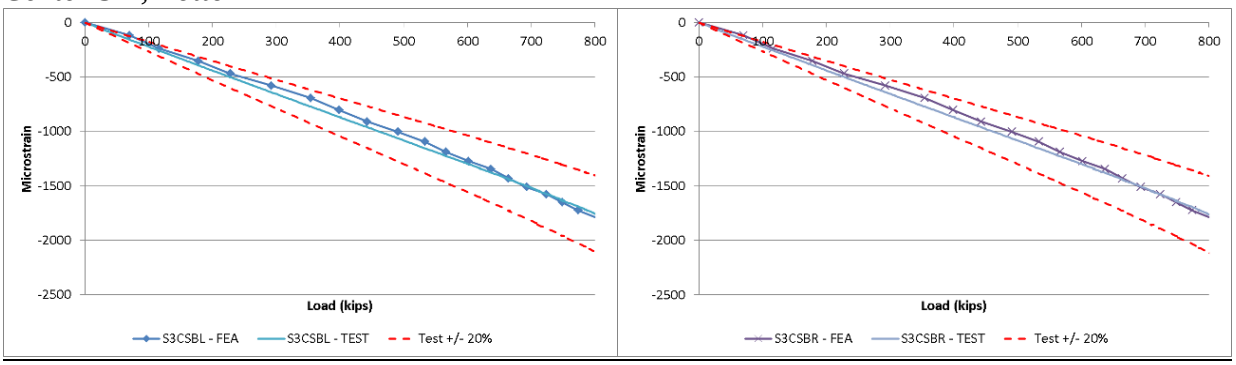

Cross-Section 4

Purlin

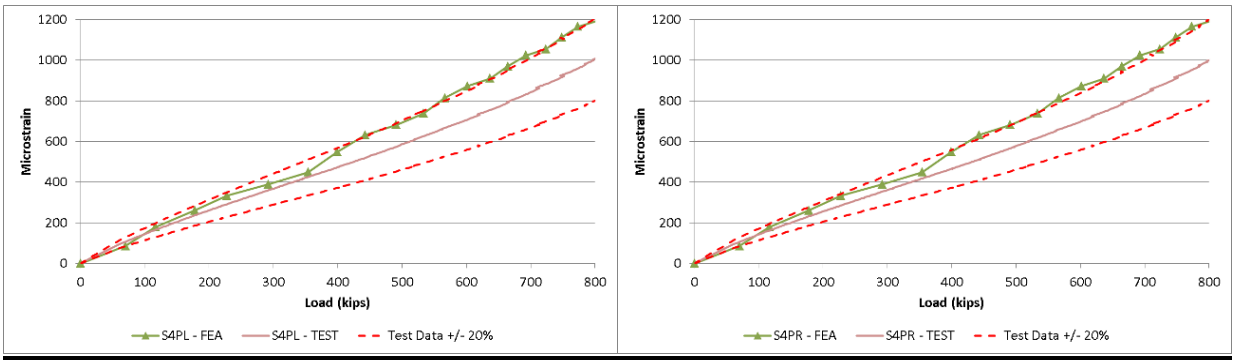

Roof Rail

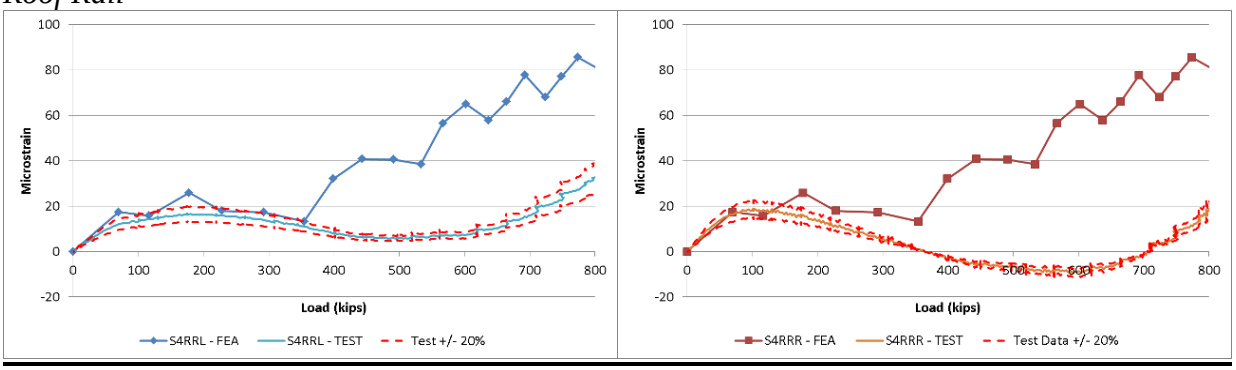

Belt Rail

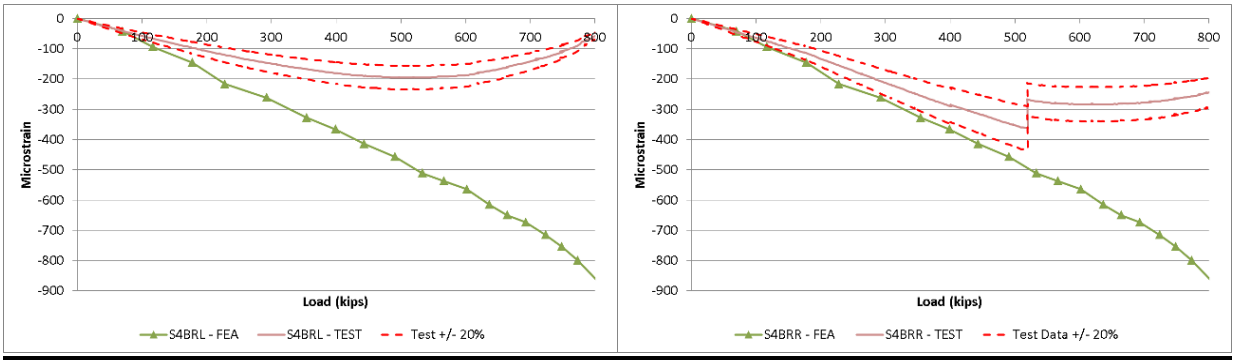

Side Sill

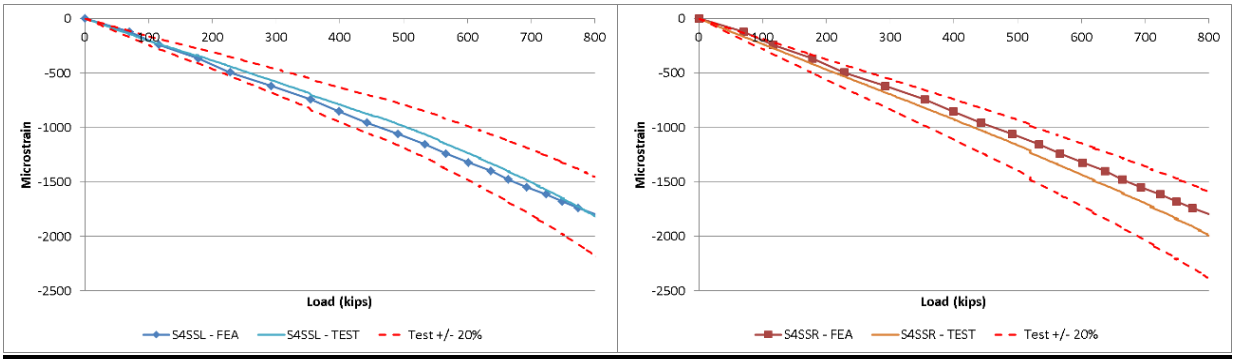

Center Sill, Top

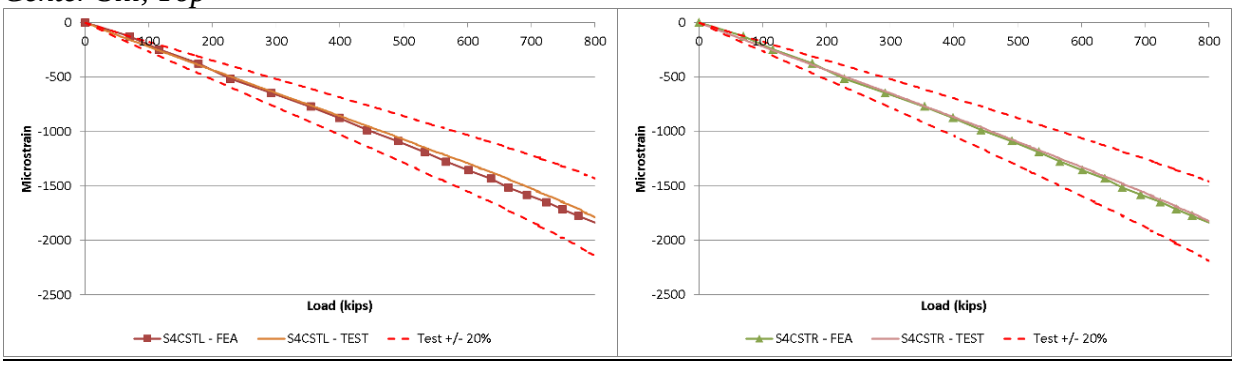

Center Sill, Bottom

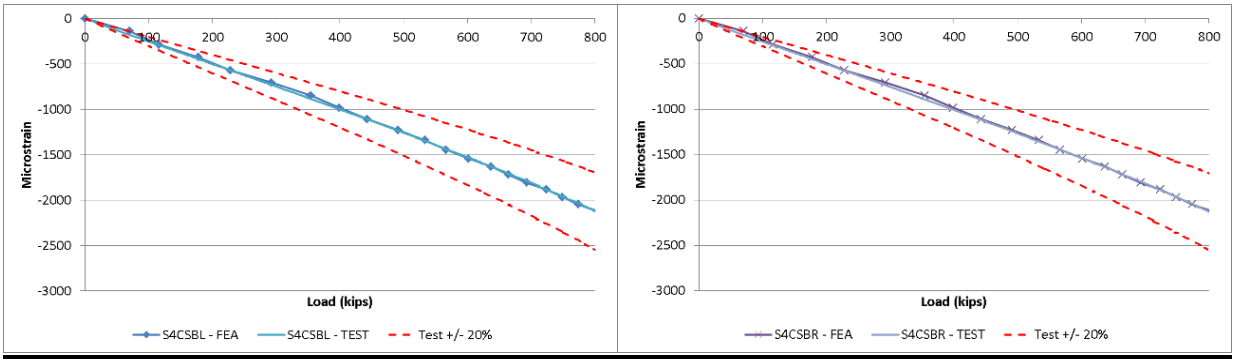

Cross-Section 5

Purlin

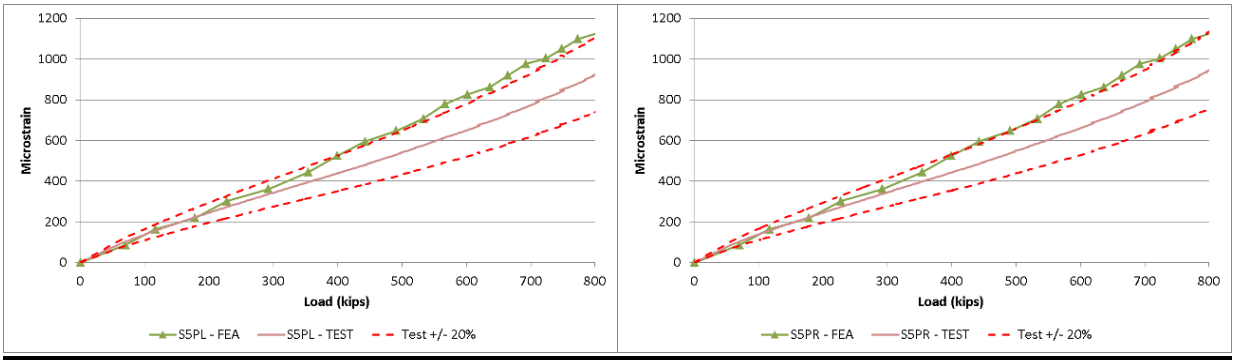

Roof Rail

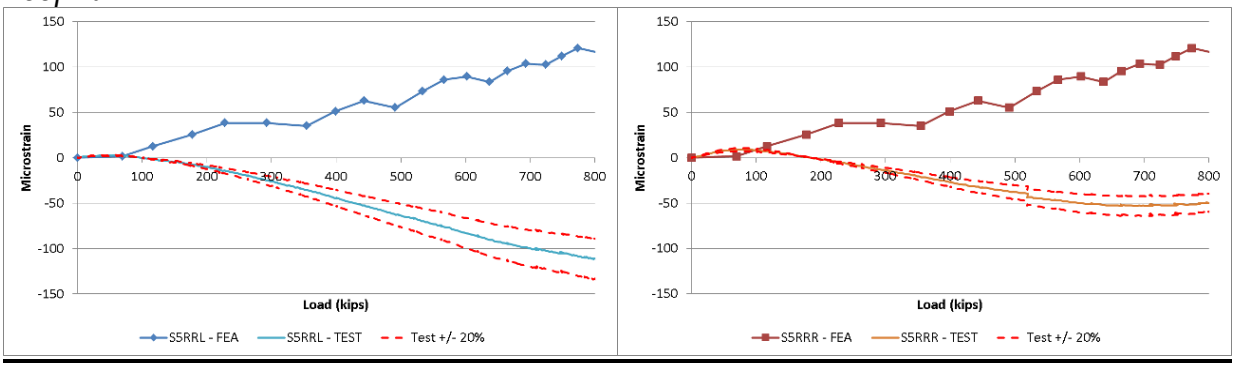

Belt Rail

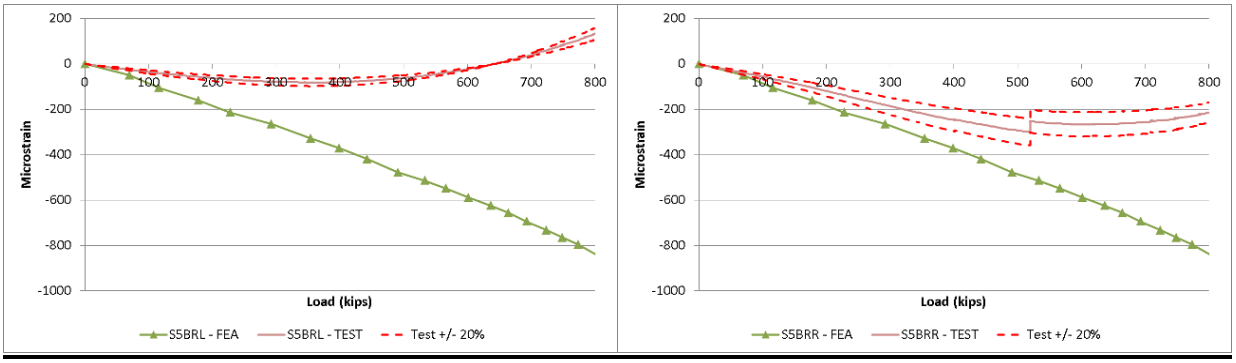

Side Sill

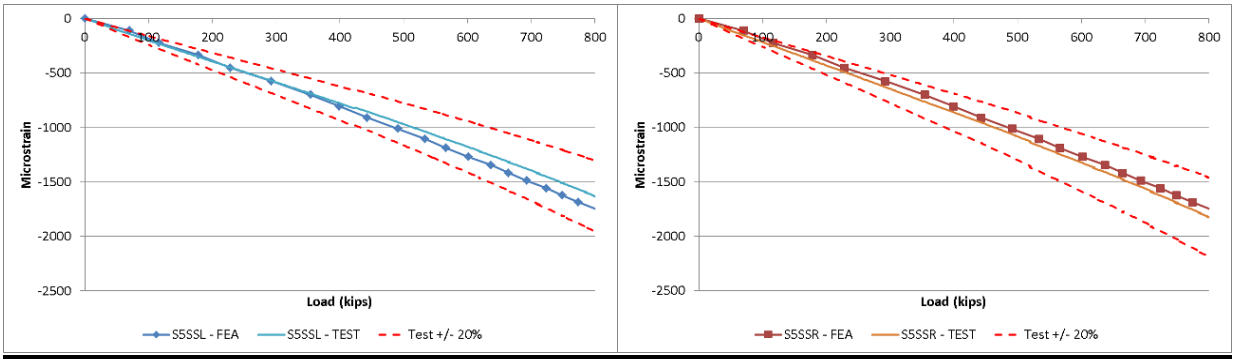

Center Sill, Top

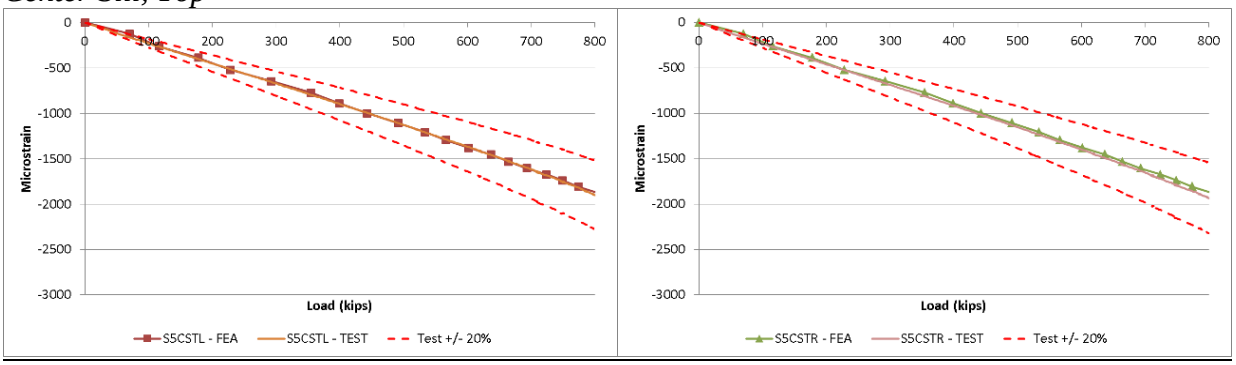

Center Sill, Bottom

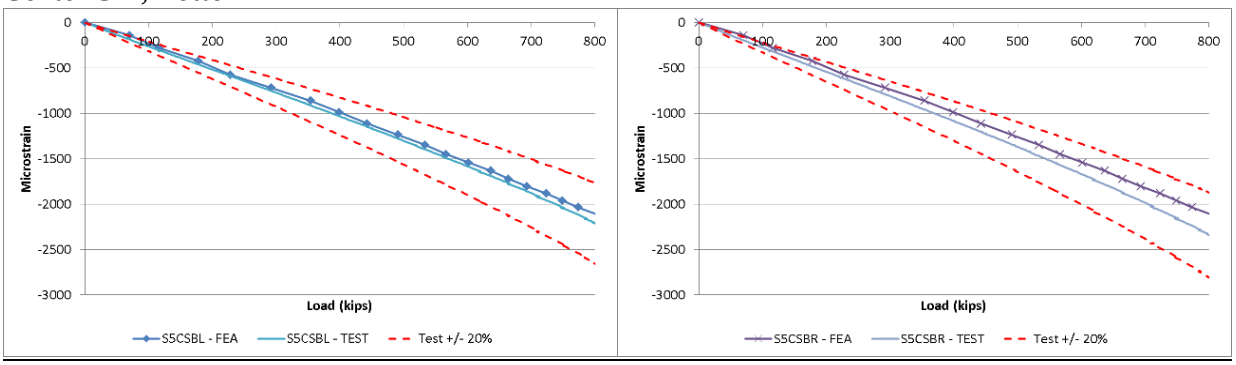

Cross-Section 6

Belt Rail

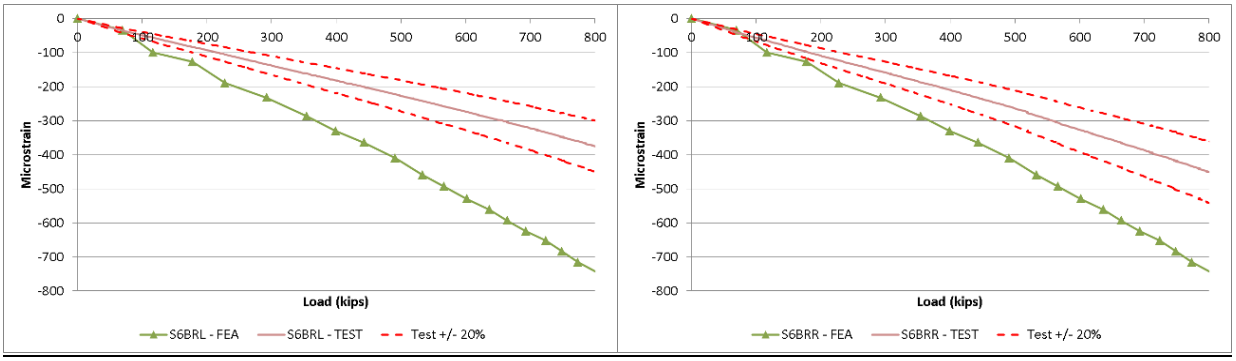

Side Sill

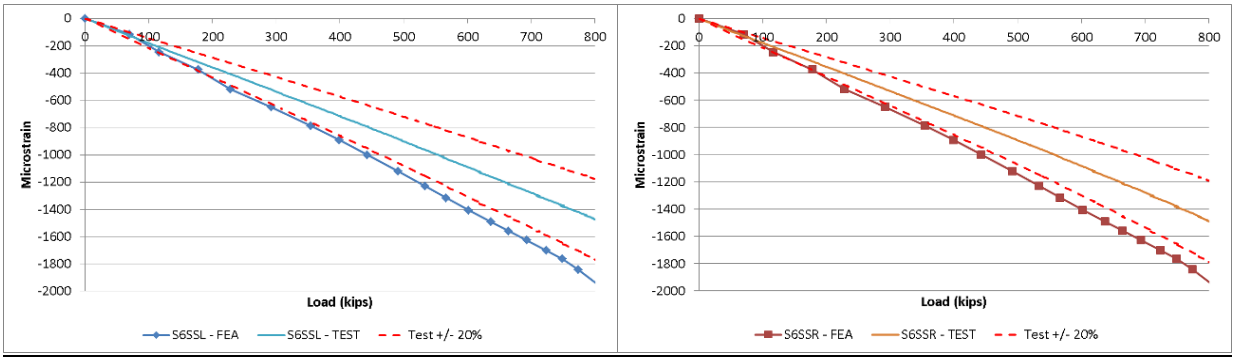

Crippling Test of Car 244

The strain data measured in the roof and floor energy absorber supports during the crippling test of Car 244 are plotted in this section. These instrumented locations are indicated in Figure 38 and Figure 39.

Roof Energy Absorber Supports

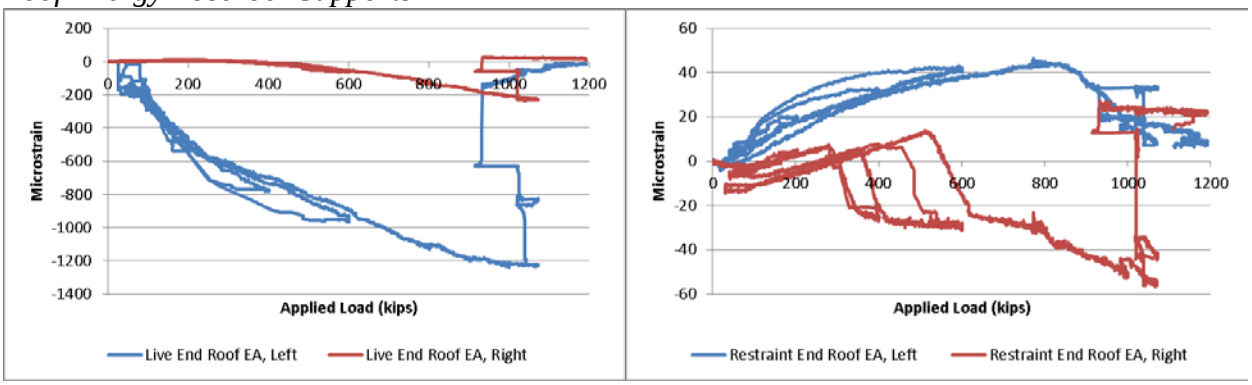

Outboard Floor Energy Absorber Support Location

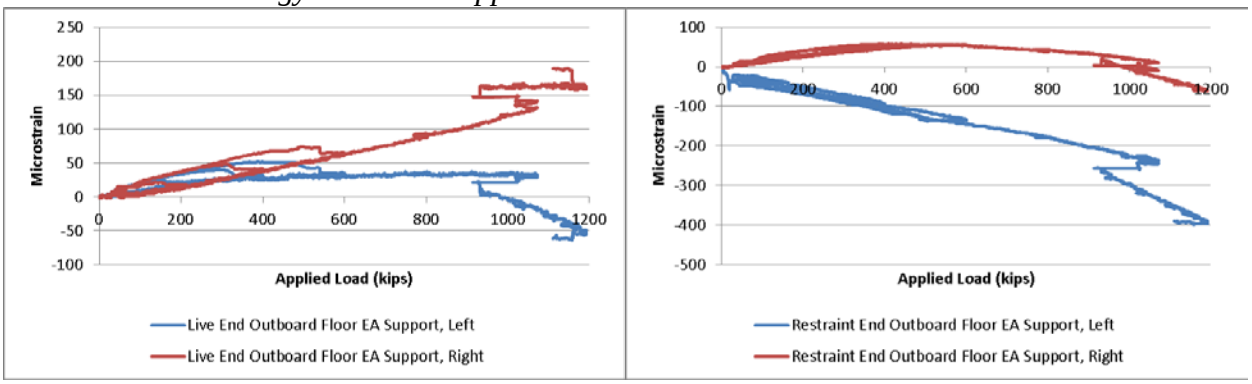

Inboard Floor Energy Absorber Support Location

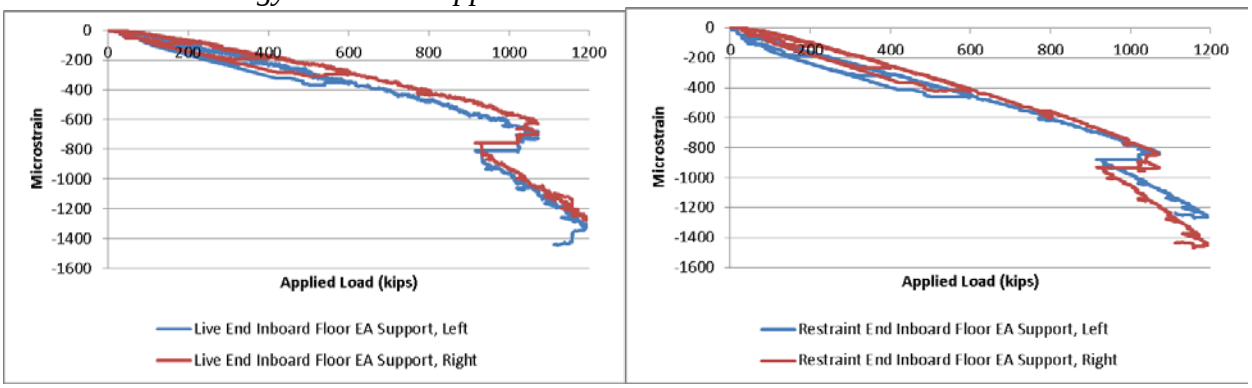

The strain data from the crippling test of Car 244 are plotted against the results of the FE analysis at the corresponding locations in the six cross-sections through the occupant volume.

Cross-Section 1

Purlin

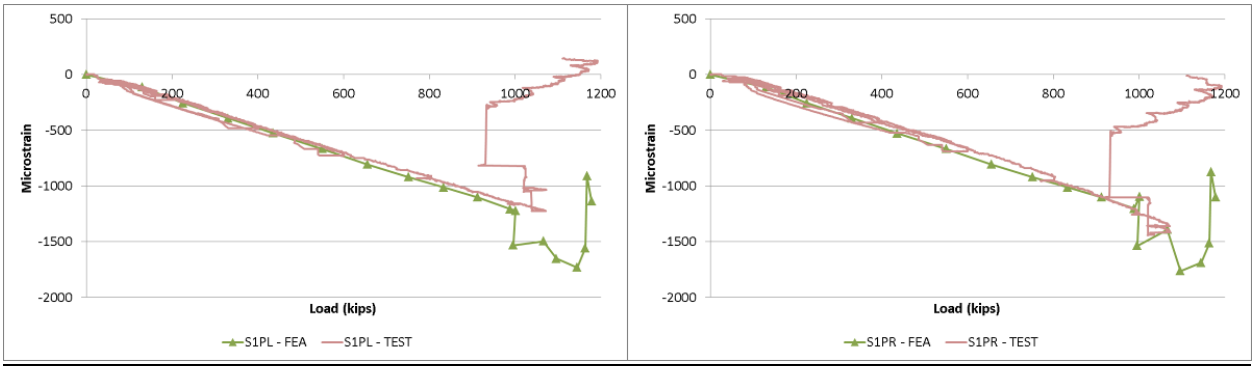

Roof Rail

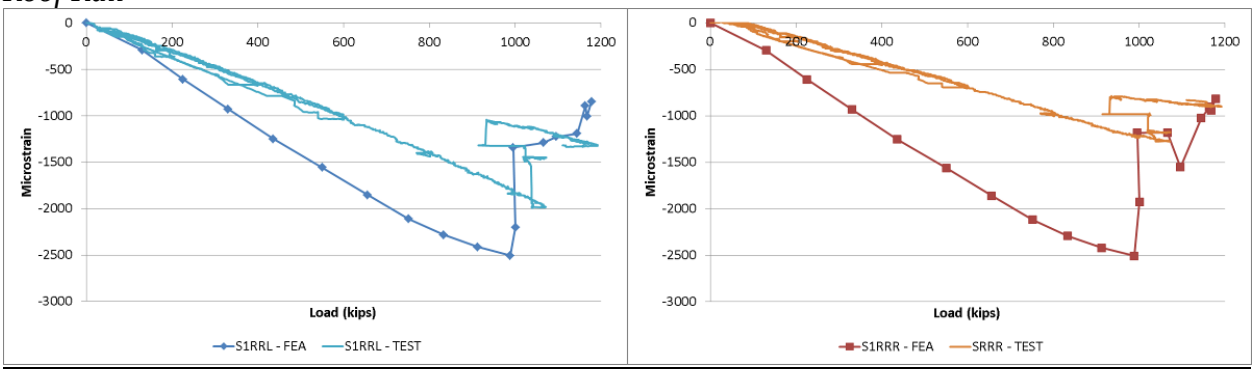

Belt Rail

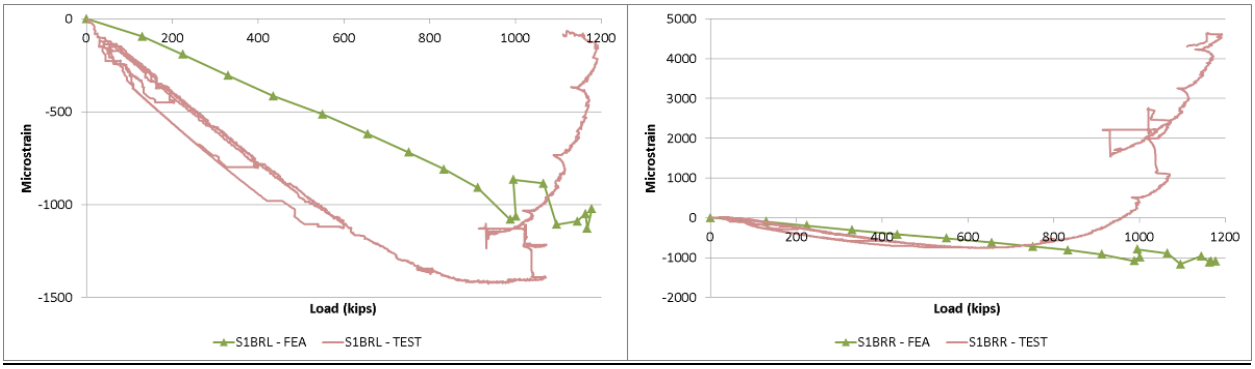

Side Sill

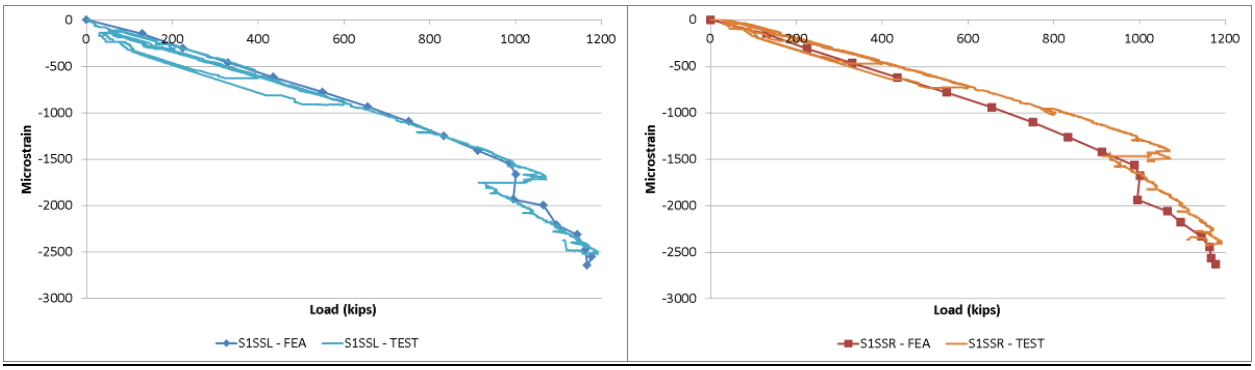

Center Sill, Top

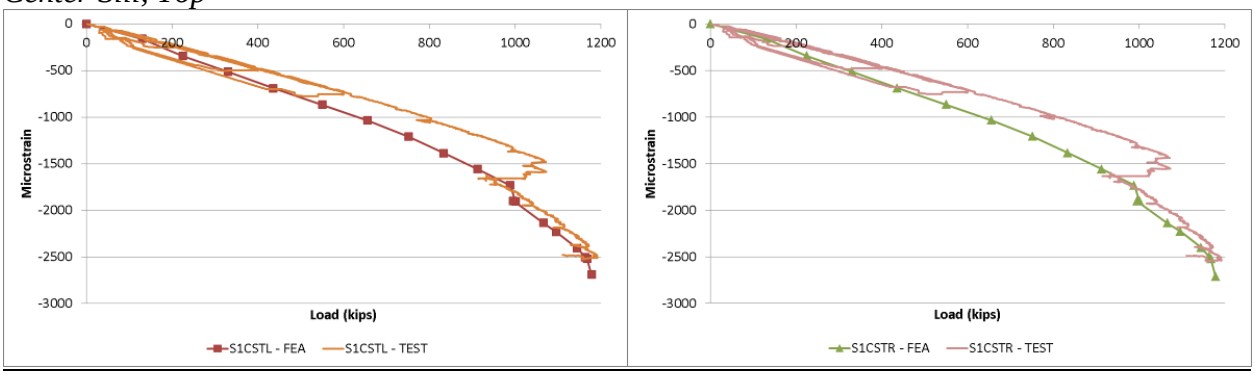

Center Sill, Bottom

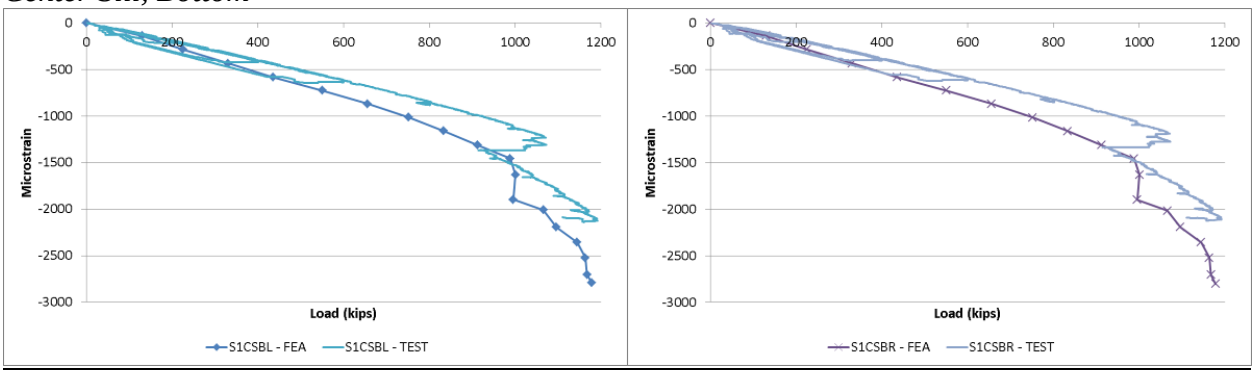

Cross-Section 2

Purlin

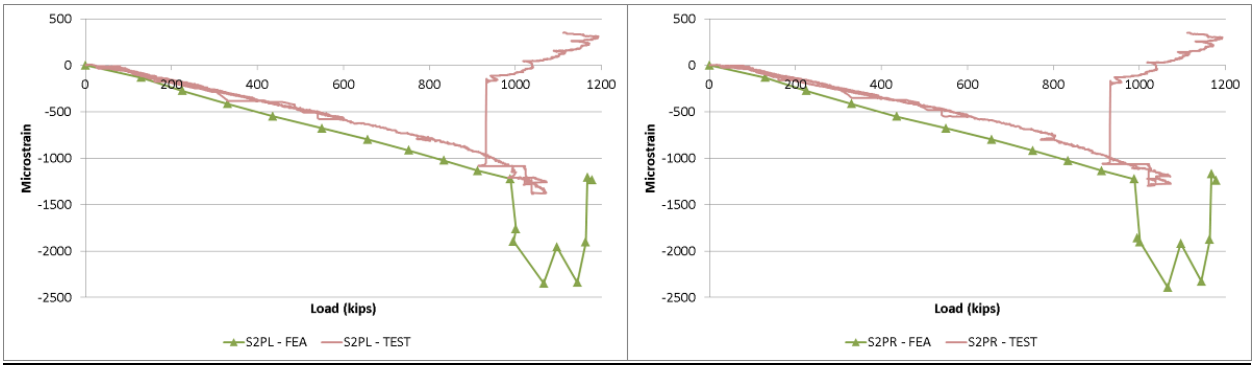

Roof Rail

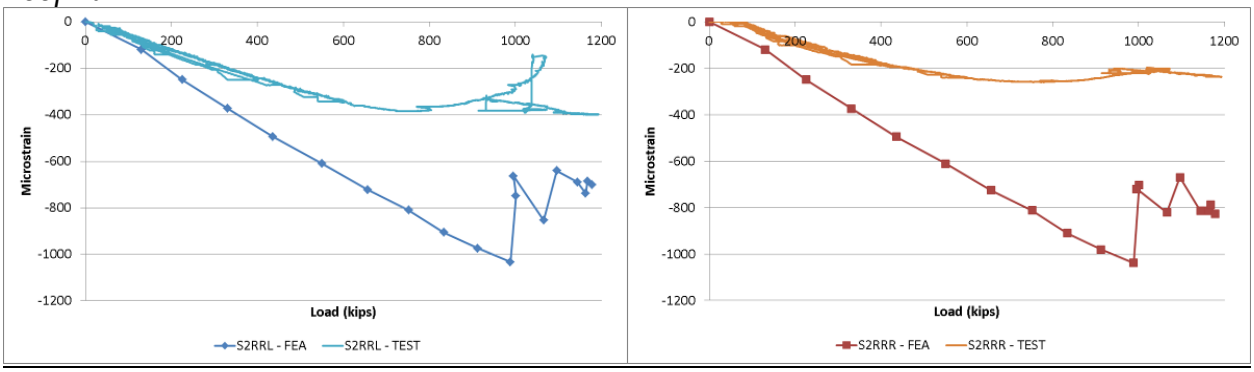

Belt Rail

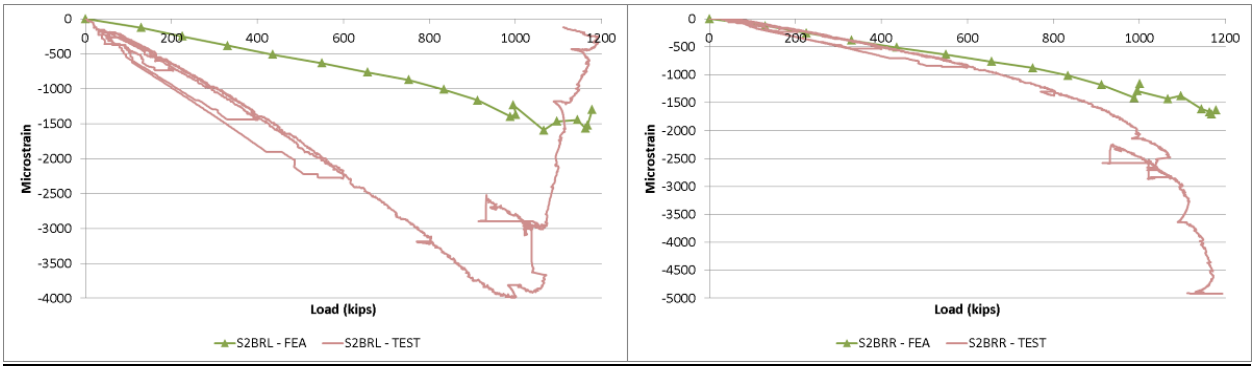

Side Sill

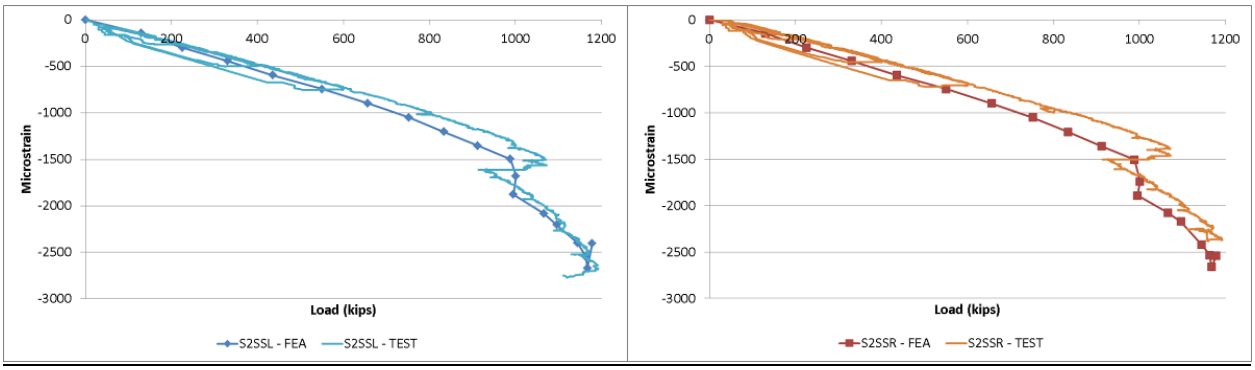

Center Sill, Top

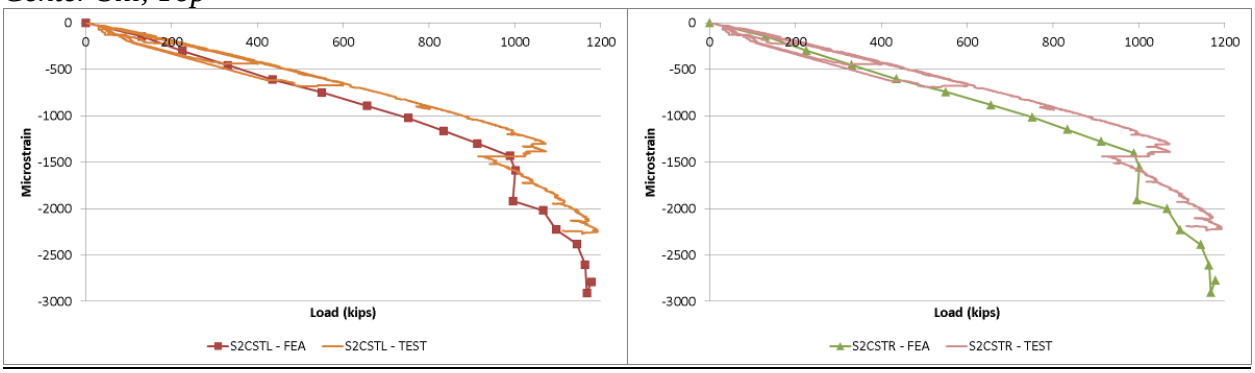

Center Sill, Bottom

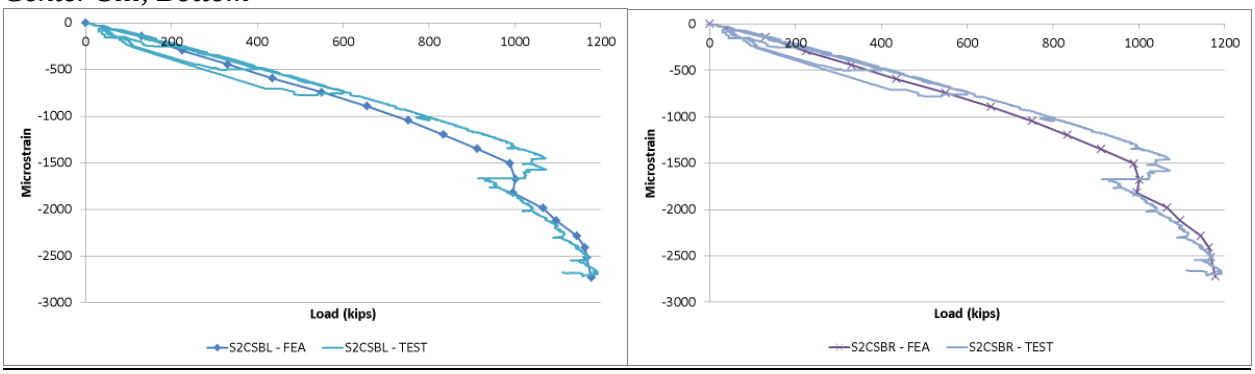

Cross-Section 3

Purlin

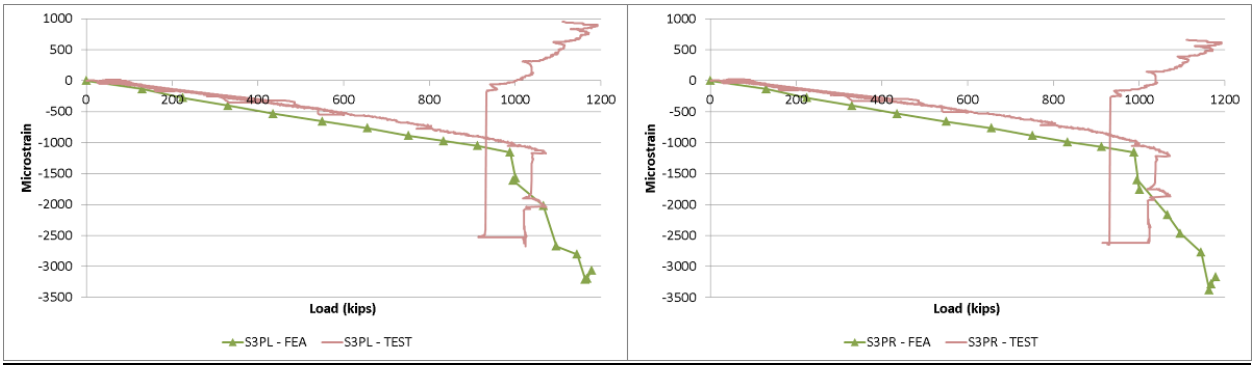

Roof Rail

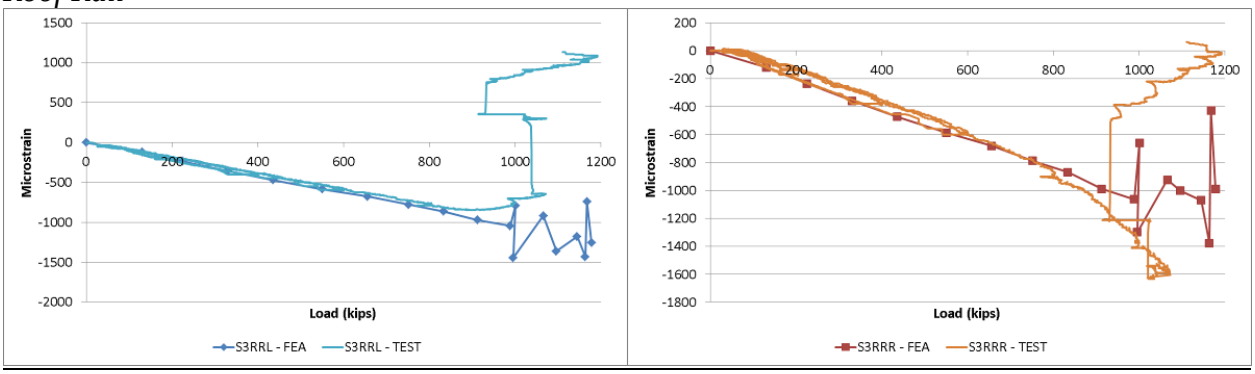

Belt Rail

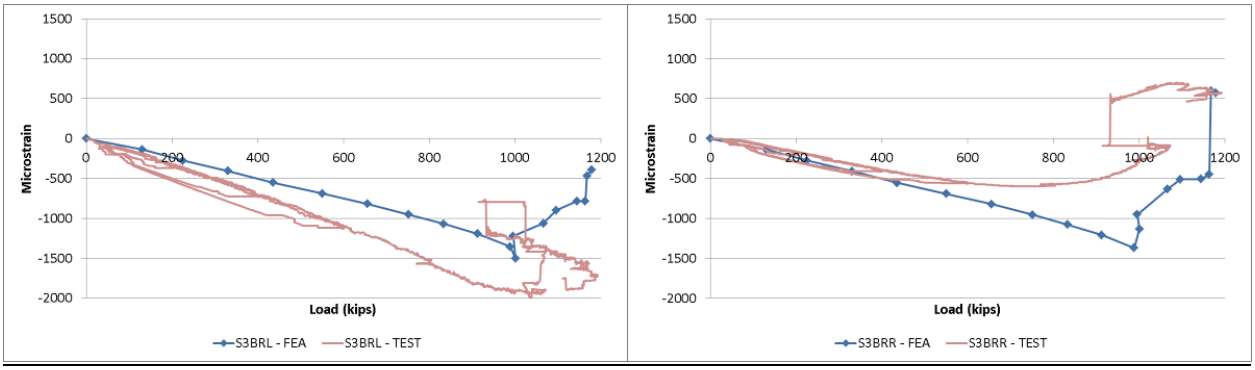

Side Sill

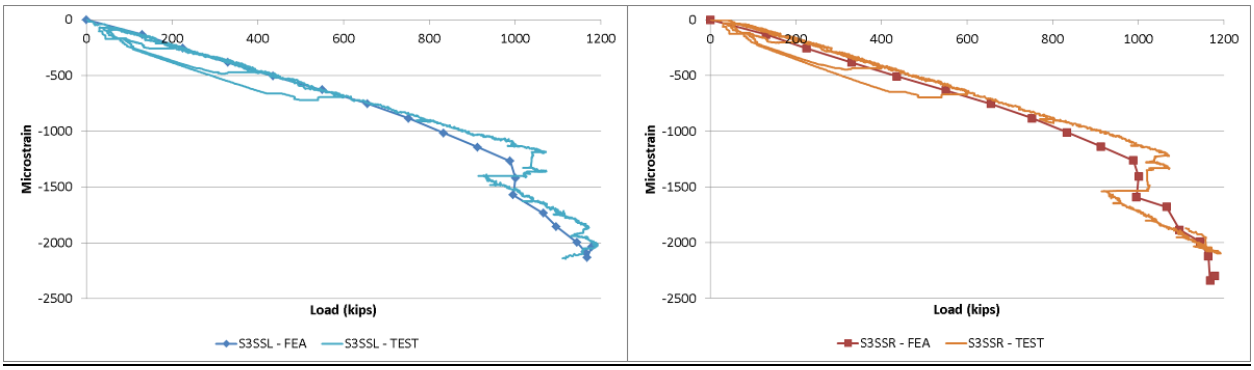

Center Sill, Top

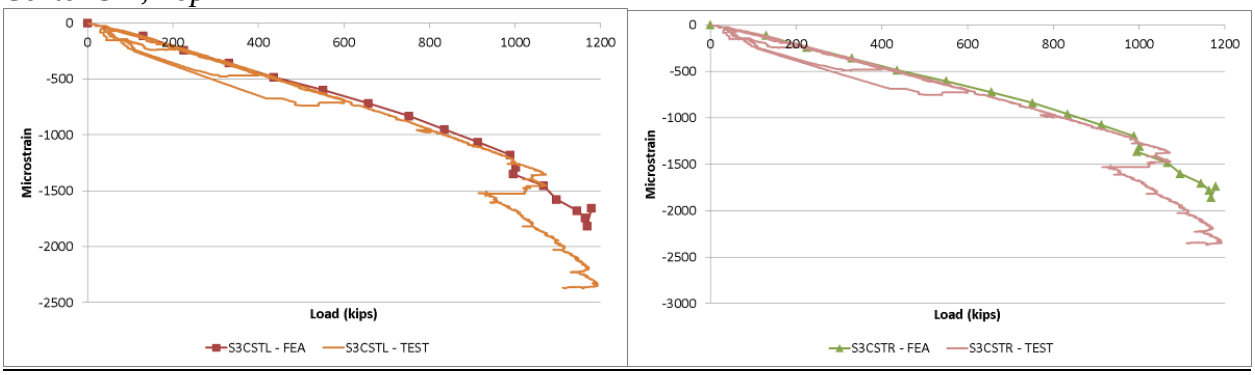

Center Sill, Bottom

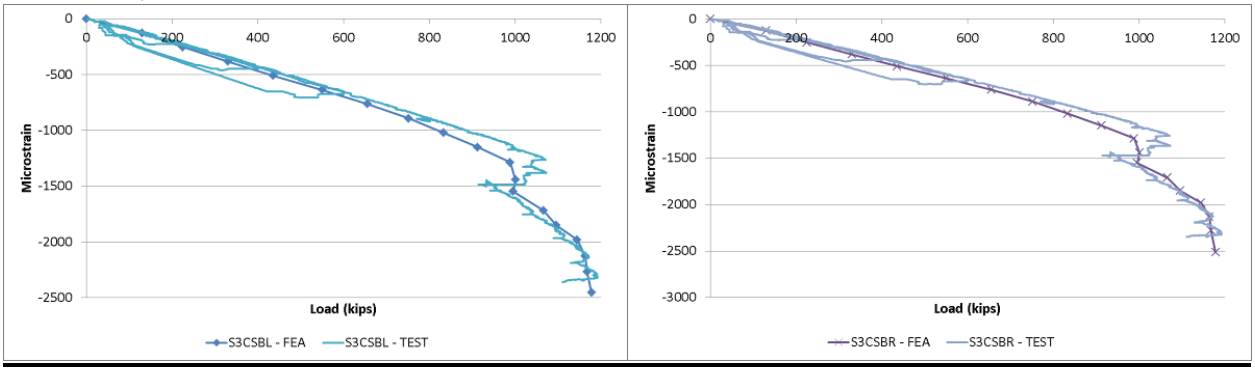

Cross-Section 4

Purlin

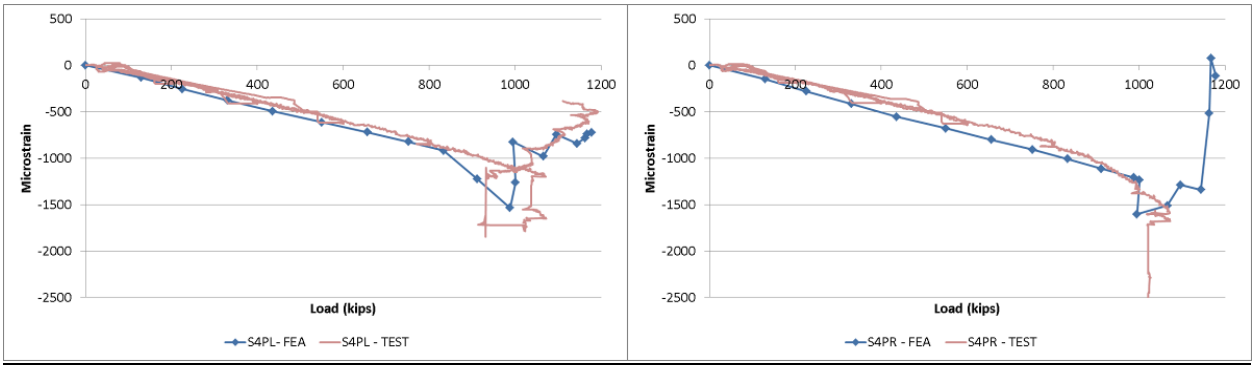

Roof Rail

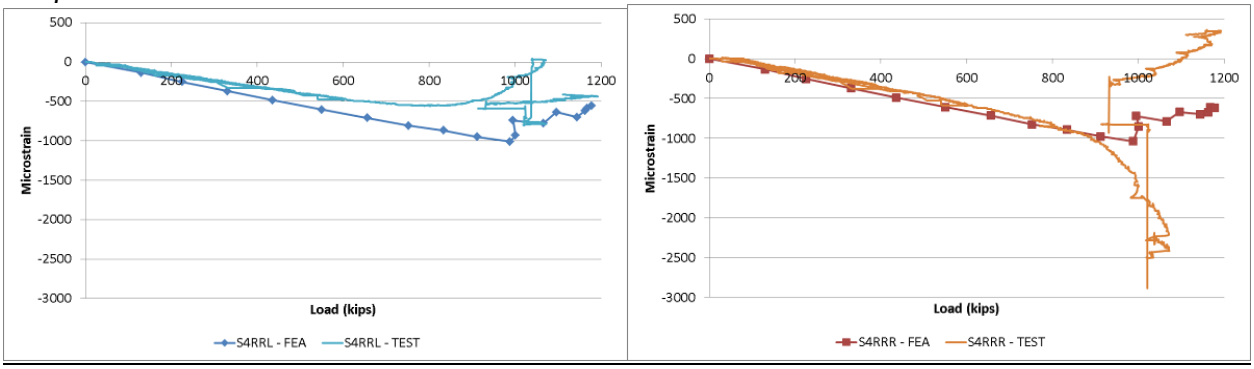

Belt Rail

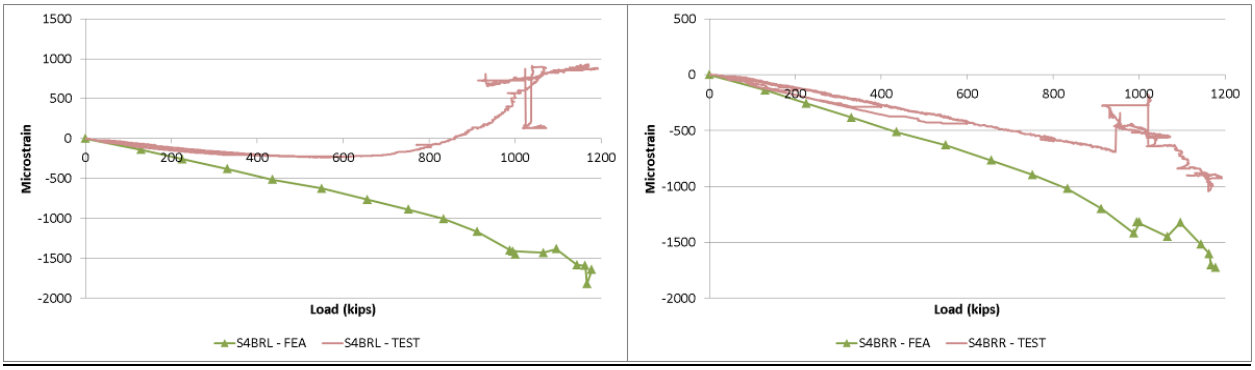

Side Sill

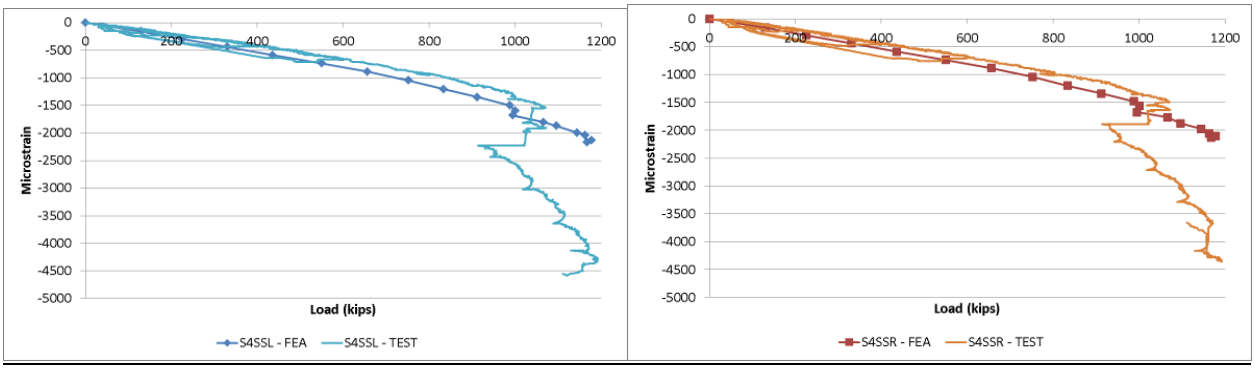

Center Sill, Top

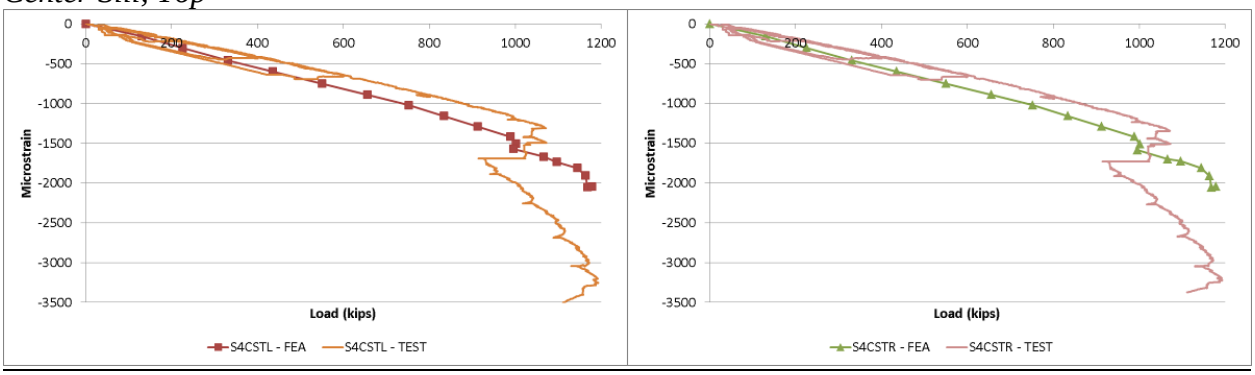

Center Sill, Bottom

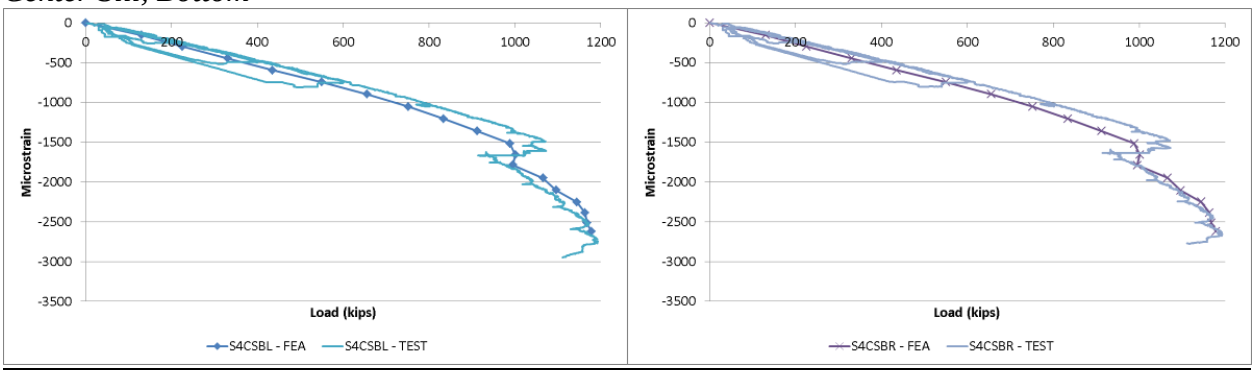

Cross-Section 5

Purlin

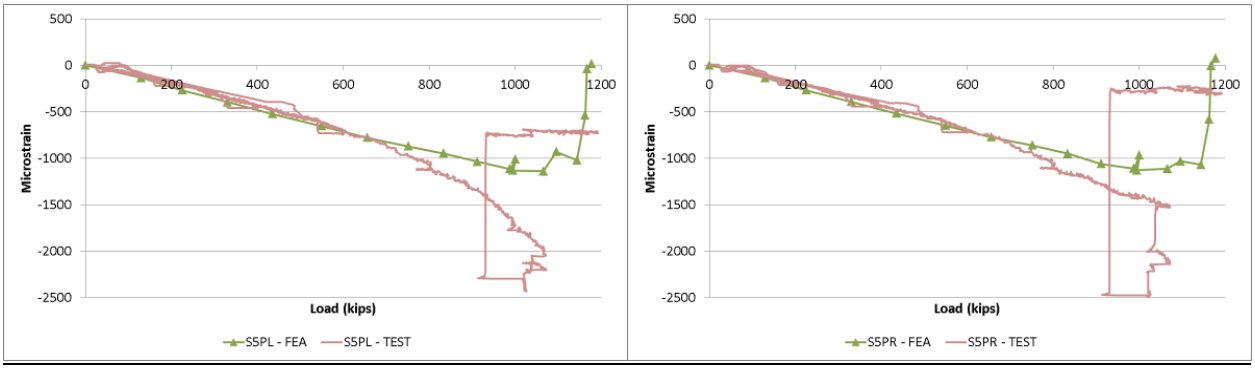

Roof Rail

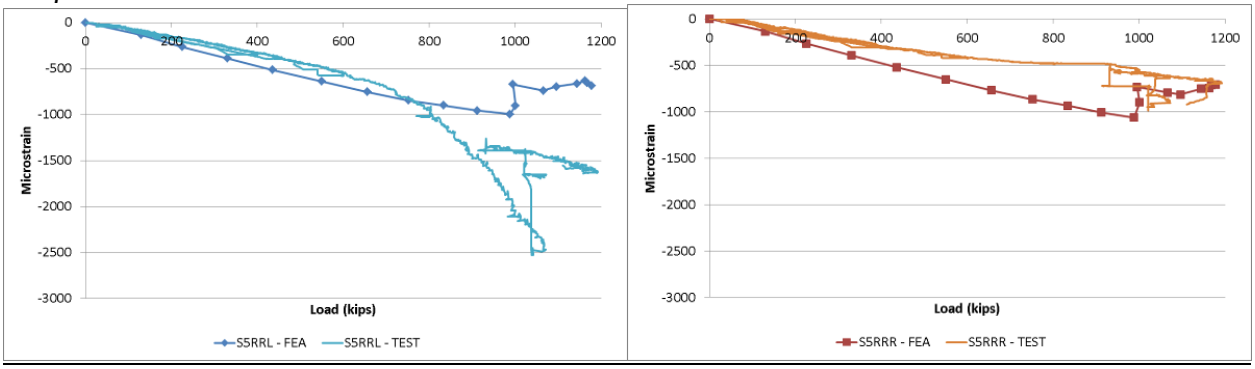

Belt Rail

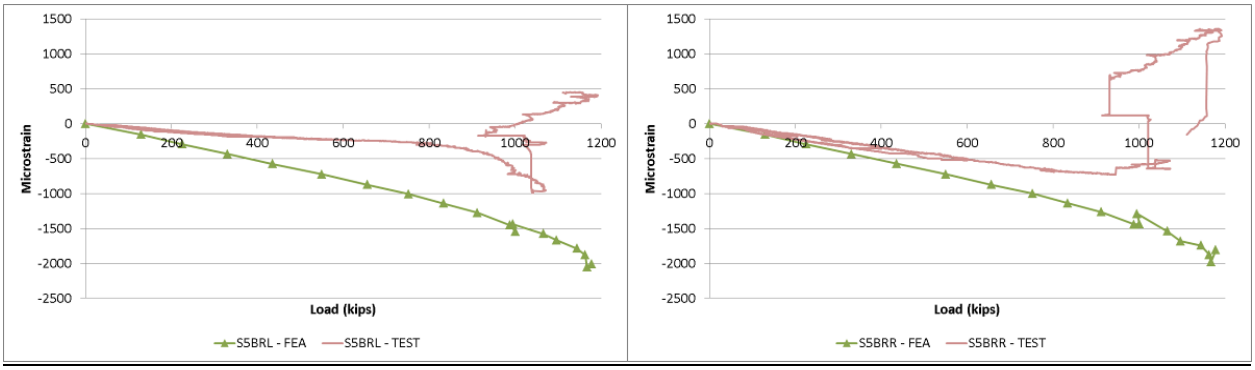

Side Sill

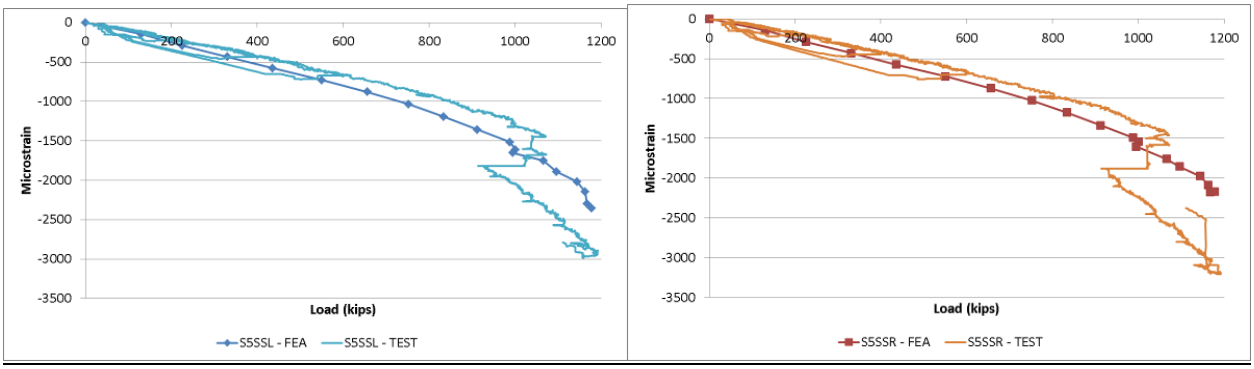

Center Sill, Top

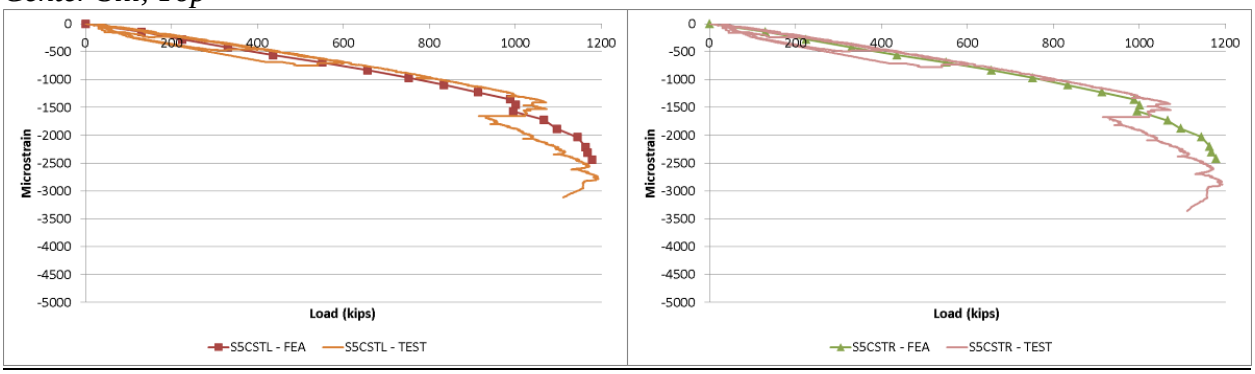

Center Sill, Bottom

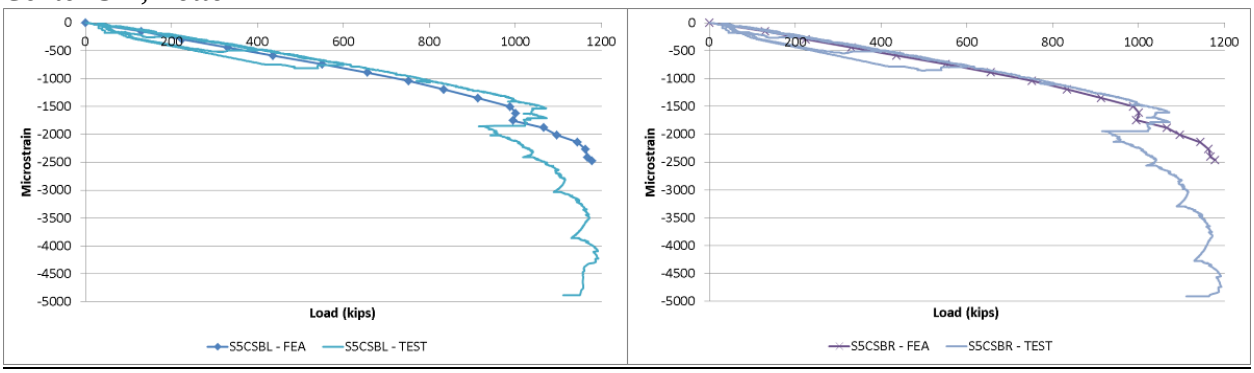

Cross-Section 6

Belt Rail

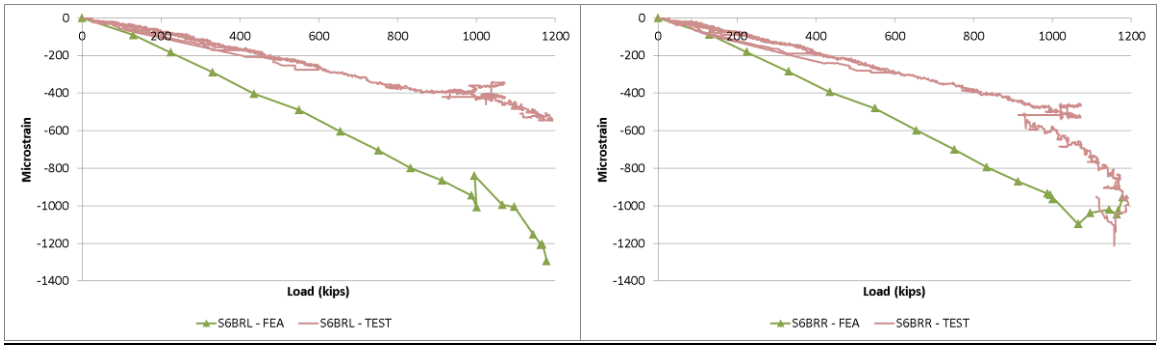

Side Sill

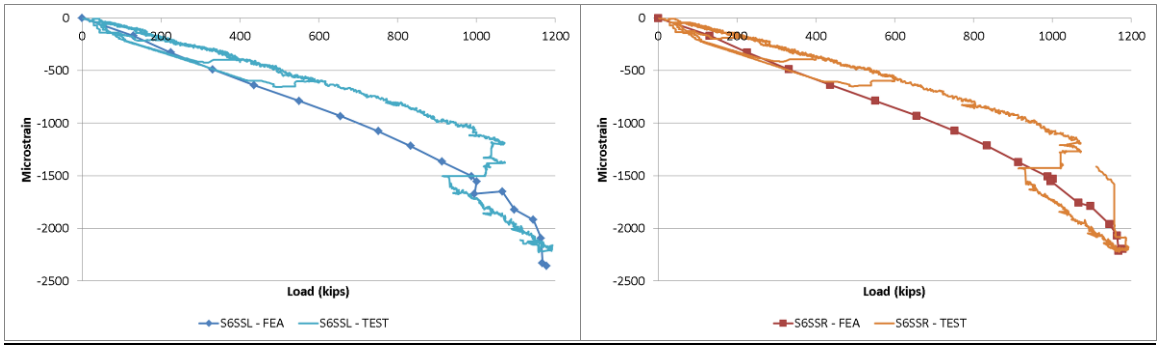

Appendix D.
Car 244 Displacement Data and FE Results

String potentiometers were placed on the underframe of Car 244 both during the 800-kip elastic validation test and during the crippling test to measure the displacements experienced by the car. In the elastic test, a total of nine locations on the center and side sills of the car were instrumented with string pots. In the crippling test a total of 11 locations were instrumented. These locations are indicated in Figure 10.

Because any point on the car may simultaneously experience motion in the vertical, lateral, and longitudinal (VLL) directions, it was necessary to instrument each location with a VLL array of string pots (Figure A 3). Although each string pot was initially oriented with its string along a single axis, motion of the instrumented point in any one direction could result in a change in length to all three strings. It was necessary to process the test data and resolve the recorded changes to the length of each string in the VLL directions.

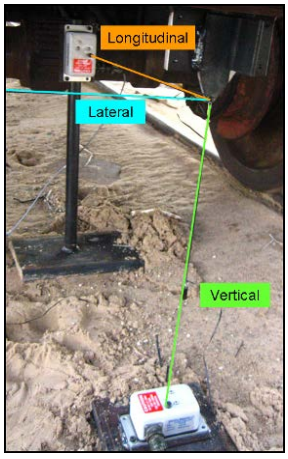

Figure A 3. VLL Array of String Pots

Processing the raw change-in-string-length data accomplished two goals. First, the data were transformed from each array's local coordinate system to a universal coordinate system for the test car. Second, the change-in-length data were resolved into motion in the three principal directions, correcting each string's data for off-axis motion. Figure A 4 shows an exemplar set of labeled axes used during the processing of the string pot data. These axes represent the global coordinate system and correspond to the orientation of the string array shown in Figure A 3.

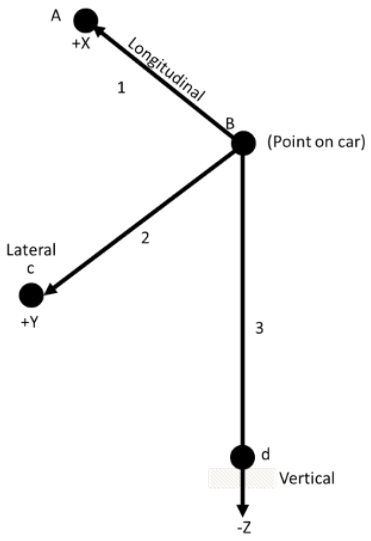

Figure A 4. Axes Used for String Pot. Data Processing

A system of equations was written to relate the change in length of each string to a corresponding displacement in the global X, Y, and Z directions. The origin for each VLL array was placed at Point B, the point on the car being measured. The initial length of each string was measured prior to application of any load to the car.

The coordinates for the position of the grounded end of each channel were then entered into the global coordinate system:

Point D (vertical): (0, 0, -Initial length)
Point A (longitudinal): (Initial length, 0, 0)
Point C (lateral): (0, Initial length, 0)

For each data point recorded during the test, the change in string length was added to the initial string length to determine the length of each string at a given point in time.

The system of equations used to resolve the data into X, Y, and Z motion is:

Equation 1. System of Equations for Resolving String Pot Data

$$\left(L_{vert_k}\right)^2 = \left(\Delta x_b - x_d\right)^2 + \left(\Delta y_b - y_d\right)^2 + \left(\Delta z_b - z_d\right)^2$$

$$\left(L_{long_k}\right)^2 = \left(\Delta x_b - x_a\right)^2 + \left(\Delta y_b - y_a\right)^2 + \left(\Delta z_b - z_a\right)^2$$

$$\left(L_{lat_k}\right)^2 = \left(\Delta x_b - x_c\right)^2 + \left(\Delta y_b - y_c\right)^2 + \left(\Delta z_b - z_c\right)^2$$

Where

L_{vert}=new length of vertically oriented string pot
L_{long}=new length of longitudinally oriented string pot
L_{lat}=new length of laterally oriented string pot
k=index
Δx_b=displacement of point B in x-direction

Δy_b=displacement of point B in y-direction
Δz_b=displacement of point B in z-direction
x_a, y_a, z_a=coordinates of point A
x_c, y_c, z_c=coordinates of point C
z_d, y_d, z_d=coordinates of point D

A solver (the commercial software MathCAD [15]) was used to solve the system for Δx_b, Δy_b, and Δz_b. This system of equations was solved at each time point where data were simultaneously collected at the three channels making up each array.

The names and locations of the string pot channels installed in VLL arrays in the validation test of Car 244 and the crippling test of Car 244 are provided in Table A 2.

Table A 2. String Pot Channel Names and Locations

Channel Name	Orientation	Location
SPAX	Longitudinal	A-end lateral cross-member
SPAY	Lateral	A-end lateral cross-member
SPAZ	Vertical	A-end lateral cross-member
SPSSALX	Longitudinal	A-end left side sill
SPSSALY	Lateral	A-end left side sill
SPSSALZ	Vertical	A-end left side sill
SPSSARX	Longitudinal	A-end right side sill
SPSSARY	Lateral	A-end right side sill
SPSSARZ	Vertical	A-end right side sill
SPCSAX	Longitudinal	Center sill between A-end and midpoint of car
SPCSAY	Lateral	Center sill between A-end and midpoint of car
SPCSAZ	Vertical	Center sill between A-end and midpoint of car
SPCSCX	Longitudinal	Center sill at midpoint of car
SPCSCY	Lateral	Center sill at midpoint of car
SPCSCZ	Vertical	Center sill at midpoint of car
SPCS4-5X*	Longitudinal	Center sill between cross-bearer 4 and 5
SPCS4-5Y*	Lateral	Center sill between cross-bearer 4 and 5
SPCS4-5Z*	Vertical	Center sill between cross-bearer 4 and 5
SPCS5X*	Longitudinal	Center sill at cross-bearer 5
SPCS5Y*	Lateral	Center sill at cross-bearer 5
SPCS5Z*	Vertical	Center sill at cross-bearer 5
SPCSBX	Longitudinal	Center sill between B-end and midpoint of car

Channel Name	Orientation	Location
SPCSBY	Lateral	Center sill between B-end and midpoint of car
SPCSBZ	Vertical	Center sill between B-end and midpoint of car
SPSSBLX	Longitudinal	B-end left side sill
SPSSBLY	Lateral	B-end left side sill
SPSSBLZ	Vertical	B-end left side sill
SPSSBRX	Longitudinal	B-end right side sill
SPSSBRY	Lateral	B-end right side sill
SPSSBRZ	Vertical	B-end right side sill
SPBX	Longitudinal	B-end lateral cross-member
SPBY	Lateral	B-end lateral cross-member
SPBZ	Vertical	B-end lateral cross-member

*Channel only used in crippling test

800-kip Validation Test of Car 244

The following series of graphs contains the displacement results from the 800-kip elastic validation test and corresponding FE analysis. In each graph the test data have been resolved into their x, y, or z components. Because the test frame stretched in response to the applied load, the test data have had the longitudinal displacement of the restraint end (SPBX) subtracted from all other longitudinal channels' data.

Longitudinal Data

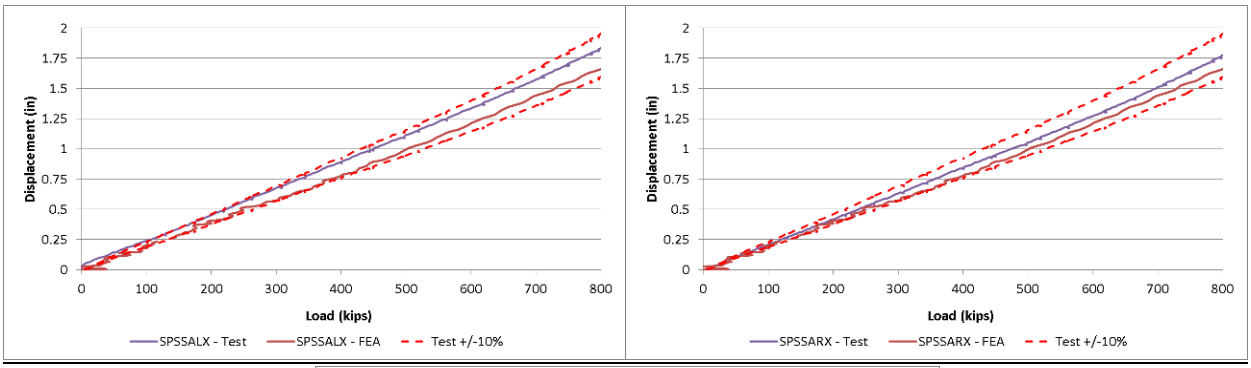

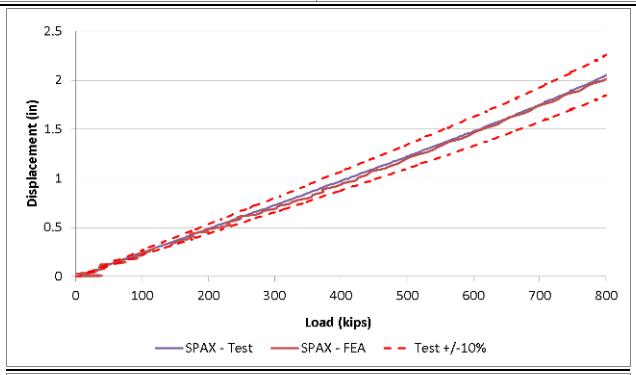

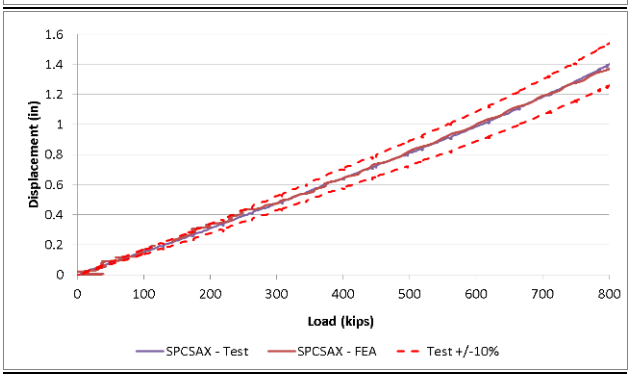

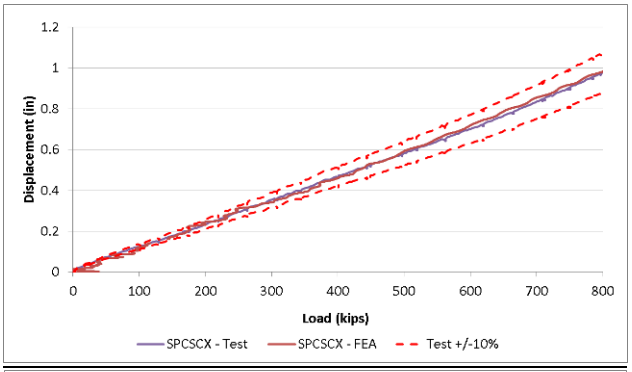
Displacement (in)
1.2
1
0.8
0.6
0.4
0.2
0
0 100 200 300 400 500 600 700 800
Load (kips)
SPCSCX - Test
SPCSCX - FEA
Test +/-10%

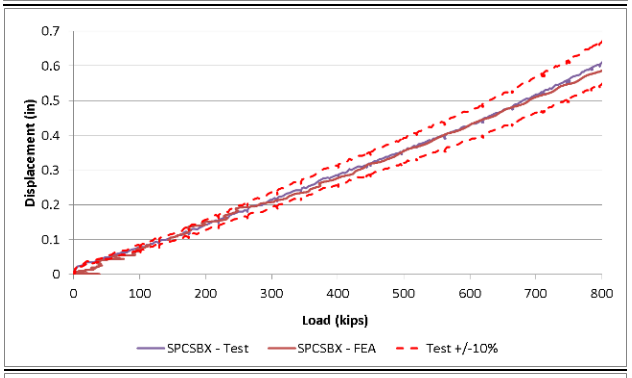
Displacement (in)
0.7
0.6
0.5
0.4
0.3
0.2
0.1
0
0 100 200 300 400 500 600 700 800
Load (kips)
SPCSBX - Test
SPCSBX - FEA
Test +/-10%

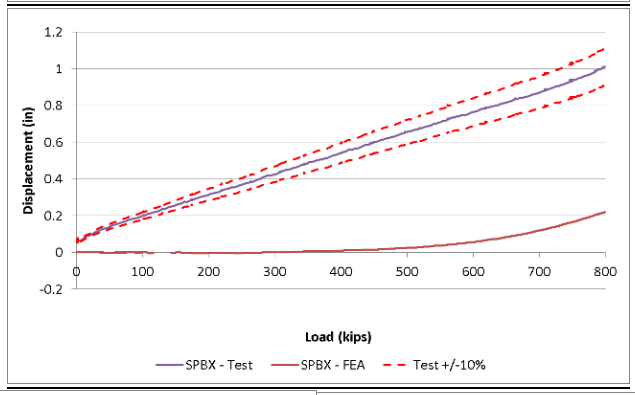
Displacement (in)
1.2
1
0.8
0.6
0.4
0.2
0
-0.2
0 100 200 300 400 500 600 700 800
Load (kips)
SPBX - Test
SPBX - FEA
Test +/-10%

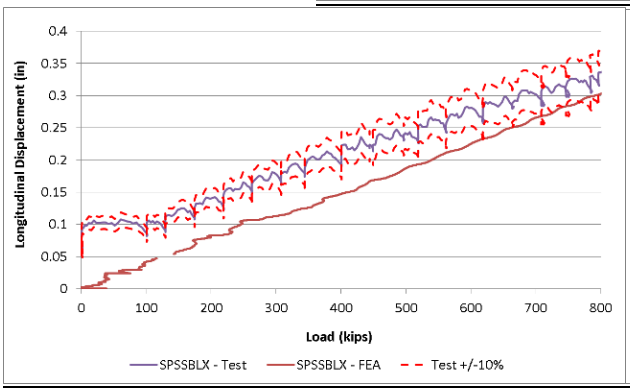
Longitudinal Displacement (in)
0.4
0.35
0.3
0.25
0.2
0.15
0.1
0.05
0
0 100 200 300 400 500 600 700 800
Load (kips)
SPSSBLX - Test
SPSSBLX - FEA
Test +/-10%

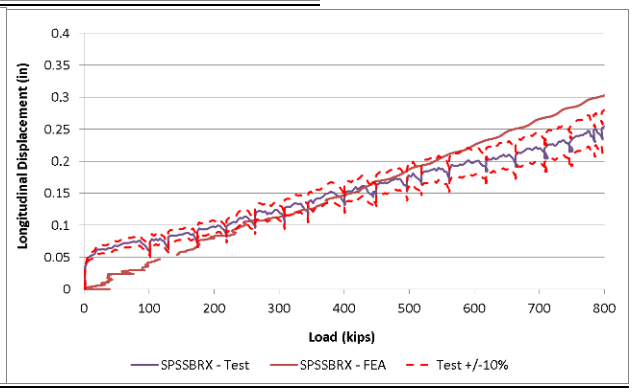
Longitudinal Displacement (in)
0.4
0.35
0.3
0.25
0.2
0.15
0.1
0.05
0
0 100 200 300 400 500 600 700 800
Load (kips)
SPSSBRX - Test
SPSSBRX - FEA
Test +/-10%

Lateral Data

Lateral displacement data were collected during the test at each of the nine VLL arrays. Corresponding lateral displacements were recorded in the FE model. Because the FE model employed longitudinal-vertical symmetry, nodes along the symmetry plane were not permitted lateral displacement. In the test, the car experienced very small lateral displacements at all locations (< 0.2 inches).

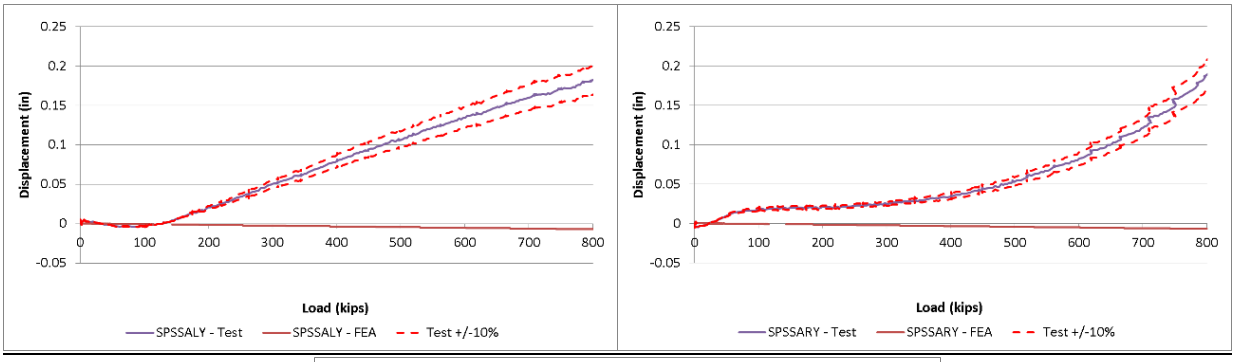

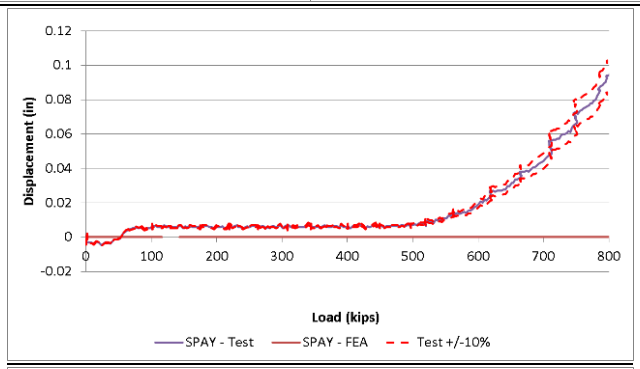

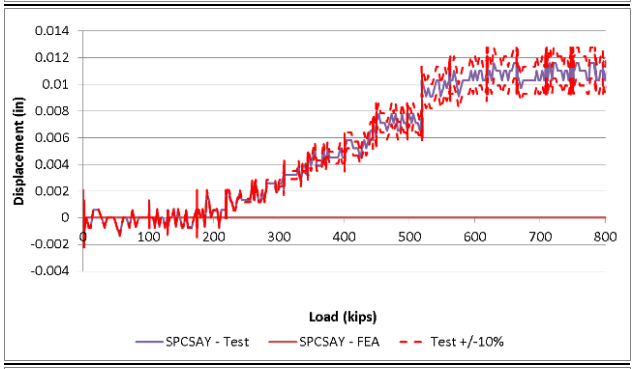

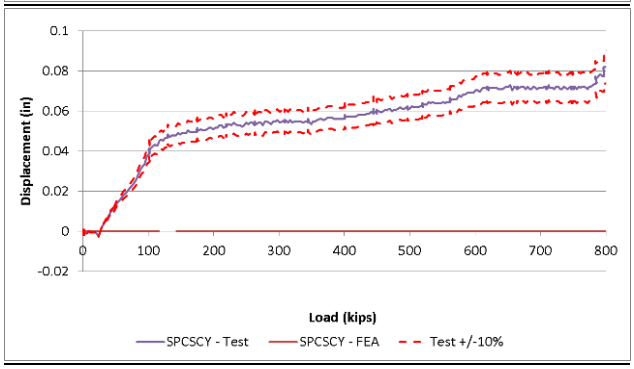

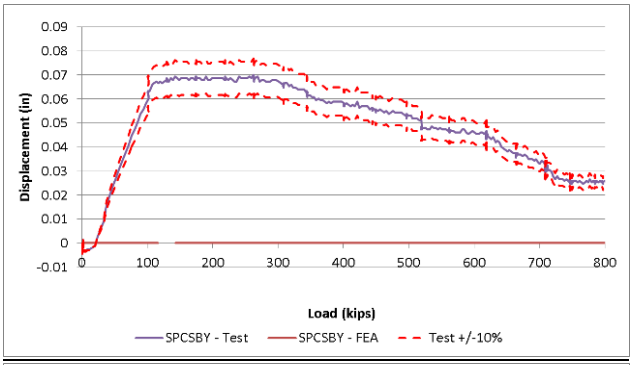
Displacement (in)
0.09
0.08
0.07
0.06
0.05
0.04
0.03
0.02
0.01
0
-0.01
0
100
200
300
400
500
600
700
800
Load (kips)
SPCSBY - Test
SPCSBY - FEA
Test +/-10%

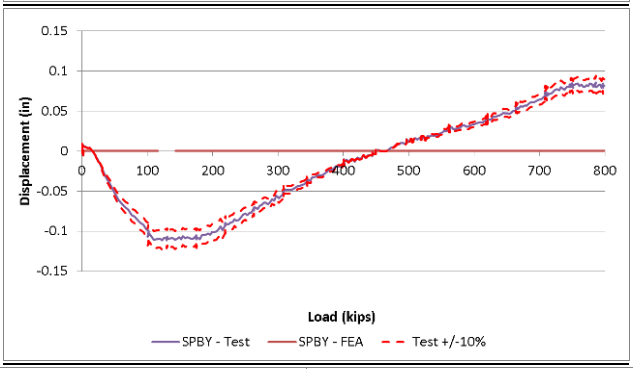
Displacement (in)
0.15
0.1
0.05
0
-0.05
-0.1
-0.15
0
100
200
300
400
500
600
700
800
Load (kips)
SPBY - Test
SPBY - FEA
Test +/-10%

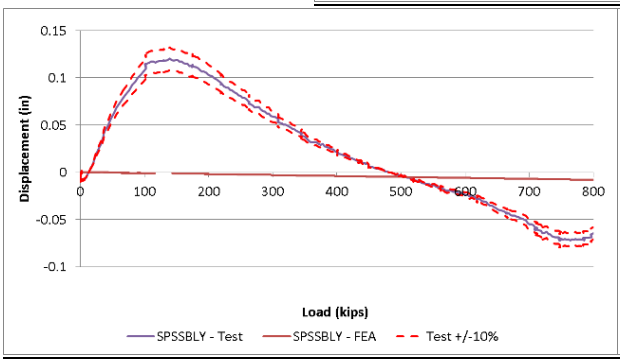
Displacement (in)
0.15
0.1
0.05
0
-0.05
-0.1
0
100
200
300
400
500
600
700
800
Load (kips)
SPSSBLY - Test
SPSSBLY - FEA
Test +/-10%

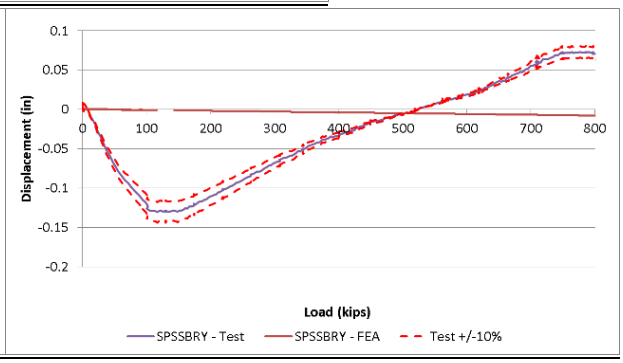
Displacement (in)
0.1
0.05
0
-0.05
-0.1
-0.15
-0.2
0
100
200
300
400
500
600
700
800
Load (kips)
SPSSBRY - Test
SPSSBRY - FEA
Test +/-10%

Vertical Data

Vertical data were recorded at each of the nine VLL array locations. Vertical displacement results were also recorded at the corresponding locations within the FE model. In general, the vertical displacement results in the FE analysis compare favorably with the vertical displacement data recorded during the test.

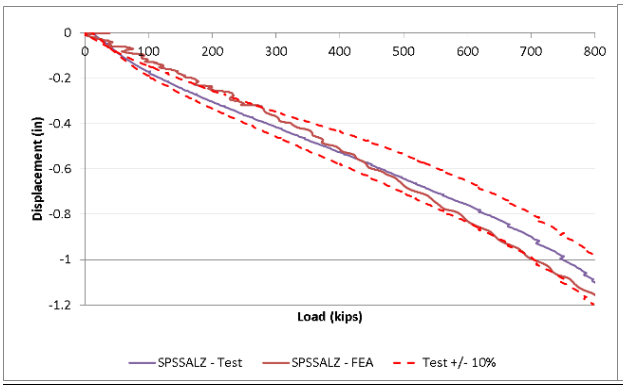

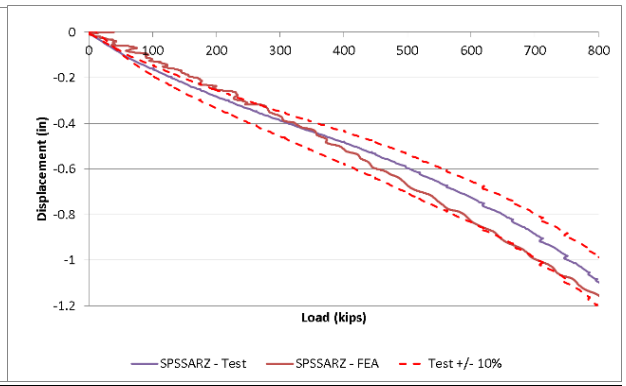

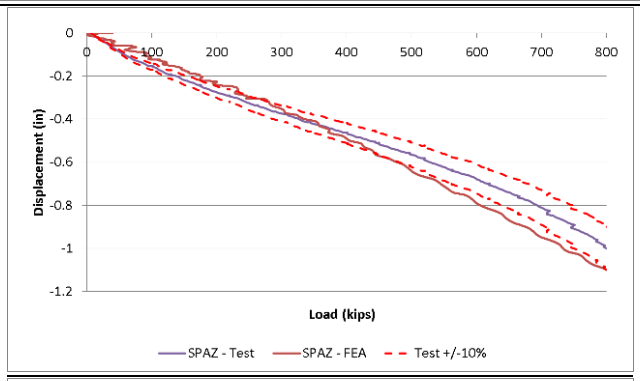

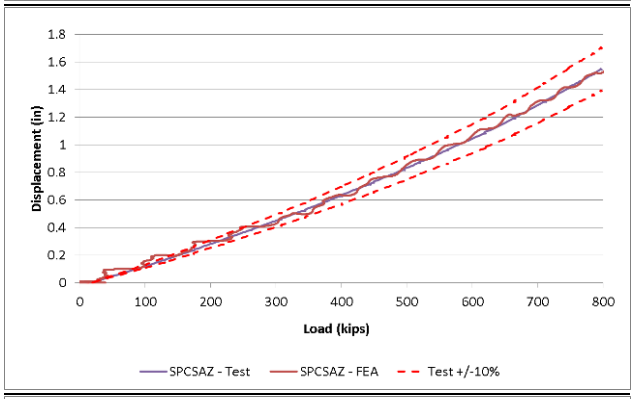

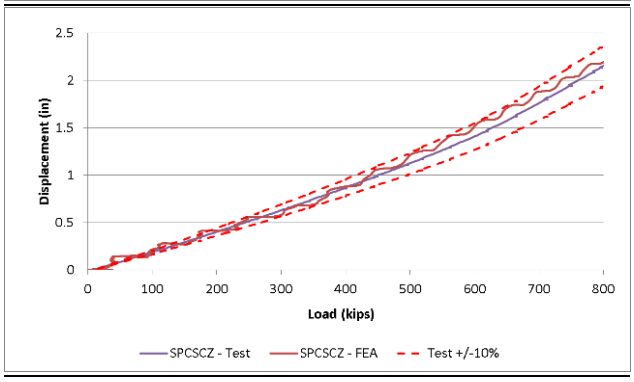

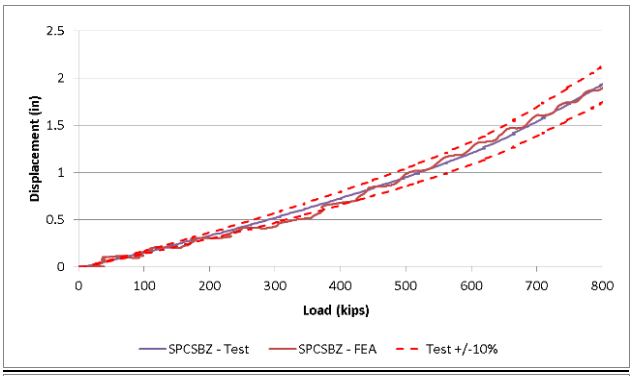
Displacement (in)
Load (kips)
SPCSBZ - Test
SPCSBZ - FEA
Test +/-10%

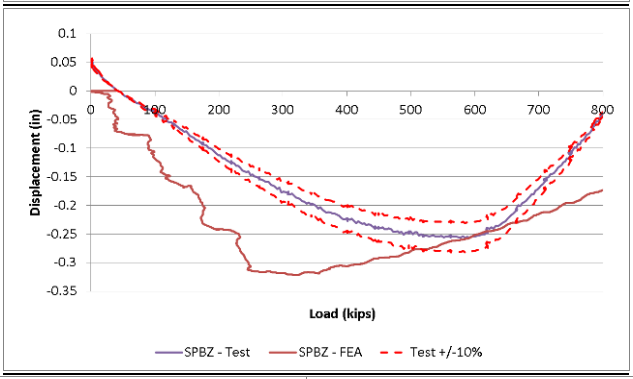
Displacement (in)
Load (kips)
SPBZ - Test
SPBZ - FEA
Test +/-10%

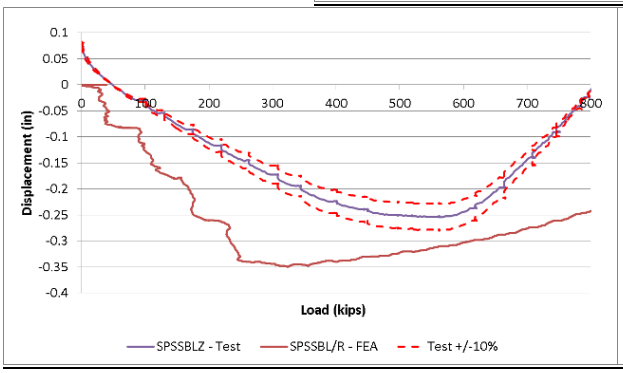
Displacement (in)
Load (kips)
SPSSBLZ - Test
SPSSBL/R - FEA
Test +/-10%

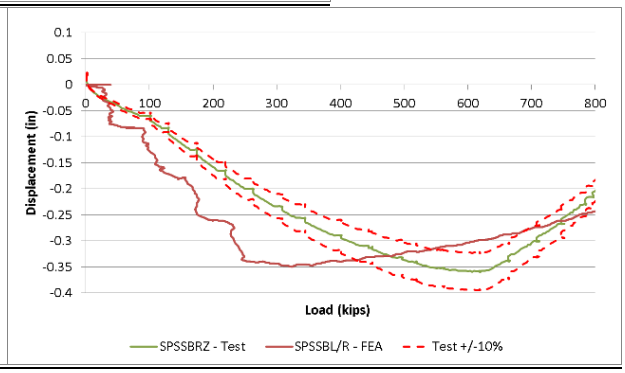
Displacement (in)
Load (kips)
SPSSBRZ - Test
SPSSBL/R - FEA
Test +/-10%

Crippling Test of Car 244

The following series of graphs contains the displacement results from the crippling test and corresponding pretest FE analysis. In each graph the test data have been resolved into their x, y, or z component. The A-end array of string pots on the center sill has been omitted from these results because of a suspected error in the data collected at this location.

Longitudinal Data

The longitudinal test data presented in each of the following figures have had the restraint-end displacement measurement subtracted from the measured longitudinal displacement data.

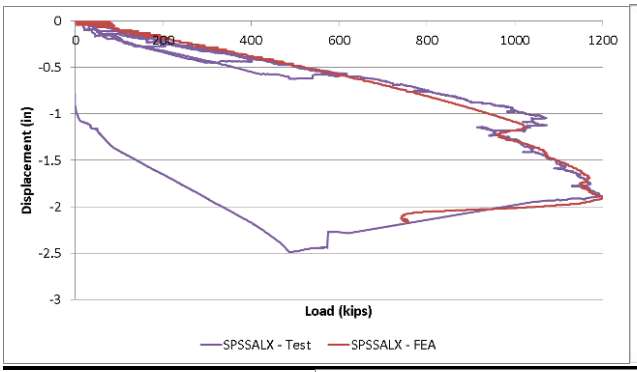

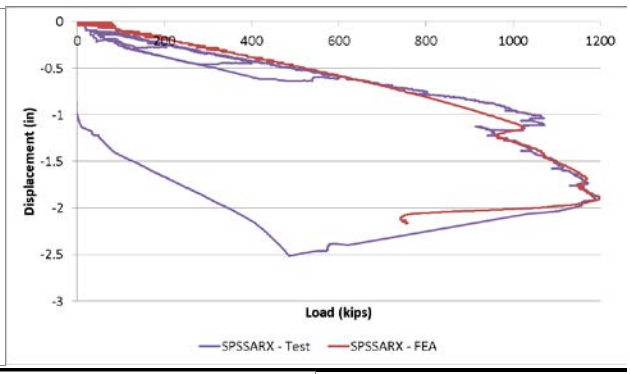

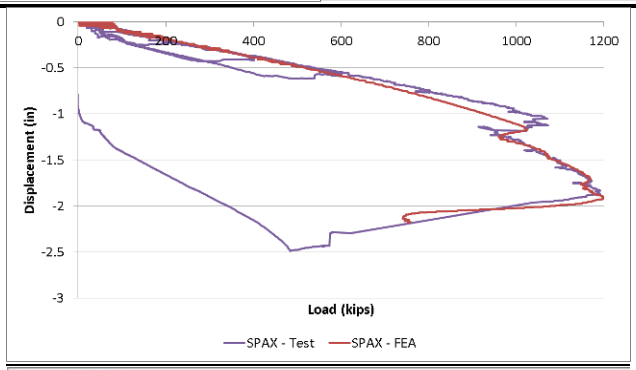

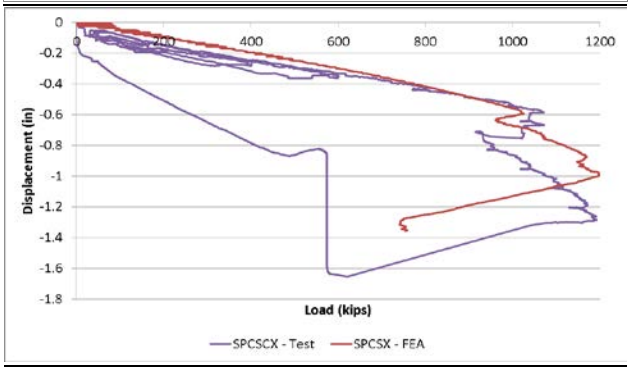

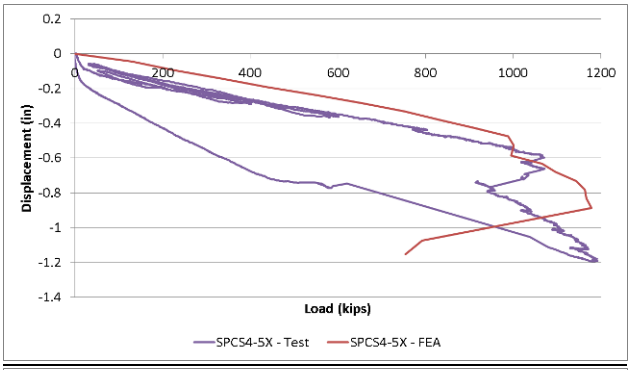
0.2
0
-0.2
-0.4
-0.6
-0.8
-1
-1.2
-1.4
0
200
400
600
800
1000
1200
Displacement (in)
Load (kips)
SPCS4-5X - Test
SPCS4-5X - FEA

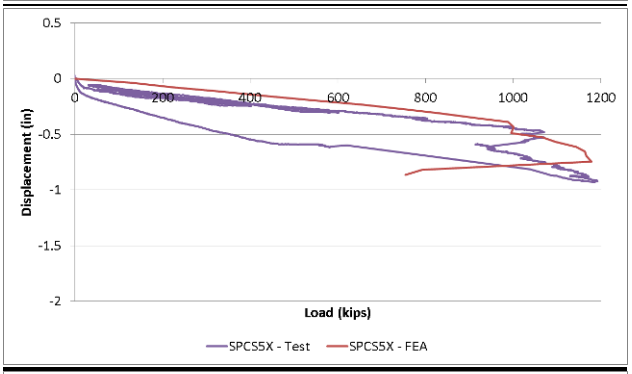
0.5
0
-0.5
-1
-1.5
-2
0
200
400
600
800
1000
1200
Displacement (in)
Load (kips)
SPCS5X - Test
SPCS5X - FEA

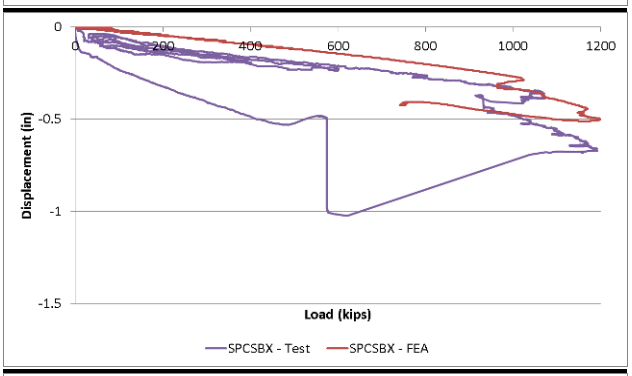
0
-0.5
-1
-1.5
0
200
400
600
800
1000
1200
Displacement (in)
Load (kips)
SPCSBX - Test
SPCSBX - FEA

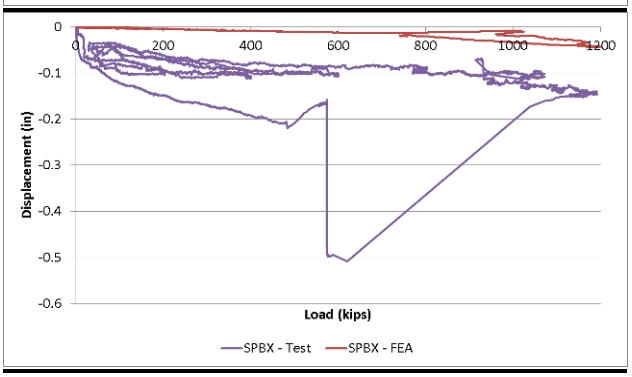
0
-0.1
-0.2
-0.3
-0.4
-0.5
-0.6
0
200
400
600
800
1000
1200
Displacement (in)
Load (kips)
SPBX - Test
SPBX - FEA

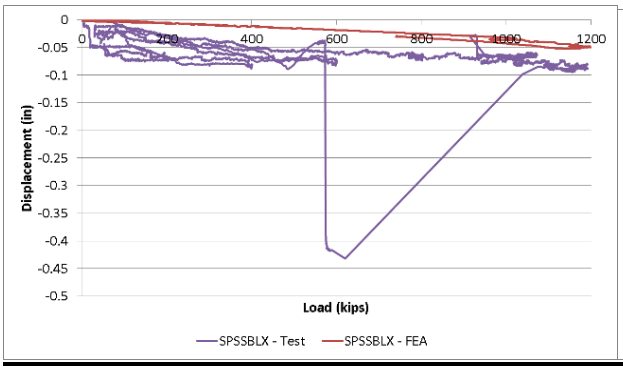
0
-0.05
-0.1
-0.15
-0.2
-0.25
-0.3
-0.35
-0.4
-0.45
-0.5
Displacement (in)
0
200
400
600
800
1000
1200
Load (kips)
SPSSBLX - Test
SPSSBLX - FEA

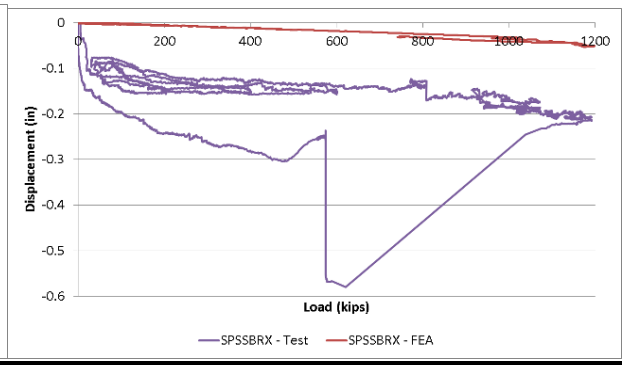
0
-0.1
-0.2
-0.3
-0.4
-0.5
-0.6
Displacement (in)
0
200
400
600
800
1000
1200
Load (kips)
SPSSBRX - Test
SPSSBRX - FEA

Lateral Data

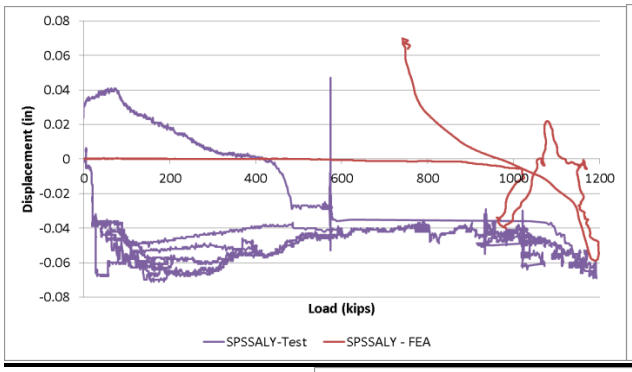

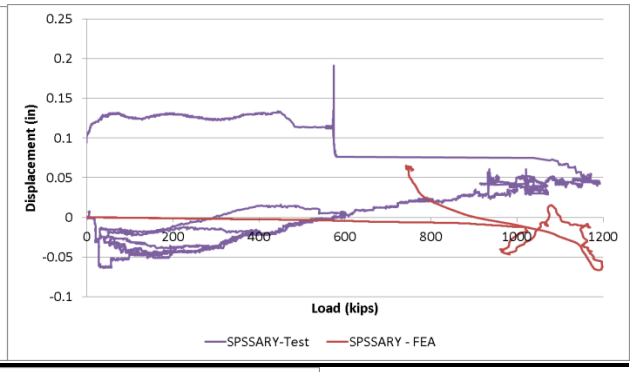

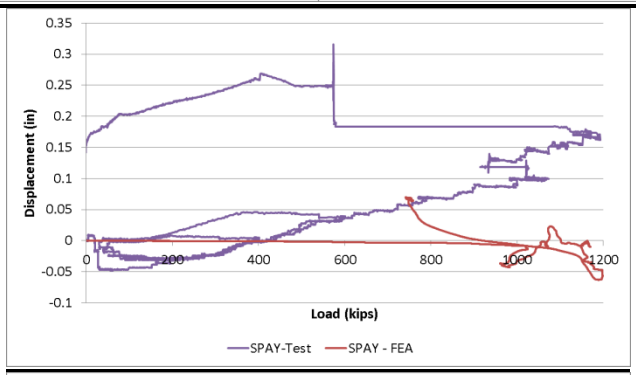

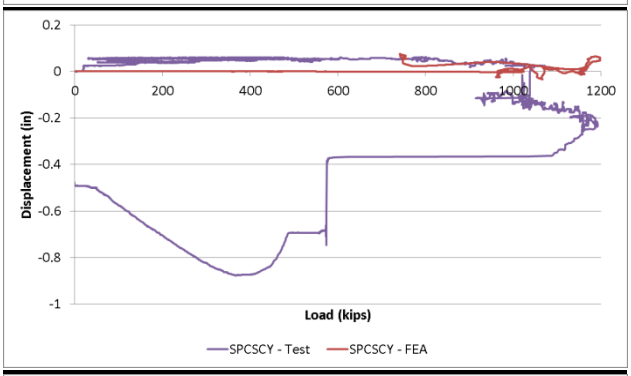

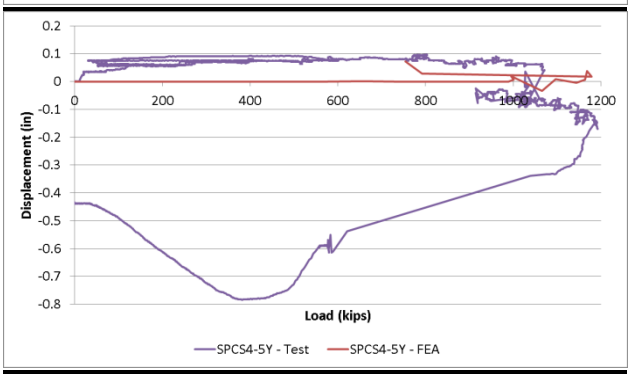

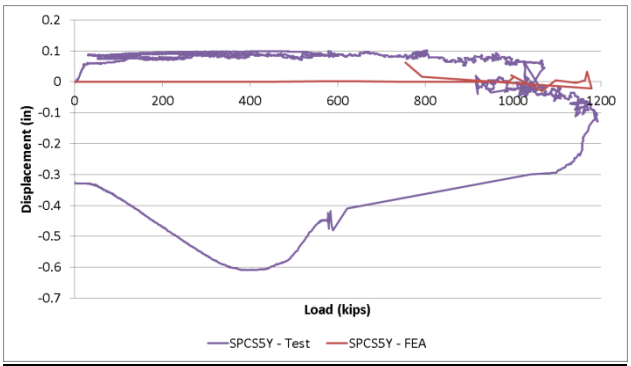
Displacement (in)
Load (kips)
SPCS5Y - Test
SPCS5Y - FEA

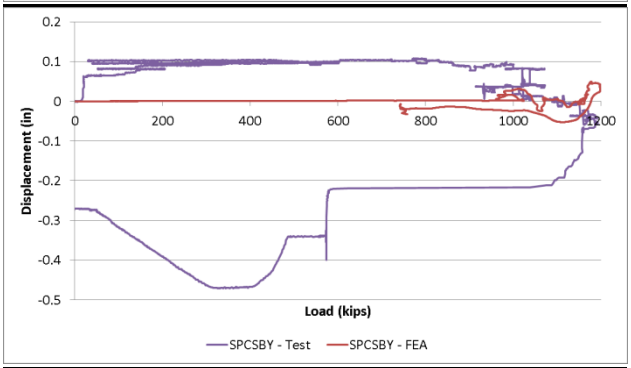
Displacement (in)
Load (kips)
SPCSBY - Test
SPCSBY - FEA

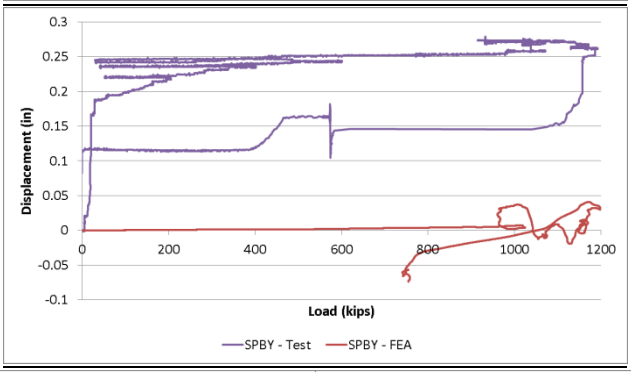
Displacement (in)
Load (kips)
SPBY - Test
SPBY - FEA

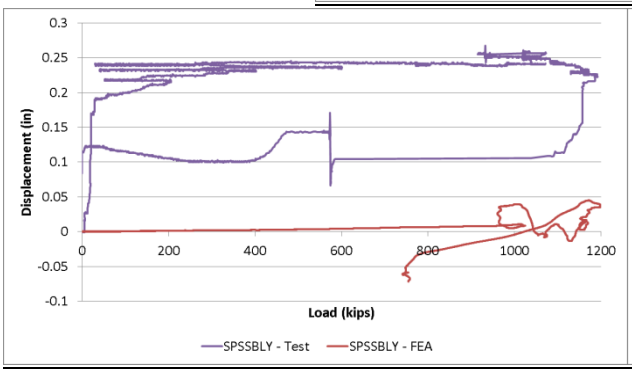
Displacement (in)
Load (kips)
SPSSBLY - Test
SPSSBLY - FEA

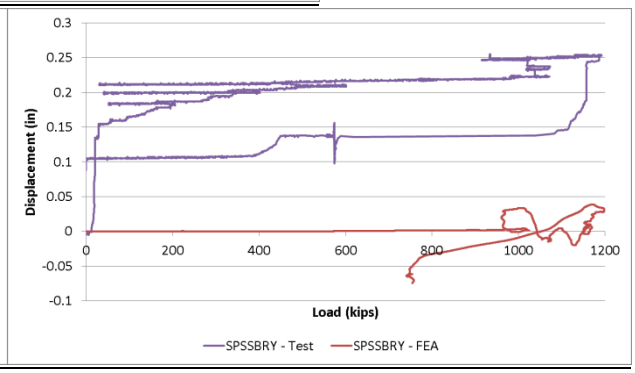
Displacement (in)
Load (kips)
SPSSBRY - Test
SPSSBRY - FEA

Vertical Data

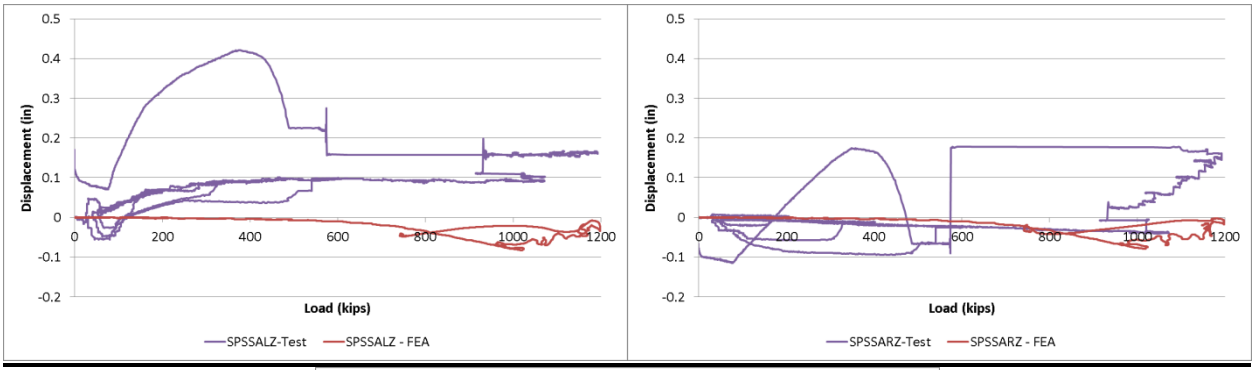

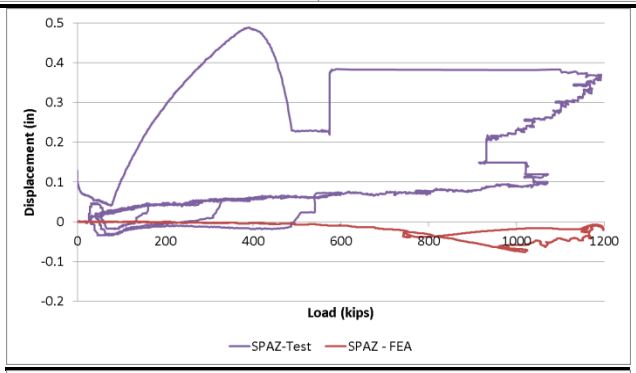

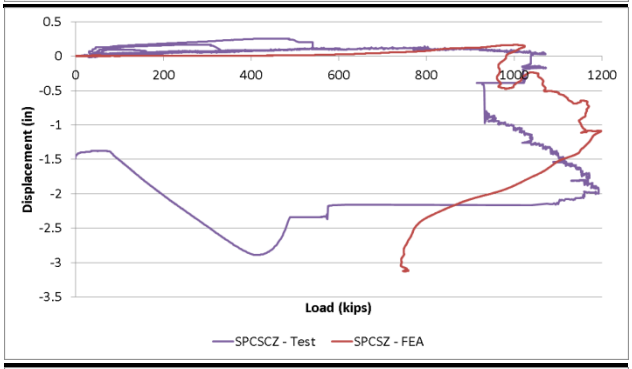

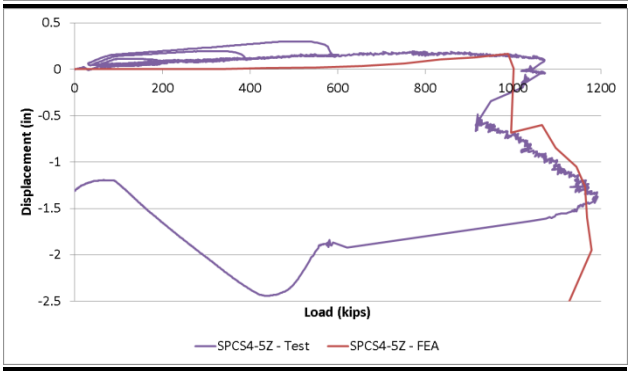

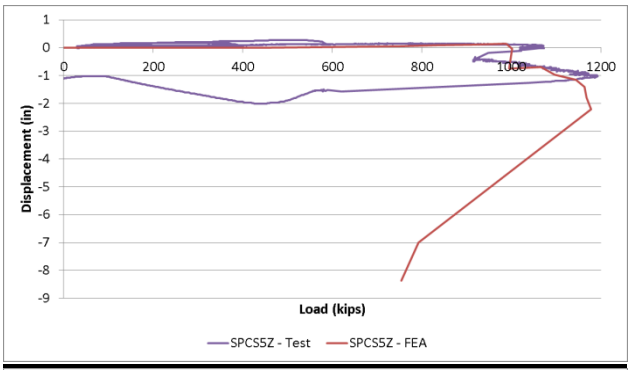
Displacement (in)
Load (kips)
SPCS5Z - Test
SPCS5Z - FEA

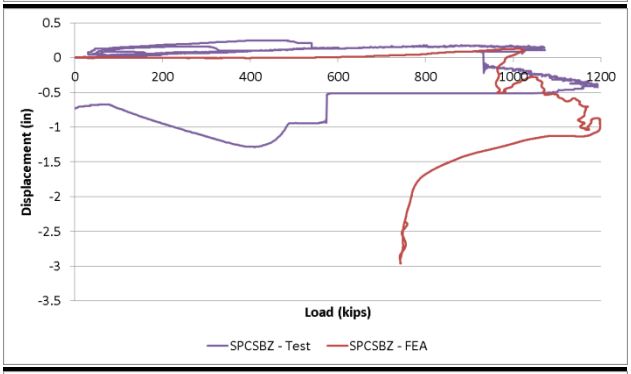
Displacement (in)
Load (kips)
SPCSBZ - Test
SPCSBZ - FEA

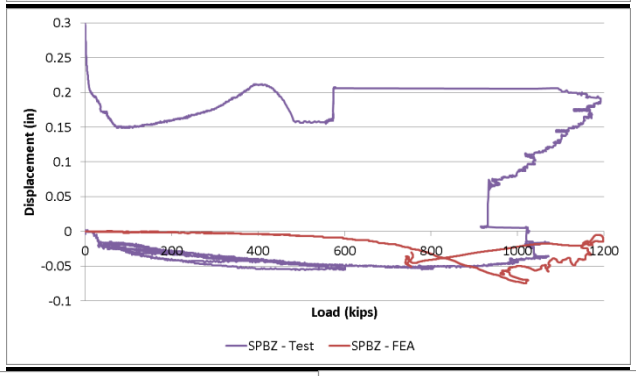
Displacement (in)
Load (kips)
SPBZ - Test
SPBZ - FEA

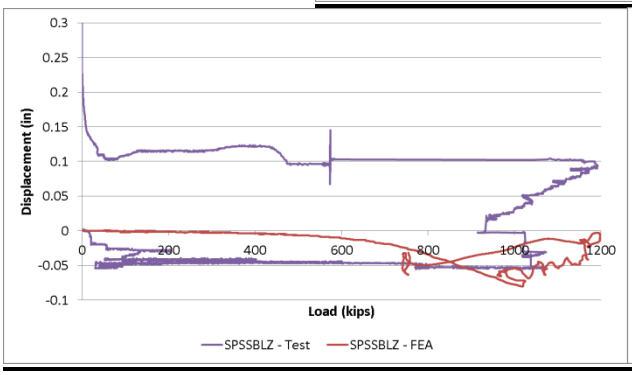
Displacement (in)
Load (kips)
SPSSBLZ - Test
SPSSBLZ - FEA

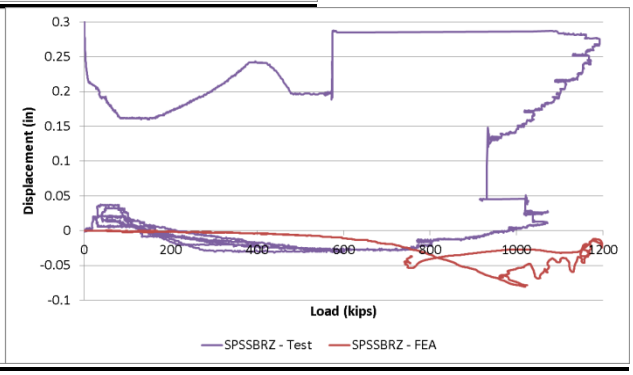
Displacement (in)
Load (kips)
SPSSBRZ - Test
SPSSBRZ - FEA

Abbreviations and Acronyms

CFR	Code of Federal Regulations
ETF	Engineering Task Force
FE	Finite Element
FRA	Federal Railroad Administration
OVI	Occupied Volume Integrity
RSAC	Railroad Safety Advisory Committee
SEPTA	Southeastern Pennsylvania Transportation Authority
VLL	Vertical, Lateral, Longitudinal